

# SSRP 2015

## 19. Steirisches Seminar über Regelungstechnik und Prozessautomatisierung

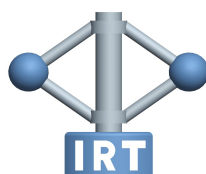
R. Seeber, M. Horn (Hrsg.)

7. - 9. 9. 2015

Schloss Retzhof, Leibnitz, Österreich

ISBN: 978-3-901439-11-7

© Institute of Automation and Control, Graz University of Technology



<http://www.irt.tugraz.at>



# Preface

For the 19th time the *Steirische Seminar über Regelungstechnik und Prozessautomatisierung* (Styrian Seminar on Control Systems Engineering and Process Automation) has taken place at *Schloss Retzhof*, an education center run by the Austrian State of Styria. This conference is organized every two years by the *Institute of Automation and Control* of *Graz University of Technology*, with the goal of discussing current works and developments in the field of control systems and process automation.

The present conference proceedings are a compilation of submissions received and presented at Schloss Retzhof. They are divided in two parts: Part I is devoted to full papers, while Part II contains abstracts and slides of the presentations. The organizers would like to thank the authors for their diligence in preparing their contributions.

Graz, November 2015

Richard Seeber, Martin Horn

# Contents

|  |           |
|--|-----------|
| <b>I. Full Papers</b>  | <b>1</b>  |
| <i>Gernot Druml</i><br>Effects of the nonlinear Arc of a 20-kV-net single-line cable fault on the Earth-Fault-Detection and -Control                     | 2         |
| <i>Alexander Schirrer, Stefan Jakubek</i><br>Optimization-based formulations of absorbing boundary conditions in discrete-time wave propagation problems | 9         |
| <i>Dimitrios Kalligeropoulos, Soultana Vasileiadou</i><br>Philon von Byzanz und seine Druckwerke über pneumatisch-hydraulische Regelsysteme              | 22        |
| <b>II. Slides</b>  | <b>32</b> |
| <i>Alexander Barth, Markus Reichhartinger, Johann Reger, Martin Horn, Kai Wulff</i><br>Lyapunov-based Design of Adaptive Sliding Mode Controllers        | 33        |
| <i>Robel Besrat, Felix Gausch, Nenad Vrhovac</i><br>Observers for Non-Linear MIMO Descriptor Systems   | 50        |
| <i>Stefan Doczy, Wolfgang Toppler</i><br>Design and Validation of an SOH Algorithm for Lithium Ion Batteries   | 65        |
| <i>Markus Freistätter, Robert Bauer, Nicolaos Dourdoumas, Wilfried Rossegger</i><br>Control-oriented Turbocharger Modelling                              | 78        |
| <i>Leonid Fridman</i><br>HOSM Based Observation, Identification and Output Based Control   | 89        |
| <i>Mikulas Huba, Peter Tapak, Stefan Chamraz</i><br>Comparing model-free and disturbance observer based control  | 110       |
| <i>Stefan Koch, Markus Reichhartinger, Martin Horn</i><br>On Discretization of Sliding Mode Based Control Algorithms                                     | 129       |
| <i>Jaime A. Moreno</i><br>Discontinuous Integral Control for Mechanical Systems  | 150       |
| <i>Johann Reger, Jerome Jouffroy</i><br>Estimating Parameters and States Using Modulating Functions  | 177       |

|  |     |
|--|-----|
| <i>Georg Stettinger, Martin Benedikt, Martin Horn, Christian Pötzsche, Josef Zehetner</i><br>Stability Analysis of Interconnected Linear Systems with Coupling Imperfections | 190 |
| <i>Christopher Zemann, Viktor Unterberger, Markus Göller</i><br>Model based control of a biomass fired steam boiler  | 205 |



**Part I.**

**Full Papers**

# Effects of the nonlinear Arc of a 20-kV-net single-line cable fault on the Earth-Fault-Detection and -Control

Gernot Druml

Linz

Austria

g.druml@ieee.org

## Abstract

The results of field tests have shown, that the behaviour of the restriking earthfault in a cable is completely different in isolated and well-tuned compensated networks. In this paper, the differences will be considered in detail and the impact on the earthfault detection and the control of the Petersen-Coil will be explained.

Due to the different behaviour, there are new possibilities to reduce the current via the fault location.

Actually the control of the Petersen-Coil is a preventive action during the healthy network operation. On the other side the control of the Petersen-Coil is currently blocked during the earth-fault. Therefore a change of the network-size during the earthfault will increase the current via the fault location. In this paper the new method "faulty phase earthing" will be presented, which finally allows the correct tuning of the Petersen-Coil even under earth-fault conditions.

In addition, the earth fault detection will be influenced by this new method. These influences and the new demands on the earth fault detection will be presented in detail.

## 1 Introduction

In many European countries the "resonant grounding" is one of the most important options in electrical network design, in order to obtain the optimal power supply quality. The main advantages of an earthfault-compensated network are:

- Self-healing of the system without any intervention of protection systems
- Continuing the network operation during a sustained single line earth-fault
- Improved power quality and reliability for the customer
- Reduction of the current via the fault location to 2% - 3% of the whole capacitive current

The first main advantage of this neutral-point-treatment is the fact, that in most cases the system is self-healing, as the arc distinguishes without any intervention of the protection system. The second main advantage is the possibility of continuing the network operation during a sustained earth fault. As a consequence this reduces the number of interruptions of the customers power supply.

With the increased use of cables the advantages of the Petersen-Coils are called into question, as the fault is always restriking until it becomes a line-to-line-to-ground-fault (LLG-fault) or a cross-country fault.

## 2 Physic of the earthfault

To explain the transient behaviour of a single-line earth fault in more detail, the scheme of a substation (Fig. 1) with three feeders (A, B and C) and an earth fault in line 1 of feeder A will be used [1].

In Fig. 2 the behaviour of the earthfault is simplified using phasors. The first picture shows the healthy state of the network. The second picture shows, that in case of an earthfault there will be an unsymmetrical system. Phase 1 is zero.

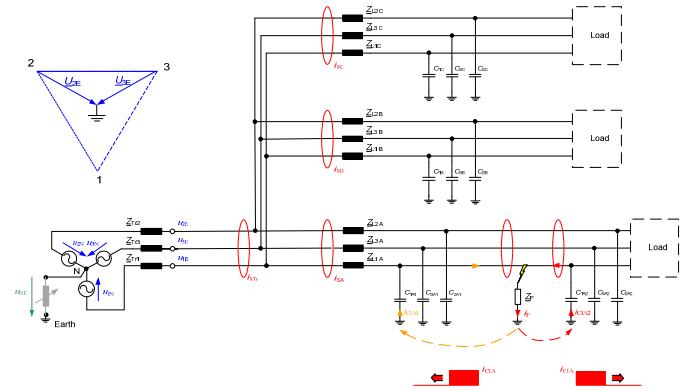


Fig. 1 Discharge of the faulty line via earth

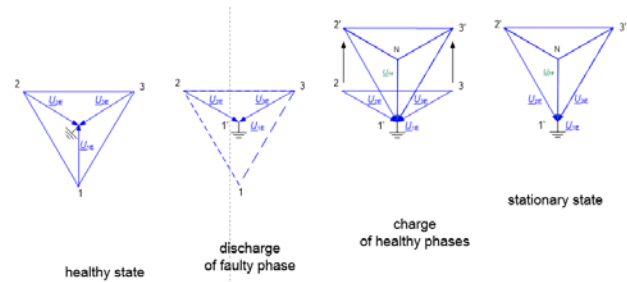


Fig. 2 Earthfault – simplified with symmetrical components

In solid and low-impedance grounded networks this distorted voltage will be seen until the fault is switched of. In resonance grounded and isolated networks the two healthy feeders will be charged, which is shown in the third picture. In reality this description is simplified too much.

The transient parts of an earthfault cannot be described exact using "symmetrical components". For the mathematical description either the  $\alpha\beta$ -components introduced by Edith Clarke [11] or the space-vector description introduced by K.P. Kovács [10] should be used. The second method is widespread, in the reduced form, for the description of frequency converters for motor drives.

Reduced, because in these applications there is no zero-sequence in use. A detailed explanation of the space vector theory applied to power systems can be found in [4][5][6]. With the beginning of the earth-fault two different processes can be superposed [1]. The following two processes are starting at the same time, but with different duration:

- discharge of the faulty line over the earth
- charging of the two healthy lines over the earth

The two processes end in the stationary state of the earth fault.

## 2.1 Discharge of the faulty line via earth

The lines can be considered as a distributed lattice network, consisting of a distributed complex serial impedance and a distributed  $Z'_{Lxx} = R' + j\omega L'_{Lxx}$  line-to-ground capacitance  $C'_{Lxx}$ . The highest probability for the first ignition is near the maximum of the line-to-ground voltage  $u_{1G}$ . At this time the line has about the maximum charge. The discharge of the lattice network of line 1 will start at the fault location and it will spread in both directions to the ends of line 1. A reflection of the waves occurs at the end of the line, respectively at every change of the characteristic impedance  $Z_c$  of the line. These reflections can be detected in form of oscillations at a high frequency in the zero-sequence-current and in the zero-sequence-voltage. The oscillation frequency essentially depends on the serial impedance and the line-to-ground capacity, which are, in a first approximation, inversely proportional to the length of the line. Therefore, the frequency is higher for small networks and it is lower for large networks. According to the time-domain equations (1) and (2) of a single-conductor line [5]

$$-\frac{\partial u(x,t)}{\partial x} = R' i(x,t) + L' \frac{\partial i(x,t)}{\partial t} \quad (1)$$

$$-\frac{\partial i(x,t)}{\partial x} = G' u(x,t) + C' \frac{\partial u(x,t)}{\partial t} \quad (2)$$

The velocity for a lossless line can be estimated as

$$v = \frac{1}{\sqrt{L'C'}} = \frac{1}{\sqrt{\mu\epsilon}} = \frac{c}{\sqrt{\mu_r\epsilon_r}} \approx \frac{c}{\sqrt{\epsilon_r}} \quad (3)$$

With  $\epsilon_r = 1$  for overhead lines and  $\epsilon_r = 2.3 \dots 3.5$  for cables [9]. For a more accurate modelling of a line, the frequency dependency of the line-parameters must be taken into account the characteristic impedance of the lossless line (surge impedance) is

$$Z_c = \sqrt{\frac{L'}{C'}} \quad (4)$$

with a value of about 400 Ohm for overhead lines and about 40 Ohm for cables. **This surge impedance limits the discharge current of the line.**

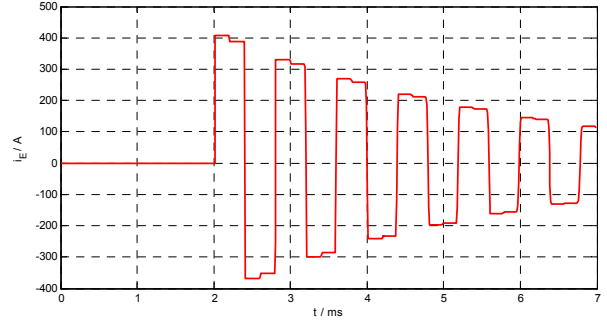


Fig. 3 Discharge current of a loaded cable ( $11.5 \text{ kV} \cdot \sqrt{2}$ , 20 km, NA2XS2Y 150 mm<sup>2</sup>)

The simulation with SimPowerSystem using a model with distributed parameters confirms, that the maximum discharge current in a standard 20 kV cable is limited to about 400 A [1], as depicted in Fig. 3

## 2.2 Charge of the two healthy lines via earth

As a result of the discharge of the faulty line, the triangle of the line-to-ground voltages is destroyed. As the supply-transformer is still delivering a symmetrical three-phase-system, the two healthy lines will be charged to the line-to-line voltage in isolated and compensated networks.

## 2.3 Stationary state of the earth fault

In an isolated network the whole capacitive current of all feeders flows via the fault location.

For compensated networks the situation is different. In this case, the current through the Petersen-Coil superposes and reduces the capacitive current over the fault location. In a well-tuned network the capacitive current over the fault location is completely compensated.

Using a Petersen-Coil, the fundamental current over the fault location can be reduced to the small wattmetric part, which is usually in the range of 2 % to 3 % of the whole capacitive line-to-ground current of the network. During the transient state of the earthfault ignition respectively during the first ms, the Petersen-Coil has no or low compensation effect [1]. But after few periods the capacitive current via the fault location is compensated more or less completely. In a well-tuned network only the wattmetric part flows over the fault location.

## 3 Restriking earthfault in a cable-section

Fig. 4 shows a line-to-ground-fault (LG-fault) in a cable. Due to the fault, an air-channel is developing with higher pressure. The isolation level of the air gap is smaller than the one of the dielectric. In overhead lines (OHL) the air is self-healing after the arc has extinguished [2][3]. The self-healing of the OHL-network is supported by the Petersen-Coil.

In cables the isolation-level of the air gap is too small, so that there will be always a re-ignition of the arc [1].



Fig. 4 LG-fault in a cable section.

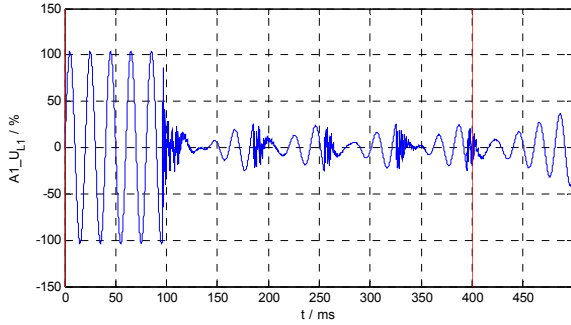


Fig. 5 Voltage  $u_{L1}$  measured at the bus-bar

Fig. 5 shows the behaviour of a restriking fault in a cable-section: During the whole earth fault, the voltage  $u_{L1}$  is zero only for very short times. The low current arc extinguishes within few milliseconds at the zero-crossing of the current. As the investigated network is a compensated network, the phase voltage  $u_{L1}$  increases slowly. The increase of the voltage in a cable network goes up to the restriking voltage, which is in the range between 2 kV and 6 kV in a 20-kV-network. This restriking voltage depends on different parameters and it is not constant, neither during an earth fault.

Fig. 3 Discharge current of a loaded cable ( $11.5 \text{ kV} \cdot \sqrt{2}$ , 20 km, NA2XS2Y 150 mm<sup>2</sup>)

shows the behaviour of the fault current via the fault location in case of a solid earthfault. In this simulation it was assumed, that there is no restriking voltage. Real measurements have confirmed, that in a well-tuned compensated network the following items are valid:

- **The arc in a cable-section with a restriking voltage will distinguish after the first zero-crossing of the current via the fault location.**
- **The length of the pulse depends on the network length.** The burning time of the arc is reduced from continuous burning to few ms with a replication of some periods
- The burning time of the arc in the real test-network was, due to the well-tuned Petersen-Coil, reduced from  $\geq 10$  ms to 1.4 ms
- **The amplitude of the discharge-current via the fault location is limited by the surge impedance of the network (Fig. 7) and is more or less constant during the pulse.**
- The time for the next restrike mainly depends on:
  - the detuning of the network
  - the damping of the network
  - restriking voltage of the cable-air-gap
  - pressure, temperature and consistency of the gas

in the cable-air-gap

- Due to the limited amplitude of the discharge current, due to the reduction of the burning time and due to the increase of the restriking time, **the converted energy at the fault location is reduced to some 100 W.** Therefore also the probability of the extension of the LG-fault to an LLG-fault at the fault location is reduced dramatically.

Fig. 8 shows the behaviour of the restriking for the case of an ideal tuned network. The time in-between the restrikes is increased.

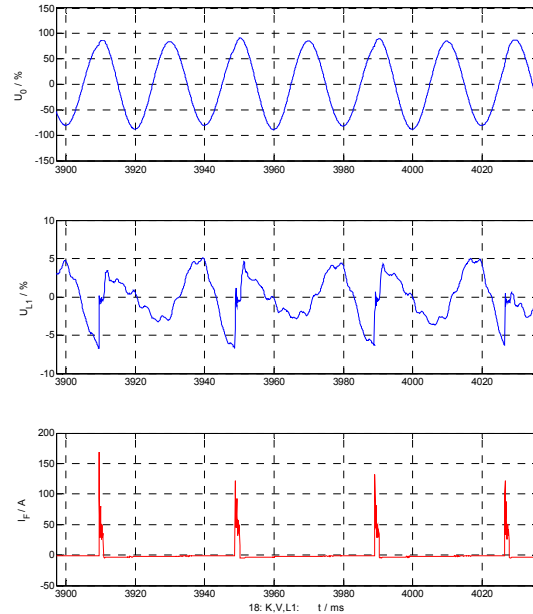


Fig. 6 Restriking fault in a cable section of a well-tuned compensated network

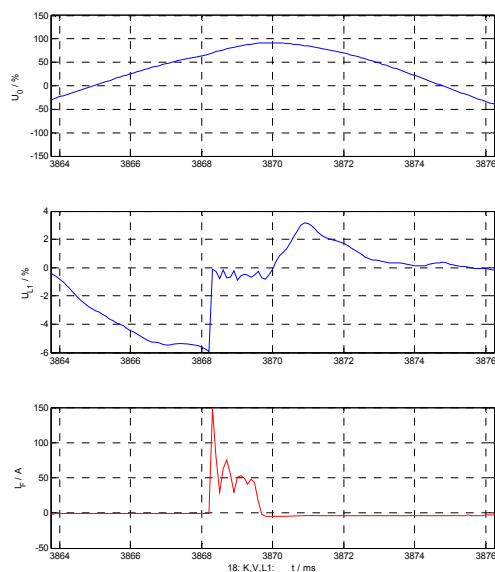


Fig. 7 Zoomed window of Fig. 6

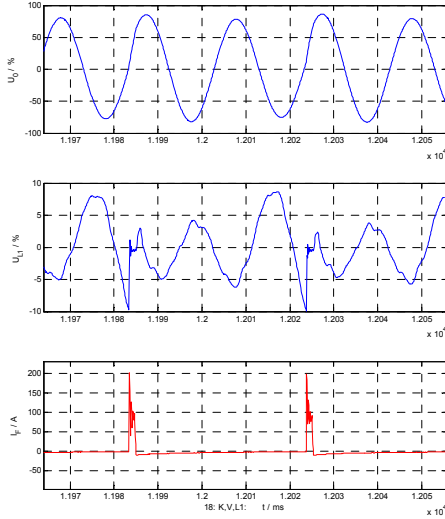


Fig. 8 Restriking fault in a cable section of an ideal tuned compensated network

Up to now the classification for the network and the handling auf SL-faults is:

- Networks with OHL ( cable / OHL < 10% )
- Mixed networks (10% < cable / OHL < 90% )
- Cable-Network (cable / OHL > 90% )

In the future, we should classify according to the point, where the fault occurs:

- Earth-fault in the cable section => restriking
- Earth-fault in the OHL section => quasi-stationary

In case of restriking earthfaults, it is possible to improve the function of the Petersen-Coil with the faulty-phase-earthing (FPE).

## 4 QU-Algorithm for directional transient earthfault detection

The following considerations are based on the transient definition of the zero-sequence-system according to the space-vector-theory.

For example, for the healthy feeder B or C, as shown in Fig. 9, of our sample-network the charging can be described with equation (5)

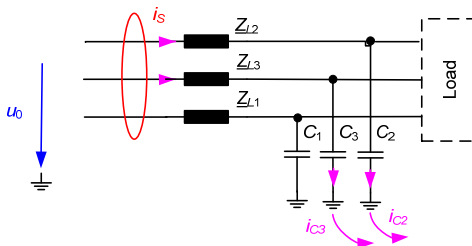


Fig. 9 Charge of one healthy feeder

$$u_0(t) = u_0(t_0) + \frac{1}{C_{eq}} \int_{t_0}^t i_s(\tau) d\tau \quad (5)$$

$$u_0(t) = u_0(t_0) + \frac{q_s(t)}{C_{eq}} \quad (6)$$

Starting the integration at a point where  $u_0(t_0) = 0$  results in:

$$u_0(t) = \frac{q_s(t)}{C_{eq}} \quad (7)$$

Drawing a diagram of this relation, with  $q_0$  on the ordinate and the zero-sequence voltage  $u_0$  on the abscissa results in a straight line with the gradient  $C_{eq}$ , which is the equivalent zero-sequence capacitance of the feeder. Subsequently, this diagram shown in Fig. 10 will be referred to as qu-diagram.

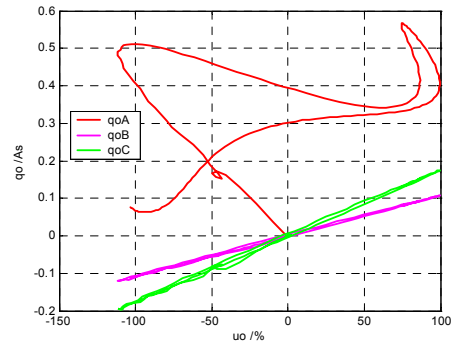


Fig. 10 qu-diagram of the three feeders in case of a low-ohmic fault in feeder A

In the case of a faulty feeder this relation is no more valid. The sum of the charging currents of all healthy feeders flows out from the faulty feeder, it starts with a negative gradient and in compensated networks it is not a straight line. The last statement can be used as additional information for the earthfault detection.

Fig. 11 and Fig. 12 shows the behaviour for a high-ohmic earthfault.

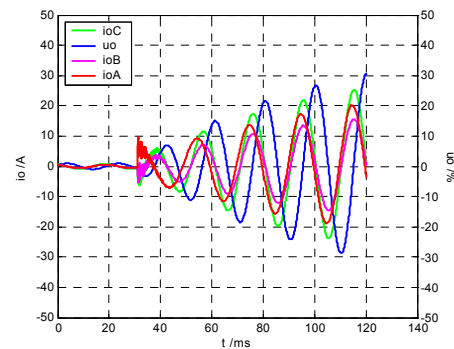


Fig. 11  $i_0$  and  $u_0$  of the three feeders in case of a high-ohmic earthfault

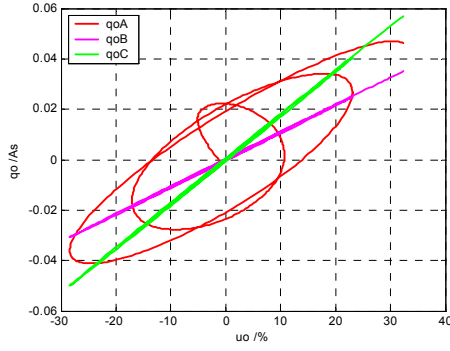


Fig. 12  $qu$ -diagram of the three feeders in case of a high-ohmic fault in feeder A

From Fig. 12, we see, that the faulty feeder A starts with a negative gradient and that the rotation of the ellipse is positive in the mathematical sense.

The  $qu$ -algorithm can be used also for restriking earthfaults.

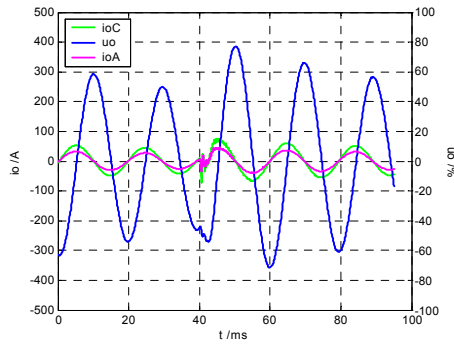


Fig. 13  $i_o$  and  $u_0$  of the three feeders; restriking fault

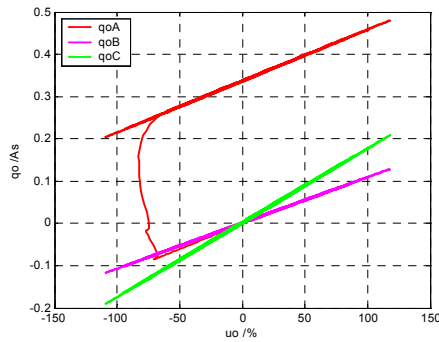


Fig. 14  $qu$ -diagram of the three feeders in case of a restriking fault in feeder A

From Fig. 14 we see that the network is healthy between the arcing earthfaults. In this healthy situation the zero-sequence voltage is decaying until the voltage in line A restrikes. A more detailed evaluation of restriking earthfaults and a presentation of the influence to other earthfault detection methods can be found in [12][13].

With the  $qu$ -algorithm a classification of the earth-fault can be done (Fig. 15). This classification is a great improvement during the real localisation of the earthfault in mixed

networks. This classification enables to reduce the time to find and to remove the earth-fault.

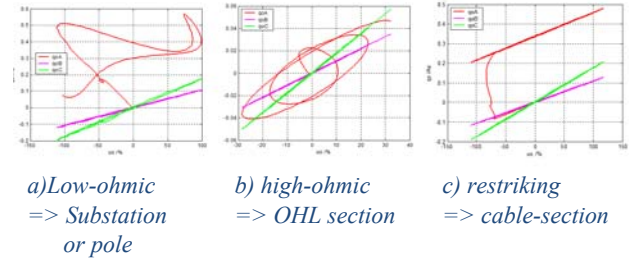


Fig. 15 Classification of the earthfault using the  $qu$ -algorithm

## 5 Faulty-Phase-Earthing (FPE)

Fig. 16 shows the situation in case of a single LG-fault. The not compensated current flows via the fault location.

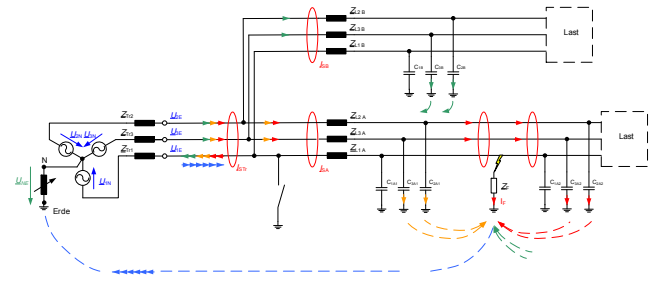


Fig. 16 Faulty-Phase-Earthing (FPE) stand by

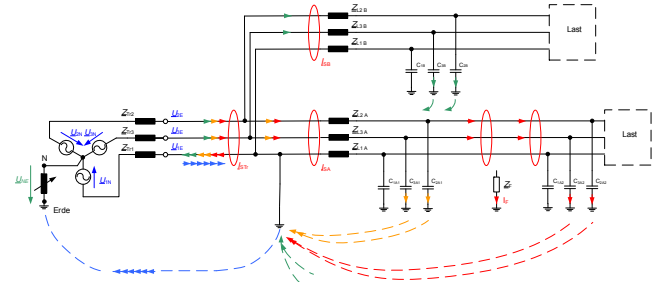


Fig. 17 Faulty-Phase-Earthing (FPE) activated

In Fig. 17 the FPE is activated and the fault current is now flowing via the grounded phase in the substation. Due to the cable, the restriking voltage at the fault location is in the range of 1... 6 kV. This restriking voltage is now the allowed voltage drop from the substation to the fault-location, as a result of the load current. Due to this high restriking voltage of the cable, the arc at the fault location will not re-ignite. High restriking voltage can be find in all faults with an air-gap with constant gap-length like in cable joints, cable sealing end and so on.

The resulting advantages of the FPE are:

- During the active FPE, the earthfault-current is moved from the fault-location to the well-grounded substation. At the point of the damaged cable no current flows to the earth and therefore no power conversion occurs at the fault location



- As there is no current via the fault location, also the touch and step-voltage is reduced
- As there is no current via the fault location, also the often discussed problems with harmonic currents in the residual current are eliminated.
- The positive-sequence-system is not influenced by the earthfault, so that the customers on the LV-network do not see the isolation problem in the MV-system.
- In addition, there is no more a restriking earthfault with corresponding voltage spikes on the two healthy phases.
- Relays for the correct and reliable recognition of restriking earthfaults already exist.
- As already mentioned above: during the active FPE the earthfault-current is moved from the fault-location to the well-grounded substation. Therefore it is now possible, to measure the current via the fault location in the substation and **to make a correct tuning operation with the Petersen-Coil, even during the earthfault.**
- Due to the control of the Petersen-Coil during the earthfault, it is now possible to react on changes in the network size and to move the Petersen-Coil to the correct tuning position. In all actual controllers on the market, the control of the Petersen-Coil is blocked during the earthfault.
- For the localisation of the fault after switching operations the FPE must be reopened to check if the earthfault is removed. In case of a restrike, the earthfault still exists in the compensated network and the FPE will be closed immediately.
- The used vacuum-switch is suitable for short-circuit-currents, so that also cross-country-faults are under control.
- The correct detection of the faulty phase under all possible earthfault scenarios is a challenge, but possible with the new E-FPE controller
- A Petersen-Coil, well-tuned to the resonance-point, supports the functionality of the FPE. The restriking voltage is increased, due to the longer available time to cool down the plasma after the last flashover.

Fig. 18 shows for example a combination of a Petersen-Coil with a ZigZag transformer and an integrated Faulty-Phase-Earthing. The real implementation of this combination is depicted in Fig. 19.

The advantage of the combination FPE and Petersen-Coil is, that the FPE will be activated by the new relays, when earthfaults occur in the cable-section. If the earthfault is in the range of the OHL all the well-known advantages of the Petersen-Coil remain available.

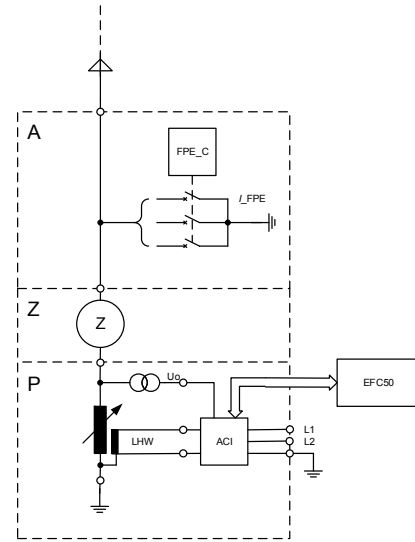


Fig. 18 Petersen-Coil combination with ZigZag-transformer and integrated Faulty-Phase-Earthing (FPE)

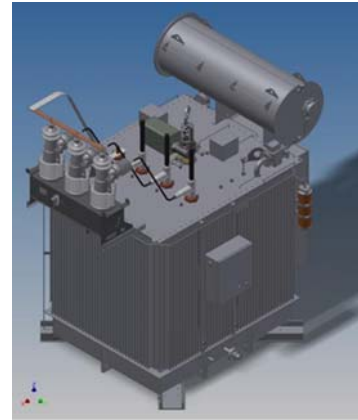


Fig. 19 Combination of Petersen-Coil with ZN-Transformer and Faulty-Phase-Earthing

## 6 Summary

Due to the new relays and the new classification of earthfaults:

- Earth-fault in the cable section => restriking
  - Earth-fault in the OHL section => quasi-stationary
- a different handling of the fault situation can be initiated.

If the fault is in the range of the OHL, the well-known advantages of the Petersen-Coil can be used.

If the fault occurs in the cable-section, the fault can be moved from the faulty cable-section to the substation by using the Faulty-Phase-Earthing (FPE) device. Due to the nonlinearity and the high restriking voltage of the cable-fault, there will be no restriking and therefore no fault-current via the original fault-location.

The FPE ideally complements the advantages of the Petersen-Coil in OHL lines in cases of earthfaults in cable sections.

In addition, using the FPE a tuning of the Petersen-Coil also during the earthfault is possible.

## 7 References

- [1] Druml G., 2013, *Innovative Methoden zur Erdschlussortung und Petersen-Spulen Regelung*, Thesis at the Institute of Electrical Power System in Graz, Austria
- [2] Druml G., Seifert O., Marketz M., 2011, "*Directional Detection of Restriking Earthfaults in Compensated Networks*", *Proceedings CIREN 2011 conference*, paper 612
- [3] Druml G., Seifert O., Zickler U., Roser M., Fickert L., 2011, "*Auswertung von nichtlinearen Erdschlüssen*", *Proceedings ETG Fachtagung STE 2011 Erfurt*, ETG-Fachbericht 129, VDE-Verlag GmbH, Berlin Offenbach, 2011
- [4] Herold G., 2002, *Elektrische Energieversorgung I*, J. Schlembach Fachverlag, Weil der Stadt, Germany
- [5] Herold G., 2002, *Elektrische Energieversorgung II*, J. Schlembach Fachverlag, Weil der Stadt, Germany
- [6] Herold G., 2002, *Elektrische Energieversorgung III*, J. Schlembach Fachverlag, Weil der Stadt, Germany
- [7] Melzer H.: 2012, "*Die aktuelle Situation der Sternpunktbehandlung in Netzen bis 110 kV (D-A-CH)*", *ETG-Fachbericht 132*, VDE Verlag GmbH, Berlin Offenbach, 2012
- [8] Tengg Ch., Schoass K., Druml G., Schmaranz R., Marketz M., Fickert L., 2013, "*Evaluation of new earth fault localization methods by earth fault experiments*", *CIREN Stockholm 2013*, paper 1317
- [9] VDEW, 1997, *Kabelhandbuch*, VDEW-Verlag, Frankfurt, Germany
- [10] Kovács K.P., Raács I., 1959, *Transiente Vorgänge in Wechselstrommaschinen*, Band 1, Verlag der ungarischen Akademie der Wissenschaften Budapest
- [11] Clarke Edith, 1950: *Circuit Analysis of A-C Power Systems*, Volume 1, 4.Aufl, John Wiley & Sons, Inc
- [12] Druml G., Seifert O., 2010, "*Gerichtete Erkennung von wiederzündenden Erdschlüssen in gelöschten Netzen*", Schutz- und Leittechnik Tutorial, VDE
- [13] Druml G., 2013, "*Innovative Methoden zur Erdschlussortung und Petersen-Spulen Regelung*", Thesis at the Institute of Electrical Power System in Graz, Austria



# Optimization-based formulations of absorbing boundary conditions in discrete-time wave propagation problems

Alexander Schirrer<sup>a</sup>

Stefan Jakubek<sup>a</sup>

This contribution discusses two optimization-based methods to generate practical and efficient absorbing boundaries for discrete-time wave propagation problems. Absorbing boundary formulations are desirable when problems given on large or infinite domains should only be studied locally at confined regions of interest, such as the near-field solution in acoustic problems or local interaction effects near contact points in catenaries or cable dynamics. We consider time-discrete approximations of the solution represented by explicit time-marching schemes.

One proposed method generates absorbing boundary conditions by direct optimization of the coefficients of the boundary stencil in a finite-difference discretization, such that the reflection coefficient is optimized [6]. Stability criteria are considered to obtain optimal and stable boundary conditions. The second proposed method shown is inspired by the “perfectly matched layer” (PML). The PML’s absorption properties are emulated by a suitable optimal boundary control law [5]. High absorption performance even on badly conditioned discretization grids is achieved with high computational efficiency. Additionally, it allows the controlled modification of impedance in the boundary region, which is not realizable with other concepts such as traditional absorbing boundary conditions.

The proposed methods are widely applicable for linear system dynamics having wave propagation and lead to simple and computationally efficient model structures with the desired absorbing properties. These features are crucial in problems with real-time requirements, e.g. when creating design models of online model predictive control. One current industrial application for these models are real-time control tasks related to railway pantograph/catenary interaction.

## 1 Introduction

Many engineering problems show low-damped distributed-parameter dynamics with wave propagation effects (“wave-like problems”), such as pressure waves in fluids or oscillations in tensioned strings or railway catenary systems. These problems may be posed on very large (essentially unbounded) domains in reality and need to be solved, however, on limited discretization domains of interest. Truncating the computational domain and installing trivial (e.g., clamped) boundary conditions is problematic in combination with low damping

---

<sup>a</sup>Institute of Mechanics and Mechatronics, Workgroup of Control and Process Automation, Technische Universität Wien, Getreidemarkt 9, 1060 Vienna, E-Mail: [alexander.schirrer@tuwien.ac.at](mailto:alexander.schirrer@tuwien.ac.at), [stefan.jakubek@tuwien.ac.at](mailto:stefan.jakubek@tuwien.ac.at)

and wave propagation: the artificial boundary conditions generate spurious reflections of waves back into the domain of interest – hence, the numerical solution becomes corrupted. Introducing “absorbing” boundary conditions or suitable dissipative layers reduces or eliminates these spurious reflections, however they may not be easily found or computed for complicated PDEs. A historic overview on developments in absorbing boundary conditions and the method of “perfectly matched layers” (PMLs) is given in [2]. Absorbing boundary conditions for various continuous as well as discretized forms of wave equations have been derived analytically, e.g. [3, 4]. A PML formulation for an Euler-Bernoulli bending beam with elastic support has been derived for a finite-element discretization in [1]. These results, however, are highly specific to the considered problem and may be computationally expensive. In this contribution, two optimization-based methods to construct absorbing boundary conditions [6] or controlled boundary layers [5] are presented which are generic in the sense that they essentially only require knowing the underlying so-called dispersion relation.

As an underlying motivation leading to the development of these methods we consider the dynamics of railway catenaries (schematically depicted in Fig. 1 (left)).

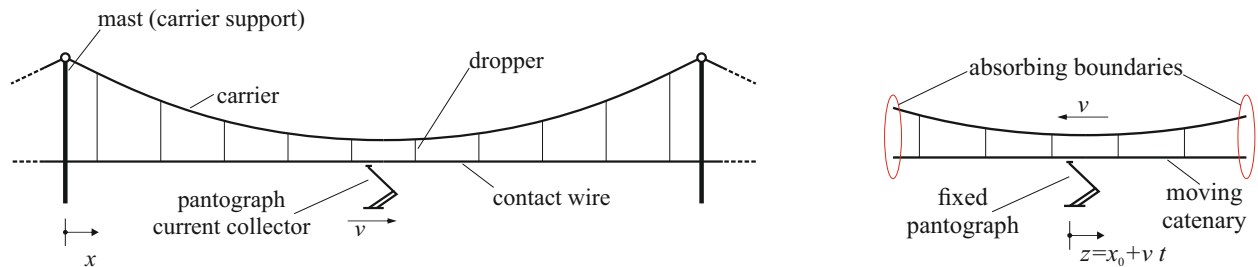


Figure 1: Left: Schematic setup of a railway catenary (1 span shown); Right: catenary model in train-fixed coordinates where absorbing boundaries are needed

The dominant dynamics therein shows wave propagation along the carrier and contact wire, low damping, and physically correct partial wave reflections at the attachment points of the droppers (which is formulated as a one-sided elastic constraint and point masses at the attachment points). In time-critical applications, such as real-time model-based control of the pantograph or real-time catenary emulation in a pantograph hardware-in-the-loop test rig, the catenary model size needs to be kept small. One promising formulation is based on moving coordinates (i.e., pantograph-fixed coordinates)  $(z, t)$  instead of  $(x, t)$  with  $z = x + vt$  for constant train velocity  $v$ . Then, only a short catenary segment around the pantograph needs to be discretized, but absorbing boundary conditions need to be implemented (see Fig. 1 (right)).

This paper is organized as follows: Section 2 outlines the significance of the dispersion relation in linear wave-like partial differential equations and summarizes the Finite Difference (FD) method. The optimization based methods to obtain absorbing boundary conditions by direct stencil optimization (summarized from [6]) and the PML-inspired approach of a controlled boundary layer (summarized from [5]) are given in Sec. 3. Then, typical results on the Euler-Bernoulli bending beam equation under axial load are shown in Sec. 4. A discussion concludes the paper in Sec. 5.

## 2 Fundamentals

### 2.1 Basic example: linear one-dimensional wave equation

When considering the second-order linear one-dimensional wave equation

$$\frac{\partial^2 w}{\partial t^2} - c^2 \frac{\partial^2 w}{\partial x^2} = 0 \quad (1)$$

with the solution  $w(x, t)$  in space  $x \in \mathbb{R}$  and time  $t \in \mathbb{R}^+ \cup \{0\}$ , note that the differential operator can be factorized:

$$\frac{\partial^2 w}{\partial t^2} - c^2 \frac{\partial^2 w}{\partial x^2} = 0 \rightarrow \left( \frac{\partial}{\partial t} - c \frac{\partial}{\partial x} \right) \left( \frac{\partial}{\partial t} + c \frac{\partial}{\partial x} \right) w = 0 \quad (2)$$

By inspection, two associated transport equations can be identified as suitable one-sided boundary conditions for the restricted spatial domain  $x \in [0, L]$ :

$$\frac{\partial w}{\partial t}(0, t) = c \frac{\partial w}{\partial x}(0, t), \quad \frac{\partial w}{\partial t}(L, t) = -c \frac{\partial w}{\partial x}(L, t) \quad (3)$$

for which the corresponding outgoing solution components of the wave equation are a solution.

### 2.2 Harmonic modes and the dispersion relation

For linear constant-coefficient PDEs, fundamental solutions can be formulated by a complex exponential form. Here, the term “harmonic wave solution” will be used, referring to purely oscillatory waves of the form

$$w(x, t) = \exp(i\omega_x x) \exp(i\omega_t t), \quad (4)$$

where  $\omega_x, \omega_t \in \mathbb{R}$ . Inserting (4) into the original wave equation (1), the temporal frequency  $\omega_t$  and the spatial frequency (wave number)  $\omega_x$  have to fulfill the following *dispersion relation*:

$$\omega_t^2 - c^2 \omega_x^2 = 0 \rightarrow \omega_t = \pm c \omega_x \quad (5)$$

This relationship is illustrated in Fig. 2.

As a generalizing idea, it turns out to be beneficial to use a PDE’s dispersion relation, which can be retrieved with little effort, when devising boundary conditions with absorbing properties.

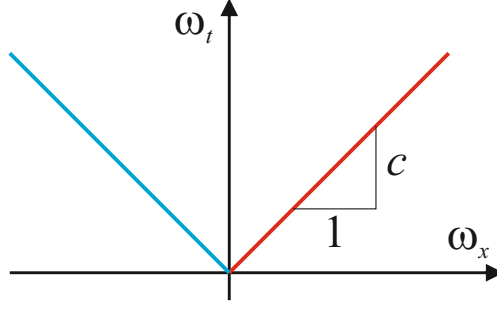


Figure 2: Dispersion relation of the linear scalar wave equation

### 2.3 Finite-Difference approximation

To numerically solve PDEs, finite-dimensional approximations (discretizations) are formulated, for example via the Finite Difference (FD) or the Finite Element (FE) method. Here, we will demonstrate the proposed methods applied to FD discretizations.

To apply the FD approximation to the wave equation (1), the approximated solution is considered point-wise on an (equidistant) grid in space and time:

$$w(k\Delta x, n\Delta t) = w_k^n$$

where  $n, k \in \mathbb{N} \cup \{0\}$ ,  $0 \leq k\Delta x \leq L$ ,  $n \geq 0$  and  $\Delta x$  and  $\Delta t$  are the spatial and temporal step sizes, respectively.

By substituting the PDE's partial derivatives with approximations by central difference quotients, for example

$$\frac{\partial^2 w}{\partial t^2}(x_k, t_n) \approx \frac{w_k^{n-1} - 2w_k^n + w_k^{n+1}}{\Delta t^2},$$

a set of time- and space-discrete evolution equations are obtained:

$$w_k^{n+1} = 2w_k^n - w_k^{n-1} + c^2 \frac{\Delta t^2}{\Delta x^2} (w_{k-1}^n - 2w_k^n + w_{k+1}^n)$$

Similar to the PDE's dispersion relation, an analogue relation can be obtained for the discretized problem by inserting the discrete harmonic wave solution

$$w_k^n = \exp(ik\omega_x\Delta x) \exp(in\omega_t\Delta t)$$

into the FD scheme, yielding the relation between the normalized grid frequencies  $\omega_t\Delta t$  and  $\omega_x\Delta x$ .

## 2.4 Euler-Bernoulli bending beam equation under axial load

The dynamic vertical displacement of railway catenaries can be modeled well by the Euler-Bernoulli bending beam (EBB) equations under axial load for both, carrier cable and contact wire, coupled via stiff or elastic droppers. The underlying EBB equation reads:

$$\rho A \ddot{w} + \beta \dot{w} = -EI w'''' + T w'' + f \quad (6)$$

where  $w = w(x, t)$  is the vertical wire displacement at time  $t \geq 0, t \in \mathbb{R}$  and longitudinal coordinate  $x \in [0, L] \subset \mathbb{R}$ ,  $f = f(x, t)$  is the vertical force density field including gravity forces, dropper coupling forces, and pantograph contact forces. The partial derivatives are denoted  $(\dot{\cdot}) = \frac{\partial}{\partial t}$  and  $(\cdot)' = \frac{\partial}{\partial x}$ . The constant parameters  $\rho A$ ,  $\beta$ ,  $EI$ , and  $T$  are the specific mass per unit length, the viscous damping coefficient, the bending stiffness and the axial tensile force, respectively.

Approximation via finite differences is considered here. With an equidistant grid in time and space, the displacement solution field is approximated at the grid points  $w_k^n \approx w(x_k, t_n)$  with  $x_k = k\Delta x$  and  $t_n = n\Delta t$ . Utilizing central differences to approximate the partial derivatives leads to an explicit evolution scheme:

$$w_k^{n+1} = {}_0\mu_2 w_{k-2}^n + {}_0\mu_1 w_{k-1}^n + {}_0\mu_0 w_k^n + {}_{-1}\mu_0 w_k^{n-1} + \nu f_k^n \quad (7)$$

As this scheme only defines the behavior of the domain interior, formulas for  $w_0^n, w_1^n$  (as well as the corresponding values at the right boundary) need to be specified to realize appropriate boundary conditions.

Transforming the beam PDE (6) to the moving coordinates  $(z, t)$  with  $z = x + vt$ , mixed derivatives up to second order appear, which results for the undamped case  $\beta = 0$  in

$$\rho A \ddot{w} = -EI w'''' + (T - \rho A v^2) w'' + 2v \rho A \dot{w}' + f \quad (8)$$

where  $(\dot{\cdot})' = \frac{\partial}{\partial z}$ . Using central finite differences to approximate the mixed derivatives, the evolution scheme is no longer explicit, but an implicit scheme is obtained:

$$\sum_{j=-2}^2 {}_1\bar{\mu}_j w_{k+j}^{n+1} = \sum_{l=-1}^0 \sum_{j=-2}^2 {}_l\bar{\mu}_j w_{k-j}^{n+l} + \bar{\nu} f_k^n \quad (9)$$

Here, the resulting FD scheme's stencil coefficients are denoted  $\mu, \bar{\mu}, \nu, \bar{\nu}$ .

## 3 Methodology

### 3.1 Direct Optimization of Absorbing Boundary Stencil Coefficients

To achieve absorbing boundary behavior in an FD-discretized system, suitable boundary stencils (see Fig. 3) need to be found. In the first formulation, the stencil coefficients are

directly considered decision variables of an optimization problem, and the objective is to maximize boundary absorption accuracy. The main steps of this optimization-based ABC construction are:

- Step 1: Formulate finite-difference approximation** of the problem interior domain as outlined in Sec. 2.3.
- Step 2: Precompute dispersion relation** of the discretized problem, see Sec. 2.3.
- Step 3: Choose ABC stencil shape** (i.e., define the parameters  $N_{t,ABC}$ ,  $N_{x,ABC}$  as defined in Fig. 3).

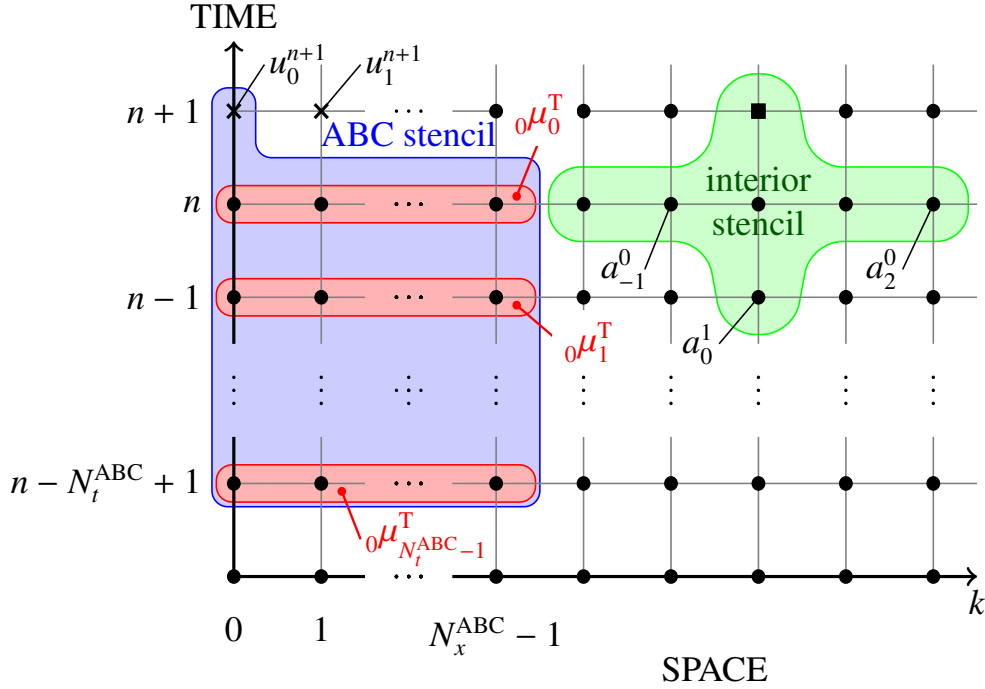


Figure 3: Generic form of an explicit boundary condition stencil for  $k = 0$  (left) and an explicit interior stencil (right), taken from [6].

The stencil coefficients are collected into the decision variable vector  $\mathbf{p}$ .

- Step 4: Select and configure optimization objectives.** Suitable objective function(s) and constraints are formulated:

**Accuracy objective** is formulated by means of the *reflection coefficient*, which describes the ratio of outgoing and incoming harmonic wave amplitudes

**Stability objective/condition** evaluates the largest magnitude of the eigenvalues of an FD test system with ABCs in place. Eigenvalues outside the unit circle indicate instability and are not admissible or need to be penalized in a multi-objective optimization formulation.

**Step 5: Formulate and solve optimization problem.** The optimization problem can now be formulated either as single-objective problem,

$$\begin{aligned} \min_{\mathbf{p}} \quad & J_{\text{accuracy}}(\mathbf{p}) \\ \text{subject to} \quad & \rho(\mathbf{A}) < 1, \end{aligned}$$

or as multi-objective problem,

$$\begin{aligned} \min_{\mathbf{p}} \quad & \mathbf{J}(\mathbf{p}), \mathbf{J} : \mathbb{R}^{N_p} \rightarrow \mathbb{R}^2 \\ \mathbf{J} = \quad & \begin{bmatrix} J_{\text{accuracy}}(\mathbf{p}) \\ J_{\text{stability}}(\mathbf{p}) \end{bmatrix} \end{aligned}$$

to study stability margin/accuracy trade-off sensitivity. Thereby,

$$J_{\text{accuracy}}(\mathbf{p}) = \sum_{k=0}^{N_{\text{ABC}}-1} \int_0^{\frac{\pi}{\Delta x}} \gamma(\omega_x) |R_k(\omega_x, \mathbf{p})| d\omega_x$$

is the accuracy error cost where  $R_k$  denotes the reflection coefficient and  $\gamma$  is a non-negative frequency weighting function, and

$$J_{\text{stability}}(\mathbf{p}) = \rho(\mathbf{A}) = \max_i \lambda_i(\mathbf{A}) < 1$$

is the stability condition formulated as second cost function.

The reflection error can be computed using the dispersion relation and the boundary stencil coefficients and turns out to be an effective cost formulation (see [6]).

The single-objective optimization problem can be efficiently solved by standard numeric optimization tools as the number of decision variables is reasonably low. In the multi-objective case, dedicated multi-objective optimization codes (such as multi-objective genetic algorithms) have been applied successfully.

### 3.2 Perfectly-Matched-Layer-based Boundary Layer via Control

The second proposed method is inspired by the behavior of the so-called “perfectly matched layer” (PML): the computation domain is being surrounded by absorbing or dissipative layers at the boundaries, see Fig. 4.

The damping properties of these additional layers are selected to produce optimal absorption properties. State-of-the-art PML formulations rely on several involved extensions to the problem formulation (complex coordinate stretching as sketched in Fig. 5, and auxiliary field variables). This increases mathematical and computational complexity significantly, especially for higher-order PDEs such as the Euler-Bernoulli beam equation.

The present approach takes a different path: the boundary layer is being controlled by a suitable optimal control law that minimizes absorption error with respect to a reference solution.

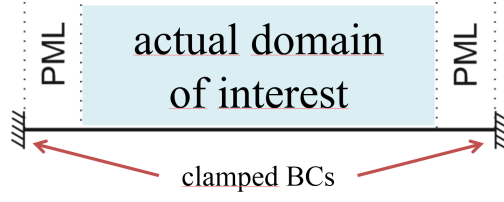


Figure 4: The actual computational domain contains the domain of interest and additional boundary layers

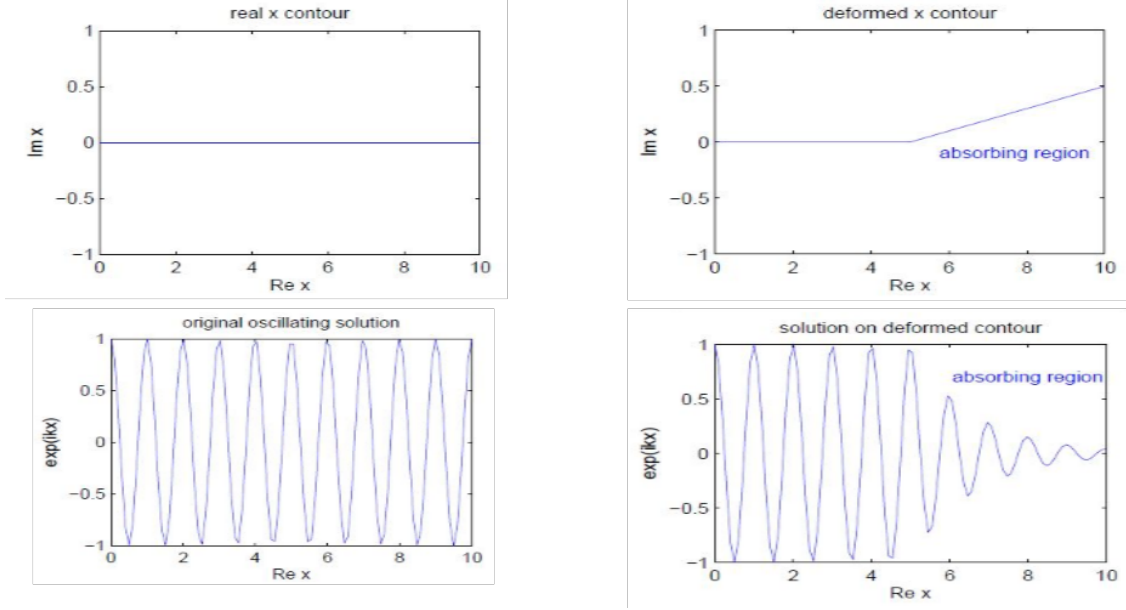


Figure 5: Choosing a continuous damping profile (top) leads to a smooth attenuation of modes across the boundary layer (bottom).

### 3.2.1 Quasi-PML as Predictive Control Problem: Concept

Consider the discretized dynamics of the system (interior domain and boundary layer(s)) as depicted in Fig. 6 given in a state space representation

$$\mathbf{x}^{n+1} = \mathbf{A}\mathbf{x}^n + \mathbf{B}u^n \quad (10)$$

$$\mathbf{w}^n = \mathbf{C}\mathbf{x}^n, \quad (11)$$

define the finite-horizon quadratic cost function

$$J = (\mathbf{Y}_{\text{ref}} - \mathbf{Y})^T (\mathbf{Y}_{\text{ref}} - \mathbf{Y}) + \mathbf{U}^T \mathbf{R} \mathbf{U} \quad (12)$$

with

$$\mathbf{Y} = \mathbf{F}\mathbf{x}^n + \Phi \mathbf{U} \quad (13)$$



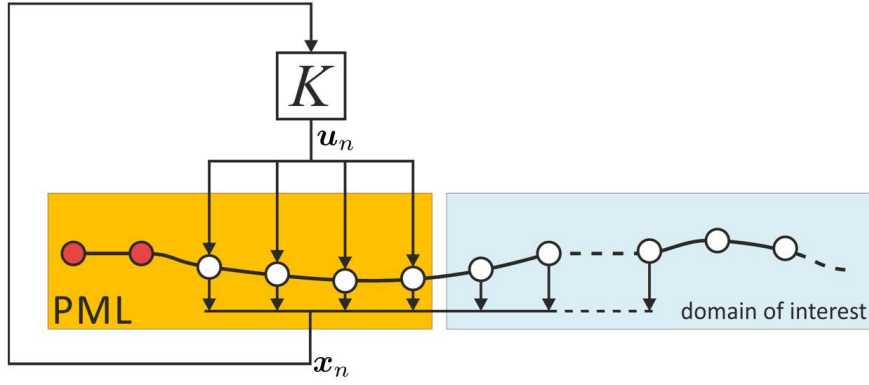


Figure 6: Schematics of controlled boundary layer system

$$\mathbf{Y} = \begin{bmatrix} \mathbf{w}^{n+1} \\ \mathbf{w}^{n+2} \\ \vdots \\ \mathbf{w}^{n+N_p} \end{bmatrix}, \mathbf{U} = \begin{bmatrix} \mathbf{u}^n \\ \mathbf{u}^{n+1} \\ \vdots \\ \mathbf{u}^{n+N_p-1} \end{bmatrix}, \mathbf{F} = \begin{bmatrix} \mathbf{CA} \\ \mathbf{CA}^2 \\ \vdots \\ \mathbf{CA}^{N_p} \end{bmatrix}, \quad (14)$$

$$\Phi = \begin{bmatrix} \mathbf{CB} & \mathbf{0} & \mathbf{0} & \dots & \mathbf{0} \\ \mathbf{CAB} & \mathbf{CB} & \mathbf{0} & \dots & \mathbf{0} \\ \mathbf{CA}^2\mathbf{B} & \mathbf{CAB} & \mathbf{CB} & \dots & \mathbf{0} \\ \vdots & & & & \vdots \\ \mathbf{CA}^{N_p-1}\mathbf{B} & \mathbf{CA}^{N_p-2}\mathbf{B} & \mathbf{CA}^{N_p-3}\mathbf{B} & \dots & \mathbf{CB} \end{bmatrix} \quad (15)$$

The optimal control sequence is then found as

$$\mathbf{U}^* = (\Phi^T \Phi + \mathbf{R})^{-1} \Phi^T (\mathbf{Y}_{\text{ref}} - \mathbf{F}\mathbf{x}^n). \quad (16)$$

Note: In this particular case all states  $\mathbf{x}^n$  can be measured but the “desired” reference signal  $\mathbf{Y}_{\text{ref}}$  is unknown.

It remains to formulate and compute  $\mathbf{Y}_{\text{ref}}$  such that the boundary layer behaves like the unbounded domain solution and thus fulfills the dispersion relation.

This can be done in a mode-wise manner: each harmonic wave mode, defined via its frequency pair  $(\omega_t, \omega_x)$  can be predicted parametrically. The key issue now is to express the current state  $\mathbf{x}^n$  in terms of modal coordinates and construct  $\mathbf{Y}_{\text{ref}}$  by the superposition of the modal predictions.

The simple prediction per mode (index  $s$ ) reads:

$$w_{k,s}^n = G_{1,s}^n \cos(k\omega_{x,s}\Delta x) + G_{2,s}^n \sin(k\omega_{x,s}\Delta x) \quad (17)$$

where

$$\mathbf{w}_{n+N,s} = \underbrace{\begin{bmatrix} \cos(\omega_{x,s}\Delta x + N\omega_{t,s}\Delta t) & \sin(\omega_{x,s}\Delta x + N\omega_{t,s}\Delta t) \\ \cos(2\omega_{x,s}\Delta x + N\omega_{t,s}\Delta t) & \sin(2\omega_{x,s}\Delta x + N\omega_{t,s}\Delta t) \\ \vdots & \vdots \\ \cos(K\omega_{x,s}\Delta x + N\omega_{t,s}\Delta t) & \sin(K\omega_{x,s}\Delta x + N\omega_{t,s}\Delta t) \end{bmatrix}}_{\mathbf{T}_s^N} \underbrace{\begin{bmatrix} G_{1,s}^n \\ G_{2,s}^n \end{bmatrix}}_{\mathbf{g}_{n,s}} \quad (18)$$

Thereby,  $(K+1)\Delta x = L$ ,  $N$  is the prediction offset, the mode prediction map  $\mathbf{T}_s^N$  is defined a priori, and  $\mathbf{g}_{n,s}$  collects the real-valued modal coordinates of mode  $s$  at time step  $n$ .

The modal mapping (modal coordinates to node displacements) for a single mode  $s$  is denoted as

$$\mathbf{w}_s^n = \begin{bmatrix} \cos(\omega_{x,s}\Delta x) & \sin(\omega_{x,s}\Delta x) \\ \cos(2\omega_{x,s}\Delta x) & \sin(2\omega_{x,s}\Delta x) \\ \vdots & \vdots \\ \cos(N\omega_{x,s}\Delta x) & \sin(N\omega_{x,s}\Delta x) \end{bmatrix} \begin{bmatrix} G_{1,s}^n \\ G_{2,s}^n \end{bmatrix} = \mathbf{L}_s \mathbf{g}_s^n, \quad (19)$$

and aggregating over the set of considered modes  $s = 1, \dots, \Omega$  yields

$$\mathbf{w}^n = \sum_{s=1}^{\Omega} \mathbf{L}_s \mathbf{g}_s^n \quad (20)$$

$$= \begin{bmatrix} \mathbf{L}_1 & \mathbf{L}_2 & \dots & \mathbf{L}_{\Omega} \end{bmatrix} \begin{bmatrix} \mathbf{g}_1^n \\ \mathbf{g}_2^n \\ \vdots \\ \mathbf{g}_{\Omega}^n \end{bmatrix} = \mathbf{L} \mathbf{g}^n. \quad (21)$$

Finally, the entire reference trajectory is expressed in the current modal coordinates,

$$\mathbf{Y}_{\text{ref}} = \mathbf{T} \mathbf{g}^n, \quad (22)$$

and the current modal coordinates are retrieved by a least-squares mapping from the current states (nodal displacements):

$$\begin{bmatrix} \mathbf{g}^n \\ \mathbf{g}^{n-1} \end{bmatrix} = \underbrace{\left( \begin{bmatrix} \mathbf{L} & \mathbf{0} \\ \mathbf{0} & \mathbf{L} \end{bmatrix}^T \begin{bmatrix} \mathbf{L} & \mathbf{0} \\ \mathbf{0} & \mathbf{L} \end{bmatrix} + \alpha \mathbf{I} \right)^{-1} \begin{bmatrix} \mathbf{L} & \mathbf{0} \\ \mathbf{0} & \mathbf{L} \end{bmatrix}}_{\mathbf{K}_{\text{mapping}}} \mathbf{x}^n. \quad (23)$$

Combining equations (16) and (23) results in a constant state vector feedback gain that optimizes boundary layer absorption:

$$\mathbf{u}^n = \mathbf{K} \mathbf{x}^n. \quad (24)$$

## 4 Numerical Results

Exemplary results for both proposed methods are shown in the following for the non-moving beam equation under axial load: both methods achieve high absorption quality without significantly increasing computational effort of the system equations. The beam's physical parameters are set to typical values of a contact wire in a high-speed railway catenary.

### 4.1 Direct ABC stencil coefficient optimization

As detailed in [6], Fig. 7 shows several time snapshots of the successful absorption of outgoing wave components in the truncated beam (bottom plots) in comparison to a significantly extended reference domain's solution (top plots). The ABC is installed at  $x = 0$  m in the truncated domain, while a clamped BC is formulated at  $x = 100$  m.

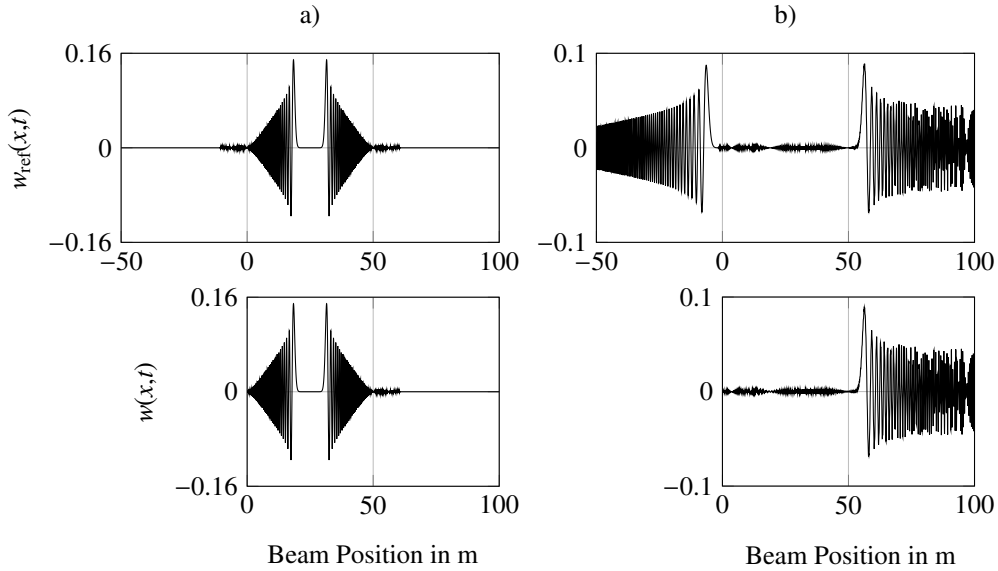


Figure 7: Typical results for an ABC-bounded beam (adopted from [6]): initial perturbation centered at  $x = 25$  m (not shown) propagates in both directions and is being absorbed by the boundary at  $x = 0$  m. Lower plots show the ABC-bounded, small domain ( $x = 0..100$  m), whereas the upper plots show the reference solution on a beam extended far to the left (shown:  $x = -50..100$  m).

### 4.2 Controlled absorbing boundary layer

Figure 8 shows the high accuracy of the controlled boundary layer absorption for low and high frequencies. The control law (24) has been found as outlined in Sec. 3.2. For detailed results the reader is referred to Ref. [5].

Numeric studies show that the controlled boundary layer provides consistent high absorption accuracy for various choices of time-/space-gridding and physical parameters of the EBB

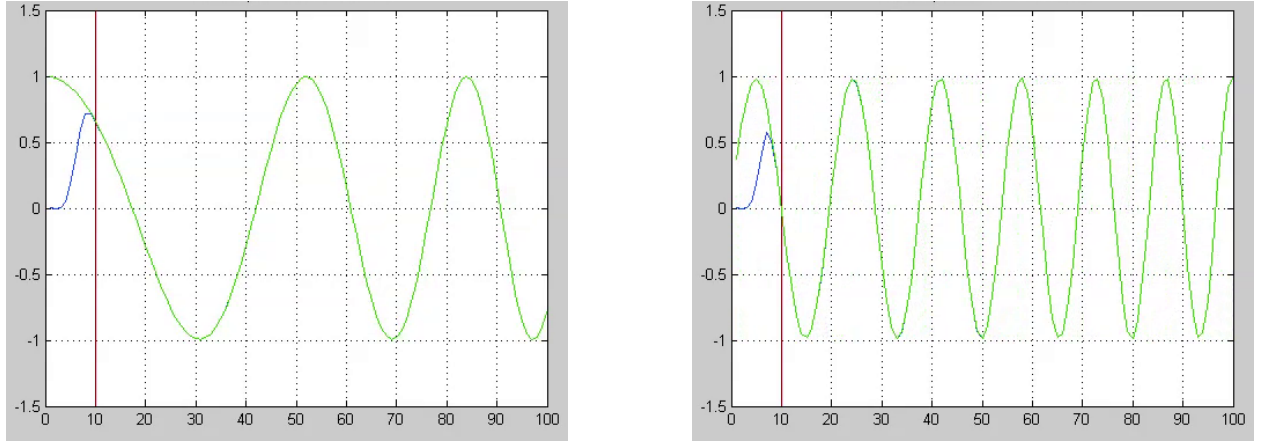


Figure 8: Controlled boundary layer absorbs low (left plot) and high (right plot) frequencies in a beam model excited by a sine sweep on the right boundary (waves travel leftwards).

equation. In the moving-coordinate case, this method is observed to stand out in the sense that unlike other methods (analytic ABCs, optimization-based ABCs as in Sec. 3.1) it reliably produces satisfying absorption results, while providing for an efficient implementation.

Finally, the finite-width boundary layer allows for great flexibility in system modeling: approaching droppers in a moving catenary description, for example, can be modeled already when entering the boundary layer (but when still outside the “domain of interest”), resulting in a regularized, realistic behavior.

## 5 Discussion & Conclusions

Absorbing boundary formulations have been presented which allow the use of small, efficient computational domains for wave-like PDEs. The key feature of these methods is that they essentially only rely on the dispersion relation of the underlying equation and can thus be generically applied to various wave problems. The first proposed method formulates an optimization problem directly in the boundary stencil coefficients as decision variables, whereas the second method follows the ideas of the well-known “perfectly matched layer” technique, but achieves the boundary layer’s absorption properties through an appropriate optimal control law. Both methods produce highly computationally efficient formulations of absorbing boundary behavior, and satisfying accuracy in the absorption task is attained. The methods are specifically useful if analytic solutions are not available or too expensive to be computed. One prominent case is the numerically difficult Euler-Bernoulli bending beam equation under axial load in moving coordinates, which is successfully treated only by the boundary control approach. One possible explanation for this observation is that detrimental grid conditioning always occurs at the incoming side in the moving-coordinate case – the broad boundary layer seems to be significantly more robust to bad grid conditioning, whereas the ABC (with smaller support and region of influence) suffers significant performance loss.

## References

- [1] ARBABI, F. FARZANIAN, M.S.: *Propagation of waves in infinite beams: PML approach*. Proceedings: 11th World Congress on Computational Mechanics, 2014.
- [2] BÉRENGER, J.-P.: *A Historical Review of the Absorbing Boundary Conditions for Electromagnetics (2015)*. Forum for Electromagnetic Research Methods and Application Technologies, 9(6), 2015.
- [3] HIGDON, R.L.: *Absorbing boundary conditions for difference approximations to the multidimensional wave equation*. Mathematics of computation, 47(176):437–459, 1986.
- [4] HIGDON, R.L.: *Numerical absorbing boundary conditions for the wave equation*. Mathematics of computation, 49(179):65–90, 1987.
- [5] RITZBERGER, D., A. SCHIRRER and S. JAKUBEK: *Emulating the properties of a perfectly matched layer with an optimal feedback controller*. -, 2015. to be submitted.
- [6] SCHIRRER, A., E. TALIC, G. ASCHAUER, M. KOZEK and S. JAKUBEK: *Determination of highly absorbing boundary conditions for linear finite difference schemes by multi-objective optimization*. Journal of Sound and Vibration, 2015. submitted, under review.

## **Philon von Byzanz und seine Druckwerke über pneumatisch-hydraulische Regelsysteme**

**Prof. Emeritus Dimitrios Kalligeropoulos<sup>1</sup>    Application Prof. Soultana Vasileiadou<sup>2</sup>**

Philon von Byzanz lebte in dritten Jahrhundert v. Chr. in Alexandria und lehrte an ihrem berühmten Museum. Er schrieb das bedeutendste technische Handbuch der hellenistischen Antike, die sogenannte «*Μηχανική Σύνταξις – Systematische Abhandlung der Mechanik*», die neun Bücher beinhaltete. Die sechs ersten von ihnen sind Lehrbücher.

Darunter sind: – Die «*Pneumatik – Πνευματικά*», das einzige Buch Philons, das in Fragmenten gerettet wurde und das Kapitel über die Theorie der Gase und die Konstruktion der pneumatischen und hydraulischen Maschinen beinhaltet.

Des Weiteren: – Die «*Konstruktion der Automaten – Αυτοματοποιητική*», die besonders die Kunst der automatischen Theater abhandelte.

Im Weiteren, werden wir uns mit drei Beispielen aus Philons *Pneumatik* befassen.

### **Beispiel 1.    Beweis der Körperlichkeit der Luft**

Die Luft ist eine unsichtbare und nicht greifbare Materie. Dass sie Philon für die Bewegung und die Regelung seiner Automaten zu benutzen konnte, musste er zuerst ihre Existenz, d.h. ihre materielle Substanz beweisen. Und er beweist sie, indem er ein Gefäß umdreht, seine Mündung ins Wasser eintaucht und es tief in das Wasser drückt.

*“Zieht man es nun allmählich heraus, so wird man finden, dass es im Inneren trocken ist und an keiner Stelle, mit Ausnahme der äußeren Mündung, nass geworden ist. Daraus ergibt sich also die Körperlichkeit der Luft., [2, II]*

---

<sup>1</sup> Piraeus University of Applied Sciences, Department of Automation Engineering, Petrou Ralli & Thivon 250, 12244 Athens, Greece, E-mail: [dkal@teipir.gr](mailto:dkal@teipir.gr)

<sup>2</sup> Piraeus University of Applied Sciences, Department of Automation Engineering, Petrou Ralli & Thivon 250, 12244 Athens, Greece, E-mail: [svasil@teipir.gr](mailto:svasil@teipir.gr)

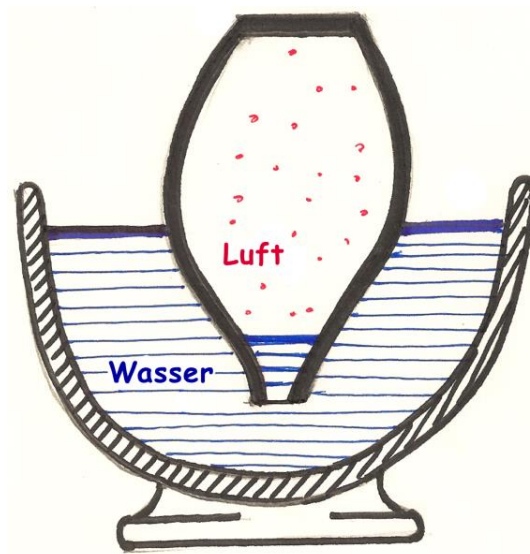


**Bild 1.** Beweis der Körperlichkeit der Luft, nach Philon

## **Beispiel 2. Die Regelung eines Wasserspiegels mittels der Luft**

Nachdem Philon die Materialität der Luft experimentell bestätigt hat, kann er sie jetzt dazu benutzen, um pneumatisch-hydraulische Regelungssysteme, d.h. geschlossene Regelkreise mit Rückkopplung, zu entwerfen.

Charakteristisch ist das Beispiel der Regelung eines Wasserstandes mittels der Luft.

Dieser Mechanismus enthält "...ein Gefäß  $\alpha\beta$  mit einem Loch  $\delta$  auf seinem Boden. Durch das Loch geht senkrecht eine oben umgebogene Röhre  $\varepsilon\delta\gamma$ . Ihr Ende  $\gamma$  geht zu einem anderen Gefäß  $\gamma\zeta\eta$ , welches unten in  $\tau$  durchbohrt ist. Die zwei Gefäße stehen untereinander in Verbindung mittels der zwei dünnen gekrümmten Röhren  $\varepsilon\delta\gamma$  und  $\rho\pi$ . Das Gefäß  $\alpha\beta$  steht höher als das Gefäß  $\zeta\eta$ , das auf einer hohlen Basis  $\mu\nu$  angepasst ist und mit ihr mittels der Öffnung  $\tau$  in Verbindung steht.

Wenn wir nun das Gefäß  $\alpha\beta$  mit Wasser bis zu einer gewissen Höhe, kleiner als  $\delta\varepsilon$ , auffüllen und die obere Öffnung des Gefäßes dicht mit dem Deckel  $\chi\psi$  verschließen, so wird das Wasser aufhören durch das Rohr  $\rho\pi$  ins Gefäß  $\zeta\eta$  zu fließen, bis die hohle Basis  $\mu\nu$  mit Wasser gefüllt ist.

So wird allmählich der Wasserstand in der Basis sich noch mehr erhöhen, die Öffnung  $\tau$  übersteigen und somit die Öffnung  $\gamma$  des Rohres  $\gamma\delta\epsilon$  mit Wasser verschließen.

Und so wird auch keine Luft mehr ins Gefäß  $\alpha\beta$  eindringen können, das Wasser wird aufhören durch das Rohr  $\rho\pi$  zu fließen und solange die Öffnung  $\gamma$  geschlossen bleibt wird auch der Wasserspiegel im Gefäß  $\zeta\eta$  konstant bleiben.

Wenn wir jedoch Wasser aus der Basis  $\mu\nu$  durch die Öffnung  $\kappa$  entnehmen und somit der Wasserpegel ins Gefäß  $\zeta\eta$  sinkt und die Öffnung  $\gamma$  öffnet, so wird Luft ins Gefäß  $\alpha\beta$  eindringen und Wasser durch das Rohr  $\rho\pi$  ins Gefäß  $\zeta\eta$  einfließen. Der Wasserstand wird somit in seinem ursprünglichen Niveau zurückgeführt und in derselben Höhe immer konstant bleiben.,, [2, XII]

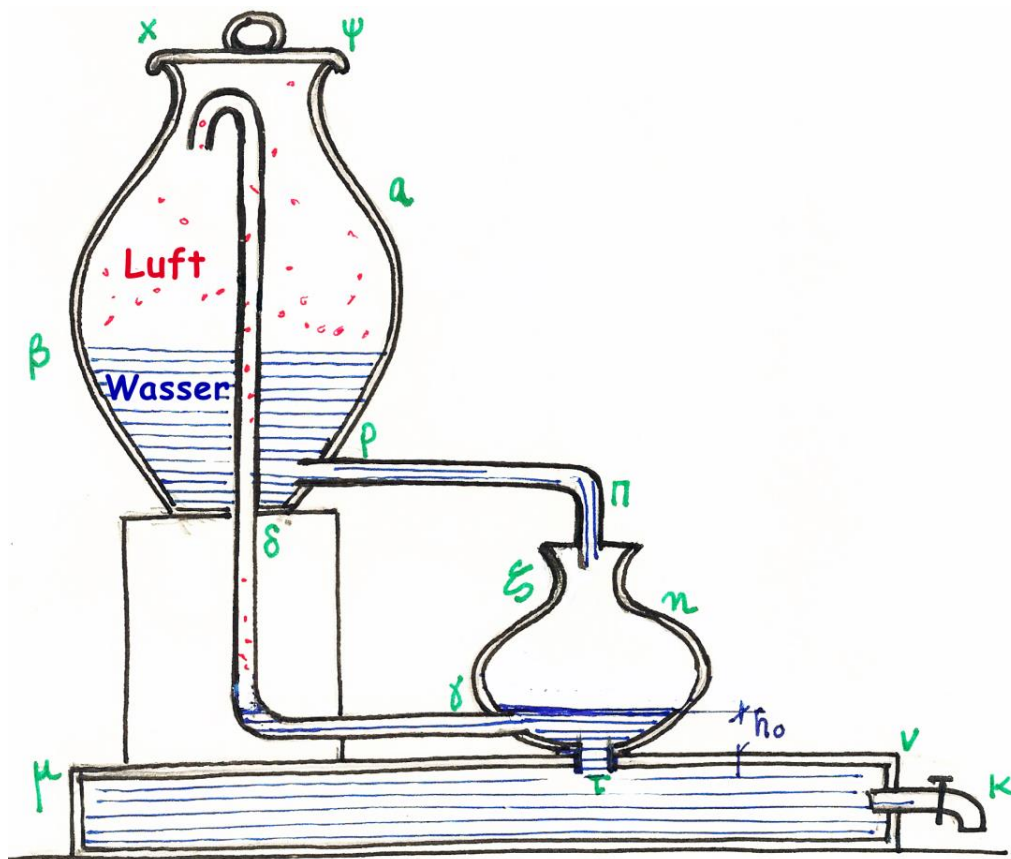


**Bild 2.** Regelung des Wasserspiegels mittels der Luft, nach Philon



### Beispiel 3. Die Hausdienerin, die automatisch Wein und Wasser ausschenkt

In dem Buch mit dem Titel *“Le livre des appareils Pneumatique et des machines hydrauliques – Pneumatische Apparate und hydraulische Maschinen,, Philons von Byzanz, findet man die erste französische Übersetzung von Baron Carra de Vaux, aus den arabischen Ausgaben von Oxford und Konstantinopel, Paris 1903. Darin findet man das Thema 30 unter dem Titel: “Description d’un autre vase plus merveilleux que celui-là – Beschreibung einer anderen Vase, wunderbarer als die vorangehende.”*

Es folgt nun die deutsche Übersetzung des entsprechenden Textes:

#### Beschreibung der äußeren Form des Apparates

*“Es handelt sich um einen Brunnen mit einem sich periodisch unterbrochenen Fluss. Der Brunnen hat die Form einer Hausdienerin, die einen Krug mit ihrer rechten Hand hält. Stellt man nun auf ihre linke flache Hand einen Becher auf, so gießt sie in den Becher Wein einer gewünschten Quantität ein. Und nachher gießt sie Wasser, das sich mit diesem Wein vermischt.,,*



**Bild 3.** Die Hausdienerin Philons

## Über die Konstruktion des Mechanismus

*“Man konstruiert zunächst aus Bronze oder aus Silber eine stehende Hausdienerin.*

*Vom Kopf bis zu ihrer Brust schafft man im Inneren einen Behälter, der durch eine Scheidewand in zwei gleiche Kammern getrennt ist. In jeder Kammer des Behälters befindet sich je eine Luftröhre, die Wein oder Wasser in den Krug ableitet. Die Röhre des Weinbehälters führt direkt zum Krug, die Röhre des Wasserbehälters ist jedoch viel länger und im Bauch der Hausdienerin um den Behälter gewickelt. Die Luftröhren sind offen, sie haben also im unteren Teil des Behälters offene Eingänge für den Eintritt der Luft. Die linke Hand ist mit der Schulter durch eine Drehachse verbunden.,,*

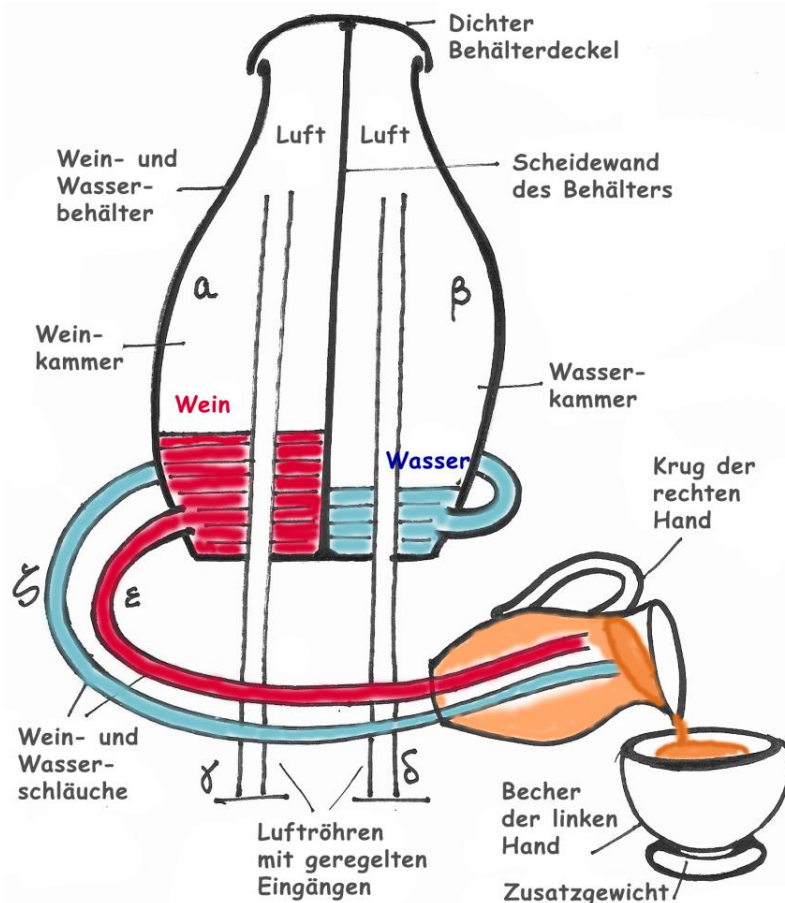


**Bild 4.** Der Mechanismus für die Wein- und Wasserlieferung im Becher der linken Hand

## Die einzelnen Teile des inneren Mechanismus

*Im Inneren der Figur befindet sich ein Krummstab, nach unten gerichtet, in der Form einer Gartenschere. Auf der Gerte, im unteren Teil dieses Stabes, sind zwei zylindrische Holzstifte angepasst, die als Verschluss oder Schlüssel dienen. Ihre Endungen passen genau in den Eingängen der Luftröhren, in denen sie mit milder Reibung eintreten. An den Stab ist unten ein kleines Zusatzgewicht angebracht. So strebt er natürlich nach unten und hebt somit die linke Hand hoch. Es heben sich so auch die zwei Holzstifte, die, als Schlüssel dienende, die zwei Eingänge der Luftröhren verschließen. Somit können die Flüssigkeiten nicht aus den Röhren fließen.,,*

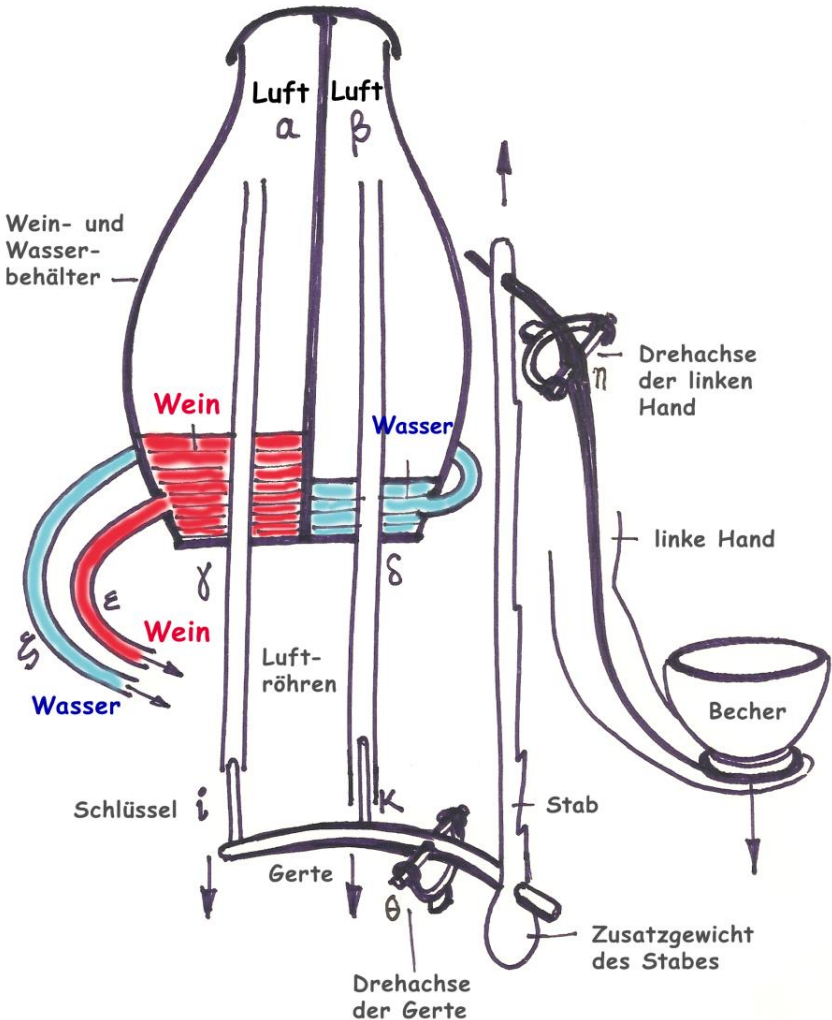


**Bild 5.** Mechanische Regelung des Wein- und Wasserflusses mittels Holzschlüsseln der Luftröhren

*“Diese ganze Konstruktion befindet sich im Inneren der Hausdienerin. Das Wasser und der Wein fließen leicht vom oberen Teil der Hausdienerin nach unten. Ihr Schädel dient als ein sehr dichter Deckel. Ihre rechte Hand bleibt unbeweglich an ihrer Stelle. So auch der Krug, den sie hält. Die zwei Schläuche ermöglichen die Zufuhr von Wein und Wasser aus den zwei Kammern des Behälters zum Krug.,,*

Die Reihenfolge des Flusses von Wein und Wasser wird hier durch die verschiedenen Höhen der Schlüsseln oder der Eingängen der Luftröhren geregelt.

### **Bezeichnungen und technische Einzelheiten des Innenraums**

*“Durch  $\alpha$  und  $\beta$  bezeichnen wir die zwei Kammern des Behälters. Mit  $\gamma$  und  $\delta$  die Luftröhren. Mit  $\varepsilon$  und  $\zeta$  die zwei Schläuche für die Zufuhr der Flüssigkeiten zum Krug. Mit  $\eta$  die Drehachse der linken Hand und mit  $\theta$  die Drehachse der Gerte. Die zwei hölzernen Schlüssel werden mit  $\iota$  und  $\kappa$  bezeichnet. Im Inneren der Hausdienerin gibt es ein Loch, verschlossen mit einem Deckel, der sich nach außen öffnet. Dieser Deckel bleibt während der ganzen Funktion des Mechanismus verschlossen, damit, wenn die Eingänge der Luftröhren sich öffnen, die Luft wieder aufgesaugt werden kann. Sonst würde der ganze Apparat nicht funktionieren.*

*Nachdem wir all das, was wir beschreiben wollten, vollendet haben, nehmt ihr einen Becher mit einem Inhalt von einem oder zwei Litern, oder auch von einem beliebigen Inhalt, entsprechend zu den Dimensionen der Röhrenbreiten, die sie gewählt haben. Zweckmäßig ist es auch die Mischung der Flüssigkeiten in Dritteln aufzuteilen, es sei zwei Drittel Wein und ein Drittel Wasser. Die Aufnahmefähigkeit des Kruges hängt von euren übrigen Auswahlen ab. Der Becher kann schwerer werden durch Zusatz in seinem unteren Teil eines geeigneten Gewichtes.,, .*

## Über die Funktion des Mechanismus

“Wenn wir nun den Becher auf die linke flache Hand der Hausdienerin aufsetzen, fällt die Hand nach unten. Der dicke Stab mit der Gerte steigt, jedoch die Holzzapfen, die als Verschluss gelten, fallen nach unten und öffnen nacheinander die verschlossenen unteren Öffnungen der Wein- und Wasserröhren. Zuerst öffnet sich die Öffnung der kürzeren Weinröhre. Der Wein fließt und füllt allmählich den Becher. Wenn der Wein fast ganz ausgeflossen und die Hand tiefer gesunken ist, öffnet sich allmählich die untere Öffnung der längeren Wasserröhre und das Wasser fängt an aus der Wasserkammer zu fließen. Wenn beide Kammern leer sind, nimmt man den Becher weg. Die Hand kehrt dann in ihre Stellung zurück. Beide Öffnungen, die den Eingang der Luft in die Luftröhren ermöglichen, werden verschlossen. Nichts fließt mehr aus dem Krug heraus. Setzt man nun wieder den leeren Becher auf die Hand der Hausdienerin, so bewegt sich die Hand nach unten, der Wein und anschließend das Wasser fließen wieder und füllen den Becher. Und das wiederholt sich solange noch Wein und Wasser vorhanden ist.,,



**Bild 6.** Der volle innere Mechanismus für die automatische Regelung der Bewegungen der Hausdienerin

## Die Schlussfolgerung Philons

*“Das war, was wir erklären wollten, in Bezug auf diesen Brunnen mit dem unterbrochen periodischen Fluss und mit der Form einer Hausdienerin. Ich hoffe sie verstehen all das, was ich Ihnen beschrieben habe. Hier zeig ich Ihnen noch die Form...., [4, 30].*

Das war der Text über die Hausdienerin, den uns Philon hinterlassen hat. Leider ist uns diese, von Philon erwähnte, originelle Form der Hausdienerin nicht erhalten.

Es existierte bis jetzt auch nicht, soviel wir wissen, eine originale deutsche Übersetzung des entsprechenden philonischen Textes.

Unser Beitrag zielte also zunächst darauf ab, diese beide Lücken zu füllen, und dabei gewisse interessante Erfindungen der hellenistischen Zeit, d.h. in dritten Jahrhundert v. Chr., aufzuzeigen:

1. Den Beweis der Materialität der Luft, um sie nachher für den Entwurf pneumatischer Systeme anzuwenden.
2. Den Entwurf von pneumatisch-hydraulischen Regelsystemen, mit geschlossenen Regelkreis und Rückkopplung.
3. Den bemerkenswerten Entwurf eines einzigartigen pneumatisch-hydraulischen und mechanischen Automaten mit der Form einer Wein und Wasser einschenkenden Hausdienerin.

Es klingt alles als wie eine Vorwegnahme von Erfindungen der viel später stattfindenden industriellen Revolution, die zusätzlich den Wasserdampf für den Maschinenantrieb einführte.

## Geschichtliche Literaturangaben

[1] Das originale Werk Philons von Byzanz *“Περί Πνευματικών – Über Pneumatik,,* in Altgriechisch, ist nicht erhalten.

[2] Es folgten, eine arabische Übersetzung, sowie die lateinischen Ausgaben von Konstantinopel und Oxford, mit dem Titel: *“Liber Philonis de ingeniis spiritualibus – Philons Buch über Erfindungen der Pneumatik,,.*

[3] Später kam die unvollständige deutsche Übersetzung eines Teils derer im Werke *“Heron Alexandrinus, Band I,,* vom Wilhelm Schmidt, Leipzig, Teubner Verlag, 1899 mit dem Titel: *“Die Druckwerke Philons von Byzanz,,* veröffentlicht wurde.

Darin ist jedoch die Beschreibung der *“Hausdienerin,,* nicht vorhanden.

[4] Es folgte die französische Übersetzung vom Baron Carra de Vaux, die in Paris, 1903, unter dem Titel: *“Le livre des appareils Pneumatique et des machines hydrauliques – Pneumatische Apparate und hydraulische Maschinen,,* veröffentlicht wurde.

Nur diese französische Übersetzung beinhaltet das Thema der Hausdienerin:

*“Thema 30. Description d’un autre vase plus merveilleux que celui-là – Beschreibung einer anderen Vase, wunderbarer als die vorangehende”.*

Das vorgehende Thema trägt den Titel:

*“Thema 29. Construction d’un vase élégant et merveilleux – Konstruktion eines eleganten und wunderbaren Gefäßes”* und betrifft der Mechanismus für eine pneumatisch-hydraulische Regelung. Dasselbe Thema findet man auch in der erwähnten deutschen Übersetzung [3], als Beispiel XII mit dem Titel: *“Ein konstanter Wasserspiegel,,.*

**Part II.**

**Slides**



# Lyapunov-based Design of Adaptive Sliding Mode Controllers

Alexander Barth<sup>a</sup> Markus Reichhartinger<sup>b</sup> Johann Reger<sup>a</sup> Martin Horn<sup>b</sup> Kai Wulff<sup>a</sup>

Consider the nonlinear system

$$\dot{\mathbf{x}} = \mathbf{f}(\mathbf{x}) + \mathbf{g}(\mathbf{x})(\Delta(\mathbf{x}, t) + u) \quad (1)$$

where  $\mathbf{x}(t) \in \mathbb{R}^n$  is the state,  $u(t) \in \mathbb{R}$  a scalar control input,  $\mathbf{f}$  and  $\mathbf{g}$  are known differentiable vector fields. Assume that the matched uncertainty  $\Delta$  may be decomposed as per

$$\Delta(\mathbf{x}, t) = \Delta_s(\mathbf{x}) + \Delta_u(\mathbf{x}, t) = \Theta^T \boldsymbol{\phi}(\mathbf{x}) + \Delta_u(\mathbf{x}, t) \quad (2)$$

such that  $\Delta_s(\mathbf{x}) = \Theta^T \boldsymbol{\phi}(\mathbf{x})$  represents the structured uncertainty, with unknown parameter vector  $\Theta$  and known base function  $\boldsymbol{\phi}$ , and  $\Delta_u(\mathbf{x}, t)$  comprises the unstructured uncertainty and external disturbances.

Let a sliding variable  $\sigma = \sigma(\mathbf{x})$  be selected such that a desired dynamics is imposed on the sliding manifold  $\sigma \equiv 0$ . Further, let  $\sigma$  be of relative degree one wrt. the input  $u$  and assume the associated internal dynamics to be stable. Thus, along the solution the derivative reads

$$\dot{\sigma} = \underbrace{\Theta^T \mathbf{a}_1(\mathbf{x}) + a_2(\mathbf{x}, t)}_{=\phi(\mathbf{x}, t)} + \omega(\mathbf{x}, u) \quad (3)$$

where  $\mathbf{a}_1(\mathbf{x})$ ,  $a_2(\mathbf{x}, t)$  as well as  $\omega(\mathbf{x}, u)$  may be expressed in terms of equations (1) and (2). Clearly, expression  $\phi(\mathbf{x}, t)$  captures the entire uncertainty and  $\omega$  is a known function, that given  $\mathbf{x}$ , is bijective wrt. the control input  $u$ .

The goal is to devise a controller  $\omega$  that stabilizes the origin of (3).

Neglecting the knowledge about the structure within the uncertainty and requiring that the entire uncertainty be uniformly bounded according to

$$|\phi(\mathbf{x}, t)| \leq \Omega_\phi |\sigma(\mathbf{x})|^{\frac{1}{2}} \quad (4)$$

for some  $\Omega_\phi > 0$  Shtessel et al. gave a solution to this problem [7, 8]. However, the square-root growth bound on the uncertainty may be restrictive in many practical situations.

Therefore, we propose to treat the structurally known part  $\Theta^T \mathbf{a}_1(\mathbf{x})$  of the uncertainty  $\phi(\mathbf{x}, t)$  separately from the unstructured part  $a_2(\mathbf{x}, t)$ . This allows to relax the requirement (4) considerably such that no upper bound is needed for the uncertainty  $\phi(\mathbf{x}, t)$ . Only for the unstructured part  $a_2(\mathbf{x}, t)$  we still require that

$$|a_2(\mathbf{x}, t)| \leq \Omega_{a_2} |\sigma(\mathbf{x})|^{\frac{1}{2}} \quad (5)$$

uniformly for some  $\Omega_{a_2} > 0$ .

---

<sup>a</sup>Fachgebiet Regelungstechnik, Technische Universität Ilmenau, Helmholtzplatz 5, D-98693 Ilmenau, E-Mail: {alexander.barth,johann.reger,kai.wulff}@tu-ilmenau.de

<sup>b</sup>Institut für Regelungs- und Automatisierungstechnik, Technische Universität Graz, Kopernikusgasse 24/II, 8010 Graz, E-Mail: {markus.reichhartinger,martin.horn}@tugraz.at

**Main result:** In view of the super-twisting algorithm [4] we propose the following dynamic state-feedback with adaptive extension:

$$\begin{aligned}\dot{\omega} &= -k_1 |\sigma(\mathbf{x})|^{\frac{1}{2}} \text{sign}(\sigma(\mathbf{x})) + \nu - \hat{\Theta}^T \mathbf{a}_1(\mathbf{x}) \\ \dot{\nu} &= -k_2 \text{sign}(\sigma(\mathbf{x})) \\ \dot{\hat{\Theta}} &= \gamma k_2 \text{sign}(\sigma(\mathbf{x})) \mathbf{a}_1(\mathbf{x})\end{aligned}\tag{6}$$

with  $\nu(0) = 0$ ,  $\hat{\Theta}(0) = \hat{\Theta}_0$  for some  $\hat{\Theta}_0$ , controller state  $\nu$ , and parameters  $k_1, k_2, \gamma > 0$ .

In view of an adaptive extension of a Lyapunov-function presented in [6], employing the weak Lyapunov-function

$$V(\mathbf{x}, \nu, \hat{\Theta}) = k_2 |\sigma(\mathbf{x})| + \frac{1}{2} \nu^2 + \frac{1}{2\gamma} (\hat{\Theta} - \Theta)^T (\hat{\Theta} - \Theta)\tag{7}$$

we show that the origin of the closed-loop system (3) is stable.

In our approach, the gains  $k_1$  and  $k_2$  of the controller (6) may be reduced significantly when compared, for example, with the adaptive-gain super-twisting algorithm [7] or its modification in [8]. For further details on our proposed approach, see [1].

As a general remark note that whenever given a Lyapunov-function for the nominal system that satisfies some continuity assumptions, e.g. in [5], the proposed approach may lead to novel families of adaptive sliding-mode controllers.

- [1] BARTH, A., REICHHARTINGER, M., REGER, J., HORN, M., and WULFF, K.: *Lyapunov-Design for a Super-Twisting Sliding-Mode Controller using the Certainty-Equivalence Principle*. In 1st MICNON, St. Petersburg, Russia, 2015.
- [2] CLARKE, F., LEDYAEV, Y., STERN, R., and WOLENSKI, P.: *Nonsmooth analysis and control theory*. Springer, New York, 1988.
- [3] KOCHALUMMOOTIL, J., SHTESSEL, Y., MORENO, J., and FRIDMAN, L.: *Adaptive twist sliding mode control: A lyapunov design*. In 50th IEEE CDC, 7623–7628, 2011.
- [4] LEVANT, A.: *Sliding order and sliding accuracy in sliding mode control*. IJC, 58(6), 1247–1263, 1993.
- [5] MORENO, J. and SÁNCHEZ, T.: *A constructive lyapunov function design method for a class of homogeneous systems*. In 53rd IEEE CDC, 5500–5505, 2014.
- [6] ORLOV, Y.: *Finite time stability and robust control synthesis of uncertain switched systems*. SIAM Journal on Control and Optimization, 43(4), 1253–1271, 2005.
- [7] SHTESSEL, Y., MORENO, J., PLESTAN, F., FRIDMAN, L. and POZNYAK, A.: *Super-twisting adaptive sliding mode control: A lyapunov design*. In 49th IEEE CDC, 5109–5113, 2010.
- [8] SHTESSEL, Y., TALEB, M. and PLESTAN, F.: *A novel adaptive-gain supertwisting sliding mode controller: Methodology and application*. Automatica, 48(5), 759–769, 2012.



# Lyapunov-based Design of Adaptive Sliding Mode Controllers

Alexander Barth<sup>†</sup>

*alexander.barth@tu-ilmenau.de*

<sup>†</sup> Control Engineering Group, TU Ilmenau, Germany  
in cooperation with Faculty of Electrical and Information Engineering, Graz University of  
Technology, Austria

8<sup>th</sup> of September 2015

Retzhof 2015, Austria

## Outline

- 1 Motivation
- 2 Problem Description
- 3 Controller Design
  - Conventional Lyapunov Function (weak)
  - Quadratic LF (strict)
  - Continuously Differentiable LF (strict)
- 4 Simulation Examples
- 5 Conclusion & Outlook

## Motivation

- enhance the super-twisting (STA) controller by a certainty-equivalence approach
- extend the class of disturbances / unbounded uncertainties
- increase the robustness of the super-twisting algorithm
- exploit *all* available information about the system
- generate less discontinuous control action
- obtain control law via Lyapunov theory



## Problem Description

### System

$$\dot{x} = f(x) + g(x)(\Delta(x, t) + u)$$

- state  $x(t) \in \mathbb{R}^n$
- scalar input  $u(t) \in \mathbb{R}$
- vector fields  $f, g$  known and differentiable
- $g(x) \neq 0, \forall x \in \mathbb{R}^n$
- scalar uncertainty  $\Delta(x, t) = \Delta_u(x, t) + \Delta_s(x)$ 
  - structured uncertainty  $\Delta_s(x) = \Theta^T \phi(x)$  :  
known function  $\phi : \mathbb{R}^n \rightarrow \mathbb{R}^p$ , unknown parameter  $\Theta \in \mathbb{R}^p$
  - unstructured uncertainty / disturbance  $\Delta_u(x, t)$



## Sliding Variable

Sliding variable:  $\sigma = \sigma(x)$  with  $\sigma : \mathbb{R}^n \rightarrow \mathbb{R}$

- desired dynamics for  $\sigma \equiv 0$
- relative degree 1 of  $\sigma$  with respect to  $u$
- stable zero dynamics

Derivation:

$$\begin{aligned}\dot{\sigma} &= \frac{\partial \sigma}{\partial x} \left( f(x) + g(x) (\Delta_s(x) + \Delta_u(x, t) + u) \right) \\ &= \underbrace{\frac{\partial \sigma}{\partial x} f(x)}_{=: a_0(x)} + \underbrace{\Theta^T \phi(x) \frac{\partial \sigma}{\partial x} g(x)}_{=: a_1(x)} + \underbrace{\frac{\partial \sigma}{\partial x} g(x) \Delta_u}_{=: a_2(x, t)} + \underbrace{\frac{\partial \sigma}{\partial x} g(x) u}_{=: b(x)} \\ &= \Theta^T a_1(x) + a_2(x, t) + \omega \quad \text{with} \quad \omega := a_0(x) + b(x) u\end{aligned}$$

**Goal:** stabilize the origin of the  $\sigma$ -system with control  $\omega$



## Outline

- 1 Motivation
- 2 Problem Description
- 3 Controller Design
  - Conventional Lyapunov Function (weak)
  - Quadratic LF (strict)
  - Continuously Differentiable LF (strict)
- 4 Simulation Examples
- 5 Conclusion & Outlook



## Controller Design

### Idea

- make use of the structure of the uncertainty
- exploit Lyapunov functions for SMC

### System

$$\dot{\sigma} = \Theta^T a_1(x) + a_2(x, t) + \omega$$

### Assumptions

- $a_1 : \mathbb{R}^n \rightarrow \mathbb{R}^p$  known base function
- $\Theta \in \mathbb{R}^p$  unknown parameter vector
- $a_2$  bounded by  $|a_2(x, t)| \leq \delta |\sigma(x)|^{\frac{1}{2}}$  with known  $\delta > 0$



6/26

## Certainty Equivalence Super-Twisting

### System

$$\dot{\sigma} = \Theta^T a_1(x) + a_2(x, t) + \omega$$

### Control Law

$$\omega = -k_1 \lceil \sigma \rceil^{\frac{1}{2}} + \nu - \hat{\Theta}^T a_1(x)$$

$$\dot{\nu} = -k_2 \text{sign}(\sigma), \quad \nu(0) = 0$$

controller parameter  $k_1, k_2 > 0$ .

Note:  $\lceil \sigma \rceil^q = \text{sign}(\sigma) |\sigma|^q$

### Adaptation Law

$$\dot{\hat{\Theta}} = \Gamma k_2 \text{sign}(\sigma) a_1(x)$$

adaptation parameter  $\Gamma > 0$



7/26

## Sketch of a Proof

### Lyapunov Function Candidate [Orlov, 2005]

$$V = k_2 |\sigma| + \frac{1}{2} \nu^2 + \frac{1}{2\Gamma} \tilde{\Theta}^T \tilde{\Theta}$$

- with  $\tilde{\Theta} = \hat{\Theta} - \Theta$
- Adaptation Parameter  $\Gamma > 0$

### Derivation

$$\begin{aligned} \dot{V} &= k_2 \operatorname{sign}(\sigma) \left( -k_1 |\sigma|^{\frac{1}{2}} \operatorname{sign}(\sigma) + a_2(x, t) - \tilde{\Theta}^T a_1 \right) + \frac{1}{\Gamma} \tilde{\Theta}^T \dot{\tilde{\Theta}} \\ &\leq \left( -k_1 k_2 |\sigma|^{\frac{1}{2}} + k_2 \delta |\sigma|^{\frac{1}{2}} \right) + \tilde{\Theta}^T \left( -a_1(x) k_2 \operatorname{sign}(\sigma) + \frac{1}{\Gamma} \dot{\tilde{\Theta}} \right) \end{aligned}$$



8/26

## Comments

### Adaptation Law

$$\dot{\hat{\Theta}} = \Gamma k_2 \operatorname{sign}(\sigma) a_1(x)$$

### Improvements

- combines adaptive and sliding-mode control
- stability is guaranteed by design
- increases the robustness of the super-twisting algorithm (STA)

### Drawbacks

- discontinuous adaptation law
- no asymptotic stability of controller state  $\nu$



9/26

## Outline

- 1 Motivation
- 2 Problem Description
- 3 Controller Design
  - Conventional Lyapunov Function (weak)
  - Quadratic LF (strict)
  - Continuously Differentiable LF (strict)
- 4 Simulation Examples
- 5 Conclusion & Outlook



10/26

## Quadratic LF (strict)

Addressing the drawbacks:

- discontinuous adaptation law
- no asymptotic stability of controller state  $\nu$

### System

$$\dot{\sigma} = \Theta^T a_1(x) + a_2(x, t) + \omega$$

### Control Law

$$\omega = -k_1 \lceil \sigma \rceil^{\frac{1}{2}} + \nu - \hat{\Theta}^T a_1(x)$$

$$\dot{\nu} = -k_2 \text{sign}(\sigma), \quad \nu(0) = 0$$

### Lyapunov Function [Moreno and Osorio, 2008]

$$V = z^T P z + \frac{1}{2\Gamma} \tilde{\Theta}^T \tilde{\Theta}$$

with  $z = (\lceil \sigma \rceil^{\frac{1}{2}}, \nu)^T$ ,  $\Gamma > 0$  and  $P = P^T > 0$



10/26



## Quadratic LF (strict)

### Derivation

$$\dot{V}(z, \tilde{\Theta}) \leq -\frac{1}{2|z_1|} z^T Q_0 z + \frac{1}{|z_1|} z^T P G_1(x) \tilde{\Theta} + \frac{1}{\Gamma} \dot{\tilde{\Theta}}^T \tilde{\Theta}$$

with  $Q_0 = -(A^T P + P A) > 0$

$$G_1(x) := \begin{pmatrix} a_1^T(x) \\ 0 \end{pmatrix} \text{ and } A := \begin{pmatrix} -\frac{k_1}{2} & \frac{1}{2} \\ -k_2 & 0 \end{pmatrix}$$

### Adaptation Law

$$\dot{\tilde{\Theta}} = \frac{\Gamma}{|z_1|} G_1^T(x) P z$$

- diagonal matrix  $P$
- restrict  $a_1$  with:  $|a_{1,i}(x)| \leq |\sigma(x)|^{q_i}$  with  $q_i > \frac{1}{2}$ ,  $\forall i = 1 \dots p$



## Quadratic LF (strict)

### Advantages

- possible to achieve asymptotic stability of  $\sigma$  and  $\nu$
- increases the robustness compared to the nominal STA
- allows combination with the adaptive-gain STA

### Drawbacks

- requires additional bounds on the known base function
- otherwise the right hand side of the adaptation law becomes unbounded



## Review: Adaptive-Gain Super-Twisting

### System

$$\dot{\sigma} = \underbrace{\Theta^T a_1(x) + a_2(x, t)}_{=:\varphi(x, \Theta, t)} + \omega$$

### Disturbance

$$|\varphi(x, \Theta, t)| \leq \delta^* |\sigma(x)|^{\frac{1}{2}}, \quad \forall x \in \mathbb{R}^n, \forall t \in \mathbb{R}^+$$

### Controller [Shtessel et al., 2010]

$$\omega = -\alpha(t) |\sigma|^{\frac{1}{2}} + \nu \quad \text{and} \quad \dot{\nu} = -\beta(t) \operatorname{sign}(\sigma)$$

$$\dot{\alpha}(t) = \begin{cases} \omega_1 \sqrt{\frac{1}{2} \gamma_1}, & \text{if } \sigma \neq 0, \\ 0, & \text{if } \sigma = 0 \end{cases}$$

$$\beta(t) = 2\varepsilon\alpha + \lambda + 4\varepsilon^2$$



## Review: Adaptive-Gain Super-Twisting

### Controller [Shtessel et al., 2010]

$$\omega = -\alpha(t) |\sigma|^{\frac{1}{2}} \operatorname{sign}(\sigma) + \nu \quad \text{and} \quad \dot{\nu} = -\beta(t) \operatorname{sign}(\sigma)$$

$$\dot{\alpha}(t) = \begin{cases} \omega_1 \sqrt{\frac{1}{2} \gamma_1}, & \text{if } \sigma \neq 0, \\ 0, & \text{if } \sigma = 0 \end{cases}$$

$$\beta(t) = 2\varepsilon\alpha + \lambda + 4\varepsilon^2$$

with  $\gamma_1, \omega_1, \lambda, \varepsilon > 0$

### Lyapunov Function

$$V_a(z, \alpha, \beta) = z^T P_a z + \frac{1}{2\gamma_1} (\alpha(t) - \alpha^*)^2 + \frac{1}{2\gamma_2} (\beta(t) - \beta^*)^2$$

$$\gamma_2, \alpha^*, \beta^* > 0 \quad \text{and} \quad P_a = \begin{pmatrix} \lambda + 4\varepsilon^2 & -2\varepsilon \\ -2\varepsilon & 1 \end{pmatrix}$$



## Outline

- 1 Motivation
- 2 Problem Description
- 3 Controller Design
  - Conventional Lyapunov Function (weak)
  - Quadratic LF (strict)
  - Continuously Differentiable LF (strict)
- 4 Simulation Examples
- 5 Conclusion & Outlook



## Continuously Differentiable LF (strict)

In order to overcome the drawbacks:

- no asymptotic stability of the controller state  $\nu$
- discontinuous / unbounded control law
- additional bounds on the base function  $a_1$  required

### Idea

- make use of recently discovered Lyapunov functions for higher-order sliding-mode [Moreno and Sánchez, 2014]

$$V_0 = \frac{2}{3}\gamma_1 |\sigma|^{\frac{3}{2}} - \gamma_{12}\sigma \nu + \frac{1}{3}\gamma_2 |\nu|^3$$

- avoid unbounded / discontinuous control laws
- extend the class of captured uncertainties compared to the design with the quadratic LF



## Continuously Differentiable LF (strict)

### System

$$\dot{\sigma} = \Theta^T a_1(x) + a_2(x, t) + \omega$$

### Control Law

$$\omega = -k_1 \lceil \sigma \rceil^{\frac{1}{2}} + \nu - \hat{\Theta}^T a_1(x)$$

$$\dot{\nu} = -k_2 \operatorname{sign}(\sigma), \quad \nu(0) = 0$$

### Lyapunov Function

$$V = \frac{2}{3} k_1 |\sigma|^{\frac{3}{2}} - \sigma \nu + \frac{1+a}{k_1^2} |\nu|^3 + \frac{1}{2\Gamma} \tilde{\Theta}^T \tilde{\Theta}$$

### Derivation

$$\begin{aligned} \dot{V} &= \tilde{\Theta}^T a_1(x) \left( k_1 \lceil \sigma \rceil^{\frac{1}{2}} - \nu \right) + \dot{V}_0 + \frac{1}{\Gamma} \tilde{\Theta}^T \dot{\tilde{\Theta}} \\ &= \dot{V}_0 + \tilde{\Theta}^T \left( \frac{1}{\Gamma} \dot{\tilde{\Theta}} + a_1(x) \left( k_1 \lceil \sigma \rceil^{\frac{1}{2}} - \nu \right) \right) \end{aligned}$$

### Adaptation Law

$$\dot{\tilde{\Theta}} = \Gamma a_1(x) \left( k_1 \lceil \sigma \rceil^{\frac{1}{2}} - \nu \right)$$



16/26

## Continuously Differentiable LF (strict)

### Adaptation Law

$$\dot{\tilde{\Theta}} = \Gamma a_1(x) \left( k_1 \lceil \sigma \rceil^{\frac{1}{2}} - \nu \right)$$

### Advantages

- combines adaptive and sliding mode control
- increases the robustness of the standard super-twisting
- no further limitations to the base function  $a_1(x)$
- continuous adaptation law

### Drawbacks

- nominal Lyapunov function limits the number of usable controller parameter  $k_1, k_2$  combinations



17/26

## Simulation Examples

### Simulation System

$$\dot{x}_1 = x_2$$

$$\dot{x}_2 = \Theta \Omega(x_1, x_2) + u$$

### Sliding Surface

$$\sigma = x_1 + x_2$$

### Disturbance

$$\Omega(x_1, x_2) = \sin(2x_2)(x_1 + x_2) \quad \text{and} \quad \Theta = 2$$

$\Rightarrow$  fails AGSTA-conditions [Shtessel et al., 2010, Shtessel et al., 2012]

### Controller Parameter

| AGSTA      |            |           |            | CESTA |       |          |
|------------|------------|-----------|------------|-------|-------|----------|
| $\omega_1$ | $\gamma_1$ | $\lambda$ | $\epsilon$ | $k_1$ | $k_2$ | $\Gamma$ |
| 0.1        | 2          | 0.5       | 0.5        | 1     | 2     | 1        |

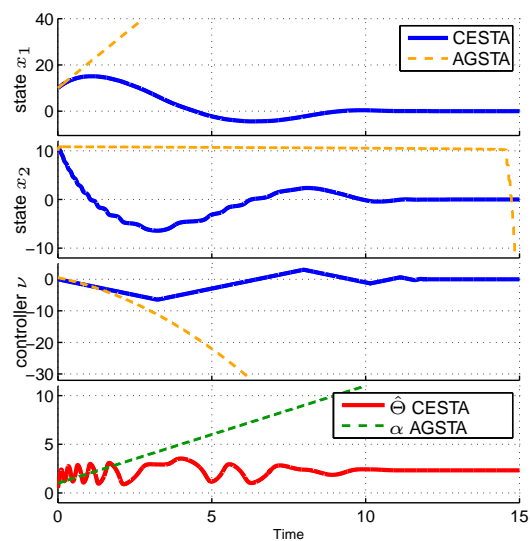
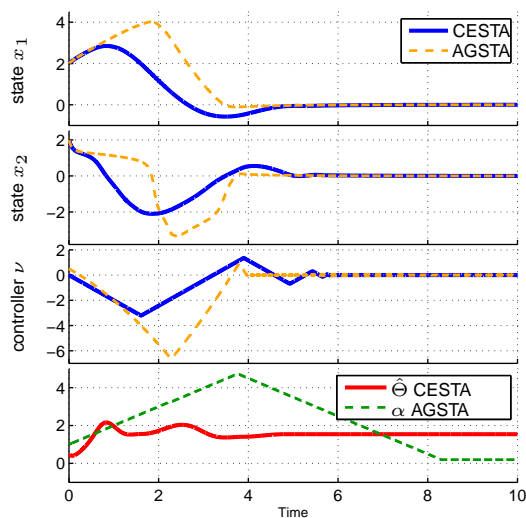


18/26

## Simulation Examples

Initial condition:  $x_0 = [2, 2]$

$x_0 = [10, 10]$



19/26

## Quadratic Lyapunov Function

### System

$$\dot{\sigma} = \Theta^T a_1(x) + a_2(x, t) + \omega$$

### Control Law

$$\omega = -k_1 \lceil \sigma \rceil^{\frac{1}{2}} + \nu - \hat{\Theta}^T a_1(x)$$

$$\dot{\nu} = -k_2 \text{sign}(\sigma)$$

### Disturbances

$$a_1 = \sigma (\cos(\sigma) + 1), \quad a_2 = 0.2 \sin(2\sigma)$$

### Initial Condition

$$\sigma(0) = 10, \quad \nu(0) = 10,$$

### Adaptation Law

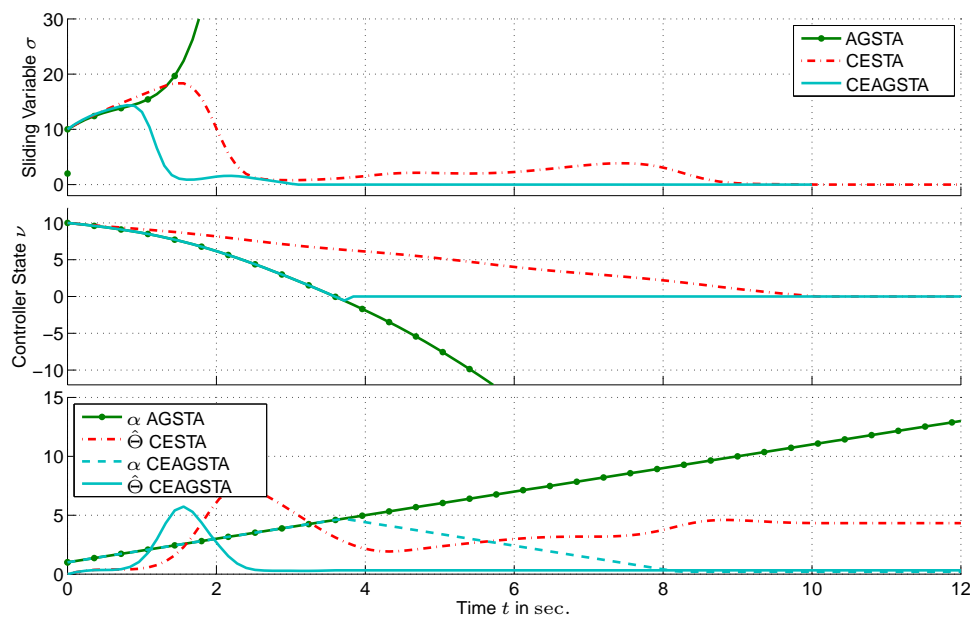
$$\dot{\hat{\Theta}} = \frac{\Gamma}{|z_1|} \begin{pmatrix} a_1(x) & 0 \end{pmatrix} P z, \quad z = (\lceil \sigma \rceil^{\frac{1}{2}}, \nu)^T$$

| Controller                      | AGSTA | CESTA | CEAGSTA |
|---------------------------------|-------|-------|---------|
| Controller Parameter $k_1, k_2$ | ✓     |       | ✓       |
| Uncertainty Parameter $\Theta$  |       | ✓     | ✓       |



20/26

## Quadratic Lyapunov Function



21/26

## Continuously Differentiable Lyapunov Function

### System

$$\dot{\sigma} = \Theta^T a_1(x) + a_2(x, t) + \omega$$

### Control Law

$$\omega = -k_1 \lceil \sigma \rceil^{\frac{1}{2}} + \nu - \hat{\Theta}^T a_1(x)$$

$$\dot{\nu} = -k_2 \operatorname{sign}(\sigma)$$

### Disturbances

$$a_1 = (\sigma + 1) (\cos(\sigma) + 1), \quad a_2 = 0.2 \sin(2\sigma)$$

### Initial Condition

$$\sigma(0) = 10, \quad \nu(0) = 10,$$

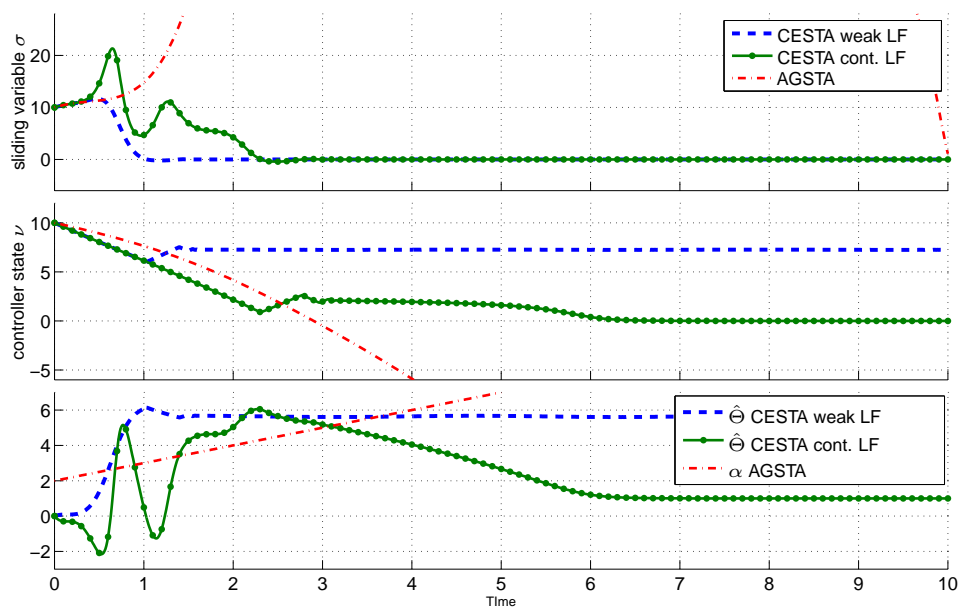
### Adaptation Law

$$\dot{\hat{\Theta}} = \Gamma a_1(x) \left( k_1 \lceil \sigma \rceil^{\frac{1}{2}} - \nu \right)$$



22/26

## Continuously Differentiable Lyapunov Function



23/26

## Conclusion & Outlook









### Conclusion

- enhanced the super-twisting algorithm by an adaptive extension
- Lyapunov based approach
- influence of the nominal Lyapunov function for the adaptation law
- simulation examples

### Outlook

- demonstrate finite time convergence
- detailed investigation of the continuously differentiable LF
- selection of controller parameters
- modifications to the adaptation scheme



-  Dávila, A., Moreno, J., and Fridman, L. (2009).  
Optimal lyapunov function selection for reaching time estimation of super twisting algorithm.  
*In 48th IEEE CDC*, pages 8405–8410.
-  Moreno, J. (2010).  
Lyapunov analysis of non homogeneous super-twisting algorithms.  
*In 11th IEEE VSS*, pages 534–539.
-  Moreno, J. and Osorio, M. (2008).  
A lyapunov approach to second-order sliding mode controllers and observers.  
*In 47th IEEE CDC*, pages 2856–2861.
-  Moreno, J. and Osorio, M. (2012).  
Strict lyapunov functions for the super-twisting algorithm.  
*IEEE Trans. Autom. Control*, 57(4):1035–1040.
-  Moreno, J. and Sánchez, T. (2014).  
A constructive lyapunov function design method for a class of homogeneous systems.  
*In 53rd IEEE CDC*, pages 5500–5505.
-  Orlov, Y. (2005).  
Finite time stability and robust control synthesis of uncertain switched systems.  
*SIAM Journal on Control and Optimization*, 43(4):1253–1271.
-  Shtessel, Y., Moreno, J., Plestan, F., Fridman, L., and Poznyak, A. (2010).  
Super-twisting adaptive sliding mode control: A lyapunov design.  
*In 49th IEEE CDC*, pages 5109–5113.
-  Shtessel, Y., Taleb, M., and Plestan, F. (2012).  
A novel adaptive-gain supertwisting sliding mode controller: Methodology and application.  
*Automatica*, 48(5):759–769.





Thank you for  
your attention!



# Observers for non-linear MIMO descriptor systems

Robel Besrat<sup>a</sup>

Felix Gausch<sup>a</sup>

Nenad Vrhovac<sup>b</sup>

This article presents non-linear observers for exact I/O-linearizable descriptor systems with a specific focus on the semi-explicit form:

$$\dot{\mathbf{x}} = \mathbf{a}(\mathbf{x}, \mathbf{z}) + \mathbf{B}(\mathbf{x}, \mathbf{z})\mathbf{u} \quad (1a)$$

$$\mathbf{0} = \mathbf{p}(\mathbf{x}, \mathbf{z}, \mathbf{u}) \quad (1b)$$

$$\mathbf{y} = \mathbf{c}(\mathbf{x}, \mathbf{z}) \quad (1c)$$

where  $\mathbf{x} \in \mathbb{R}^n$  and  $\mathbf{z} \in \mathbb{R}^p$  denote the vectors of the differential and the algebraic variables respectively. Furthermore, we assume that there are the same number of input variables  $\mathbf{u} \in \mathbb{R}^m$  and output variables  $\mathbf{y} \in \mathbb{R}^m$ .

In addition to the constraints explicitly specified in (1b) the differential algebraic equations (1a, 1b) include further implicit constraints for higher-index systems. All these constraints contained in (2) describe the manifold  $\mathcal{M}$ , where the solutions  $\mathbf{x}(t)$  and  $\mathbf{z}(t)$  of (1a, 1b) are located:

$$\mathbf{0} = \tilde{\mathbf{p}}(\mathbf{x}, \mathbf{z}, \mathbf{u}). \quad (2)$$

Following the preliminary work in [1] and [3], as part of the exact I/O-linearization for descriptor systems, an observer is developed that incorporates the impact of all the constraints during the estimation process.

To determine the observer structure, the explicit representation (3) of the non-linear descriptor system (1):

$$\begin{aligned} \dot{\mathbf{w}} = \begin{bmatrix} \dot{\mathbf{x}} \\ \dot{\mathbf{z}} \end{bmatrix} &= \begin{bmatrix} \mathbf{a}(\mathbf{x}, \mathbf{z}) + \mathbf{B}(\mathbf{x}, \mathbf{z})\mathbf{u} \\ - \left[ \frac{\partial \mathbf{p}_{k-1}}{\partial \mathbf{z}} \right]^{-1} \frac{\partial \mathbf{p}_{k-1}}{\partial \mathbf{x}} (\mathbf{a}(\mathbf{x}, \mathbf{z}) + \mathbf{B}(\mathbf{x}, \mathbf{z})\mathbf{u}) \end{bmatrix} = \mathbf{f}(\mathbf{w}) + \mathbf{G}(\mathbf{w})\mathbf{u} \\ \mathbf{y} &= \mathbf{c}(\mathbf{w}) \end{aligned} \quad (3)$$

is transferred to Byrnes-Isidori normal form by choosing a suitable transformation (diffeomorphism)  $\boldsymbol{\xi} = \boldsymbol{\varphi}(\mathbf{w}) = [\boldsymbol{\zeta}^T, \boldsymbol{\eta}^T]^T$  and subsequently introducing a state feedback  $\mathbf{u} = (\boldsymbol{\zeta}, \boldsymbol{\eta}, \mathbf{v})$  with new inputs  $\mathbf{v}$ :

$$\dot{\boldsymbol{\zeta}} = \mathbf{A}\boldsymbol{\zeta} + \mathbf{B}\mathbf{v} \quad (4a)$$

$$\dot{\boldsymbol{\eta}} = \boldsymbol{\vartheta}(\boldsymbol{\zeta}, \boldsymbol{\eta}) \quad (4b)$$

$$\mathbf{y} = \mathbf{C}\boldsymbol{\zeta}. \quad (4c)$$

The linear subsystem (4a, 4c) is observable independent of  $\mathbf{v}$  and  $\boldsymbol{\vartheta}$ , while the non-linear subsystem (4b) describes the non-observable internal dynamics. In case of a asymptotic

<sup>a</sup>Institut für Elektrotechnik und Informationstechnik, Universität Paderborn, Pohlweg 47-49, 33098 Paderborn, E-Mail: [robel.besrat@uni-paderborn.de](mailto:robel.besrat@uni-paderborn.de), [gausch@uni-paderborn.de](mailto:gausch@uni-paderborn.de)

<sup>b</sup>Former member of the "Steuerungs- und Regelungstechnik" workgroup at the above

minimum-phase system (3) the overall system (4) is detectable, and it is appropriate to design a high-gain observer for subsystem (4a, 4c) using the Luenberger method (5):

$$\begin{aligned}\dot{\hat{\zeta}} &= \mathbf{A}\hat{\zeta} + \mathbf{B}\hat{v} + \mathbf{K}(\mathbf{y} - \hat{\mathbf{y}}) \\ \dot{\hat{\eta}} &= \vartheta(\hat{\zeta}, \hat{\eta}) \\ \hat{\mathbf{y}} &= \mathbf{C}\hat{\zeta}.\end{aligned}\tag{5}$$

In the original coordinates ( $\hat{\mathbf{w}} = \hat{\varphi}^{-1}(\hat{\xi})$ ), the observer gain  $\mathbf{K}_{HGR}$  is determined via the Moore-Penrose inverse of the reduced observability matrix, which is calculated from the time derivatives of the (known) output variables (4c):

$$\begin{aligned}\dot{\hat{\mathbf{w}}} &= \mathbf{f}(\hat{\mathbf{w}}) + \mathbf{G}(\hat{\mathbf{w}})\mathbf{u} + \mathbf{K}_{HGR}(\hat{\mathbf{w}})(\mathbf{y} - \mathbf{c}(\hat{\mathbf{w}})) \\ \hat{\mathbf{y}} &= \mathbf{c}(\hat{\mathbf{w}}).\end{aligned}\tag{6}$$

With the correction approach suggested in [2] the convergence of the high-gain observer solution, against that of the system, can be improved. To achieve this, the observer (6) is extended by the implicit and explicit constraints contained in the vector  $\tilde{\mathbf{p}}(\mathbf{w})$ :

$$\begin{aligned}\dot{\hat{\mathbf{w}}} &= \mathbf{f}(\hat{\mathbf{w}}) + \mathbf{G}(\hat{\mathbf{w}})\mathbf{u} - \Delta\mathbf{P}_{\mathcal{M}}(\hat{\mathbf{w}})\mathbf{M}\tilde{\mathbf{p}}(\hat{\mathbf{w}}) + \mathbf{K}_{HGR}(\hat{\mathbf{w}})(\mathbf{y} - \mathbf{c}(\hat{\mathbf{w}})) \\ \hat{\mathbf{y}} &= \mathbf{c}(\hat{\mathbf{w}}).\end{aligned}\tag{7}$$

In this equation  $\mathbf{M}$  denotes a free design parameter, while  $\Delta\mathbf{P}_{\mathcal{M}}$  describes an orthogonal projection of the deviations in the constraints on the tangent bundle of the solution manifold  $\mathcal{M}$ .

Finally the extended observer (7) is implemented using a suitable example, and the results are discussed.

- [1] GAUSCH, F. und N. VRHOVAC: *Feedback Linearization of Descriptorsystems - A Classification Approach*. IJAA - International Journal Automation Austria, 18(1):1–18, 2010.
- [2] VRHOVAC, N.: *Beobachtungsaufgabe bei nichtlinearen Deskriptorsystemen*. Dissertation, Universität Paderborn, 2015.
- [3] VRHOVAC, N. und F. GAUSCH: *Beobachterentwurf für nichtlineare SISO-Deskriptorsysteme vom Index  $k=1$* . In: HORN, M., M. HOFBAUR und N. DOURDOUMAS (Herausgeber): *16. Steirisches Seminar über Regelungstechnik und Prozessautomatisierung*, Seiten 16–28, Schloss Retzhof - Leibniz/Österreich, 2009. Institut für Regelungs- und Automatisierungstechnik, Technische Universität Graz.

|          |                              |                        |                                      |                               |
|----------|------------------------------|------------------------|--------------------------------------|-------------------------------|
| Overview | Descriptor Systems<br>○<br>○ | Feedback Linearization | Observer Design SISO<br>○○○○<br>○○○○ | Observer Design MIMO<br>○○○○○ |
|----------|------------------------------|------------------------|--------------------------------------|-------------------------------|

# Observers for Non-Linear MIMO Descriptor Systems

Robel Besrat, Nenad Vrhovac

University of Paderborn  
Department of Electrical Engineering  
Automatic Control Group  
Prof. Dr. techn. F. Gausch

9 September 2015

|                          |  |        |
|--------------------------|--|--------|
| Besrat, R. , Vrhovac, N. | Observers for Non-Linear MIMO Descriptor Systems | 1 / 26 |
|--------------------------|--|--------|

|          |                              |                        |                                      |                               |
|----------|------------------------------|------------------------|--------------------------------------|-------------------------------|
| Overview | Descriptor Systems<br>○<br>○ | Feedback Linearization | Observer Design SISO<br>○○○○<br>○○○○ | Observer Design MIMO<br>○○○○○ |
|----------|------------------------------|------------------------|--------------------------------------|-------------------------------|

## Overview

A well known procedure for non-linear

- **explicit state models**  
differential equations  
output equations
- **input and coord. transformation**  
L-Operator
- **BYRNES–ISIDORI NF**  
observer design for linear part
- **inverse transformation**  
set up as high-gain observer

Presented procedure for non-linear

- **semi-explicit descriptor models**  
differential equations  
**algebraic equations**  
output equations
- **input and coord. transformation**  
**N-Operator**  
**mod. shuffle algorithm**
- **BYRNES–ISIDORI NF**  
observer design for linear part
- **inverse transformation**  
set up as high-gain observer  
**error affected by algebr. constraints**

|                          |  |        |
|--------------------------|--|--------|
| Besrat, R. , Vrhovac, N. | Observers for Non-Linear MIMO Descriptor Systems | 2 / 26 |
|--------------------------|--|--------|

## 3 / 26

## 4 / 26



Overview
Descriptor Systems
Feedback Linearization
Observer Design SISO
Observer Design MIMO

## ...Feedback Linearization

Besrat, R. , Vrhovac, N.
Observers for Non-Linear MIMO Descriptor Systems
7 / 26

Overview
Descriptor Systems
Feedback Linearization
Observer Design SISO
Observer Design MIMO

## Diffeomorphism

$$\begin{aligned} \dot{\zeta} &= A\zeta + bv \\ \eta &= \vartheta(\zeta, \eta) \\ y &= c^T \zeta \end{aligned}$$

$$\xi = \varphi(w) = \begin{bmatrix} N^0 h \\ N^1 h \\ \vdots \\ N^{\gamma-1} h \\ \eta_{\gamma+1} \\ \vdots \\ \eta_{n+p} \end{bmatrix} = \begin{bmatrix} \zeta \\ \eta \end{bmatrix}$$

Besrat, R. , Vrhovac, N.
Observers for Non-Linear MIMO Descriptor Systems
8 / 26

Overview   Descriptor Systems   Feedback Linearization   **Observer Design SISO**   Observer Design MIMO

## ...Diffeomorphism

BYRNES-ISIDORI Normal Form

$$\xi = \varphi(w) = \begin{bmatrix} N^0 h(w) \\ \vdots \\ N^{\gamma-1} h(w) \\ \eta_{\gamma+1} \\ \vdots \\ \eta_{n+p} \end{bmatrix} \quad \text{with} \quad \begin{bmatrix} N^0 h(w) \\ \vdots \\ N^{\gamma-1} h(w) \end{bmatrix} = \zeta \quad \text{and} \quad \begin{bmatrix} \eta_{\gamma+1} \\ \vdots \\ \eta_{n+p} \end{bmatrix} = \eta :$$

$$\begin{aligned} \dot{\zeta} &= A\zeta + b v \\ \dot{\eta} &= \vartheta(\zeta, \eta) \\ y &= c^T \zeta \end{aligned}$$

**Zero Dynamics:**  
 $\dot{\eta} = \vartheta(0, \eta) \quad \text{with} \quad \zeta = 0$

**Condition:**  
 Equilibrium  $\eta = 0$  asymptotically stable

Besrat, R. , Vrhovac, N.   Observers for Non-Linear MIMO Descriptor Systems   9 / 26

Overview   Descriptor Systems   Feedback Linearization   **Observer Design SISO**   Observer Design MIMO

## Luenberger Observer

$\dot{\zeta} = A\zeta + b v$   
 $\dot{\eta} = \vartheta(\zeta, \eta)$   
 $y = c^T \zeta$

$$\xi = \varphi(w) = \begin{bmatrix} N^0 h \\ N^1 h \\ \vdots \\ N^{\gamma-1} h \\ \eta_{\gamma+1} \\ \vdots \\ \eta_{n+p} \end{bmatrix} = \begin{bmatrix} \zeta \\ \eta \end{bmatrix}$$

$u = \frac{1}{(N^{\gamma-1}h)' b(w)} \left[ - (N^{\gamma-1}h)' a(w) + v \right]$   
 $\dot{w} = \begin{bmatrix} a(w) + b(w)u \\ - \left[ \frac{\partial p_{k-1}}{\partial z} \right]^{-1} \frac{\partial p_{k-1}}{\partial x} (a(w) + b(w)u) \end{bmatrix}$   
 $y = h(w), \quad w = \begin{bmatrix} x \\ z \end{bmatrix}$

$\dot{\xi} = A\xi + b\hat{v} + k(y - \hat{y})$   
 $\dot{\eta} = \vartheta(\hat{\xi}, \hat{\eta})$   
 $\hat{y} = c^T \hat{\xi}$   
 $\hat{w} = \varphi^{-1}(\hat{\xi})$

Besrat, R. , Vrhovac, N.   Observers for Non-Linear MIMO Descriptor Systems   10 / 26



## ...Luenberger Observer

- Luenberger Method:**

$$\begin{aligned} \dot{\zeta} &= A\zeta + bv, & \zeta(0) &= \zeta_0 \\ \dot{\eta} &= \vartheta(\zeta, \eta), & \eta(0) &= \eta_0 \\ y &= c^T \zeta \end{aligned} \quad \begin{aligned} \dot{\hat{\zeta}} &= A\hat{\zeta} + b\hat{v} + k(y - \hat{y}), & \hat{\zeta}(0) &= \hat{\zeta}_0 \\ \dot{\hat{\eta}} &= \vartheta(\hat{\zeta}, \hat{\eta}), & \hat{\eta}(0) &= \hat{\eta}_0 \\ \hat{y} &= c^T \hat{\zeta} \end{aligned}$$

- Error Dynamics:**

$$\dot{e} = \begin{bmatrix} (A - kc^T)e_\zeta + b(v - \hat{v}) \\ \vartheta(\hat{\zeta}, \hat{\eta}) - \vartheta(\zeta, \eta) \end{bmatrix}$$

$$\text{mit } e = \begin{bmatrix} e_\zeta \\ e_\eta \end{bmatrix} = \begin{bmatrix} \hat{\zeta} - \zeta \\ \hat{\eta} - \eta \end{bmatrix} \text{ und } e(0) = e_0 = \hat{\xi}_0 - \xi_0$$

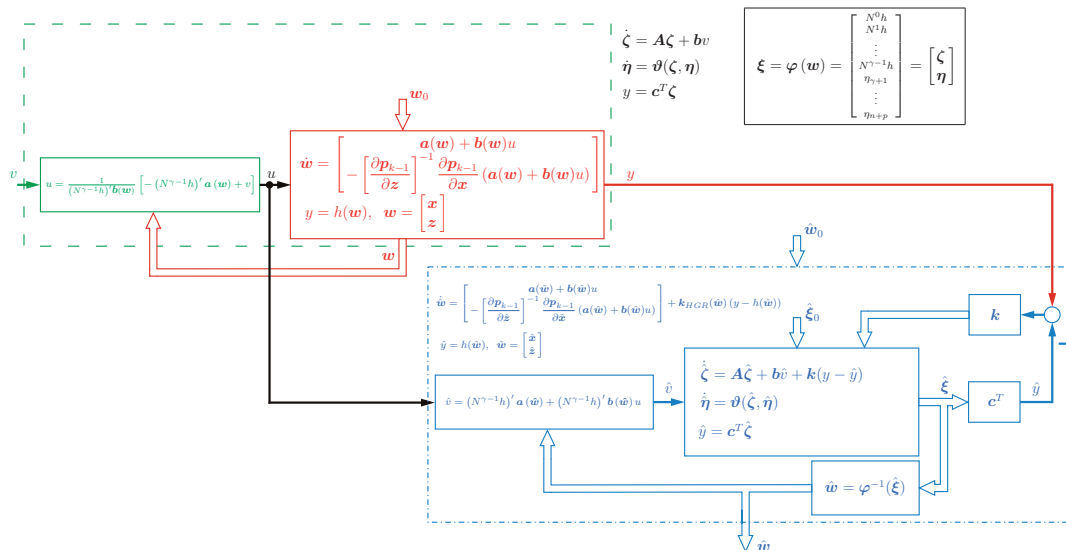
- Condition:** Constants  $L_1, L_2 \geq 0$  exist for bounded inputs  $u$

$$|\hat{v}(\hat{\zeta}, \hat{\eta}, u) - v(\zeta, \eta, u)| \leq L_1 \|\hat{\zeta} - \zeta\| + L_2 \|\hat{\eta} - \eta\|$$

### High-Gain Observer:

Choose  $k$  so that the equilibrium  $e = 0$  is asymptotically stable (the convergence behavior  $e(t) \rightarrow 0$  for  $t \rightarrow \infty$  is dominated by the linear part of the system).

## High-Gain Observer





Overview   Descriptor Systems   Feedback Linearization   **Observer Design SISO**   Observer Design MIMO

## ...High-Gain Observer

$$\dot{\zeta} = A\zeta + bv$$

$$\dot{\eta} = \vartheta(\zeta, \eta)$$

$$y = c^T \zeta$$

$$\xi = \varphi(w) = \begin{bmatrix} N^0 h \\ N^1 h \\ \vdots \\ N^{\gamma-1} h \\ \eta_{\gamma+1} \\ \vdots \\ \eta_{n+p} \end{bmatrix} = \begin{bmatrix} \zeta \\ \eta \end{bmatrix}$$

$$\dot{\hat{w}} = \begin{bmatrix} a(\hat{w}) + b(\hat{w})u \\ -\left[\frac{\partial p_{k-1}}{\partial \hat{z}}\right]^{-1} \frac{\partial p_{k-1}}{\partial \hat{x}} (a(\hat{w}) + b(\hat{w})u) \\ + k_{HGR}(\hat{w}) (y - h(\hat{w})) + M\hat{p}(\hat{w}) \end{bmatrix}$$

$$\hat{y} = h(\hat{w}), \quad \hat{w} = \begin{bmatrix} \hat{x} \\ \hat{z} \end{bmatrix}$$

$$\dot{\hat{\xi}} = \begin{bmatrix} a(\hat{w}) + b(\hat{w})u \\ -\left[\frac{\partial p_{k-1}}{\partial \hat{z}}\right]^{-1} \frac{\partial p_{k-1}}{\partial \hat{x}} (a(\hat{w}) + b(\hat{w})u) \\ + k_{HGR}(\hat{w}) (y - h(\hat{w})) \end{bmatrix}$$

$$\hat{y} = h(\hat{w}), \quad \hat{w} = \begin{bmatrix} \hat{x} \\ \hat{z} \end{bmatrix}$$

$$\dot{\hat{\zeta}} = A\hat{\zeta} + b\hat{v} + k(y - \hat{y})$$

$$\dot{\hat{\eta}} = \vartheta(\hat{\zeta}, \hat{\eta})$$

$$\hat{y} = c^T \hat{\zeta}$$

$$\hat{w} = \varphi^{-1}(\hat{\xi})$$

$$M\hat{p}(\hat{w})$$

Besrat, R., Vrhovac, N.   Observers for Non-Linear MIMO Descriptor Systems   15 / 26

Overview   Descriptor Systems   Feedback Linearization   **Observer Design SISO**   Observer Design MIMO

## Example: SISO

Semi-explicit Model:

$$\dot{x} = \begin{bmatrix} x_2(z+1) \\ \sin(x_1) + u \end{bmatrix}$$

$$0 = z - 1$$

$$y = x_1$$

Explicit Model:

$$\dot{w} = \begin{bmatrix} w_2(w_3+1) \\ \sin(w_1) + u \\ 0 \end{bmatrix}$$

$$y = w_1$$

Observer:

$$\dot{\hat{w}} = \begin{bmatrix} \hat{w}_2(\hat{w}_3+1) \\ \sin(\hat{w}_1) + u \\ 0 \end{bmatrix} + \begin{bmatrix} k_1 \\ k_2 \frac{\hat{w}_3+1}{(\hat{w}_3+1)^2 + \hat{w}_2^2} \\ k_2 \frac{\hat{w}_2}{(\hat{w}_3+1)^2 + \hat{w}_2^2} \end{bmatrix} (y - \hat{w}_1) + \underbrace{\begin{bmatrix} \mu_1 \\ \mu_2 \\ \mu_3 \end{bmatrix} (\hat{w}_3 - 1)}_{M\hat{p}(\hat{w})}$$

$M\hat{p}(\hat{w}) = ? \implies$  Orthogonal Projection

Besrat, R., Vrhovac, N.   Observers for Non-Linear MIMO Descriptor Systems   16 / 26

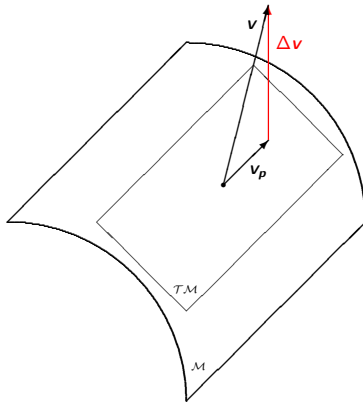
# Orthogonal Projection

Explicit and implicit constraint equations

$$\tilde{\mathbf{p}}(\mathbf{w}) = \begin{bmatrix} \tilde{\mathbf{p}}_1(\mathbf{w}) \\ \vdots \\ \tilde{\mathbf{p}}_p(\mathbf{w}) \end{bmatrix}, \quad \tilde{\mathbf{p}}_i := \begin{bmatrix} p_{i,0}(\mathbf{w}) \\ p_{i,1}(\mathbf{x}, \mathbf{z}, \mathbf{u}) \\ \vdots \\ p_{i,k_i-1}(\mathbf{w}) \end{bmatrix} \quad \forall i \in \{1, \dots, p\}$$

span the solution manifold  $\mathcal{M}$ :

$$\mathcal{M} = \{ \mathbf{w} \mid \tilde{\mathbf{p}}(\mathbf{w}) = \mathbf{0} \}$$



Orthogonal projection  $\mathbf{v}_p$  of a vector  $\mathbf{v}$  on  $\mathcal{T}\mathcal{M}$ :

$$\mathbf{v}_p = \mathbf{v} - \Delta \mathbf{v} = \mathbf{v} - \Delta \mathbf{P}_{\mathcal{M}}(\mathbf{w}) \mathbf{v}$$

Corrective Projection

$$\Delta \mathbf{P}_{\mathcal{M}}(\mathbf{w}) = \left[ \frac{\partial \tilde{\mathbf{p}}}{\partial \mathbf{w}} \right]^T \left( \frac{\partial \tilde{\mathbf{p}}}{\partial \mathbf{w}} \left[ \frac{\partial \tilde{\mathbf{p}}}{\partial \mathbf{w}} \right]^T \right)^{-1} \frac{\partial \tilde{\mathbf{p}}}{\partial \mathbf{w}}$$

## ...Example: SISO

Semi-explicit Model:

$$\begin{aligned} \dot{\mathbf{x}} &= \begin{bmatrix} x_2(z+1) \\ \sin(x_1) + u \end{bmatrix} \\ 0 &= z - 1 \\ y &= x_1 \end{aligned}$$

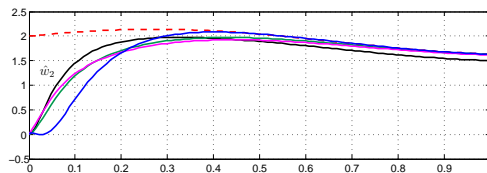
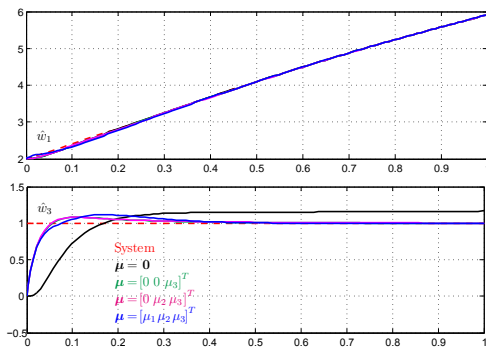
$$\begin{bmatrix} x_1 \\ x_2 \\ z \end{bmatrix} = \begin{bmatrix} w_1 \\ w_2 \\ w_3 \end{bmatrix}$$

Explicit Model:

$$\begin{aligned} \dot{\mathbf{w}} &= \begin{bmatrix} w_2(w_3+1) \\ \sin(w_1) + u \\ 0 \end{bmatrix} \\ y &= w_1 \end{aligned}$$

Observer:

$$\dot{\hat{\mathbf{w}}} = \begin{bmatrix} \hat{w}_2(\hat{w}_3+1) \\ \sin(\hat{w}_1) + u \\ 0 \end{bmatrix} + \begin{bmatrix} k_1 \frac{\hat{w}_3+1}{(\hat{w}_3+1)^2 + \hat{w}_2^2} \\ k_2 \frac{\hat{w}_2}{(\hat{w}_3+1)^2 + \hat{w}_2^2} \end{bmatrix} (y - \hat{w}_1) + \underbrace{\begin{bmatrix} \mu_1 \\ \mu_2 \\ \mu_3 \end{bmatrix}}_{\mathbf{M}\tilde{\mathbf{p}}(\hat{\mathbf{w}})} (\hat{w}_3 - 1)$$



$$\mathbf{M}\tilde{\mathbf{p}}(\hat{\mathbf{w}}) \longrightarrow \Delta \mathbf{P}_{\mathcal{M}}(\hat{\mathbf{w}}) \mathbf{M}\tilde{\mathbf{p}}(\hat{\mathbf{w}}) = \begin{bmatrix} 0 \\ 0 \\ \mu_3 \end{bmatrix} (\hat{w}_3 - 1)$$

Overview Descriptor Systems Feedback Linearization Observer Design SISO Observer Design MIMO

## Modified High-Gain Observer

$$\dot{\hat{w}} = \begin{bmatrix} a(\hat{w}) + b(\hat{w})u \\ -\left[\frac{\partial p_{k-1}}{\partial z}\right]^{-1} \frac{\partial p_{k-1}}{\partial x} (a(\hat{w}) + b(\hat{w})u) \end{bmatrix} + k_{HGR}(\hat{w})(y - h(\hat{w})) + \Delta P_{\mathcal{M}}(\hat{w})M\tilde{p}(\hat{w})$$

$$\hat{y} = h(\hat{w}), \quad \hat{w} = \begin{bmatrix} \hat{x} \\ \hat{z} \end{bmatrix}$$

Besrat, R., Vrhovac, N. Observers for Non-Linear MIMO Descriptor Systems 19 / 26

Overview Descriptor Systems Feedback Linearization Observer Design SISO Observer Design MIMO

## Observer Design MIMO

Similar design steps as in SISO case:

**Modified High-Gain Observer**

$$\dot{\hat{w}} = f(\hat{w}) + G(\hat{w})u + K_{HGR}(\hat{w})(y - h(\hat{w})) + \Delta P_{\mathcal{M}}(\hat{w})M\tilde{p}(\hat{w})$$

$$\hat{y} = h(\hat{w})$$

$$\hat{w} \in \mathbb{R}^{n+p}, \quad y, u \in \mathbb{R}^m$$

**Observer Gain MIMO**

With observer gain of the SISO subsystems:

$$K_{HGR}(\hat{w}) = \begin{bmatrix} k_{HGR,1}(\hat{w}) & \dots & k_{HGR,m}(\hat{w}) \end{bmatrix}$$

$$k_{HGR,i}(\hat{w}) = Q_{BR,i}^+(\hat{w})k_i, \quad \forall i \in \{1, \dots, m\}$$

$$K_{HGR}(\hat{w}) = \begin{bmatrix} Q_{BR,1}^+(\hat{w}) & \dots & Q_{BR,m}^+(\hat{w}) \end{bmatrix} \begin{bmatrix} k_1 & 0 & \dots & 0 \\ 0 & k_2 & \dots & 0 \\ \vdots & \vdots & \ddots & \vdots \\ 0 & \dots & 0 & k_m \end{bmatrix} = Q_{BR}^+(\hat{w})K$$

Constant gain  $K$  via pole placement for matrix  $A - KC$

Besrat, R., Vrhovac, N. Observers for Non-Linear MIMO Descriptor Systems 20 / 26

## Example: MIMO

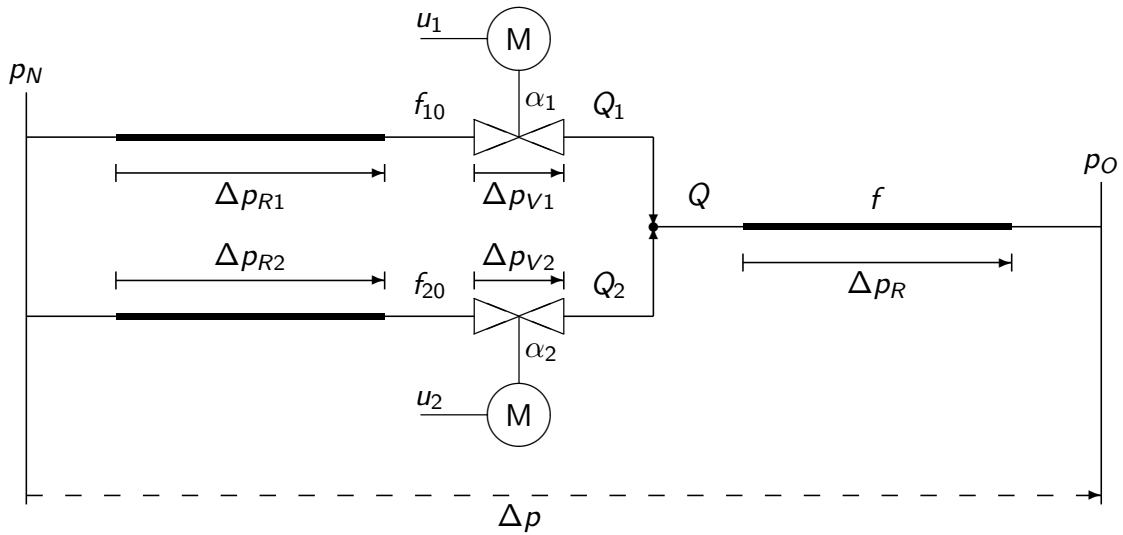


Figure: Gas mixing pipe system

## ...Example: MIMO

Semi-Explicit Model:

$$\begin{aligned} \dot{\mathbf{x}} &= \frac{1}{T} \mathbf{u} \\ 0 &= \begin{bmatrix} c_{R1} z_1^2 + c_V z_1^q \Psi(x_1) + c_R (z_1 + z_2)^2 - \Delta p \\ c_{R2} z_2^2 + c_V z_2^q \Psi(x_2) + c_R (z_1 + z_2)^2 - \Delta p \end{bmatrix} = \mathbf{p}(\mathbf{x}, \mathbf{z}) \\ \mathbf{y} &= \begin{bmatrix} \frac{1}{z_1 + z_2} (f_{10} z_1 + f_{20} z_2) \end{bmatrix} \end{aligned}$$

$$\text{with } \mathbf{x} = [\alpha_1 \ \alpha_2]^T, \quad \mathbf{z} = [Q_1 \ Q_2]^T, \quad \mathbf{y} = [f \ Q]^T, \quad \mathbf{u} = [u_1 \ u_2]^T$$

Explicit Model:

$$\begin{aligned} \dot{\mathbf{w}} &= \begin{bmatrix} \dot{w}_1 \\ \dot{w}_2 \\ w_3 \\ w_4 \end{bmatrix} = \begin{bmatrix} \frac{1}{T} \mathbf{u} \\ -\frac{1}{T} \left[ \frac{\partial \mathbf{p}(\mathbf{x}, \mathbf{z})}{\partial \mathbf{z}} \right]^{-1} \left[ \frac{\partial \mathbf{p}(\mathbf{x}, \mathbf{z})}{\partial \mathbf{x}} \right] \mathbf{u} \end{bmatrix} \\ \mathbf{y} &= \begin{bmatrix} \frac{1}{w_3 + w_4} (f_{10} w_3 + f_{20} w_4) \end{bmatrix} \end{aligned}$$

$$\text{with } \mathbf{w} = [\mathbf{x}^T \ \mathbf{z}^T]^T, \quad \mathbf{y} = [f \ Q]^T, \quad \mathbf{u} = [u_1 \ u_2]^T$$

## ...Example: MIMO

Observer:

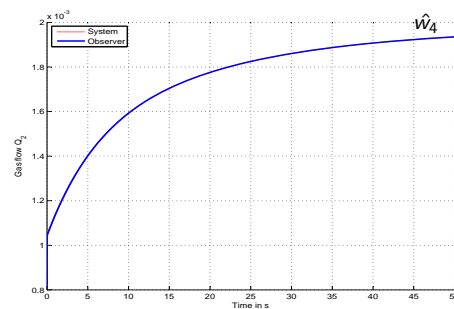
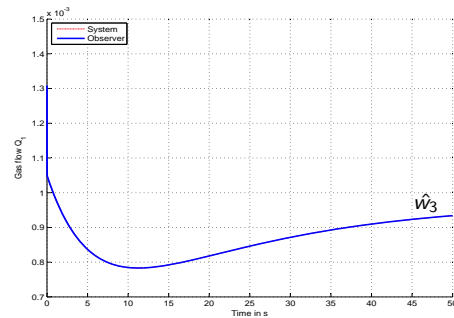
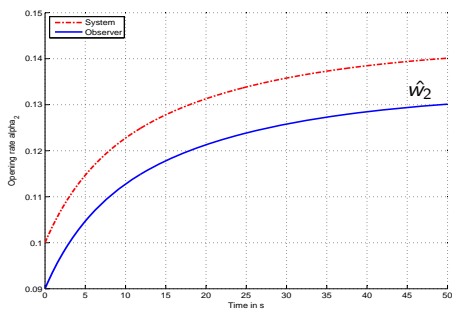
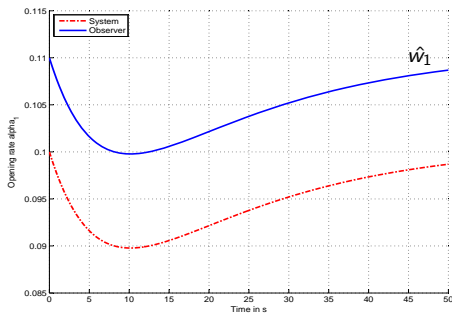
$$\dot{\hat{\mathbf{w}}} = \begin{bmatrix} \frac{1}{T} \mathbf{u} \\ -\frac{1}{T} \left[ \frac{\partial \mathbf{p}(\hat{\mathbf{x}}, \hat{\mathbf{z}})}{\partial \hat{\mathbf{z}}} \right]^{-1} \left[ \frac{\partial \mathbf{p}(\hat{\mathbf{x}}, \hat{\mathbf{z}})}{\partial \hat{\mathbf{x}}} \right] \mathbf{u} \end{bmatrix} + \underbrace{\begin{bmatrix} 0 & 0 \\ k_1 \frac{\hat{w}_3 + \hat{w}_4}{f_{10} - f_{20}} & k_2 \frac{\hat{w}_3}{\hat{w}_3 + \hat{w}_4} \\ -k_1 \frac{\hat{w}_3 + \hat{w}_4}{f_{10} - f_{20}} & k_2 \frac{\hat{w}_3}{\hat{w}_3 + \hat{w}_4} \end{bmatrix}}_{\mathbf{K}_{HGR}(\hat{\mathbf{w}})} \left( \mathbf{y} - \underbrace{\begin{bmatrix} 1 \\ \hat{w}_3 + \hat{w}_4 \end{bmatrix} \frac{(f_{10} \hat{w}_3 + f_{20} \hat{w}_4)}{\hat{w}_3 + \hat{w}_4}}_{\hat{\mathbf{y}}} \right) + \Delta \mathbf{P}_{\mathcal{M}}(\hat{\mathbf{w}}) \mathbf{M} \tilde{\mathbf{p}}(\hat{\mathbf{w}})$$

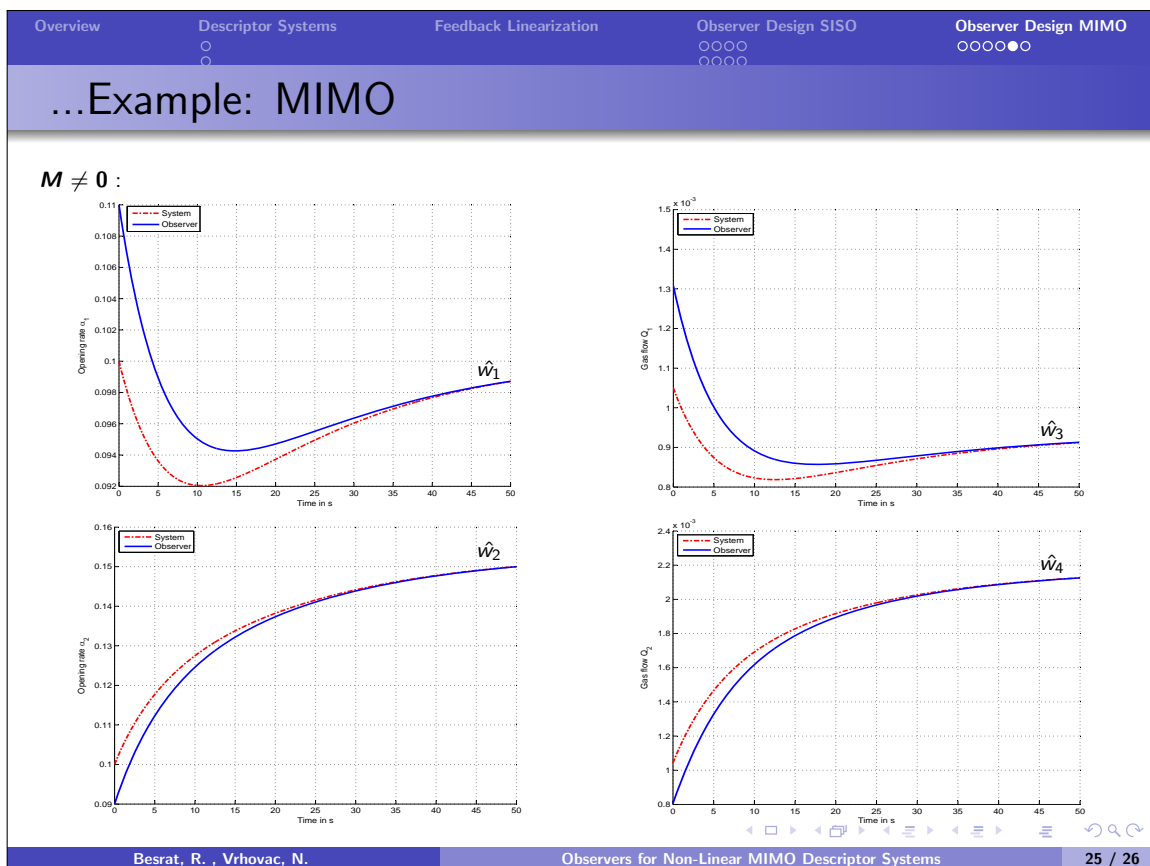
- Index-1 system  $\Rightarrow \tilde{\mathbf{p}}(\hat{\mathbf{w}}) = \mathbf{p}(\hat{\mathbf{w}}) \Rightarrow \Delta \mathbf{P}_{\mathcal{M}}(\mathbf{w}) = \left[ \frac{\partial \mathbf{p}}{\partial \mathbf{w}} \right]^T \left( \frac{\partial \mathbf{p}}{\partial \mathbf{w}} \left[ \frac{\partial \mathbf{p}}{\partial \mathbf{w}} \right]^T \right)^{-1} \frac{\partial \mathbf{p}}{\partial \mathbf{w}}$

- $\mathbf{M} = \begin{bmatrix} \mu_{11} & \mu_{12} \\ \mu_{21} & \mu_{22} \\ \mu_{31} & \mu_{32} \\ \mu_{41} & \mu_{42} \end{bmatrix}$

## ...Example: MIMO

$\mathbf{M} = \mathbf{0}$ :





Overview   Descriptor Systems   Feedback Linearization   Observer Design SISO   **Observer Design MIMO**

## References

Vrhovac, N.: *Beobachtungsaufgabe bei nichtlinearen Deskriptorsystemen*. Berichte aus der Steuerungs- und Regelungstechnik, Shaker Verlag, Aachen, 2015.

Gausch, F. and Vrhovac, N.: *Feedback Linearization of Descriptorsystems - A Classification Approach*. IJAA - International Journal Automation Austria, 18(1):1-18, 2010.

Vrhovac, N. and Gausch, F.: *Beobachterentwurf für nichtlineare SISO-Deskriptorsysteme vom Index  $k=1$* . 16. Steirisches Seminar über Regelungstechnik und Prozessautomatisierung, Schloss Retzhof - Leibniz/Österreich, 2009.

Besrat, R. , Vrhovac, N.   Observers for Non-Linear MIMO Descriptor Systems   26 / 26



# Design and Validation of an SOH-Algorithm for Lithium Ion Batteries

Stefan Doczy<sup>a</sup>

Wolfgang Toppler<sup>a</sup>

The usage of modern lithium ion batteries in the hybrid powertrain of buses and commercial vehicles allows significant fuel savings. Therefore the reliable prediction of the usable energy window and the power limits over life time of the battery is very important for the optimal energy management of the vehicle.

In the presented project a high voltage (700V) and high power (120kW) battery for hybrid electric vehicles was developed. For the battery management a state of health (SOH) algorithm was designed to estimate the current ageing status, which is described by several, partially dependent values. Among these, the battery capacity, limited by the minimum cell capacity, is representative for the usable energy window and will decrease over life time. The internal charge resistance and discharge resistance are limiting charge power and discharge power ability and will increase over life time. For an accurate validation of the ageing status the battery must perform reference tests on a suitable test bench (i.e. static capacity test, hybrid pulse power characterisation).

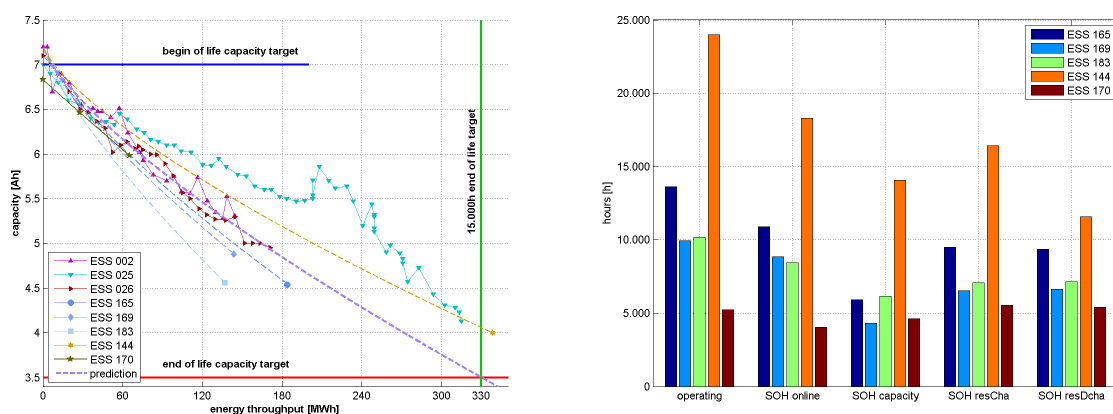


Figure 1: Reference test results for battery capacity (left) and ageing status (right)

Life time testing of batteries on test bench, using a customer defined power profile, started in an early phase of the project, but was not finished at start of production. For validation reasons several batteries used in vehicles were provided by the customer for reference tests. Test results for some of these batteries are shown in Figure 1.

The SOH algorithm is slightly underestimating the ageing mechanisms of the batteries used in the vehicles and therefore prevents the systems to be overloaded, which was an important project target.

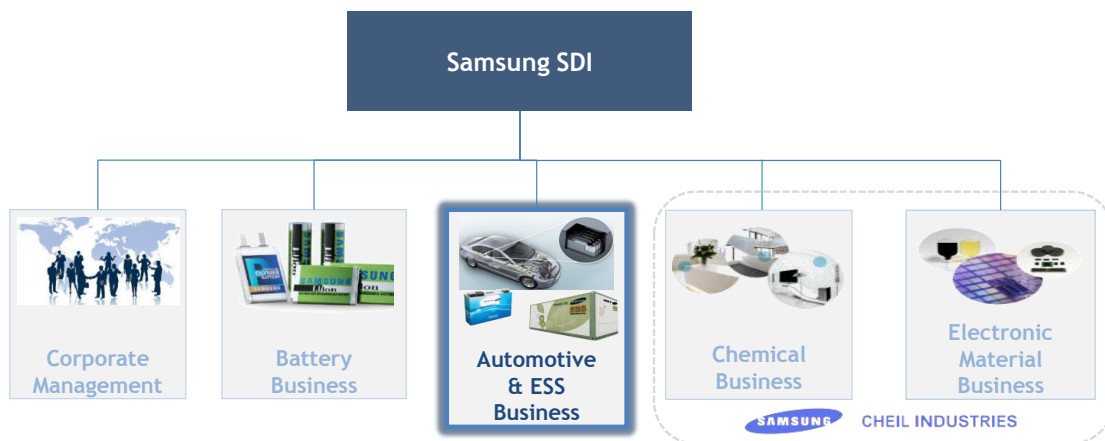
The life time requirements defined at start of the project were achieved by batteries used in vehicles and on test bench for more than five years.

<sup>a</sup>Samsung SDI Battery Systems, Frikusweg 1, 8141 Zettling, E-Mail: s.doczy@samsung.com

## Design and Validation of an SOH Algorithm for Lithium Ion Batteries

Stefan Doczy - Schloss Retzhof - 9th Sept. 2015

## Integration SDIBS into Samsung SDI



# Battery Systems Zettling (AT)

## Zettling (HQ)

- **Employees:** 340
- **Plant Size:** 14,060 m<sup>2</sup>
- **Functions**
  - Engineering, Testing and Validation
  - Prototype Battery Production
  - Battery Pack Production



## Overview

- System description
- System requirements
  - Power ability and system resistance
  - Energy content and system capacity
  - Life time requirements
- Design of algorithm
  - Cyclic ageing
  - Calendaric ageing
  - Online reference resistance determination
  - Usage logging
- Validation
  - System test on test bench
  - EHEV – Eco Drive for Hybrid Electric Vehicles
  - Systems returned from customer



## System description

- Technical details
  - Energy content: 4,9 kWh
  - Power: 120 kW nom. voltage: 600 V
  - Weight: 210 kg volume: 230 l
  - Cells: cylindrical – Li-Iron Phosphate 3,5 Ah
    - 2 cells in parallel
    - 192 cell pairs in series
  - Number of modules: 11 (10+1)
  - Dimensions (L/W/D): 740mm/615mm/505mm
  - Design start: 02/2007
  - SOP: Q3/2009 – first to market

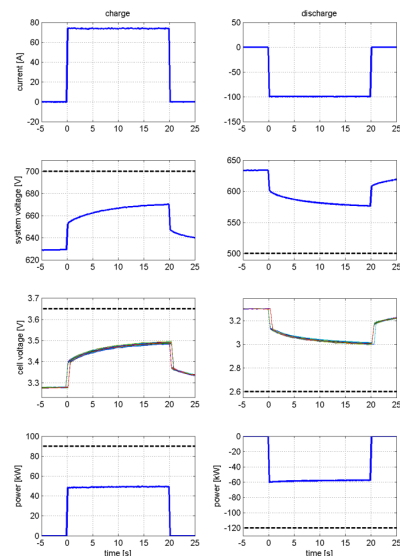


- HEV application
  - High power
  - High energy throughput
  - Up to 5000 operating hours a year



## Power ability and system resistance

- System power ability is depending on
  - System and cell voltage range
  - Temperature
  - State of charge (SOC)
  - Pulse duration
- Voltage range
  - System: 500V to 700V
  - Cell: 2,6V to 3,65V
- HPPC (Hybrid Pulse Power Characterisation)
  - Same current profile to be used for entire system life time



## Power ability and system resistance

- System power ability is depending on
  - System and cell voltage range
  - Temperature
  - State of charge (SOC)
  - Pulse duration

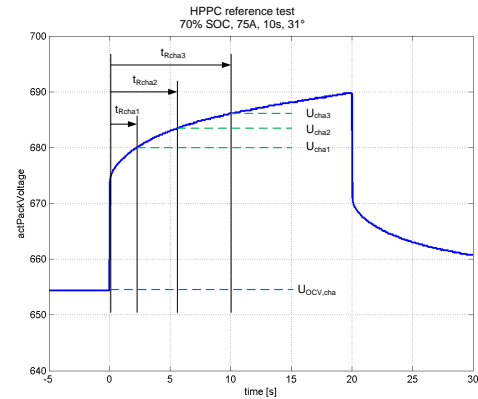
- Voltage range
  - System: 500V to 700V
  - Cell: 2,6V to 3,65V

- Internal resistance

$$R_{10s} = \frac{U_{10s} - U_{OCV}}{I}$$

- Maximum power ability

$$P_{10s,max} = \frac{U_{max} - U_{OCV}}{R_{10s}} U_{max}$$

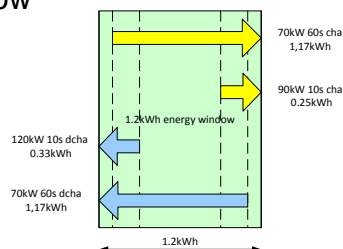


## Energy content and system capacity

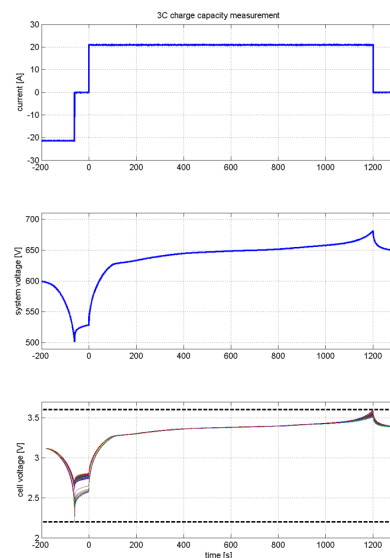
- System energy content is depending on
  - Cell voltage range
  - Temperature
  - Current (C-rate)

- Voltage range
  - Cell: 2,2V to 3,6V

- Energy window

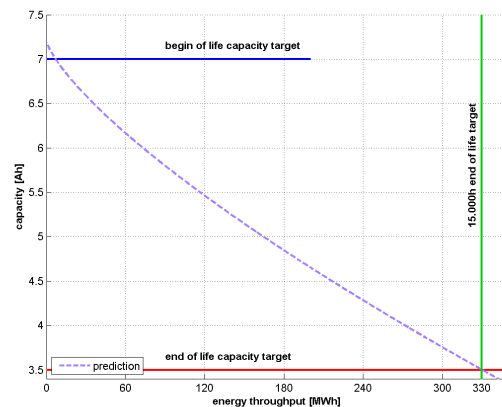


- SOC window is chosen according to power demand and power ability



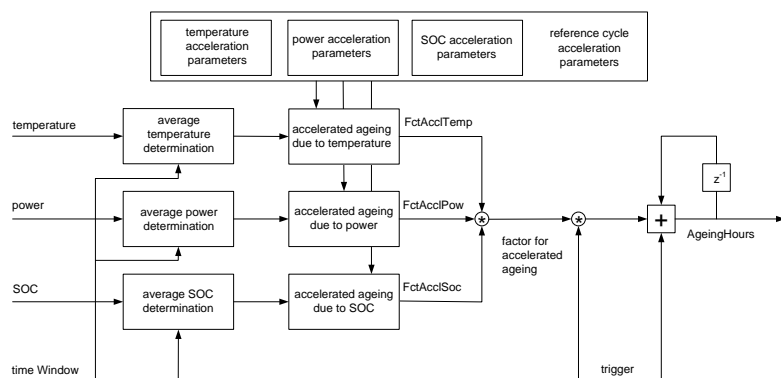
## Life time requirements

- Begin of Life (BoL)
  - Discharge power 120kW, 31°C, 10s
  - Charge power 90kW, 31°C, 10s
  - Energy window 1.200Wh
    - SOC window 30% to 60% of BoL capacity
- End of Life (EoL)
  - Discharge power 90kW, 31°C, 10s
  - Charge power 67.5kW, 31°C, 10s
  - Energy window 600Wh
    - SOC window of 30% to 45% of BoL capacity
- 15.000 operating hours
  - 5.000 operating hours a year
- Cycle definition – reference driving cycle
  - CBR85 (city bus route Gothenburg)
  - Average power 22kW
- Energy throughput 330MWh



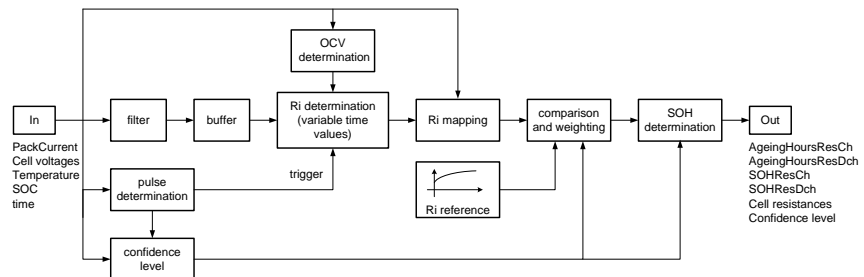
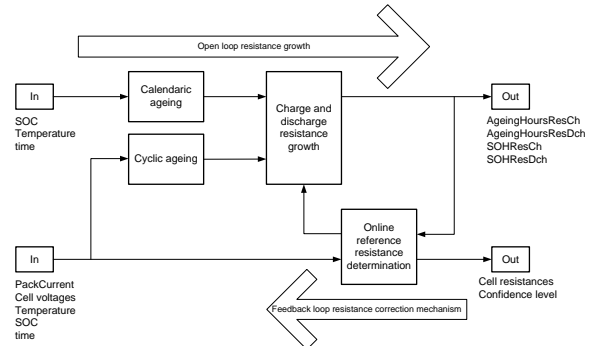
## Design of algorithm – cyclic ageing

- Usage of the system in real application must be mapped to ageing caused by reference driving cycle
  - Open loop determination of resistance growth based on ageing hours
- Main influencing parameters
  - Temperature
  - Power
  - SOC
- Data base
  - Cell testing results
  - System testing results



## Design of algorithm – updates

- Calendric ageing
  - Ageing based on storage test data on cell level
  - Main influencing parameters
    - temperature
    - SOC
  - Real time clock (RTC) necessary
- Online reference resistance determination
  - Determination of system (cell) resistance during operation



9/9/2015

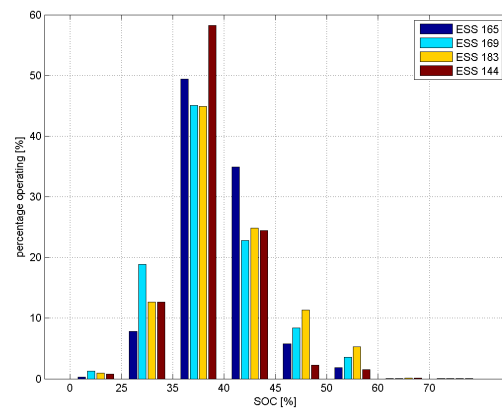
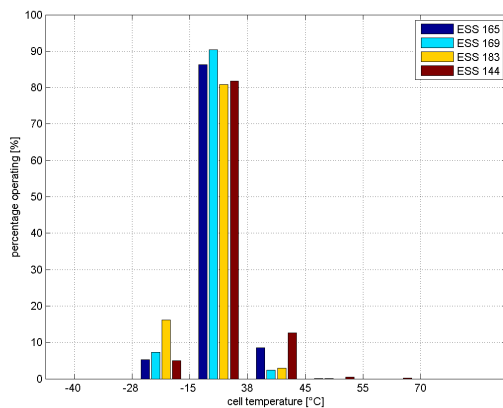
Author: Stefan Doczy

Disclosure or duplication without consent is prohibited

11

## Design of algorithm – usage logging

- Data stored during operation to ensure proper usage of the system
  - Cell temperature histogram
  - SOC histogram
  - Power limit violation
  - Cell voltage violation



9/9/2015

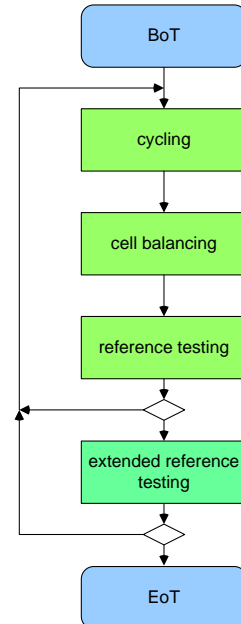
Author: Stefan Doczy

Disclosure or duplication without consent is prohibited

12

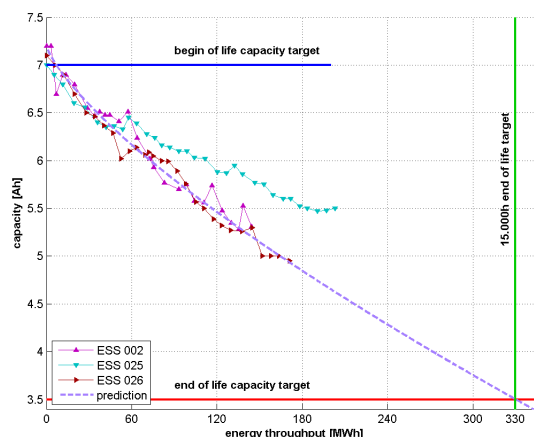
## Validation – system test on test bench

- Test start April 2009
  - 3 systems using different coolant inlet temperature
  - Reference driving cycle CBR85
- ESS 002
  - Coolant inlet temperature up to 47°C
  - Same temperature for 2 reference driving cycles (2,5h)
- ESS 025
  - Coolant inlet temperature 27°C
- ESS 026
  - Coolant inlet temperature up to 52°C
  - Same temperature for approx. 2 weeks



## Validation – system test on test bench

- Test start April 2009
  - 3 systems using different coolant inlet temperature
  - Reference driving cycle CBR85
- First part finished August 2010
  - 200MWh
  - 9.000 operating hours
- ESS 002
  - Test stopped August 2010
- ESS 025
  - Test continued to April 2015
  - 315MWh
  - 14.000 operating hours
- ESS 026
  - Test stopped August 2010
  - Disassembled
  - Capacity check for 192 cell pairs





## Validation – EHEV

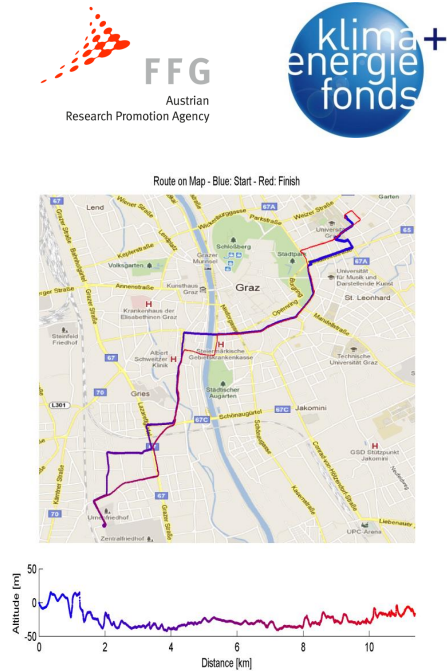
### • EHEV - Eco Drive for Hybrid Electric Vehicles

- Analysis of system usage in the vehicle
- Analysis of battery ageing
- Analysis of influence of different driving styles on ageing of the battery

### • ESS 170 - System equipped with additional measurement devices

- GPS module
- UMTS data module for data exchange

| Date:                   |            | 07/16/2012             |           |
|-------------------------|------------|------------------------|-----------|
| Start Time:             | 04:57:37   | Stop Time:             | 06:01:26  |
| Distance:               | 11.38 km   | Run Time:              | 1h 3m 49s |
| Difference in Altitude: | 894.48 m   | Average Altitude:      | 402.1 m   |
| Increasing Altitude: ↗  | 438.88 m   | Decreasing Altitude: ↘ | -455.60 m |
| Maximum Speed:          | 24.47 km/h | Average Speed:         | 5.8 km/h  |
| Energy Throughput:      | 13.58 kW/h | SOH:                   | 100.00 %  |
|                         |            |                        |           |
|                         | Minimum    | Maximum                | Average   |
| Power:                  | -99.98 kW  | 99.68 kW               | 12.79 kW  |
| Current:                | -194.65 A  | 153.35 A               | 20.42 A   |
| Voltage:                | 569.15 V   | 672.85 V               | 633.51 V  |
| Cell Voltage:           | 2.93 V     | 3.53 V                 | 3.31 V    |
| Ambient Temperature:    | 19.90 °C   | 21.80 °C               | 21.00 °C  |
| SOC:                    | 34.09 %    | 41.23 %                | 38.35 %   |
|                         |            |                        |           |
|                         | Start      | Stop                   | Δ         |
| SOC:                    | 38.53 %    | 37.97 %                | 0.56 %    |



9/9/2015

Author: Stefan Doczy

Disclosure or duplication without consent is prohibited

15

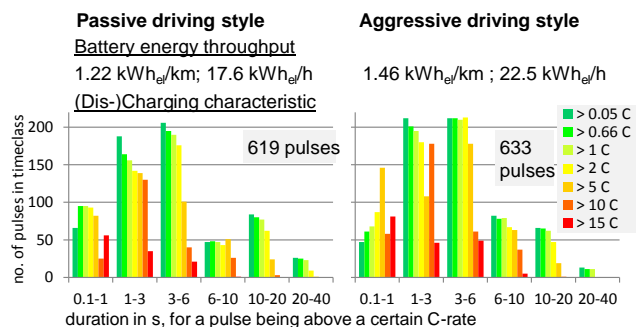
## Validation – EHEV

### • Influence of different driving styles on ageing of the battery

|         | duration | temp_avg | SOC_avg | P_avg | energy | rel ageing |
|---------|----------|----------|---------|-------|--------|------------|
|         | [s]      | [°C]     | [%]     | [kW]  | [kWh]  | [1]        |
| pass_T1 | 5320     | 27,9     | 38,4    | 17,1  | 25,56  | 0,813      |
| pass_T2 | 5050     | 32,1     | 38,8    | 18,8  | 26,61  | 0,956      |
| aggr_T1 | 4870     | 33,2     | 37,9    | 23,3  | 31,75  | 1,120      |
| aggr_T3 | 4625     | 31,2     | 37,4    | 23,5  | 30,28  | 1,062      |

### • Conclusion

- Passive driving style
  - predicted life time 11% or 1.650 operating hours longer
  - energy throughput 300MWh
- Aggressive driving
  - predicted life time 7% or 1.050 operating hours shorter
  - energy throughput 326MWh



9/9/2015

Author: Stefan Doczy

Disclosure or duplication without consent is prohibited

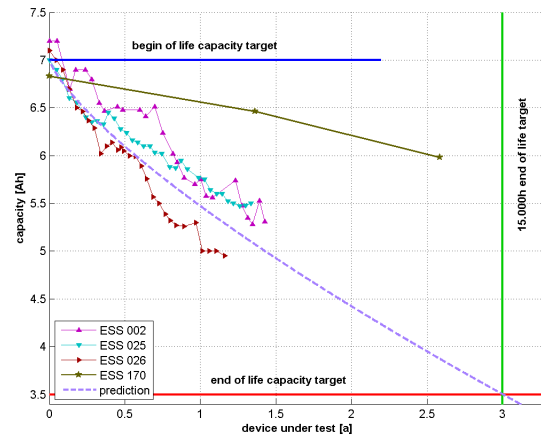
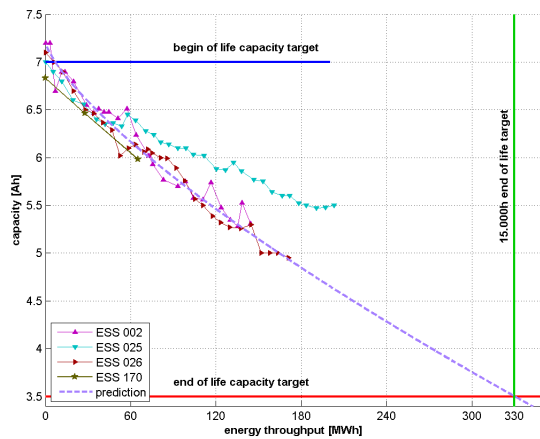
16

## Validation – EHEV



- 3 reference measurements on test bench

| date     | operating hours | energy throughput | capacity |
|----------|-----------------|-------------------|----------|
|          | [h]             | [MWh]             | [Ah]     |
| 20101222 | 0,0             | 0,0               | 6,83     |
| 20120502 | 2344,5          | 27,9              | 6,46     |
| 20130723 | 5251,4          | 65,2              | 5,98     |



9/9/2015

Author: Stefan Doczy

Disclosure or duplication without consent is prohibited

17

## Validation – systems returned from customer



- 3 systems returned April to June 2013
- 1 system returned June 2015
- Reference measurements
  - Capacity determination
  - HPPC

|        | operating hours | energy throughput | capacity | production date | reference measurement |
|--------|-----------------|-------------------|----------|-----------------|-----------------------|
|        | [h]             | [MWh]             | [Ah]     |                 |                       |
| ESS165 | 13626,3         | 184               | 5,67     | 20100608        | 20130614              |
| ESS169 | 9932,5          | 143,6             | 6,06     | 20100616        | 20130426              |
| ESS183 | 10177,4         | 137,0             | 5,61     | 20100817        | 20130426              |
| ESS144 | 23994,2         | 338,6             | 4,00     | 20100505        | 20150707              |

9/9/2015

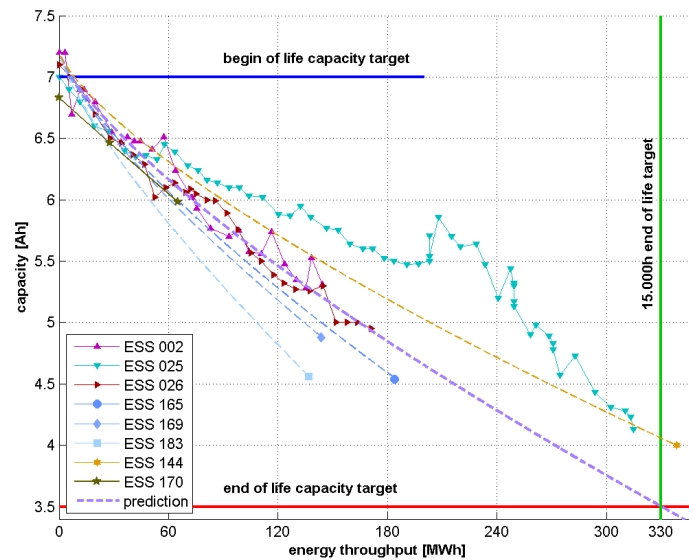
Author: Stefan Doczy

Disclosure or duplication without consent is prohibited

18

## Validation – summary

- Capacity vs. energy throughput



9/9/2015

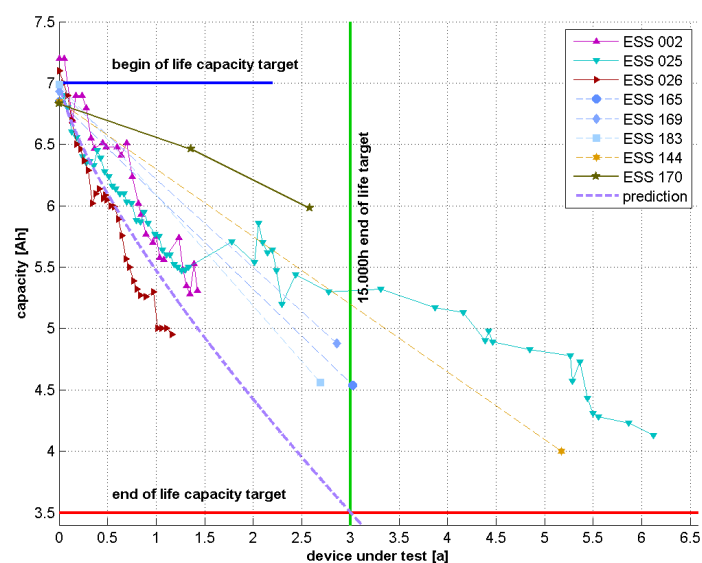
Author: Stefan Doczy

Disclosure or duplication without consent is prohibited

19

## Validation – summary

- Capacity vs. time



9/9/2015

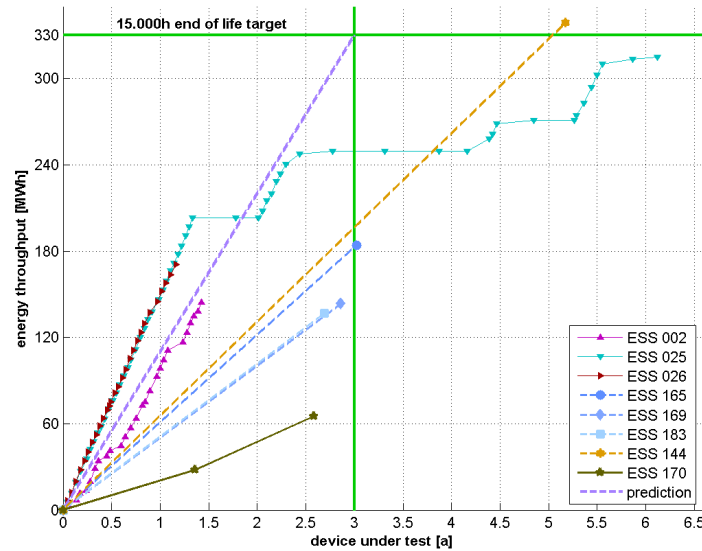
Author: Stefan Doczy

Disclosure or duplication without consent is prohibited

20

## Validation – summary

- Energy throughput vs. time



9/9/2015

Author: Stefan Doczy

Disclosure or duplication without consent is prohibited

21

## Validation – SOH algorithm

- Comparison of ageing hours value determined during usage of the battery in the vehicle to ageing hours values determined due to reference measurements on test bench
  - SOHcapacity → AgeingHoursCap
  - SOHResCh → AgeingHoursResCh
  - SOHResDch → AgeingHoursResDch

|         | SOH algorithm |             | reference measurements |                      |                       |
|---------|---------------|-------------|------------------------|----------------------|-----------------------|
|         |               |             | capacity               | HPPC test            |                       |
|         | operating     | AgeingHours | AgeingHours<br>Cap     | AgeingHours<br>ResCh | AgeingHours<br>ResDch |
|         | [h]           | [h]         | [h]                    | [h]                  | [h]                   |
| ESS 165 | 13626         | 10913       | 5905                   | 9497                 | 9359                  |
| ESS 169 | 9933          | 8861        | 4318                   | 6529                 | 6648                  |
| ESS 183 | 10177         | 8442        | 6164                   | 7090                 | 7137                  |
| ESS 144 | 23994         | 18284       | 14062                  | 16436                | 11589                 |
| ESS 170 | 5251          | 4048        | 4621                   | 5533                 | 5404                  |

9/9/2015

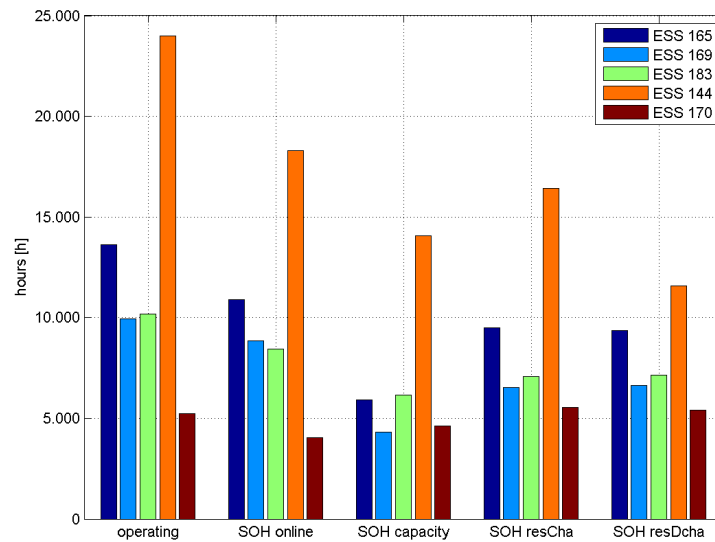
Author: Stefan Doczy

Disclosure or duplication without consent is prohibited

22

## Validation – SOH algorithm

- Comparison of ageing hours value determined during usage of the battery in the vehicle to ageing hours values determined due to reference measurements on test bench



# Control-oriented Turbocharger Modeling

**Markus Freistätter<sup>ab</sup>**

**Robert Bauer<sup>b</sup>**

**Nicolaos Dourdoumas<sup>a</sup>**

**Wilfried Rossegger<sup>b</sup>**

The use of turbochargers in the automotive industry has grown significantly over the past years. Almost every Diesel engine and an increasing number of gasoline engines are equipped with a turbocharger. Research and testing of turbochargers is often done using hot gas test beds. In such an unit a mixture of natural gas and air is burnt in a combustion chamber and the hot burnt gas is used to drive the turbine. Models are needed of the test bench itself as well as of the device under test (the turbocharger).

There already exists a variety of turbocharger models of differing complexity. Kessel presents in [1] very detailed models for turbine and compressor. However, they don't fit the measured data obtained on the test bench very well. The newly developed model resembles one of the methods of Moraals overview in [2] as physical modeling is combined with curve fitting. The modeled quantities include mass flow, pressure ratio, efficiency and temperatures of compressor and turbine. Compressor instabilities, the influence of Wastegate valves and Variable Geometry Turbines are considered as well.

- [1] KESSEL, JENS-ACHIM: *Modellbildung von Abgasturboladern mit variabler Turbinengeometrie an schnellaufenden Dieselmotoren*. Doktorarbeit, TU Darmstadt, Mai 2004.
- [2] MORAAL, PAUL und ILYA KOLMANOVSKY: *Turbocharger modeling for automotive control applications*. Technischer Bericht, SAE Technical Paper, 1999.

---

<sup>a</sup>Institut für Regelungs- und Automatisierungstechnik, Technische Universität Graz, Kopernikusgasse 24/II, 8010 Graz, E-Mail: [markus.freistaetter@tugraz.at](mailto:markus.freistaetter@tugraz.at), [nicolaos.dourdoumas@tugraz.at](mailto:nicolaos.dourdoumas@tugraz.at)

<sup>b</sup>Kristl, Seibt & Co GmbH, Baiernstraße 122a, 8052 Graz, E-Mail: [robert.bauer@ksengineers.at](mailto:robert.bauer@ksengineers.at), [wilfried.rossegger@ksengineers.at](mailto:wilfried.rossegger@ksengineers.at)

# Control-oriented Turbocharger Modelling

Markus Freistätter, Institute of Automation and Control

09.09.2015



► [www.tugraz.at](http://www.tugraz.at)



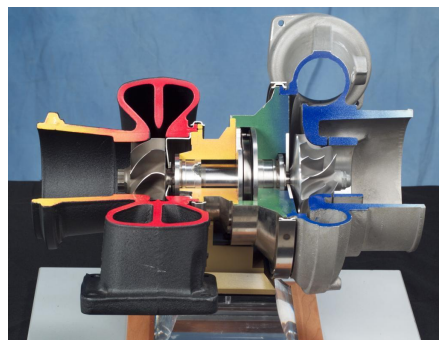
## Turbocharger

Turbine and compressor wheel

Exhaust gas drives turbine

Turbine drives compressor

- Compressed air leads to increase of power or efficiency



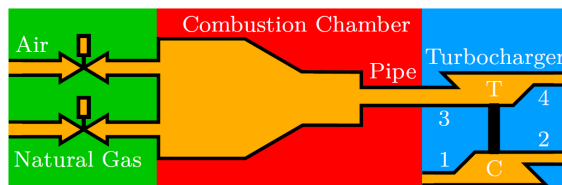
Markus Freistätter, Institute of Automation and Control  
09.09.2015



## Hot gas test bed

Relevant quantities (control):

- Turbine mass flow (speed)
- Hot gas temperature
- Compressor mass flow

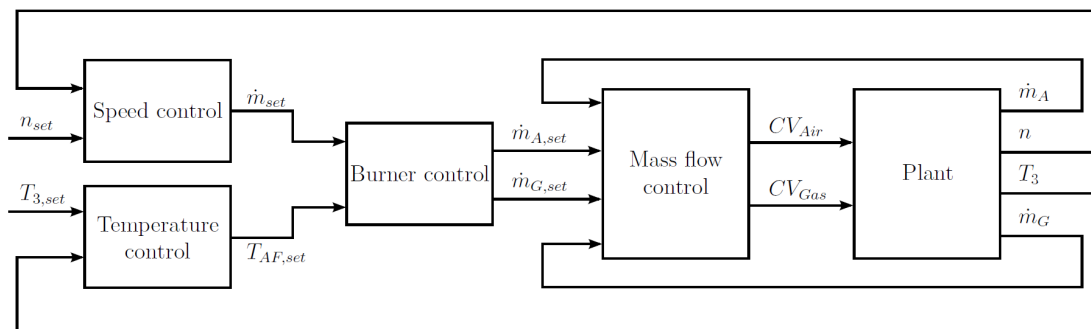


Markus Freistätter, Institute of Automation and Control  
09.09.2015

## Hot gas test bed control

Modelling:

- Temperature
- Mass flow and pressure
- Turbocharger



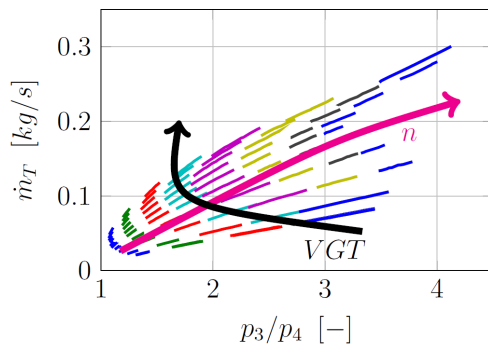
Markus Freistätter, Institute of Automation and Control  
09.09.2015



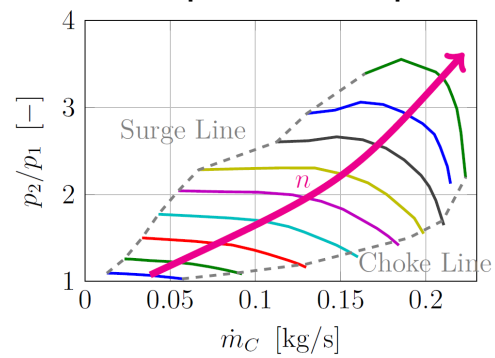
## Turbocharger maps

Model

Turbine map



Compressor map



- Simple models
- Few parameters
- Cover the essential effects

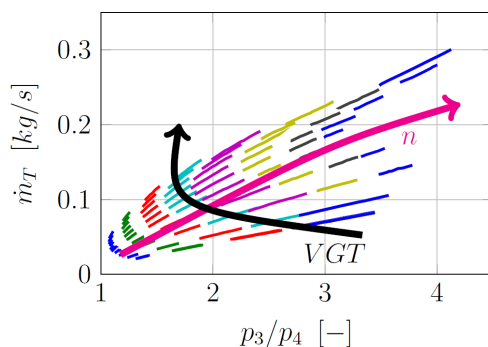
Markus Freistätter, Institute of Automation and Control  
09.09.2015



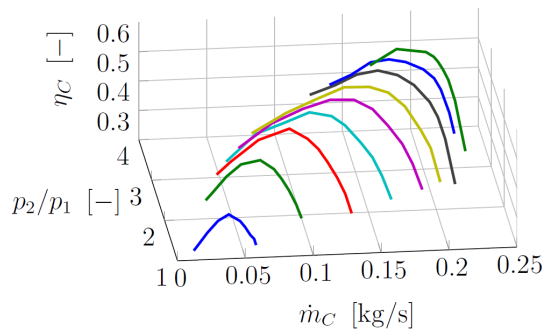
## Turbocharger maps

Model

Turbine map



Compressor map



- Simple models
- Few parameters
- Cover the essential effects

Markus Freistätter, Institute of Automation and Control  
09.09.2015



## Motivation for new model

Models based on turbine and compressor power balance [1] don't fit well

$$J_{TC}\dot{\omega}_{TC} = \Theta_C + \Theta_T + \Theta_F$$

with

$$\Theta_C = \dot{m}_C(r_2 C_{2,\phi} - r_3 C_{3,\phi})$$

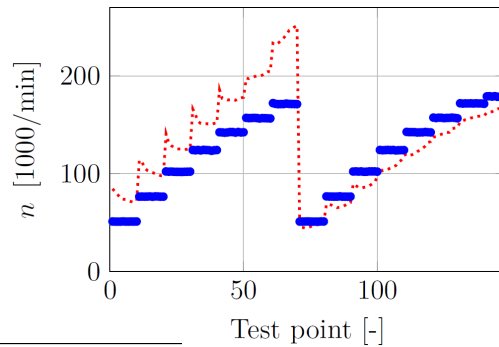
$$\Theta_T = \dot{m}_T(r_4 C_{4,\phi} - r_5 C_{5,\phi})$$

$$\Theta_F = -k_F \omega_{TC}$$

...

Approximation:

$$n = \frac{\dot{m}_C}{4c_n} - \frac{k_F}{4c_M \dot{m}_C} + \sqrt{\left(\frac{\dot{m}_C}{4c_n} - \frac{k_F}{4c_M \dot{m}_C}\right)^2 + \frac{k_{VGT} \dot{m}_T^2}{2c_M \dot{m}_C}}$$

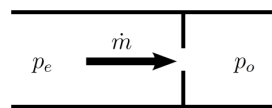


- [1] Kessel, J.-K.: Modellbildung von Abgasturboladern mit variabler Turbinengeometrie an schnelllaufenden Dieselmotoren. PhD Thesis. TU Darmstadt, 2003.

Markus Freistätter, Institute of Automation and Control  
09.09.2015

## Basic models

Orifice:

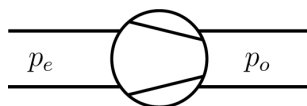


$$\Delta p = p_e - p_o = R_e \dot{V}^2$$

$$R_e = \frac{\rho}{2\alpha^2 A^2}$$

$\alpha$  ... flow coefficient

Fan:



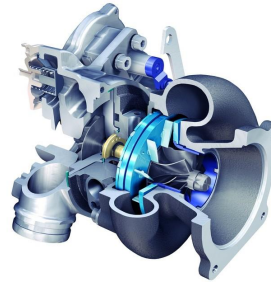
$$\Delta p = p_o - p_e = c f^2$$

Markus Freistätter, Institute of Automation and Control  
09.09.2015

## Turbine mass flow (1/2)

Orifice:

$$\dot{V}_T = \sqrt{\frac{p_3 - p_4}{R_e}}$$



Turbine mass flow:

$$\begin{aligned} \dot{m}_T &= \rho_3 \dot{V}_T = \rho_3 \sqrt{p_3 - p_4} \sqrt{\frac{2\alpha^2 A^2}{\rho_3}} = \\ &= k_{0,T} \sqrt{\frac{p_3}{R_{Gas} T_3}} \sqrt{p_3 - p_4} \end{aligned}$$

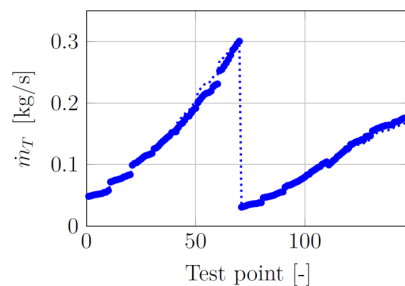
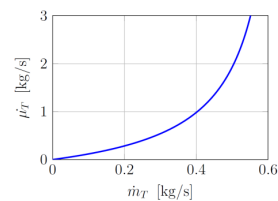
Problem: Choke line

## Turbine mass flow (2/2)

Choke line  $\Rightarrow$  virtual mass flow (no physical meaning)

$$\frac{1}{\dot{\mu}_T} = \frac{1}{\dot{m}_T} - \frac{1}{\dot{m}_{Ch,T}}$$

$$\dot{\mu}_T = k_{0,T} \sqrt{\frac{p_3}{R_{Gas} T_3}} \sqrt{p_3 - p_4}$$



Neglect compressor influence

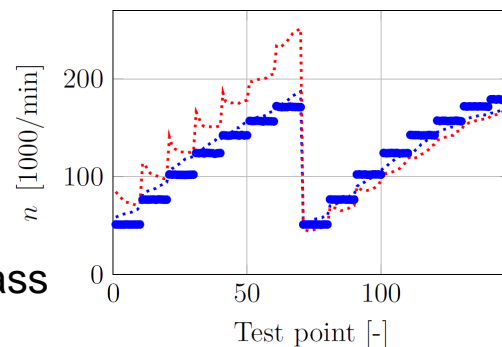
## Turbocharger speed

Power balance model:

$$n = \frac{\dot{m}_C}{4c_n} - \frac{k_F}{4c_M \dot{m}_C} + \sqrt{\left( \frac{\dot{m}_C}{4c_n} - \frac{k_F}{4c_M \dot{m}_C} \right)^2 + \frac{k_{VGT} \dot{m}_T^2}{2c_M \dot{m}_C}}$$

New model:

$$n = \frac{c_{n,T}}{\sqrt{k_{0,T}}} \dot{m}_T \sqrt{\frac{R_{Gas} T_3}{p_3}}$$

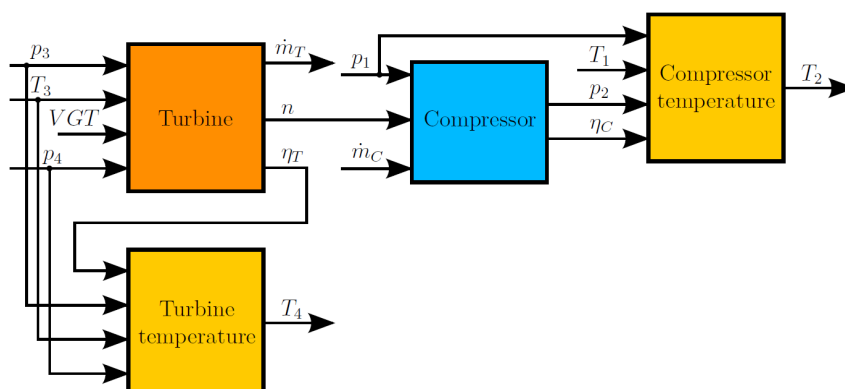
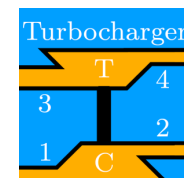


Dynamic behaviour: Low pass

## Turbocharger modelling

Speed and compressor mass flow control

Turbine and compressor models

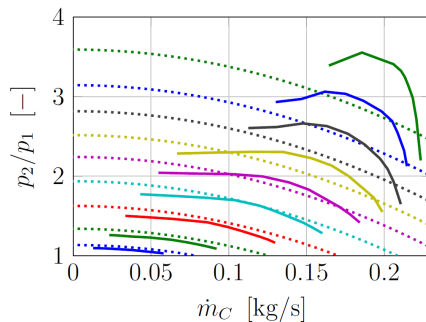
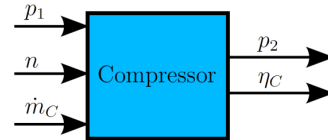


## Compressor pressure (1/3)

Combine orifice with fan

$$p_1 - R_1 \dot{V}^2 = p_2 - c f^2$$

Approximation:  $\frac{p_2}{p_1} = 1 + c_{n,C} n^2 - c_{m,C} \dot{m}_C^2$



Good:

- Low speeds
- Maximum pressure rise

Bad:

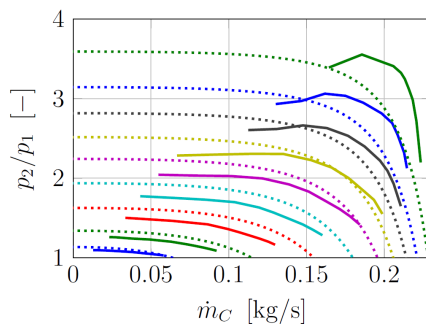
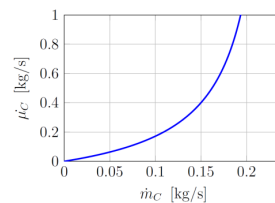
- Choke line

## Compressor pressure (2/3)

Choke line  $\Rightarrow$  virtual mass flow (no physical meaning)

$$\frac{1}{\dot{\mu}_C} = \frac{1}{\dot{m}_C} - \frac{1}{\dot{m}_{Ch}}$$

$$\frac{p_2}{p_1} = 1 + c_{n,C} n^2 - c_{m,C} \dot{\mu}_C^2$$



Good:

- Choke line

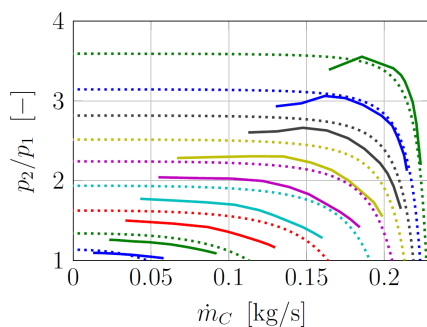
Bad:

- Speed dependency

## Compressor pressure (3/3)

Speed dependent weighting:

$$\frac{p_2}{p_1} = 1 + c_{n,C} n^2 - c_{m,C} \frac{\dot{m}_C^2}{n^4} \quad \text{with} \quad \frac{1}{\dot{m}_C} = \frac{1}{\dot{m}_C} - \frac{1}{\dot{m}_{Ch}}$$



Cause – Effect?

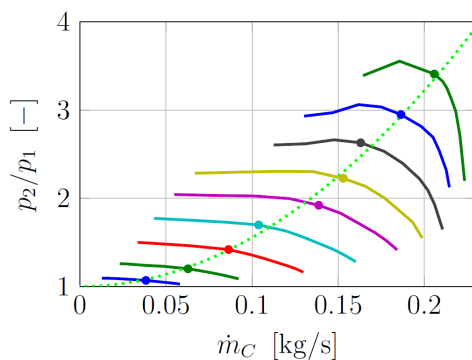
Input: Mass flow

Output: Pressure ratio

Dynamic behaviour: Low pass

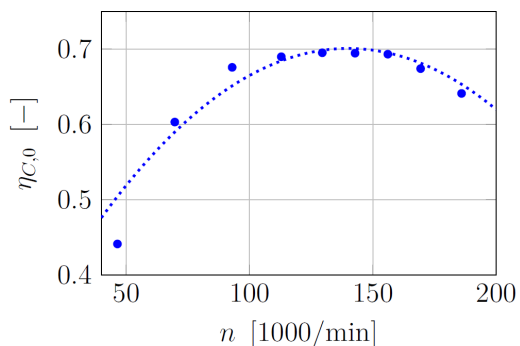
## Isentropic compressor efficiency (1/2)

Points of maximum efficiency



$$\frac{p_2^*}{p_1} = 1 + c_{opt} \dot{m}_C^2$$

Maximum efficiency against speed

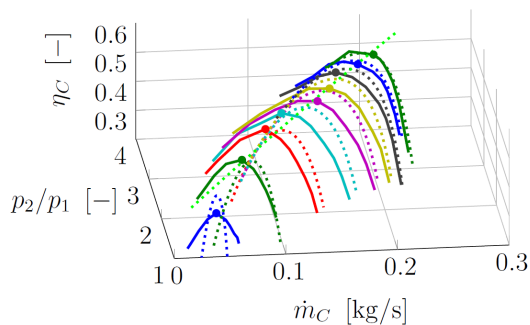


$$\eta_{C,0} = \beta n^2 + \gamma n + \delta$$

## Isentropic compressor efficiency (2/2)

Maximum efficiency and distance to it

$$\eta_C = \eta_{C,0} - \frac{c_\eta}{n^2} (\dot{m}_{C,\eta_{opt}} - \dot{m}_C)^2 \quad \eta_{C,0} = \beta n^2 + \gamma n + \delta$$



$$\dot{m}_{C,\eta_{opt}} = \sqrt{\frac{\frac{p_2}{p_1} - 1}{c_{opt}}}$$

## Compressor outlet temperature (1/2)

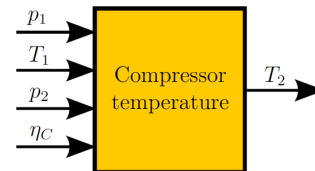
Ideal gas law:  $pV = mRT$

Isentropic change:

$$\frac{T_{2,is}}{T_1} = \left(\frac{p_2}{p_1}\right)^{\frac{\kappa-1}{\kappa}} \quad \kappa \dots \text{isentropic exponent}$$

Isentropic efficiency (compressor):  $\eta_C = \frac{T_{2,is} - T_1}{\bar{T}_2 - T_1}$

$$\bar{T}_2 = T_1 \frac{\eta_C - 1 + \frac{p_2}{p_1}^{\frac{\kappa-1}{\kappa}}}{\eta_C}$$



## Compressor outlet temperature (2/2)

Dynamic behaviour is modelled similar to thermal model of combustion chamber [2]

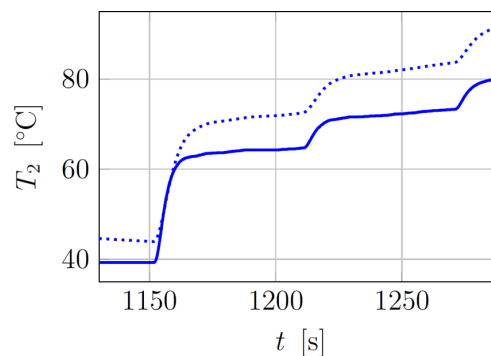
$$\frac{dx}{dt} = \mathbf{A}(\dot{m}) \mathbf{x} + \mathbf{b}(\dot{m}) u$$

$$y = \mathbf{c}^T \mathbf{x}$$

with

$$u = \bar{T}_2$$

$$y = T_2$$



[2] Bauer, R.: Modellierung und modellbasierte Regelungsstrategien am Beispiel einer Biomasse-Feuerungsanlage

Markus Freistätter, Institute of Automation and Control  
09.09.2015



## Conclusion

Hot gas test beds and turbocharger testing

Necessity of turbocharger modelling

Turbocharger model consisting of

- Pressure ratio
- Efficiency
- Temperature

for turbine and compressor

Markus Freistätter, Institute of Automation and Control  
09.09.2015





# HOSM Based Observation, Identification and Output Based Control

**Leonid Fridman**

Departamento de Ingenieria de Control y Robotica,  
Facultad de Ingenieria UNAM, Mexico

The key point of this study are *Robust Exact Differentiators*[1,2]. Such differentiators in the absence of noise, converge to the true derivatives of the signal after a finite time. Moreover, they provide best possible asymptotic precision with respect to sampling steps and measurement noise.

The paper presents The presentation contains the overview of results of Sliding Mode Control Laboratory on higher order sliding mode observation.

*Fixed-time robust exact differentiators*[3,4].An arbitrary order differentiator that, in the absence of noise, converges to the true derivatives of the signal after a fixed time independent of the initial differentiator error is presented.

*Robust exact observation of strongly observable and detectable systems*[5-7]. A global observer is designed for strongly detectable LTI systems with bounded unknown inputs. The design of the observer is based on three steps. Firstly, the system is extended taking the unknown inputs (and possibly some of their derivatives) as a new state; then, using a HSOM differentiator, a new output of the system is generated in order to fulfil, what we will call, the strong observability condition, which finally decomposing the system, in new coordinates, into two subsystems; the first one being unaffected directly by the unknown inputs, and the state vector of the second subsystem is obtained directly from the original system output.

Such decomposition permits designing of a Luenberger observer for the first subsystem, which satisfies the strong observability condition, i.e. all the outputs have relative degree one w.r.t. the unknown inputs. This procedure enables one to estimate the state and the unknown inputs using the least number of differentiations possible.

*Robust exact output control based on HOSM observation*[8,9]. Semi-global finite-time exact stabilization of linear time-invariant systems with matched disturbances is attained using a dynamic output feedback, provided the system is controllable, strongly observable and the disturbance has a bound affine in the state norm. The novel non-homogeneous HOSM control strategy is based on the gain adaptation of both the controller and the differentiator included in the feedback. A robust criterion is developed for the detection of differentiator convergence to turn on the controller at a proper time.

*Robust exact output control based on HOSM identification of perturbation*[10-12].The problem of robust exact output control for linear systems with smooth bounded matched unknown inputs is considered. The higher order sliding mode observers provide both theoretically exact observation and unknown input identification. A methodology is proposed to select the most adequate output control strategy for matched perturbations compensation. The possibility for theoretically exact uncertainties compensation using signals identified by HOSM observers. Towards this aim, we modify the hierarchical super-twisting observer in order to have the best possible observation and identification accuracy. Then,

two controllers are compared. The first one is an integral sliding mode controller based on the observed values of the state variables. The other strategy is based on the direct compensation of matched perturbations using their identified values. The performance of both controllers is estimated in terms of the deterministic noise upper bounds, sampling step and execution time. Based on these estimations, the designer may select the proper controller for the system.

A collection of the papers with different type of HOSM based observers, can be found on the web site <http://verona.fi-p.unam.mx/~lfridman/>

## REFERENCES

1. Levant, A. (1998). Robust exact differentiation via sliding mode technique. *Automatica*, 34(3), 379–384.
2. Levant, A. (2003). High-order sliding modes: differentiation and output feedback control. *International Journal of Control*, 76(9–10), 924–941.
3. Cruz-Zavala, E.; Moreno, J.; Fridman, L. Uniform Robust Exact Differentiator, *IEEE TRANSACTIONS ON AUTOMATIC CONTROL*, 2011, v.56, no. 11, pp.2727-2733, doi:10.1109/TAC.2011.2160030
4. M. T. Angulo, J. Moreno, and L. Fridman. Robust Exact Uniformly Convergent Arbitrary Order Differentiator, *Automatica*, Volume 49, Issue 8, August 2013, Pages 2489-2495, doi:10.1016/j.automatica.2013.04.034
5. F. J. Bejarano, L. Fridman. High order sliding mode observer for linear systems with unbounded unknown inputs, *International Journal of Control* 2010, v.83, no. 9, pp.1920 — 1920.
6. L. Fridman, J. Dávila, A. Levant. High-order sliding-mode observation for linear systems with unknown inputs, *Nonlinear Analysis: Hybrid Systems*, v. 5, no. 2, 189-205, 2011.
7. L. Fridman, Y. Shtessel, C. Edwards and Xing-Gang Yan. Higher-order sliding-mode observer for state estimation and input reconstruction in nonlinear systems *International Journal of Robust and Nonlinear Control* 18(4-5), 2008, pp. 399-413
8. M. T. Angulo, L. Fridman and A. Levant. Output-feedback finite-time stabilization of disturbed LTI systems; *Automatica*, Volume 48, Issue 4, April 2012, Pages 606-611 doi:10.1016/j.automatica.2012.01.003.
9. M. T. Angulo, L. Fridman, and J. Moreno. Output feedback finite-time stabilization of distributed feedback linearizable nonlinear systems, *Automatica*, 49(9), 2767-2773, <http://dx.doi.org/10.1016/j.automatica.2013.05.013>
10. A. Ferreira, F. J. Bejarano, L. Fridman. Robust Control With Exact Uncertainties compensation: With or Without Chattering? *IEEE TRANSACTIONS ON CONTROL SYSTEMS, TECHNOLOGY*, 2011, 19(5), p. 969 – 975
11. A. Ferreira de Loza, E. Punta, Leonid Fridman, G. Bartolini, S. Delprat. Nested backward compensation of unmatched perturbations via HOSM observation. *Journal of Franklin Institute*, 2014, v. 351, no 4, pp.2397–2410, doi:10.1016/j.jfranklin.2013.12.011
12. Ferreira, Alejandra; Cieslak, Jérôme ; Henry, David; Zolghadri, Ali; Fridman, L. Output tracking of systems subjected to perturbations and a class of actuator faults based on HOSM observation and identification, *Automatica*, v. 51.

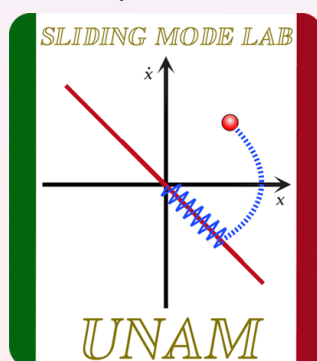
# Higher Order Sliding Mode Observers

## Theory and Practice

**Leonid Fridman**

UNAM

Retzhof, September 8<sup>th</sup>, 2015



1



Francisco Bejarano



Jorge Davila



Alejandra Ferreira



Marco Tulio Angulo



Emmanuel Cruz



Héctor Ríos

2

## Outline

- ① Background
  - Unknown input observers
- ② Strong Observability - Invariant Zeros - Relative Degree
  - Relation of concepts for SUIISO Systems
  - HOSM Observers for linear systems with unknown inputs
- ③ Applications

3

## Outline

- ① Background
  - Unknown input observers
- ② Strong Observability - Invariant Zeros - Relative Degree
  - Relation of concepts for SUIISO Systems
  - HOSM Observers for linear systems with unknown inputs
- ③ Applications

4

## Outline

### 1 Background

- Unknown input observers

### 2 Strong Observability - Invariant Zeros - Relative Degree

- Relation of concepts for SUIISO Systems
- HOSM Observers for linear systems with unknown inputs

### 3 Applications

5

## Linear systems with unknown inputs

### The system.

Consider

$$\Sigma : \begin{cases} \dot{x} = Ax + Bu + Dw, & x(0) = x_0, \\ y = Cx, \end{cases} \quad (1)$$

where

- $x(t) \in \mathbb{R}^n$  is the state,  $w(t) \in \mathbb{R}^m$  is the **unknown input**;
- $u(t) \in \mathbb{R}^q$  is the control,  $y(t) \in \mathbb{R}^p$  is the measured output.

### Strong Observability:

The system is strongly observable if for any  $x(0)$  and  $w(t)$  it follows from  $y(t) \equiv 0 \ \forall t \geq 0$  that  $x(t) \equiv 0$  [Hautus: 83].

### Strong Detectability:

The system is strongly detectable if for any  $x(0)$  and  $w(t)$  it follows from  $y(t) \equiv 0 \ \forall t \geq 0$  that  $x(t) \rightarrow 0$  as  $t \rightarrow \infty$  [Hautus: 83].

6

### Invariant zeros

The Rosenbrock of  $(A, C, D)$ :

$$R(s) = \begin{bmatrix} sI - A & -D \\ C & 0 \end{bmatrix}.$$

The values  $s_0 \in \mathbb{C}$  such that  $\text{rank } R(s_0) < n + m$  are called **invariant zeros** of  $(A, C, D)$ .

7

## Linear systems with unknown inputs

### Problem formulation:

Estimate  $x(t)$  **based on output measurements only**  $\{y(t), t \in [0, T]\}$ .

### State reconstruction without differentiation[Hautus: 1983]

- The system does not have invariant zeroes.
- All the matrices are known i.e.,  $A, B, C, D$ .
- $C$  and  $D$  are full rank matrices.
- If  $\text{rank}(C) = p$  and  $\text{rank}(D) = m$ , then  $p \geq m$ .
- $\text{rank}(CD) = m$  **Relative degree condition**.

### Canonical form

$$\begin{pmatrix} dy^\perp/dt \\ dy_1/dt \\ dy_2/dt \end{pmatrix} = \begin{pmatrix} A_{11} & A_{12} & A_{13} \\ A_{21} & A_{22} & A_{23} \\ A_{31} & A_{32} & A_{33} \end{pmatrix} \begin{pmatrix} y^\perp \\ y_1 \\ y_2 \end{pmatrix} + Bu + \begin{pmatrix} 0 \\ 0 \\ w(t) \end{pmatrix}$$

8

## Outline

### 1 Background

- Unknown input observers

### 2 Strong Observability - Invariant Zeros - Relative Degree

- Relation of concepts for SUIISO Systems
- HOSM Observers for linear systems with unknown inputs

### 3 Applications

9

## Mechanical system

Let us consider the following mechanical system:

$$M(q)\ddot{q} + C(q, \dot{q})\dot{q} + P(\dot{q}) + G(q) + \Delta(t, q, \dot{q}) = \tau$$

State space form  $x_1 = q, x_2 = \dot{q}, u = \tau$

$$\begin{aligned}\dot{x}_1 &= x_2, \\ \dot{x}_2 &= f(t, x_1, x_2, u) + w(t, x_1, x_2); \quad y = x_1\end{aligned}$$

Relative degree condition(linearized case)

$$C = [1 \quad 0], \quad D = \begin{bmatrix} 0 \\ 1 \end{bmatrix}, \quad CD = 0.$$

### Remark:

When the relative degree of  $w(t)$  w.r.t.  $y(t)$  is **higher than one**, i.e.  $\text{rank}(CD) < m$ , **output differentiations** are necessary.

10

## A simple observer for Mechanical Systems

### Formulation of the problem:

Estimate the **velocity** through position, when **acceleration is bounded**.

$$\dot{x}_1 = x_2, \quad \dot{x}_2 = f(x_1, x_2, t) + w, \quad y = x_1.$$

### A simple observer [Davila et.al. 05].

The observer

$$\begin{aligned}\dot{\hat{x}}_1 &= -1,5\sqrt{L}|y - \hat{x}_1|^{\frac{1}{2}} \text{sign}(y - \hat{x}_1) + \hat{x}_2, \\ \dot{\hat{x}}_2 &= f(x_1, \hat{x}_2, t) - 1,1L \text{sign}(y - \hat{x}_1), \quad |f(x_1, \hat{x}_2, t) - f(x_1, x_2, t) + w| < L\end{aligned}$$

The terms depending on  $x_1$  only are not taken into account!!!

- **finite-time** estimation of  $x_2$ , i.e.,  $\hat{x}_2(t) = x_2(t), \forall t \geq T$ ;
- the **best asymptotic precision** in the sense of [Kolmogorov:62].

11

## Outline

- 1 Background
  - Unknown input observers
- 2 Strong Observability - Invariant Zeros - Relative Degree
  - Relation of concepts for SUIO Systems
  - HOSM Observers for linear systems with unknown inputs
- 3 Applications

12



## Single Unknown Input- Single Output Case

### Strong Observability - Invariant Zeros Relation

Strong observability requires that for any input  $w$ , the equality  $y \equiv 0$  implies  $x \equiv 0$ . The existence of invariant zeros  $s_0$  implies the existence of inputs  $w(s_0)$  such that  $y \equiv 0$  for  $x \neq 0$

Absence of invariant zeros is sufficient and necessary condition for strong observability (Hautus, 1983)

13

## Single Unknown Input- Single Output Case

### Strong Observability - Relative Degree Relation

Taking the first  $n - 1$  derivatives of the output

$$\begin{aligned}y &= Cx \\ \dot{y} &= C\dot{x} = CAx(t) + CDw \\ &\vdots \\ y^{(n-1)} &= CA^{n-1}x + CA^{n-2}Dw + \dots + CDw^{(n-2)}\end{aligned}$$

Relative degree  $n$  is required

to obtain a set of  $n$  equations independent on  $w$ :

$$\begin{bmatrix} CD \\ CAD \\ \vdots \\ CA^{n-2}D \end{bmatrix} = \begin{bmatrix} 0 \\ 0 \\ \vdots \\ 0 \end{bmatrix}$$

14

## Single Unknown Input- Single Output Case

### Invariant zeros - Relative Degree Relation

Rosenbrock matrix for the tuple  $(A, C, D)$ :

$$R(s) = \begin{bmatrix} sI - A & -D \\ C & 0 \end{bmatrix}.$$

Determinant of the Rosenbrock matrix

$$\det(R) = (s^{n-1} + a_n s^{n-2} + \dots + a_2)CD + (s^{n-2} + a_n s^{n-3} + \dots + a_3)CAD + \dots + (s + a_n)CA^{n-2}D + CA^{n-1}D$$

### Relative degree $n$ is necessary:

The determinant does not depend on  $s$  iff:

$$\begin{bmatrix} CD \\ \vdots \\ CA^{n-2}D \end{bmatrix} = \begin{bmatrix} 0 \\ \vdots \\ 0 \end{bmatrix}$$

15

### Methodology

The Unknown Input Observer (UIO) design problem for strongly observable systems is **reduced to evaluate in real-time derivatives** of the output.

The  $k$ -th order HOSM differentiator for  $y_j$

$$\begin{aligned} \dot{z}_0 &= \nu_0 = -\lambda_k L^{\frac{1}{k+1}} |z_0 - y_j|^{\frac{k}{k+1}} \text{sign}(z_0 - y_j) + z_1, \\ \dot{z}_1 &= \nu_1 = -\lambda_{k-1} L^{\frac{1}{k}} |z_1 - \nu_0|^{\frac{k-1}{k}} \text{sign}(z_1 - \nu_0) + z_2, \\ &\vdots \\ \dot{z}_{k-1} &= \nu_{k-1} = -\lambda_1 L^{\frac{1}{2}} |z_{k-1} - \nu_{k-2}|^{\frac{1}{2}} \text{sign}(z_{k-1} - \nu_{k-2}) + z_k, \\ \dot{z}_k &= -\lambda_0 L \text{sign}(z_k - \nu_{k-1}), \end{aligned} \tag{2}$$

$$\lambda_0 = 1, \lambda_1 = 1.5, \lambda_2 = 2, \lambda_3 = 3, \lambda_4 = 5, \lambda_5 = 8.$$

### Convergence of the HOSM differentiator [Levant:03].

If the gain  $L$  satisfies  $L > |y_j^{(k+1)}(t)|$  for all  $t$ , then  $z_i = y_j^{(i)}$  after finite-time.

16

### Uniform Robust Exact First-Order Differentiator [Cruz et. al. 11].

$$\dot{z}_0 = -k_1\phi_1(z_0 - y_j) + z_1, \quad \dot{z}_1 = -k_2\phi_2(z_0 - y_j),$$

where

$$\begin{aligned}\phi_1(\sigma_0) &:= \lceil \sigma_0 \rceil^{1/2} + \lceil \sigma_0 \rceil^{3/2}, \\ \phi_2(\sigma_0) &:= 0,5 \operatorname{sign}(\sigma_0) + 2\sigma_0 + 1,5 \lceil \sigma_0 \rceil^2.\end{aligned}$$

and  $\lceil v \rceil^p := |v|^p \operatorname{sign}(v)$ .

#### Remarks.

- the differentiator is **uniform with respect to the initial differentiation error**;
- this means that the resulting observer converges in **prescribed time**;
- useful for systems with strictly positive **dwell-time**.

17

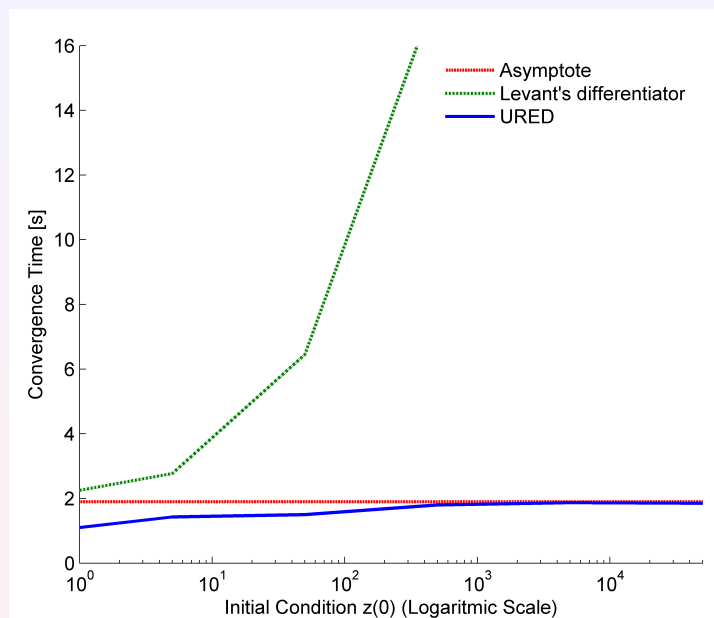


Figura: Convergence time of the Uniform Robust Exact Differentiator (URED).

18

### Arbitrary Order Uniform HOSM differentiator [Angulo et.al: 13, Automatica].

Given a signal  $y_j(t)$  to be differentiated  $(n - 1)$ -times, the differentiator

$$\begin{aligned}\dot{\hat{x}}_i &= -\lambda_i [y_j - \hat{x}_1]^{\frac{n-i}{n}} - k_i [y_j - \hat{x}_1]^{\frac{n+\alpha i}{n}} + \hat{x}_{i+1}, \quad i = 1, \dots, n-1, \\ \dot{\hat{x}}_n &= -\lambda_n \text{sign}(y_j - \hat{x}_1) - k_n [y_j - \hat{x}_1]^{1+\alpha},\end{aligned}\quad (3)$$

with  $\{\lambda_i\}_{i=1}^n$  chosen as Levant's,  $\alpha > 0$  small enough and  $\{k_i\}_{i=1}^n$  such that is  $P(s) = k_n s^{n-1} + k_{n-1} s^{n-2} + \dots + k_2 s + k_1$ , provides is stable polynomial, provides

- uniform finite-time estimation, i.e.,  $\exists T$  independent of  $|\hat{x}_i(0) + y_j^{i-1}(0)|$ ,  $i = 1, \dots, n$ , such that

$$\hat{x}_i(t) = y_j^{(i-1)}(t), \quad \forall t \geq T, \quad i = 1, \dots, n;$$

- the best asymptotic precision under measurement noise [Kolmogorov:62].

19

## Outline

### 1 Background

- Unknown input observers

### 2 Strong Observability - Invariant Zeros - Relative Degree

- Relation of concepts for SUIISO Systems
- HOSM Observers for linear systems with unknown inputs

### 3 Applications

20

## Linear systems with unknown inputs

### The system

Consider

$$\Sigma : \begin{cases} \dot{x} = Ax + Bu + Dw, & x(0) = x_0, \\ y = Cx, \end{cases} \quad (4)$$

where

- $x(t) \in \mathbb{R}^n$  is the state,  $w(t) \in \mathbb{R}^m$  is the **unknown input**;
- $u(t) \in \mathbb{R}^q$  is the control,  $y(t) \in \mathbb{R}^p$  is the measured output.

### Relative degree

The integer-scalar  $r$  such that

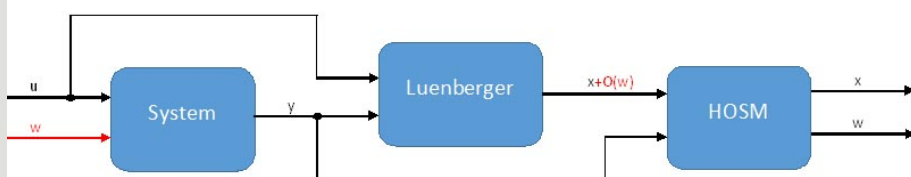
$$\begin{aligned} c_i A^j D &= 0, \quad j = 0, \dots, r_i - 2, \quad c_i A^{r_i-1} D \neq 0, \\ r_i &\leq n - 1 \end{aligned}$$

where  $c_i$  is the  $i$ th row of  $C$ .

21

## Observers for linear systems with unknown inputs

### A cascade concept [Fridman et al. 2007]



22

## Observers for linear systems with unknown inputs

### A HOSM observer [Fridman et al. 2007]

Observer for the strongly observable case and  $\sum_{i=1}^m r_i = n$

$$\begin{aligned}\dot{z} &= Az + Bu + L(y - Cz), \\ \dot{v} &= W(y - Cz, v), \\ \hat{x} &= z + Kv\end{aligned}\tag{5}$$

- $L \in \mathbb{R}^n$  is the correction term chosen such that  $A - LC$  is Hurwitz;
- for  $i=1, \dots, m$ :

$$K^{-1} = \begin{bmatrix} P_1 \\ \vdots \\ P_m \end{bmatrix}, \quad P_i = \begin{bmatrix} c_i \\ \vdots \\ c_i(A - LC)^{n-1} \end{bmatrix};$$

- $W(\cdot)$  is a nonlinear HOSM term.

23

## Observers for linear systems with unknown inputs

### A HOSM observer [Fridman et al. 2007]

Nonlinear HOSM term  $W^T = [v_1 \ v_2 \ \dots \ v_n]$

$$\begin{aligned}\dot{v}_1 &= w_1 = -\alpha_n N^{1/n} |v_1 - (y - Cz)|^{(n-1)/n} \text{sign}(v_1 - (y - Cz)) + v_2 \\ \dot{v}_2 &= w_2 = -\alpha_{(n-1)} N^{1/(n-1)} |v_2 - w_1|^{(n-2)/(n-1)} \text{sign}(v_2 - w_1) + v_3 \\ &\vdots \\ \dot{v}_{n-1} &= w_{n-1} = -\alpha_2 N^{1/2} |v_{n-1} - w_{n-2}|^{1/2} \text{sign}(v_{n-1} - w_{n-2}) + v_n \\ \dot{v}_n &= -\alpha_1 N \text{sign}(v_n - w_{n-1})\end{aligned}\tag{6}$$

where  $N > |C(A - LC)^{n-1} Dw(t)|$ .

24

## Observers for linear systems with unknown inputs

### Canonical form of the estimation error $x - z$

The form is composed for Brunovsky blocks.

$$\begin{bmatrix} \dot{\xi}_{11} \\ \dot{\xi}_{12} \\ \vdots \\ \dot{\xi}_{1r_1-2} \\ \dot{\xi}_{1r_1-1} \\ \vdots \\ \dot{\xi}_{m_1} \\ \dot{\xi}_{m_2} \\ \vdots \\ \dot{\xi}_{mr_m-2} \\ \dot{\xi}_{mr_m-1} \end{bmatrix} = \begin{bmatrix} 0 & 1 & \cdots & 0 & 0 & \cdots & \cdots & 0 & 0 & \cdots & 0 & 0 \\ 0 & 0 & \cdots & 0 & 0 & \cdots & \cdots & 0 & 0 & \cdots & 0 & 0 \\ \vdots & \vdots & & \ddots & \vdots & \cdots & \cdots & \vdots & \vdots & & \vdots & \vdots \\ 0 & 0 & \cdots & 0 & 1 & \cdots & \cdots & 0 & 0 & \cdots & 0 & 0 \\ * & * & \cdots & * & * & \cdots & \cdots & 0 & 0 & \cdots & 0 & 0 \\ \vdots & & & \vdots & \ddots & & & \vdots & \vdots & & \vdots & \vdots \\ \vdots & & & \vdots & \vdots & \ddots & & \vdots & \vdots & & \vdots & \vdots \\ 0 & 0 & \cdots & 0 & 0 & \cdots & \cdots & 0 & 1 & \cdots & 0 & 0 \\ 0 & 0 & \cdots & 0 & 0 & \cdots & \cdots & 0 & 0 & \cdots & 0 & 0 \\ \vdots & \vdots & & \vdots & \vdots & \cdots & \cdots & \vdots & \vdots & & \vdots & \vdots \\ 0 & 0 & \cdots & 0 & 0 & \cdots & \cdots & 0 & 0 & \cdots & 0 & 1 \\ * & * & \cdots & * & * & \cdots & \cdots & * & * & \cdots & * & * \end{bmatrix} \begin{bmatrix} \xi_{11} \\ \xi_{12} \\ \vdots \\ \xi_{1r_1-2} \\ \xi_{1r_1-1} \\ \vdots \\ \xi_{m_1} \\ \xi_{m_2} \\ \vdots \\ \xi_{mr_m-2} \\ \xi_{mr_m-1} \end{bmatrix} + \begin{bmatrix} 0 & \cdots & 0 \\ 0 & \cdots & 0 \\ \vdots & & \vdots \\ 0 & \cdots & 0 \\ * & \cdots & * \\ \vdots & & \vdots \\ 0 & \cdots & 0 \\ 0 & \cdots & 0 \\ \vdots & & \vdots \\ 0 & \cdots & 0 \\ * & \cdots & * \end{bmatrix} \begin{bmatrix} w_1 \\ w_2 \\ \vdots \\ w_{m-1} \\ w_m \end{bmatrix}$$

25

## Observers for linear systems with unknown inputs

### HOSM Observer [Fridman et al. 2007]

Advantages:

- ① Finite-time theoretically exact observation of the system states
- ② The cascade structure of observer allows to use any pre-filters or stabilizers

### Question

What can we do when the system is strongly observable but  $\sum_{i=1}^m r_i < n$ ?

26

## Weakly unobservable subspace

### Invariant zeros

The Rosenbrock of  $(A, C, D)$ :

$$R(s) = \begin{bmatrix} sI - A & -D \\ C & 0 \end{bmatrix}.$$

The values  $s_0 \in \mathbb{C}$  such that  $\text{rank } R(s_0) < n + m$  are called **invariant zeros** of  $(A, C, D)$ .

### The weakly unobservable subspace $\mathcal{V}^*$

A state  $x_0 \in \mathcal{X}$  is called weakly unobservable, if there exist an input  $w$  such that the corresponding output  $y_w(t, x_0) = 0$  for all  $t \geq 0$ . The set of all the weakly unobservable points is denoted by  $\mathcal{V}^*$  and it is called the **weakly unobservable subspace** of the system.

27

## Molinari Decoupling Algorithm [Molinari: 1976]

### The Molinari's algorithm

The algorithm is given as follows:

- Step 0: Let  $i = 0$  and  $M_0 = 0$  (a null dimension matrix).
- Step 1: Compute  $\Gamma_i = \begin{bmatrix} M_i D & M_i A \\ 0 & C \end{bmatrix}$ , Find  $T_i$  such that  $\Gamma_i$  is reduced to

$$T_i \Gamma_i = \begin{bmatrix} G_{i+1} & H_{i+1} \\ 0 & M_{i+1} \end{bmatrix},$$

where  $G_{i+1}$  has full row rank.

- Step 2: Let  $i = i + 1$  and back to Step 1.

### Remark

The algorithm ends when  $\text{rank } M_i = \text{rank } M_{i+1}$ . The matrix  $M_i$ , for which the equality was satisfied, is denoted by  $M_n$ .

28



## Molinari Decoupling Algorithm [Molinari: 1976]

### Theorem

$$\ker M_n = \mathcal{V}^*$$

### Importance of the Molinari's algorithm

Molinari's algorithm for strongly observable systems gives an explicit algebraic relation between the output, and its derivatives, and the state

$$v(y, \dot{y}, \dots, y^{(k)}) = M_n x \quad (7)$$

### Relations for strong observability

- i) The system is **strongly observable**;
- ii) the triplet  $(A, C, D)$  does not have invariant zeros;
- iii)  $\mathcal{V}^*$  contains only the zero vector, i.e.  $\mathcal{V}^* = \{0\}$ .

29

## Observers for strongly observable systems with unknown inputs

### Canonical form

Let  $\sum_{i=1}^p m r_i = r_p < n$ . The canonical form is composed by Brunovsky blocks and a  $w$  dependent block.

$$\begin{bmatrix} \dot{\xi}_{11} \\ \dot{\xi}_{12} \\ \vdots \\ \dot{\xi}_{1r_1-2} \\ \dot{\xi}_{1r_1-1} \\ \vdots \\ \dot{\xi}_{p1} \\ \dot{\xi}_{p2} \\ \vdots \\ \dot{\xi}_{p_{r_p-2}} \\ \dot{\xi}_{p_{r_p-1}} \\ \dot{\xi}_{r_p+1} \\ \vdots \\ \dot{\xi}_n \end{bmatrix} = \begin{bmatrix} 0 & 1 & \dots & 0 & 0 & \dots & \dots & 0 & 0 & \dots & 0 & 0 \\ 0 & 0 & \dots & 0 & 0 & \dots & \dots & 0 & 0 & \dots & 0 & 0 \\ \vdots & \vdots & & \ddots & & \dots & \dots & \vdots & & & \vdots & \\ 0 & 0 & \dots & 0 & 1 & \dots & \dots & 0 & 0 & \dots & 0 & 0 \\ * & * & \dots & * & * & \dots & \dots & 0 & 0 & \dots & 0 & 0 \\ \vdots & & & \vdots & \ddots & & & \vdots & & & \vdots & \\ \vdots & & & \vdots & & \ddots & & \vdots & & & \vdots & \\ 0 & 0 & \dots & 0 & 0 & \dots & \dots & 0 & 1 & \dots & 0 & 0 \\ 0 & 0 & \dots & 0 & 0 & \dots & \dots & 0 & 0 & \dots & 0 & 0 \\ \vdots & \vdots & & \vdots & & \dots & \dots & \vdots & & & \ddots & \\ 0 & 0 & \dots & 0 & 0 & \dots & \dots & 0 & 0 & \dots & 0 & 1 \\ * & * & \dots & * & * & \dots & \dots & * & * & \dots & * & * \\ * & * & \dots & * & * & \dots & \dots & * & * & \dots & * & * \\ \vdots & & & \vdots & & & & \vdots & & & \vdots & \\ * & * & \dots & * & * & \dots & \dots & * & * & \dots & * & * \end{bmatrix} \begin{bmatrix} \xi_{11} \\ \xi_{12} \\ \vdots \\ \xi_{1r_1-2} \\ \xi_{1r_1-1} \\ \vdots \\ \xi_{p1} \\ \xi_{p2} \\ \vdots \\ \xi_{p_{r_p-2}} \\ \xi_{p_{r_p-1}} \\ \xi_{r_p+1} \\ \vdots \\ \xi_n \end{bmatrix} + \begin{bmatrix} 0 & \dots & 0 \\ 0 & \dots & 0 \\ \vdots & & \vdots \\ 0 & \dots & 0 \\ * & \dots & * \\ \vdots & & \vdots \\ 0 & \dots & 0 \\ 0 & \dots & 0 \\ \vdots & & \vdots \\ 0 & \dots & 0 \\ * & \dots & * \\ * & \dots & * \\ \vdots & & \vdots \\ * & \dots & * \end{bmatrix} \begin{bmatrix} w_1 \\ w_2 \\ \vdots \\ w_{m-1} \\ w_m \end{bmatrix}$$

30

## Observers for linear systems with unknown inputs

### Observer in [Fridman et al. 2007]

1. The estimated states converge theoretically exactly in finite/fixed time
2. The cascade structure of observer allows:
  - ✓ observation of unstable systems with finite differentiators gains;
  - ✓ prefiltering

31

## Outline

- 1 Background
  - Unknown input observers
- 2 Strong Observability - Invariant Zeros - Relative Degree
  - Relation of concepts for SUIISO Systems
  - HOSM Observers for linear systems with unknown inputs
- 3 Applications

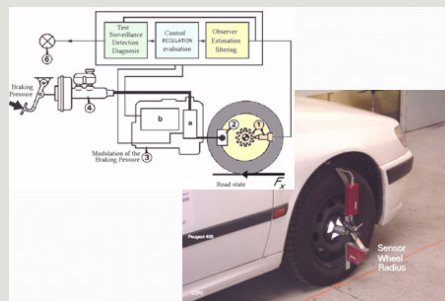
32

## Automotive application

### Peugeot 406, IFFSTAR



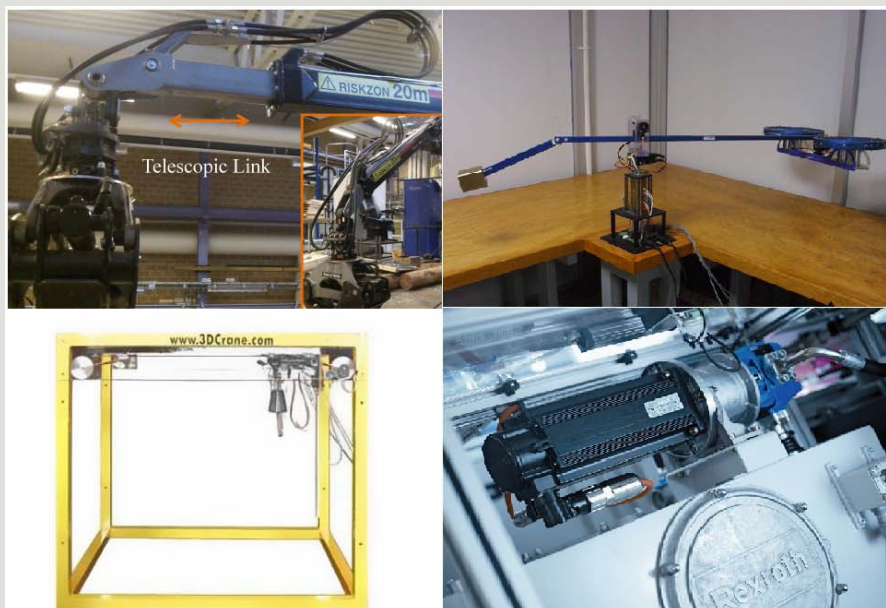
### Instrumentation



33

## More Applications

### 3DCrane, 3DOF Helicopter, Industrial Crane, Hydraulic Pneumatics



34

## Conclusions

# HOSM Observers

- provide theoretically exact observation and unknown inputs and fault estimation under sufficient and necessary conditions of the strong observability/ detectability of states or unknown inputs or faults;
- provide best possible asymptotic approximation w.r.t. discretization step and/or bounded deterministic noises;
- can ensure prescribed time convergence independent from any initial conditions.

35

## Conclusions

# HOSM Observers are designed for

- strongly detectable systems;
- for observation of the functional of the states for the systems which are even not strongly detectable;
- observation of different classes of non- linear systems;
- for theoretically exact finite time parameter identification.

36

## References

### REFERENCES

Y. Shtessel, C. Edwards , L. Fridman, A. Levant. Sliding Mode Control and Observation, Series: Control Engineering, Birkhauser: Basel, 2014.

L. Fridman, A. Levant and J. Davila Robust Exact Observation and Identification via High-Order Sliding Modes, in: The Industrial Electronics Handbook Volume; Control and Mechatronics, Editors: Bogdan Wilamowski, J. David Irwin. CRC Press, Taylor & Francis Inc., 2011, ISBN: 9781439802878.

<http://verona.fi-p.unam.mx/~lfridman/>

# Comparing model-free and disturbance observer based control

Mikulas Huba<sup>a</sup>

Peter Tapak<sup>a</sup>

Stefan Chamraz<sup>a</sup>

The iP controller [1] represents the simplest intelligent (model free) PID controller. Based on the flatness theory, it may successfully be used for control of broad spectrum of nonlinear systems. Though, to demonstrate its properties, it will be analyzed in control of a simple integrator with an input disturbance.

Similarly, in Motion Control the frequently used control structures may be characterized as disturbance observer (DO) based PI control [5, 6, 10, 9, 7]. These are still explored from various points of view as robustness, or noise attenuation [8, 2, 3, 4]. Again, in the simplest case they may be illustrated by control of a single integrator with an input disturbance.

The paper deals with comparison of both types of control with focus on the performance and noise attenuation trade off.

- [1] FLIESS, MICHEL und CEDRIC JOIN: *Model-free control*. International Journal of Control, 86(12):2228–2252, 2013.
- [2] HUBA, M.: *Performance Portrait Method: a new CAD Tool*. In: *10th Symposium on Advances in Control Education (ACE)*. IFAC, Sheffield, UK, 2013.
- [3] HUBA, M.: *Robustness analysis of a disturbance-observer based PI control*. In: *8th Int. Conf. and Exposition on Electrical and Power Eng. - EPE*, Iasi, Romania, 2014.
- [4] HUBA, M.: *Robustness versus performance in PDO FPI Control of the IPDT plant*. In: *IEEE/IES International Conference on Mechatronics, ICM2015*, Nagoya, Japan, 2015.
- [5] OHISHI, K.: *A new servo method in mechatronics*. Trans. Jpn. Soc. Elect. Eng., 107-D:83–86, 1987.
- [6] OHISHI, KIYOSHI, MASATO NAKAO, KOUHEI OHNISHI und KUNIO MIYACHI: *Microprocessor-Controlled DC Motor for Load-Insensitive Position Servo System*. IEEE Trans. Industrial Electronics, IE-34(1):44–49, feb. 1987.
- [7] RADKE, A. und ZHIQIANG GAO: *A survey of state and disturbance observers for practitioners*. In: *American Control Conference, 2006*, june 2006.
- [8] SARIYILDIZ, EMRE und KOUHEI OHNISHI: *Analysis the robustness of control systems based on disturbance observer*. International Journal of Control, 86(10):1733–1743, 2013.
- [9] SCHRIJVER, ERWIN und JOHANNES VAN DIJK: *Disturbance Observers for Rigid Mechanical Systems: Equivalence, Stability, and Design*. ASME, J. Dyn. Sys., Meas., Control, 124 (4):539–548, 2002.

---

<sup>a</sup>Institut of Automotive Mechatronics, Slovak University of Technology in Bratislava, Faculty of Electrical Engineering and Information Technology, mikulas.huba@stuba.sk, peter.tapak@stuba.sk

- [10] UMENO, T. und Y. HORI: *Robust speed control of dc servomotors using modern two-degree-of-freedom controller design*. IEEE Trans. Ind. Electr., 38:363–368, 1991.

## Comparing model-free and disturbance observer based control

Mikulas Huba   Peter Tapak   Stefan Chamraz  
Slovak University of Technology in Bratislava,  
Faculty of Electrical Engineering and Information Technology,  
Institut of Automotive Mechatronics,  
Slovakia

19. Steirisches Seminar  
über Regelungstechnik und Prozessautomatisierung  
7.9. - 9.9.2015 Retzhof, Austria

## Motivation

There exist two similar approaches to disturbance reconstruction and compensation for the first order systems:

---

Question

**Which one is better in context of the noise attenuation and speed of transients?**

---

- Disturbance observer based (filtered) PI control - DO-(F)PI?
  - "Model-free" intelligent P control - iP?
- 

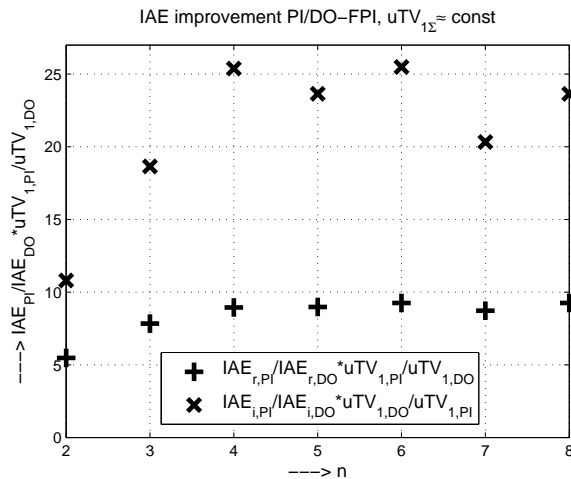
Another Question

**Why it is not enough to use the traditional PI control?**



## Motivation: huge progress in a DC motor speed control

- IAE improvements when replacing 2DOF PI by DO FPI control under the same torque ripple [7]

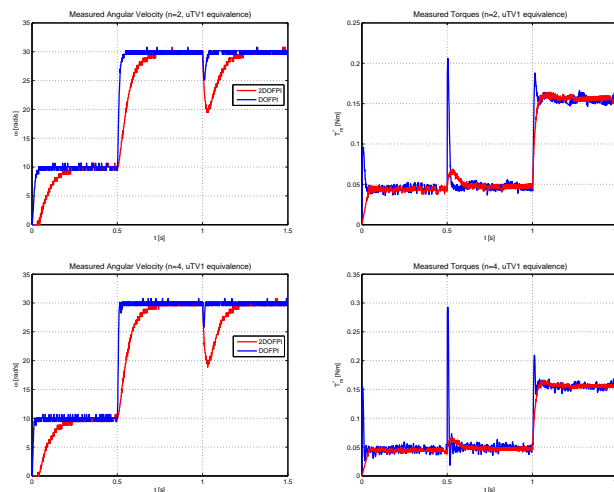


M.Huba, P. Tapak, S. Chamraz, STU Bratislava, Slovakia

Comparing model-free and disturbance observer based control

## Motivation: progress in a DC motor speed control

- 2DOF PI and DO-FPI control for  $n = 2$  (above) and  $n = 4$  (below) under  $uTV_1$  equivalence - real time control [7]



M.Huba, P. Tapak, S. Chamraz, STU Bratislava, Slovakia

Comparing model-free and disturbance observer based control

## Presentation outline

- Introduction
- Dynamical classes of control
- Shape and time related performance specifications
- Model-free iP control
- DO-(F)PI control
- 2DOF PI control
- Nominal analysis results
- Noise characteristics
- Conclusions

## Dynamical classes of control

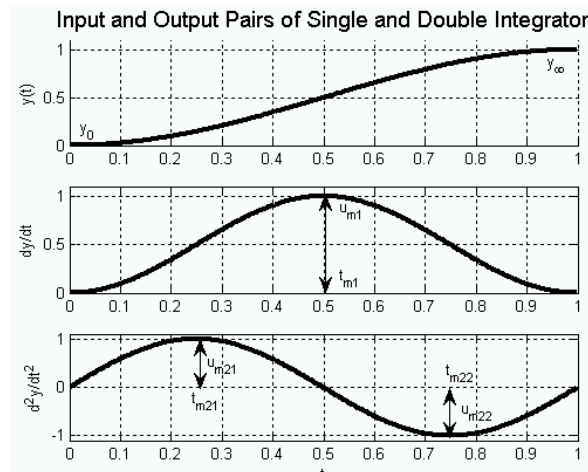
### Shape Related Performance Specifications

- The simplest possible signal changes are monotonic (MO)
- Monotonicity - central role in mathematics,
- but also in the physical & technological requirements, as e.g.
  - no/limited output overshooting,
  - non-oscillatory transients, etc.
- Deviations from ideal shapes [3-10] - important both at the plant input and output- applicable to characterization of
  - additional control effort,
  - high frequency oscillations,
  - noise impact,
  - actuator wear,
  - fuel consumption, etc.

## Dynamical classes of control

Shape Related Performance Specifications (Single and Double Integrator)

- Monotonic (MO) plant output
- One-Pulse (1P) integrator input = derivative of the output
- Two-Pulse (2P) plant input = second output derivative



M.Huba, P. Tapak, S. Chamraz, STU Bratislava, Slovakia

Comparing model-free and disturbance observer based control

## Dynamical classes of control

Shape Related Performance Specifications

- MO output of stable first order systems - may also be achieved by MO input (not just by the 1P input as for the single integrator)
- Minimal number of MO intervals at the input corresponding to a MO output = number of unstable poles+1
- Number of MO intervals at the input may be increased by increasing speed of transients up to  $n + 1$ ,  $n$  = plant order
- Systems with stable modes - **degrees of freedom** in specifying the closed loop dynamics.
- **Dynamical class (DC)** of control [2] - design parameter showing *difference between the number of MO intervals at the plant input corresponding to a MO plant output.*
- **The most important DCs are 0, 1 and 2**

M.Huba, P. Tapak, S. Chamraz, STU Bratislava, Slovakia

Comparing model-free and disturbance observer based control

## Basic Dynamical Classes of Control

Classification according to the input-output setpoint step responses pairs

To enrich observation from iPID [1], we are considering setpoint step reponse pairs characterized by:

- **DC0**: MO Output / MO Input
  - may include all stable systems
  - the simplest system represented by a **gain**
- **DC1**: MO Output / 1P Input
  - dominant dynamics with the relative degree  $\geq 1$
  - systems with one unstable/marginally stable pole
  - the simplest system represented by a **single integrator**
- **DC2**: MO Output / 2P Input
  - dominant dynamics with the relative degree  $\geq 2$
  - systems with two unstable/marginally stable poles
  - the simplest system represented by a **double integrator**

Navigation icons: back, forward, search, etc.

M.Huba, P. Tapak, S. Chamraz, STU Bratislava, Slovakia

Comparing model-free and disturbance observer based control

## Disturbance responses of DC0 and DC1

Classification according to the input-output pairs

- **DC0**: 1P Output (MO output return) / MO Input
- **DC1**: 1P Output (MO output return) / 1P Input
- Note different impact of the parameter uncertainty

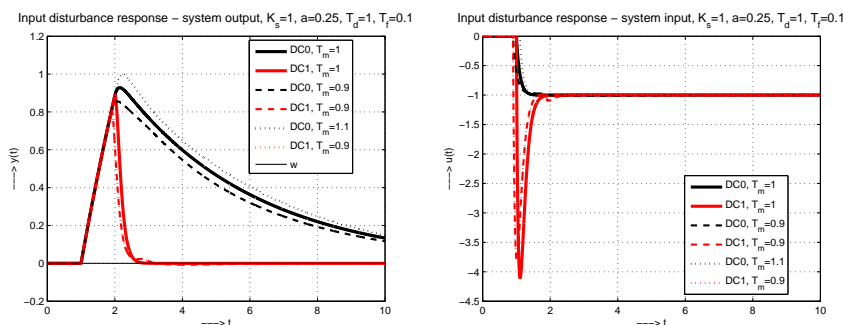


**Figure:** To show transients from both DCs we have to consider stable FOTD plant  $K_s e^{-T_d s} / (s + a)$ : Input disturbance step responses for different values of the dead time estimate  $T_m$ ;  $T_d = 1, K_s = 1$

Navigation icons: back, forward, search, etc.

M.Huba, P. Tapak, S. Chamraz, STU Bratislava, Slovakia

Comparing model-free and disturbance observer based control

## Table: Basic Controllers of DCs 0-2 [2]

Classification/acronyms according to their input-output pairs and the dominant dynamics

- Just the most frequent situations (may yet be extended)
- Note two DCs of PI and PD controllers and three DCs of the PID control  $\Leftrightarrow$  inflation in “optimal” controller tuning
- Systems with stable modes - the dynamical class of control has to be chosen by the designer = not given apriori

| Dynamic class | I-action | Dominant dynamics |             |                   |                              |  |  |                             |  |
|---------------|----------|-------------------|-------------|-------------------|------------------------------|--|--|-----------------------------|--|
|               |          | $K$               | $Ke^{-T_d}$ | $\frac{K_s}{s+a}$ | $\frac{K_s e^{-T_d s}}{s+a}$ | $\frac{K_{s1} + K_{s2}}{s+a_1} \frac{K_{s2}}{s+a_2}$ | $\left[ \frac{K_{s1} + K_{s2}}{s+a_1} \frac{K_{s2}}{s+a_2} \right] e^{-T_d s}$ | $\frac{K_s}{s^2+a_1 s+a_0}$ | $\frac{K_s e^{-T_d s}}{s^2+a_1 s+a_0}$ |
| 0             | N        | FF                | FF          | FF                | FF                           | FF   | FF   | FF                          | FF                                     |
|               | Y        | I                 | PrI         | PI                | PrPI                         | PID  | PrPID  | PID                         | PrPID                                  |
| 1             | N        | -                 | -           | P                 | PrP                          | P-P  | PrP-P  | PD                          | PrPD                                   |
|               | Y        | -                 | -           | PI                | PrPI                         | P-PI   | PrP-PI   | PID                         | PrPID                                  |
| 2             | N        | -                 | -           | -                 | -                            | -  | -  | PD                          | PrPD                                   |
|               | Y        | -                 | -           | -                 | -                            | -  | -  | PID                         | PrPID                                  |

## Shape Related Performance Specifications

Deviations from output ideal shapes - **monotonicity**

- Monotonicity Index [11]
- Total Variance [13] - total control effort

$$TV(u) = \int_0^\infty \left| \frac{du}{dt} \right| dt \approx \sum_i |u_{i+1} - u_i| \quad (1)$$

- Simple calculation in Matlab `sum(abs(diff(u)))`
- relative measures = finer resolution
- $TV_0$  - Deviations from monotonicity [3-10]

$$TV_0(y) = \sum_i |y_{i+1} - y_i| - |y_\infty - y_0| \quad (2)$$

- $TV_0(y) = 0$  just for strictly MO response, else  $TV_0(y) > 0$ .

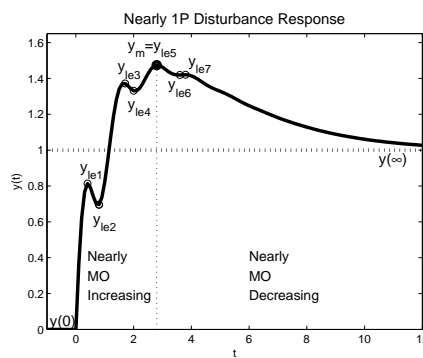
## Shape Related Performance Specifications

Deviations from output ideal shapes - disturbance responses

- $TV_1$  - Deviations from 1P shapes

$$TV_1(y_d) = \sum_i |y_{i+1} - y_i| - |2y_m - y_\infty - y_0| ; y_m = \max(y)$$

- $TV_1(y_d) = 0$  just for strictly 1P response, else  $TV_1(y_d) > 0$ .



M.Huba, P. Tapak, S. Chamraz, STU Bratislava, Slovakia

Comparing model-free and disturbance observer based control

## Time Related Performance Specifications

### As fast as possible transients

- Settling time  $t_s = \min$
- Minimal Integral of Absolute Error (IAE)

$$IAE = \int_0^\infty |w - y(t)| dt = \int_0^\infty |e(t)| dt \approx T_s \sum_i |e(i)| \Rightarrow \min \quad (3)$$

- Shape related constraints IAE=IE (Laplace Transform)

$$IE = \int_0^\infty (w - y(t)) dt = \int_0^\infty e(t) dt \quad (4)$$

$$IE = \lim_{s \rightarrow 0} E(s) \quad (5)$$

- Analysis of the input disturbance step responses ( $w = 0$ )

$$J = IAE_d \Rightarrow \min \quad (6)$$

M.Huba, P. Tapak, S. Chamraz, STU Bratislava, Slovakia

Comparing model-free and disturbance observer based control

$$\begin{aligned} TV_0(y_s) &\leq \epsilon_{ys}; & TV_1(y_d) &\leq \epsilon_{yd} \\ TV_0(u_s) &\leq \epsilon_{us}; & TV_0(u_d) &\leq \epsilon_{ud} \end{aligned} \quad (7)$$

$$\begin{aligned} TV_0(y_s) &\leq \epsilon_{ys}; & TV_1(y_d) &\leq \epsilon_{yd} \\ TV_1(u_s) &\leq \epsilon_{us}; & TV_1(u_d) &\leq \epsilon_{ud} \end{aligned} \quad (8)$$

Ideally

$$\epsilon = \epsilon_{ys} = \epsilon_{yd} = \epsilon_{us} = \epsilon_{ud} \rightarrow 0 \quad (9)$$

- We will analyze, how the “speed” of disturbance step responses  $IAE_d$  depends on the shape related deviations at the input  $TV_1(u_d)$  and output  $TV_1(y_d)$

- “Ultra-local” models - notion introduced by Fliess et al. [1]
- Based on the theory of “flat systems” - simplicity and easy manipulation in solving different control problems.
- One of the conclusions - it is enough to deal with control of the single, or double integrators
- For these systems, from a MO output the dynamics inversion yields one-pulse (1P), or two-pulse (2P) inputs consisting of 2, or 3 MO intervals [5-6]
- But, it is to remember that an useful information follows from using & comparing ultra-local and local linear models,
- Furthermore, for many problems the plant dynamics may be sufficiently approximated by a constant corresponding to MO input/MO output pairs.

## Model-free iP control

Ultra-local-models = integral models

For first-order dominant dynamics

$$\dot{y} = F + \alpha u \quad (10)$$

$\alpha \in \mathbb{R}$  - in general, a non-physical constant parameter.

$\bar{\alpha}$  - its estimate

$F$  - an equivalent disturbance at the integrator input

$\phi$  a piecewise constant approximation of  $F$  from a measured output  $y_m$  according to

$$\phi = \dot{y}_m - \bar{\alpha} u \quad (11)$$

The first critical question - how to determine  $\dot{y}_m$

In iP controller we simply use the available Simulink block

M.Huba, P. Tapak, S. Chamraz, STU Bratislava, Slovakia

Comparing model-free and disturbance observer based control

## Model-free iP control

Low-path disturbance filter

To avoid algebraic loops, to increase the loop robustness and to attenuate effects of the measurement noise, the estimation of  $\phi$  can be expanded by a low-pass filter in form of an integral

$$\phi = \frac{1}{L} \int_{t-L-T_s}^{t-T_s} (\dot{y}_m - \bar{\alpha} u) d\sigma =$$

where  $L$  is "small" (what does it mean "small"?),  $T_s \ll L$  - the sampling period

Preferably accomplished in a discrete-time form by a FIR filter

$$Q_d(z) = \frac{1}{N} \sum_{i=1}^N z^{-i}; \quad N = IP\left(\frac{L}{T_s}\right) \quad (12)$$

$T_s \ll L$ ,  $z^{-1}$  - the shift operator,

IP - an integer part.

M.Huba, P. Tapak, S. Chamraz, STU Bratislava, Slovakia

Comparing model-free and disturbance observer based control



## Model-free iP control

Overall control algorithm

Substitution (with  $u_0$  = new control signal)

$$u = \frac{u_0 - \phi}{\bar{\alpha}} \quad (13)$$

yields transformed differential equation

$$\dot{y} = F - \phi + \frac{\alpha}{\bar{\alpha}} u_0 \quad (14)$$

An ideal case with  $\alpha = \bar{\alpha}$ ,  $F = \phi$  corresponds to a single integrator

$$\dot{y} = u_0 \quad (15)$$

This explains, why it may seem enough to deal with the single integrator control. Problems occur just when considering nonmodelled dynamics (not considered in this contribution).

## Model-free iP control

Overall control algorithm

Required output reference trajectory

$$y^*, \dot{y}^* \quad (16)$$

The tracking error trajectory

$$e = y - y^*, \dot{e} = \dot{y} - \dot{y}^* \quad (17)$$

An **exponential error decrease**  $\dot{e} = \lambda e$  with  $\lambda < 0$  being the closed loop pole yields control

$$u_0 = \dot{y}^* - \bar{K}_P e \quad (18)$$

It means that the iP control algorithm may finally be written as

$$u = \frac{\dot{y}^* - \bar{K}_P e - \phi}{\bar{\alpha}} \quad (19)$$

$\bar{K}_P = -\lambda$  is the **proportional gain** defined by  $\lambda$ , or by the closed loop time constant  $T_c = -1/\lambda$  as  $\bar{K}_P = 1/T_c$

## Model-free iP control

Some remarks

- The reference trajectory may be defined by the technology.
- In the simplest case, for a given reference step  $w$ , the reference trajectory may be given by  $y^* = w, \dot{y}^* = 0$ .
- Else, for an initial steady state  $y_0$  it may be calculated as a trajectory of a disturbance free system:
  - analytically as  $\dot{y}_0 = K_P(w - y_0); \dot{y}^*(t) = e^{\lambda t} \dot{y}_0$ ,  
 $y^*(t) = y_0 + (w - y_0)(1 - e^{\lambda t})$ ,
  - or by a primary loop including the single integrator (15) + the P controller (18).
- Since the input disturbances may only be compensated by a controller output at the plant input, it may be found as more appropriate to consider the plant model in the form

$$\dot{y} = K_s(u + d_i); \quad K_s = \alpha, \quad d_i = F/\alpha \quad (20)$$

M.Huba, P. Tapak, S. Chamraz, STU Bratislava, Slovakia

Comparing model-free and disturbance observer based control

## Model-free iP control in new variables

$Q_u = 1; Q_y = ?; K_P = ?; Q_d(s) = (1 - e^{-sL})/(Ls); L = ?; Q_P = 1$

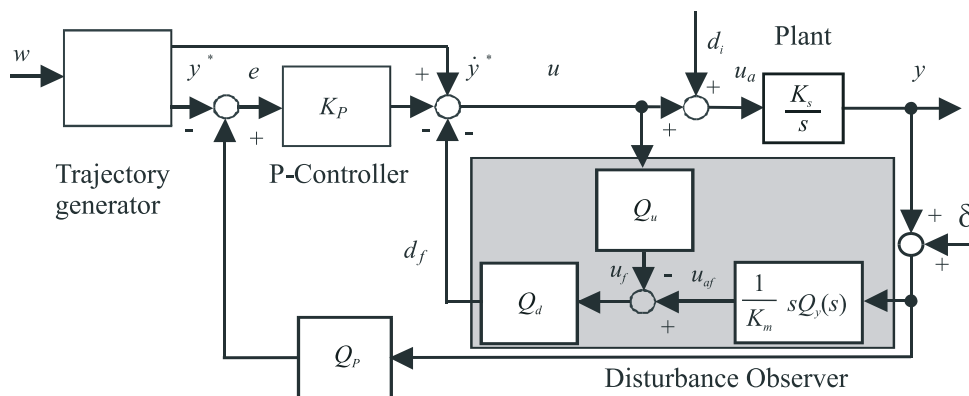


Figure:  $Q_y$ - usually not specified ( $= 1$ );  $Q_P, Q_u$  - not considered (i.e.  $= 1$ );  $\delta$  - measurement noise

M.Huba, P. Tapak, S. Chamraz, STU Bratislava, Slovakia

Comparing model-free and disturbance observer based control

## Disturbance observer based (filtered) PI control

$$Q_u = 1/(1 + T_n s)^n; Q_y = Q_u; Q_P = Q_u; Q_d = 1 \text{ [2-5, 8]}$$

DO-PI: traditional solution with  $Q_P = 1; K_P = 1/(K_s T_c)$

$$\text{DO-FPI: } K_P = \min\{K_P, K_{Pn}\}; K_{Pn} = \frac{1}{K_s T_n} \frac{1}{(n+1)(1+1/n)^n}$$

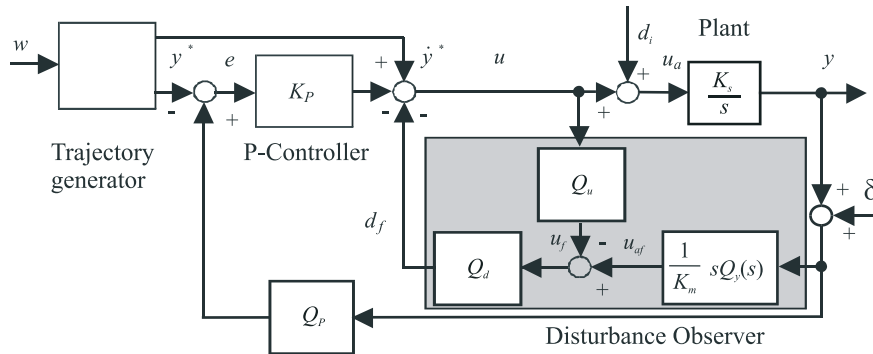


Figure: DO-FPI and DO-PI control;  $Q_u = \frac{1}{(1 + T_n s)^n}$  - binomial filter

## Traditional PI control

- The most frequently used control structure
- No filtration at higher frequencies [9, 10, 12]
- Superfluous integration - windup
- Typical overshooting - motivation for IP, or prefilter+PI control [5]

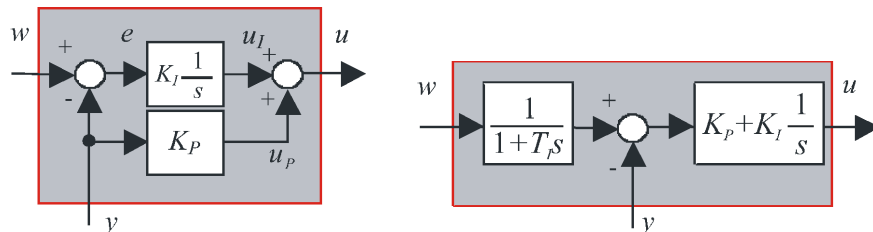


Figure: IP control and prefilter+PI control  $K_I = K_P/T_i$

## Disturbance responses

### Two step comparison

Since the setpoint step responses may significantly be modified by the dynamical feedforward, we are going to focus on [9]

- ① Net dynamics of the disturbance step responses (no noise)
- ② Noise attenuation characteristics of the disturbance step responses

### Numerical values

=====

$K_s=1$ ;  $T_c=1$ ;  $K_P=1$ ;  
 $T_s=0.001$ ;  $T_n = L = T_i/100 \in [0.005, 0.5]$   
 DO-PI and DO-FPI control with  $n \in [1, 4]$

## Comparative framework, $T_n = L = T_i/100 \in [0.005, 0.5]$ ; Net dynamics of disturbance step responses, DO-PI/FPI control with $n \in [1, 4]$

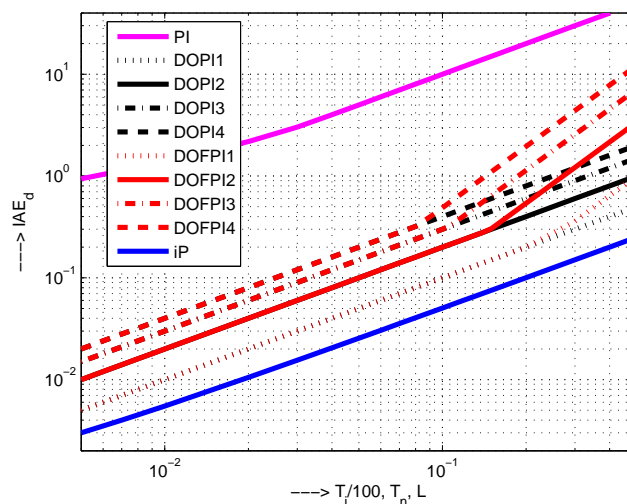


Figure: Performance measures versus  $T_i/100$ ,  $T_n$ , or  $L$ , no noise

Comparative framework,  $T_n = L = T_i/100 \in [.005, 0.5]$ ;  
Net dynamics of disturbance step responses, DO-PI/FPI control with  $n \in [1, 4]$

Output/Input 1P responses just for  $L \geq 0.03$  and  $T_i \geq 4$   
Disturbance response of the PI control is the slowest one DO-PI  
and DO-FPI are able to yield the fastest 1P responses

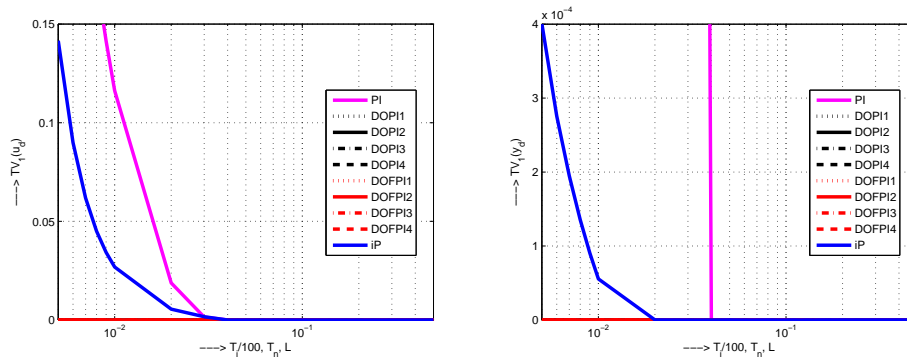


Figure: Performance measures versus  $T_i/100$ ,  $T_n$ , or  $L$ , no noise

Comparative framework,  $T_n = L = T_i/100 \in [.005, 0.5]$ ;  
Net dynamics of disturbance step responses

- 2DOF PI -  $TV_1$  increase due to complex closed loop poles
- The optimal tuning corresponds to the aperiodicity border (double real closed loop pole)
- iP -  $TV_1$  increase due to the continuous-time design and discrete-time implementation
- Improved performance may be achieved by the discrete time design (not analyzed by this paper)
- Performance decrease due to discrete time implementation may appear also for the DO-PI/FPI solutions
- However, performance achievable by the simplified continuous-time design is better than for previous solutions and for  $T_n \rightarrow T_s$  also here it is still possible to apply the discrete-time design (see also the noise characteristics)

## Comparative framework

### Noise characteristics

$$T_n = L = T_i/100 \in [0.005, 0.5]$$

Starting with parameters  $T_n = L = T_i/100 = 5 T_s$

(For lower values we should already use discrete-time design)

Both evaluations consider “**speed**” ( $IAE_d$ ) versus “**abundant control**” ( $TV_1$ ) characteristics at the **input** ( $u_d$ ) and **output** ( $y_d$ ), that is

- $IAE_d$  versus  $TV_1(u_d)$
- $IAE_d$  versus  $TV_1(y_d)$

Evaluation time  $t \in [0, 200]$ s

(Such a long evaluation time is necessary with respect to the slow PI responses)

Navigation icons

M.Huba, P. Tapak, S. Chamraz, STU Bratislava, Slovakia

Comparing model-free and disturbance observer based control

## Comparative framework, $T_n = L = T_i/100 \in [0.005, 0.5]$ ;

### Noise characteristics - main result

Noise generated by “Uniform Random Number” block in Matlab/Simulink,  $|\delta| \leq 0.01$

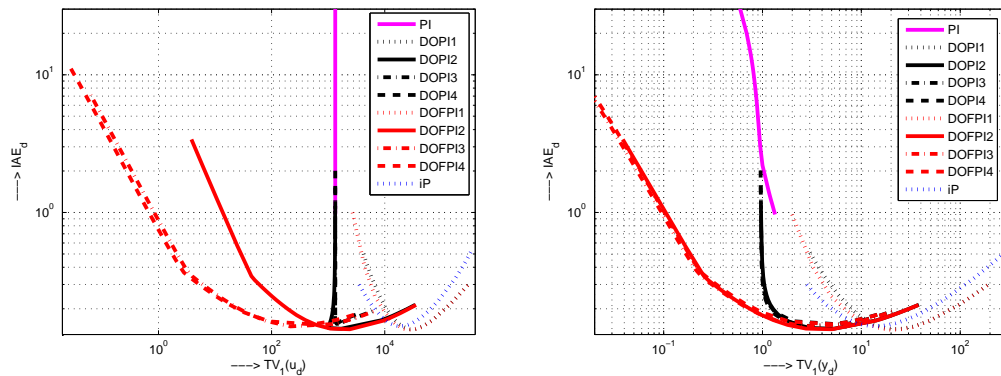


Figure: “Speed” versus shape related deviations at the input and output

Navigation icons

M.Huba, P. Tapak, S. Chamraz, STU Bratislava, Slovakia

Comparing model-free and disturbance observer based control

## Conclusions

- PI control yields the slowest transients with high noise impact
- For longer  $L$ , iP control yields faster/better attenuated transients than DO-PI and DO-FPI for  $n = 1$  and  $T_n = L$
- DO based solution allow to reach lower IAE values than iP
- To decrease the noise impact at the **output** use  $n \geq 2$
- To decrease the noise impact at the **input** use  $n \geq 3$
- DO-FPI control significantly increases the range of noise attenuation with respect to other types of control
- Possible improvements against PI control offered by newer alternatives may be characterized by 2-3 digit figures
- Experimentally confirmed for the DO based filtered PI and PID control of industrial drives [7, 14]
- Higher order filters influence also the loop robustness [8]
- After being equipped by GUI, all Matlab files will be made available in Moodle (for the address see ResearchGate)

## References: iP, DO-FPI and filtered PI/PID control

- 1 M. Fliess and C. Join, Model-free control, IJC 86, 2228-2252
- 2 M. Huba, and M. Šimunek, Modular Approach to Teaching PID Control. In: IEEE Transactions on Industrial Electronics. 54, 6, 2007, 3112-3120
- 3 M. Huba, Open and flexible P-controller design, AMC Sarajevo, BIH, 2012
- 4 M. Huba, Modular disturbance observer based constrained PI controller design, Int. Conf. AMC Sarajevo, BIH, 2012
- 5 M. Huba, Comparing 2DOF PI and Predictive Disturbance Observer Based Filtered PI Control, JPC 23 2013, 1379-1400.
- 6 M. Huba, Modular PID-controller design with different filtering properties, 39th Annual Conference of the IEEE Industrial Electronics Society (IECON). Vienna, Austria: IEEE, 2013.
- 7 M. Huba and I. Belai, Noise attenuation motivated controller design. Part I: Speed control, Speedam, Capri, Italy, 2014.
- 8 M. Huba, Robustness versus performance in PDO FPI Control of the IPDT plant, ICM2015. Nagoya, Japan.
- 9 M. Huba, Filter choice for an effective measurement noise attenuation in PI & PID controllers, ICM2015 Nagoya, Japan.
- 10 M. Huba, Analyzing limits of one type of disturbance observer based PI control by the performance portrait method. MED'15. Torremolinos, Spain.
- 11 K. J. Aström and T. Hägglund, Advanced PID Control. NC: ISA, Research Triangle Park, 2006.
- 12 V. R. Segovia, T. Hägglund and K. J. Aström, Measurement noise filtering for PID controllers, JPC 24, 299 - 313
- 13 S. Skogestad. Simple analytic rules for model reduction and PID controller tuning. JPC 13, 291-309.
- 14 M. Huba and I. Belai, Experimental Evaluation of a DO-FPID Controller with Different Filtering Properties. IFAC WC 2015 Cape Town

Thank you for your attention

Invitation to IFAC ACE'2016 Bratislava



M.Huba, P. Tapak, S. Chamraz, STU Bratislava, Slovakia      Comparing model-free and disturbance observer based control



# On Discretization of Sliding Mode Based Control Algorithms

Stefan Koch<sup>a</sup>

Markus Reichhartinger<sup>a</sup>

Martin Horn<sup>a</sup>

Variable structure control techniques are one proper method to deal with control problems for uncertain or disturbed systems. In the last decades especially sliding mode concepts which can be used in controllers or observers have stood out over classical approaches, due to their simplicity and advantages such as robustness and finite time convergence. In order to achieve an ideal sliding mode, it is assumed that the switching of a discontinuous control input takes place at an infinitely high frequency. However, when it comes to digital implementations of such controllers this assumption cannot hold true anymore and switching delays limit the existence of a true sliding mode. Consequently, in a time discretized sliding mode system, the invariance property of the sliding manifold is deteriorated and trajectories form limit cycles around the sliding surface. The characteristics of this effects, which often are referred to as discretization chattering, are influenced by the discretization method, the selected sampling frequency as well as the choice of parameters [3, 4]. In order to maintain good control performance or estimation precision after digitization, the discrete time sliding mode system may be modified compared to its explicit discretized continuous time counterpart [1, 2].

This talk will focus on discretization effects in conventional (first-order) and super-twisting based sliding mode control systems. Recent approaches involving various discretization schemes of equivalent control based methods are summarized. The influence of the choice of the sampling frequency and controller parameters on the control precision are discussed.

- [1] HUBER, O., V. ACARY und B. BROGLIATO: *Comparison between explicit and implicit discrete-time implementations of sliding-mode controllers*. In: *Decision and Control (CDC), 2013 IEEE 52nd Annual Conference on*, Seiten 2870–2875, Dec 2013.
- [2] LIVNE, M. und A. LEVANT: *Homogeneous discrete differentiation of functions with unbounded higher derivatives*. In: *Decision and Control (CDC), 2013 IEEE 52nd Annual Conference on*, Seiten 1762–1767, Dec 2013.
- [3] QU, SHAOCHENG, XIAOHUA XIA und JIANGFENG ZHANG: *Dynamical Behaviors of an Euler Discretized Sliding Mode Control Systems*. *Automatic Control, IEEE Transactions on*, 59(9):2525–2529, Sept 2014.
- [4] YAN, YAN, XINGHUO YU und CHANGYIN SUN: *Discretization behaviors of a super-twisting algorithm based sliding mode control system*. In: *Recent Advances in Sliding Modes (RASM), 2015 International Workshop on*, Seiten 1–5, April 2015.

---

<sup>a</sup>Institute of Automation and Control, Graz University of Technology, Kopernikusgasse 24/II, 8010 Graz, E-Mail: stefan.koch@tugraz.at

# On Discretization of Sliding Mode Based Control Algorithms

**Stefan Koch, Institute of Automation and Control**

Graz, 08. September 2015

 [www.irt.tugraz.at](http://www.irt.tugraz.at)



## Contents

1. First Order Sliding Mode
  - Explicit Euler Discretization
  - Zero-Order-Hold Discretization
  - Implicit Discretization
  
2. Second-Order Sliding Mode
  - Euler Discretization of Super Twisting Algorithm

## Notation

Terms including  $|x|^\gamma \text{sign}(x)$  are abbreviated in the compact way

$$[\cdot]^\gamma := |\cdot|^\gamma \text{sign}(\cdot)$$

$$\text{sign}(\sigma) := \begin{cases} 1 & \sigma > 0 \\ [-1, 1] & \sigma = 0 \\ -1 & \sigma < 0 \end{cases}$$

examples are

$$[x]^{\frac{1}{2}} = |x|^{\frac{1}{2}} \text{sign}(x)$$

$$[x]^0 = \text{sign}(x)$$

In difference equations the following notation is used

$$x' := x_{k+1}$$

$$x := x_k$$

## First Order Sliding Mode

$$\frac{dx}{dt} = Ax + bu \quad (1)$$

where  $x \in \mathbb{R}^n$ ,  $u \in \mathbb{R}$

$$A = \begin{bmatrix} 0 & 1 & 0 & \cdots & 0 \\ 0 & 0 & 1 & \cdots & 0 \\ \vdots & \vdots & \ddots & \ddots & \vdots \\ 0 & 0 & \cdots & 0 & 1 \\ -a_1 & -a_2 & \cdots & -a_{n-1} & -a_n \end{bmatrix}, \quad b = \begin{bmatrix} 0 \\ 0 \\ \vdots \\ 0 \\ 1 \end{bmatrix}$$

# First Order Sliding Mode

Specify a sliding manifold

$$S := \{\mathbf{x} | \sigma(\mathbf{x}) = 0\}, \quad \text{where } \sigma = \mathbf{c}^T \mathbf{x}$$

The coefficients  $\mathbf{c}^T = (c_1, c_2, \dots, c_{n-1}, 1)$  are chosen such that the characteristic polynomial of the compensated dynamics

$$x_1^{(n-1)} + c_{n-1}x_1^{(n-2)} + \dots + c_2\dot{x}_1 + c_1x_1 = 0$$

is Hurwitz and  $\mathbf{c}^T$  is rescaled s.t.  $\mathbf{c}^T \mathbf{b} = 1$ .

$$\dot{\sigma} < 0$$

and thus drives  $\sigma$  to zero. Choosing the control

$$u = \underbrace{-\mathbf{c}^T \mathbf{A} \mathbf{x}}_{u_{\text{equ}}} - \alpha [\sigma]^0$$

will ensure that the sliding mode is reached in finite time and maintained.

# First Order Sliding Mode

$$u = -\mathbf{c}^T \mathbf{A} \mathbf{x} - \alpha [\sigma]^0$$

The closed loop system results in:

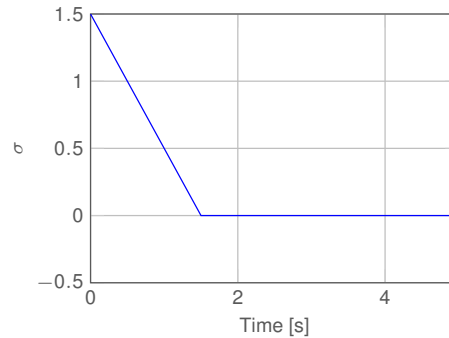
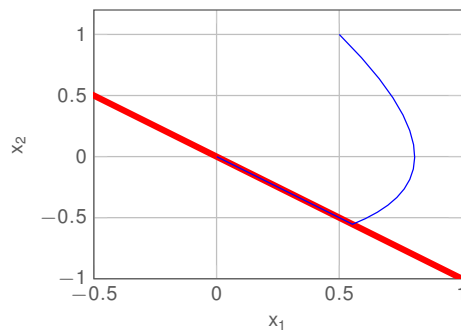
$$\frac{d\mathbf{x}}{dt} = \underbrace{(\mathbf{A} - \mathbf{b}\mathbf{c}^T \mathbf{A})}_{=: \mathbf{A}_c} \mathbf{x} - \alpha \mathbf{b} [\sigma]^0$$

and the dynamics of the switching function take the form:

$$\dot{\sigma} = -\alpha [\sigma]^0 \quad (2)$$

## System of Order $n = 2$

$$\mathbf{A}_c = \begin{bmatrix} 0 & 1 \\ 0 & -c_1 \end{bmatrix}, c_1 > 0$$



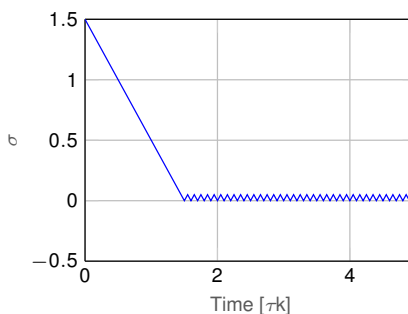
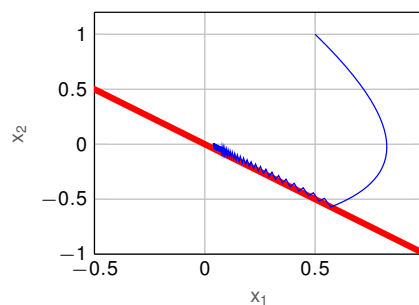
$\mathbf{x}_0 = [0.5 \ 1]^T$ ,  $\alpha = 1$ . Trajectories reach  $\mathcal{S} := \{\mathbf{x} | \mathbf{c}^T \mathbf{x} = 0\}$  in finite time and asymptotically converge to the origin. In sliding mode the the system is insensitive to matched bounded disturbances.  $\frac{d\mathbf{x}}{dt} = \mathbf{A}\mathbf{x} + \mathbf{b}(u + \Delta)$

## Discretization using Euler Forward Method

$$\mathbf{x}' = (\mathbf{I} + \tau \mathbf{A}_c) \mathbf{x} - \tau \alpha \mathbf{b} [\sigma]^0, \quad \sigma = \mathbf{c}^T \mathbf{x}$$

where  $\tau$  denotes the discretization step size. The switching function dynamics results in:

$$\sigma' = \sigma - \tau \alpha [\sigma]^0$$



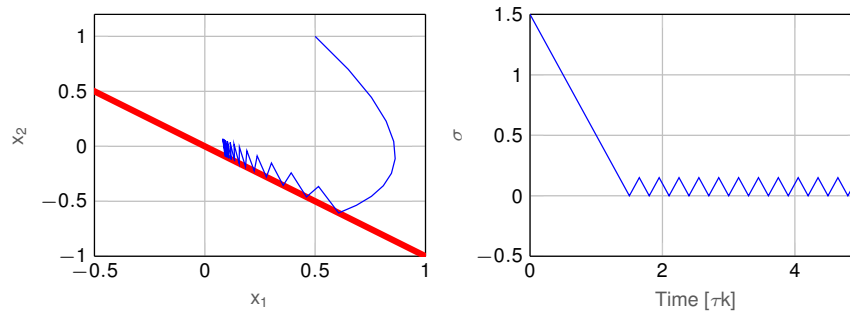
$\mathbf{x}_0 = [0.5 \ 1]^T$ ,  $\alpha = 1$  and  $\tau = 0.05$

## Discretization using Euler Forward Method

$$\mathbf{x}' = (\mathbf{I} + \tau \mathbf{A}_c) \mathbf{x} - \tau \alpha \mathbf{b} [\sigma]^0, \quad \sigma = \mathbf{c}^T \mathbf{x}$$

where  $\tau$  denotes the discretization step size. The switching function dynamics results in:

$$\sigma' = \sigma - \tau \alpha [\sigma]^0$$



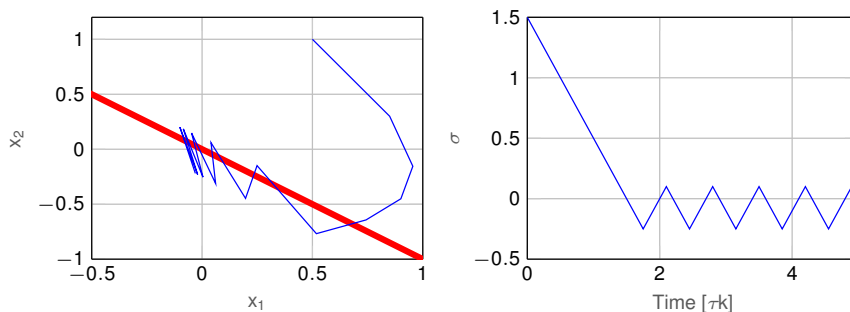
$$\mathbf{x}_0 = [0.5 \quad 1]^T, \quad \alpha = 1 \text{ and } \tau = 0.15$$

## Discretization using Euler Forward Method

$$\mathbf{x}' = (\mathbf{I} + \tau \mathbf{A}_c) \mathbf{x} - \tau \alpha \mathbf{b} [\sigma]^0, \quad \sigma = \mathbf{c}^T \mathbf{x}$$

where  $\tau$  denotes the discretization step size. The switching function dynamics results in:

$$\sigma' = \sigma - \tau \alpha [\sigma]^0$$



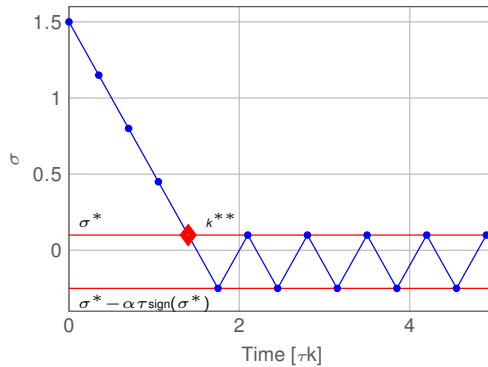
$$\mathbf{x}_0 = [0.5 \quad 1]^T, \quad \alpha = 1 \text{ and } \tau = 0.35$$

# Euler Discretization

According to Qu et al.<sup>1</sup>:

Switching function  $\sigma$  starting from  $\mathbf{x}_0$  converges to an **asymmetric** periodic-2 orbit.

$$\{\sigma^*, \sigma^* - \tau\alpha \cdot \text{sign}(\sigma^*)\} \in [\alpha\tau, -\alpha\tau]$$



Switching function is bounded by

$$|\sigma| \leq \tau\alpha$$

System States are bounded by

$$|x_1| \leq \frac{\tau\alpha}{c_1(2 - \tau c_1)}$$

$$|x_2| \leq \frac{\tau\alpha}{(2 - \tau c_1)}$$

$$\sigma' = \sigma - \tau\alpha[\sigma]^0$$

<sup>1</sup>S. Qu, X. Xia, and J. Zhang, Dynamical behaviors of an euler discretized sliding mode control systems, Automatic Control, IEEE Transactions on, vol. 59, pp. 25252529, Sept 2014.

# Euler Discretization

Using a constant plus proportional rate reaching law as suggested by [1]

$$u = -\mathbf{c}^T \mathbf{A} \mathbf{x} - \beta\sigma - \alpha[\sigma]^0$$

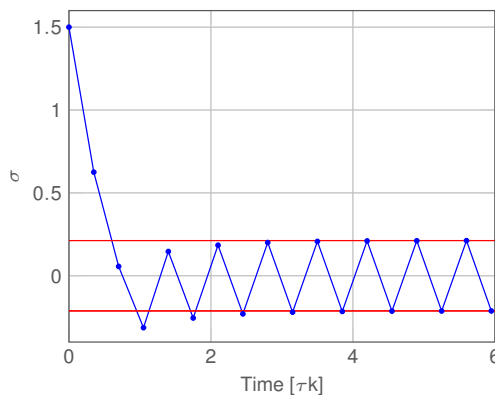
dynamics of the switching function are:

$$\sigma' = (1 - \beta\tau)\sigma - \tau\alpha[\sigma]^0 \quad (3)$$

for  $0 < 1 - \beta\tau \leq 1$  and  $\beta > 0$ :

Switching function  $\sigma$  starting from any  $\mathbf{x}_0$  converges to a **symmetric** periodic-2 orbit.

$$\left\{ \frac{-\alpha\tau}{2 - \beta\tau}, \frac{-\alpha\tau}{2 - \beta\tau} \right\}$$



## Zero Order Hold (ZOH) Discretization

$u(t) = u$  in the interval  $[k\tau, (k+1)\tau)$

$$\mathbf{x}' = \Phi \mathbf{x} + \mathbf{h}u$$

where  $\Phi = e^{\mathbf{A}\tau}$  and  $\mathbf{h} = \int_0^\tau e^{\mathbf{A}s} \mathbf{b} ds$

## Implicit Discretization

Let us choose the equivalent control for the nominal system

$$u_{equ} = -(\mathbf{c}^T \mathbf{h})^{-1} [\mathbf{c}^T (\Phi - \mathbf{I}) \mathbf{x}]$$

s.t. the switching function is of the form:

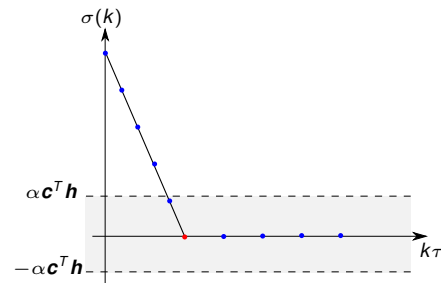
$$\sigma' = \sigma + \mathbf{c}^T \mathbf{h} u_s$$

where  $u_s$  is the discontinuous control. Now use an implicit discretization of the discontinuous part as suggested by Huber et al.<sup>2</sup>

$$\begin{cases} \sigma' = \sigma + \mathbf{c}^T \mathbf{h} u_s \\ u_s \in -\alpha \cdot \text{sign}(\sigma') \end{cases}$$

The set-valued equation can be solved by

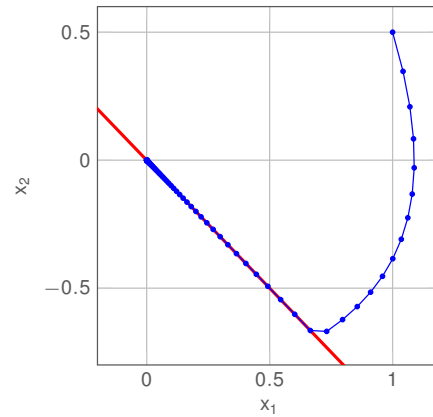
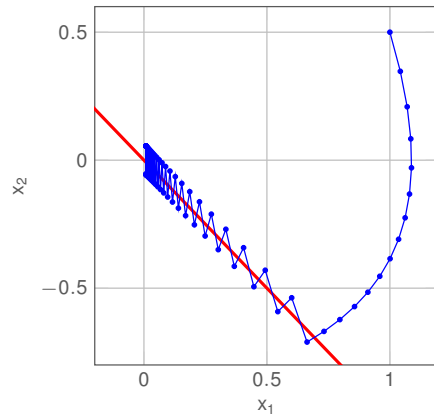
$$u_s = \begin{cases} -\alpha [\sigma]^0 & \text{if } |\sigma| > \alpha \mathbf{c}^T \mathbf{h} \\ -\frac{\sigma}{\mathbf{c}^T \mathbf{h}} & \text{else} \end{cases}$$



<sup>2</sup>O. Huber, V. Acary, and B. Brogliato, Comparison between explicit and implicit discrete-time implementations of sliding-mode controllers, in Decision and Control (CDC), 2013 IEEE 52nd Annual Conference on, pp. 28702875, Dec 2013.

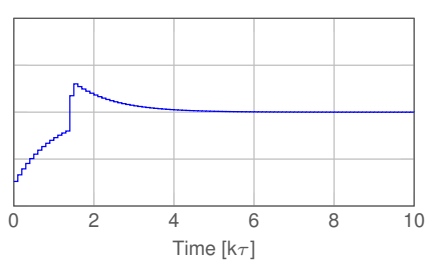
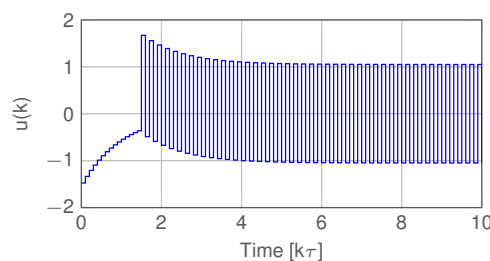
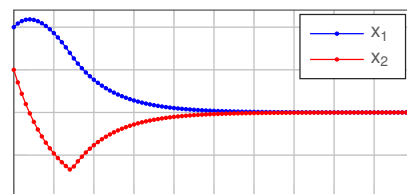
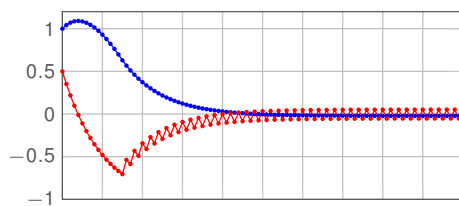


# Explicit vs. Implicit Discretization



parameters are selected  $\tau = 0.1$ ,  $c_1 = 1$ ,  $\alpha = 1$

# Explicit vs. Implicit Discretization



parameters are selected  $\tau = 0.1$ ,  $c_1 = 1$ ,  $\alpha = 1$

## Implicit Discretization with Disturbance

Assume that disturbance changes 'sufficiently' slow i.e.  $\Delta \approx \Delta'$  and appears matched. From the open loop system

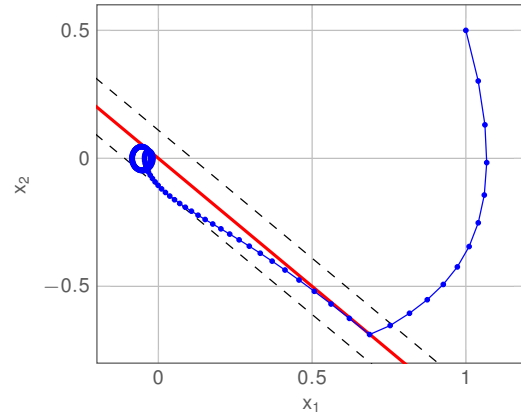
$$\mathbf{x}' = \Phi \mathbf{x} + \mathbf{h}(u + \Delta)$$

solve for  $\Delta$

$$\mathbf{h}\Delta = \mathbf{x}' - \Phi \mathbf{x} - \mathbf{h}u$$

and shifting gives an estimate of the disturbance linear in the input vector

$$\mathbf{h}\Delta_{k-1} = \mathbf{x}_k - \Phi \mathbf{x}_{k-1} - \mathbf{h}u_{k-1}$$



$$|\sigma| \leq \alpha \mathbf{c}^T \mathbf{h} \text{ where } \mathbf{c}^T \mathbf{h} = \mathcal{O}(\tau)$$

$$\Delta = -0.5 + 0.5 \sin(1.5k\tau)$$

## Implicit Discretization with Disturbance

$\mathbf{c}^T \mathbf{b} = 1$  is chosen in the design. By using the relation

$$\mathbf{h} = \int_0^\tau e^{\mathbf{A}s} \mathbf{b} ds = \mathbf{A}^{-1}(\Phi - \mathbf{I})\mathbf{b}$$

solving for  $\mathbf{b}$  and multiplying from left side by  $\mathbf{c}^T$  gives

$$\mathbf{c}^T \mathbf{b} = \mathbf{c}^T (\Phi - \mathbf{I})^{-1} \mathbf{A} \mathbf{h} = 1$$

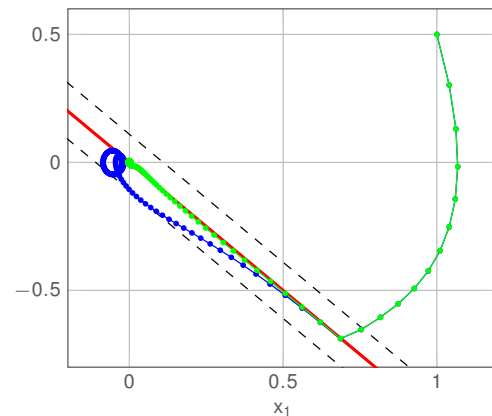
premultiplication of  $\mathbf{h}\Delta_{k-1}$  yields

$$\mathbf{c}^T (\Phi - \mathbf{I})^{-1} \mathbf{A} \mathbf{h} \Delta_{k-1} = \Delta_{k-1}$$

The control law then is given by

$$u_{eq} = (\mathbf{c}^T \mathbf{h})^{-1} \mathbf{c}^T (\mathbf{I} - e^{\mathbf{A}h}) \mathbf{x}$$

$$u_s = \begin{cases} -\alpha [\sigma]^0 & \text{if } |\sigma| > \alpha \mathbf{c}^T \mathbf{h} \\ -\frac{\sigma}{\mathbf{c}^T \mathbf{h}} - \Delta_{k-1} & \text{else} \end{cases}$$



— Implicit with disturbance compensation  
 $\Delta = -0.5 + 0.5 \sin(1.5k\tau)$

# Bounds for the Switching Function

If derivative of disturbance is bounded

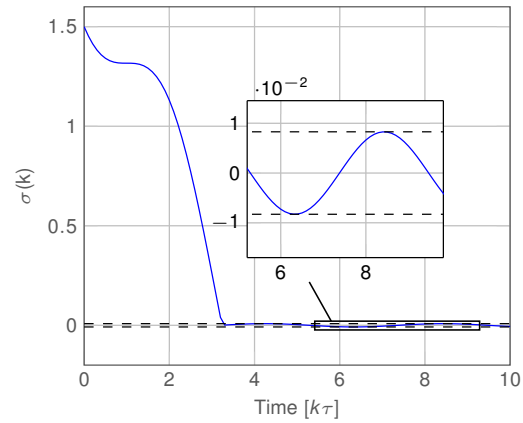
$$\frac{d\Delta}{dt} \approx \frac{\Delta_{k+1} - \Delta_k}{\tau} \leq \bar{\Delta}$$

Error is bounded by

$$\min\{\bar{\Delta}\tau\mathbf{c}^T\mathbf{h}, \alpha\mathbf{c}^T\mathbf{h}\}$$

and

$$\tau\mathbf{c}^T\mathbf{h} = \mathcal{O}(\tau^2)$$



Disturbance  $\Delta = 0.5 + 0.5 \sin(1.5k\tau)$ ,  $\tau = 0.1$ ,  
 $|\sigma| \leq \bar{\Delta}\tau\mathbf{c}^T\mathbf{h} = 0.0083$

# Super Twisting (STW) Controller

Consider again the relative-degree-one system

$$\sigma = \mathbf{c}_1\mathbf{x}_1 + \mathbf{x}_2$$

and applying the control

$$u = -u_{equ} - k_1[\sigma]^{\frac{1}{2}} - k_2 \int_0^t [\sigma]^0 ds$$

leads to the following the switching function dynamics

$$\dot{\sigma} = -k_1[\sigma]^{\frac{1}{2}} + v + \Delta(t)$$

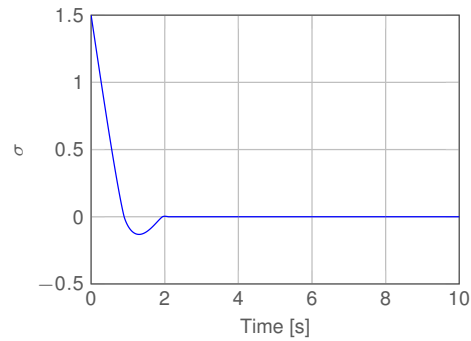
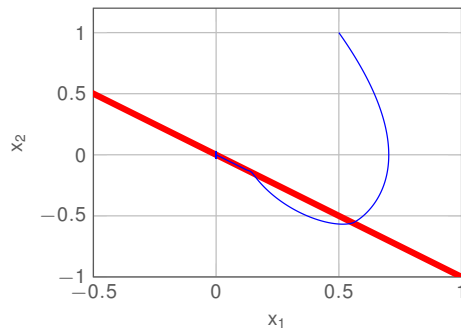
$$\dot{v} = -k_2[\sigma]^0$$

Assume that  $\dot{\Delta}(t)$  is bounded. Introducing the variable  $w := v + \Delta(t)$  we can rewrite the system as

$$\dot{\sigma} = -k_1[\sigma]^{\frac{1}{2}} + w$$

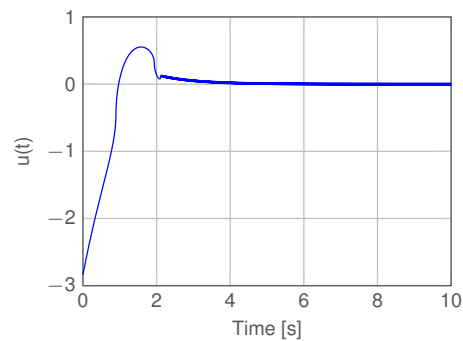
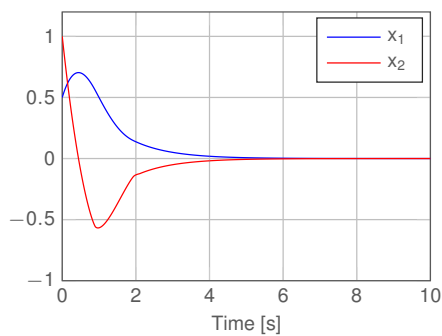
$$\dot{w} = -k_2[\sigma]^0 + \dot{\Delta}(t)$$

## Example: Double Integrator



$$\mathbf{x}_0 = [0.5 \ 1]^T, k_1 = 1.5, k_2 = 1.1$$

## Example: Double Integrator



$$\mathbf{x}_0 = [0.5 \ 1]^T, k_1 = 1.5, k_2 = 1.1$$

Remark: under bounded Lipschitz perturbations  $|\dot{\Delta}| \leq L$  a proper choice of parameters is

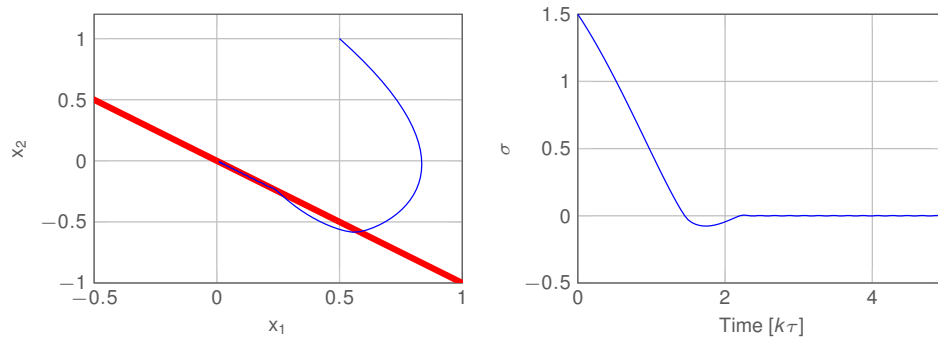
$$\begin{aligned} k_1 &= \lambda_1 \sqrt{L} \\ k_2 &= \lambda_0 L \end{aligned}$$

with  $\lambda_0 = 1.1$  and  $\lambda_1 = 1.5$

$$\begin{aligned} \dot{\sigma} &= -k_1 [\sigma]^{\frac{1}{2}} + w \\ \dot{w} &= -k_2 [\sigma]^0 + \dot{\Delta}(t) \end{aligned}$$

# Discretization using Euler Forward Method

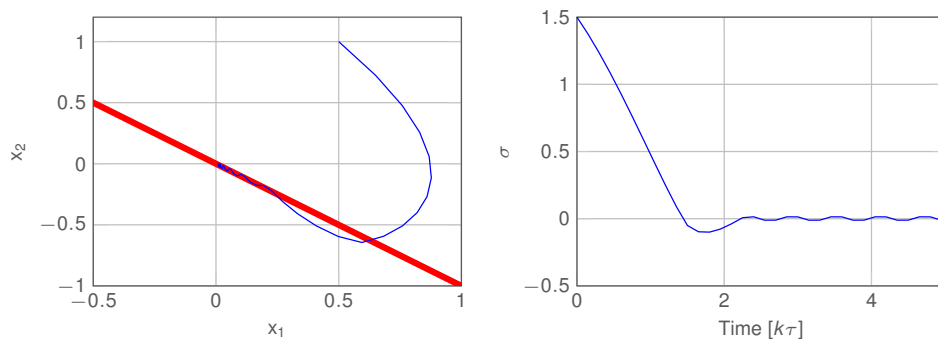
$$\begin{aligned}\sigma' &= \sigma - \tau k_1 [\sigma]^{\frac{1}{2}} + \tau w \\ w' &= w - \tau k_2 [\sigma]^0\end{aligned}$$



$\mathbf{x}_0 = [0.5 \ 1]^T$ ,  $k_1 = 1.5$ ,  $k_2 = 1.1$  and  $\tau = 0.05$

# Discretization using Euler Forward Method

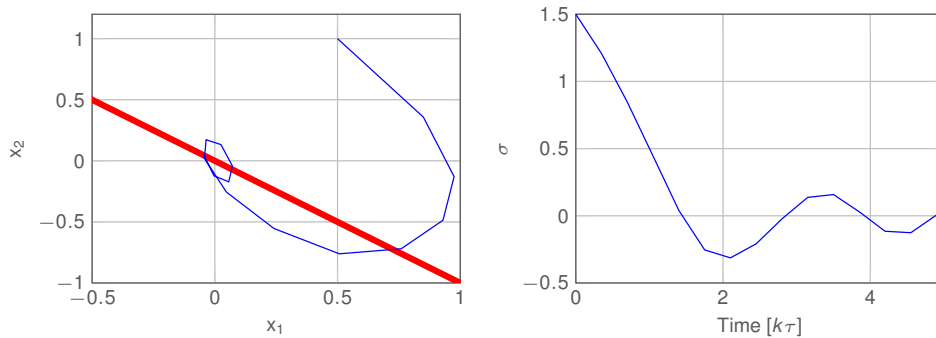
$$\begin{aligned}\sigma' &= \sigma - \tau k_1 [\sigma]^{\frac{1}{2}} + \tau w \\ w' &= w - \tau k_2 [\sigma]^0\end{aligned}$$



$\mathbf{x}_0 = [0.5 \ 1]^T$ ,  $k_1 = 1.5$ ,  $k_2 = 1.1$  and  $\tau = 0.15$

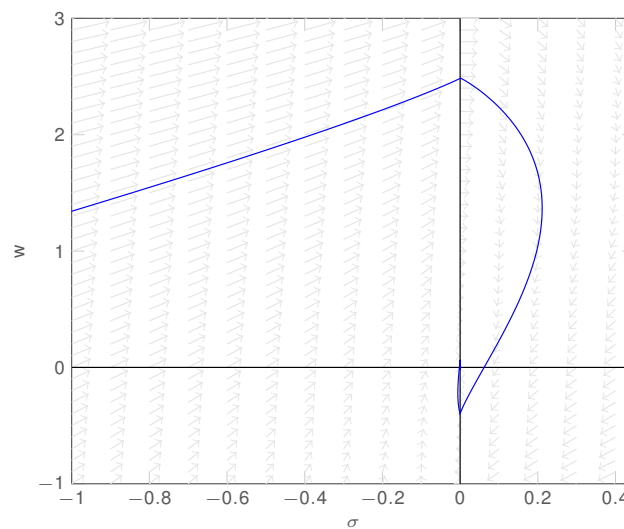
# Discretization using Euler Forward Method

$$\begin{aligned}\sigma' &= \sigma - \tau k_1 [\sigma]^{\frac{1}{2}} + \tau w \\ w' &= w - \tau k_2 [\sigma]^0\end{aligned}$$

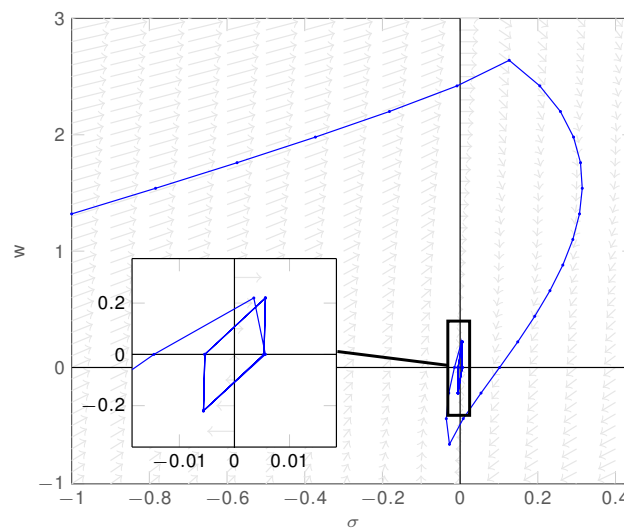


$\mathbf{x}_0 = [0.5 \ 1]^T$ ,  $k_1 = 1.5$ ,  $k_2 = 1.1$  and  $\tau = 0.35$

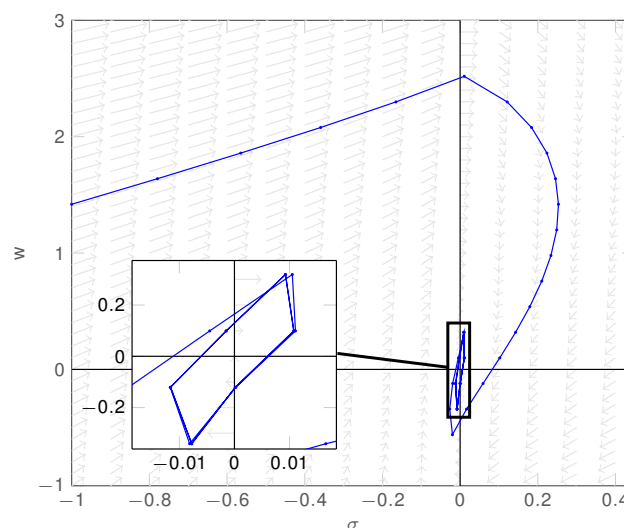
# Periodic Orbits



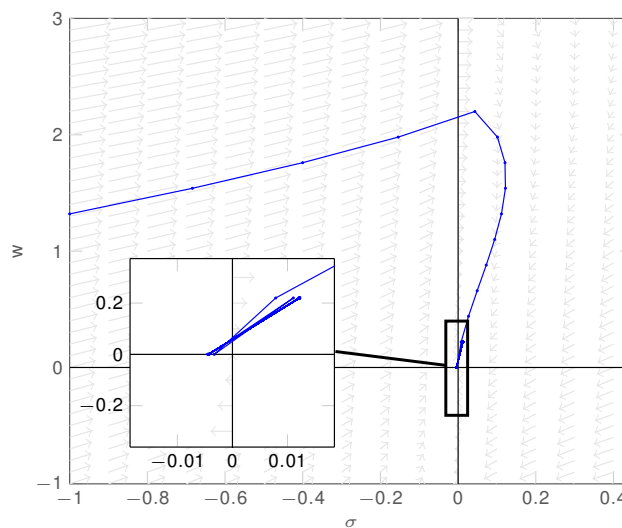
# Periodic Orbits



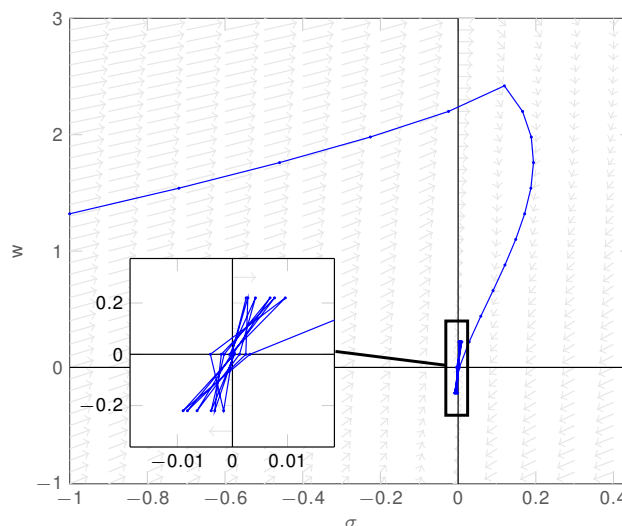
# Periodic Orbits



# Periodic Orbits



# Periodic Orbits



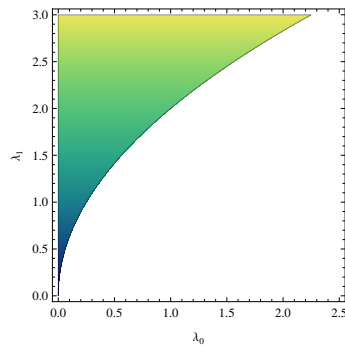


## Error Bounds in DTSTW

Bounds for  $\sigma$  and  $w_0$  can be found by solving for the fixed points of the period map

$$\begin{bmatrix} \sigma \\ w_0 \end{bmatrix}' = F(\sigma, w), \quad \text{where} \quad F = \underbrace{f \circ f \circ \dots \circ f}_{p\text{-times}}$$

If the trajectory eventually converges to a symmetric 2-periodic orbit then  $\lambda_0, \lambda_1$  is from the below set and  $w_0 = (n + 0.5)\lambda_0 L\tau$ ,  $n \in \mathbb{Z}$ .

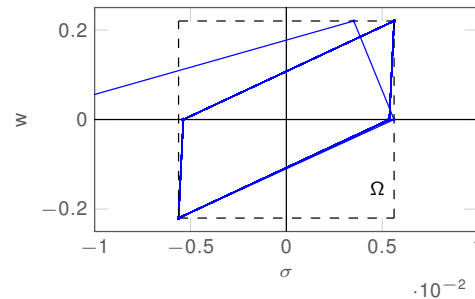
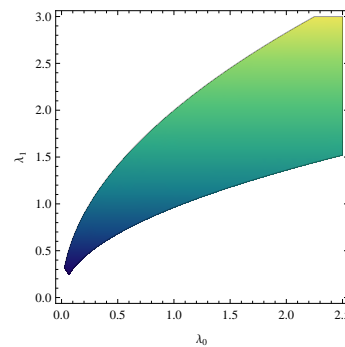


## Error Bounds in DTSTW

Bounds for  $\sigma$  and  $w_0$  can be found by solving for the fixed points of the period map

$$\begin{bmatrix} \sigma \\ w_0 \end{bmatrix}' = F(\sigma, w), \quad \text{where} \quad F = \underbrace{f \circ f \circ \dots \circ f}_{p\text{-times}}$$

If the trajectory eventually converges to a symmetric 4-periodic orbit then  $\lambda_0, \lambda_1$  is from the below set and  $w_0 = n\lambda_0 L\tau$ ,  $n \in \mathbb{Z}$ .

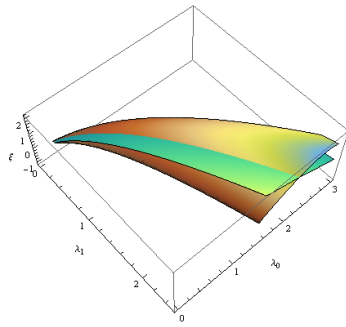


$$\lambda_0 = 1.1, \lambda_1 = 1.5, \tau = 0.05, L = 4 \text{ and } \xi = 0.562$$

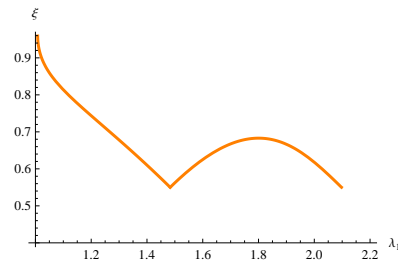
## Error Bounds in DTSTW

The fixed points of the time-4 map are

$$\begin{bmatrix} \sigma^* \\ w^* \end{bmatrix} = \left( \pm \begin{bmatrix} \tau^2 \xi_1(\lambda_0, \lambda_1) L \\ \tau \lambda_0 L \end{bmatrix}, \pm \begin{bmatrix} \tau^2 \xi_2(\lambda_0, \lambda_1) L \\ 0 \end{bmatrix} \right)$$



Parameters leading to minimum values for  $\sigma$  are found at the intersection of  $\xi_1$  and  $\xi_2$ .



The trajectory will eventually be bounded by:

$$\begin{aligned} |\sigma| &\leq \max(\xi_1, \xi_2) L \tau^2 \\ |w| &\leq \lambda_0 L \tau \end{aligned}$$

Fixing  $\lambda_0 = 1.1$  one finds  $\lambda_1 = 1.483$

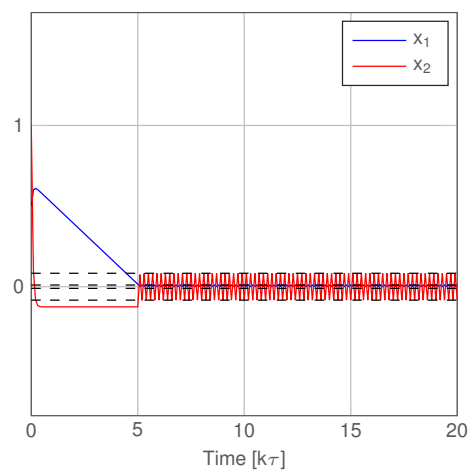
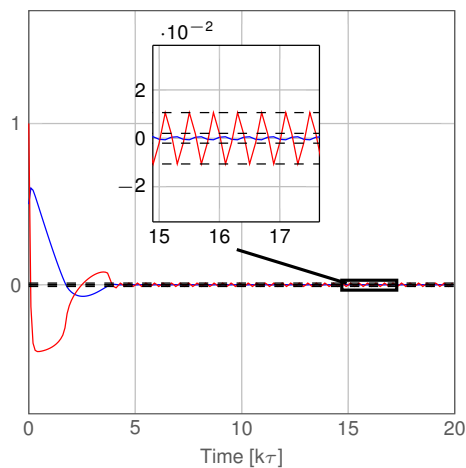
## Bounds of System States FOSM vs. STW

$$|x_1| < \bar{x}_1 = \xi L \tau^2 + \bar{x}_2$$

$$|x_2| \leq \bar{x}_2 = \frac{\tau^2 (\lambda_1 L \sqrt{\xi} (1 - c_1 \sqrt{\tau}) + c_1 L \lambda_0 \tau)}{2 + c_1 \tau (c_1 \tau - 2)}$$

$$|x_1| \leq \frac{\tau \alpha}{c_1 (2 - \tau c_1)}$$

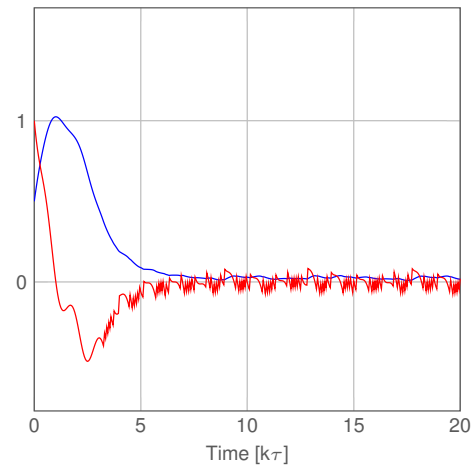
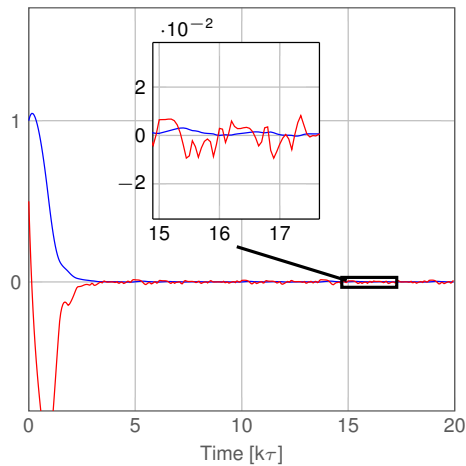
$$|x_2| \leq \frac{\tau \alpha}{(2 - \tau c_1)}$$



# STW vs. FOSM with perturbation

$$L = 2.5, \lambda_0 = 1.1, \lambda_1 = 1.5$$

$$\alpha = \lambda_0$$

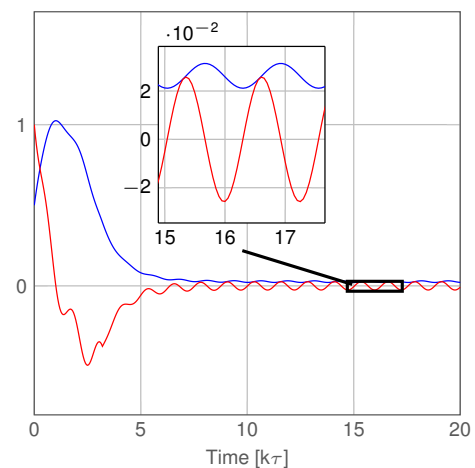
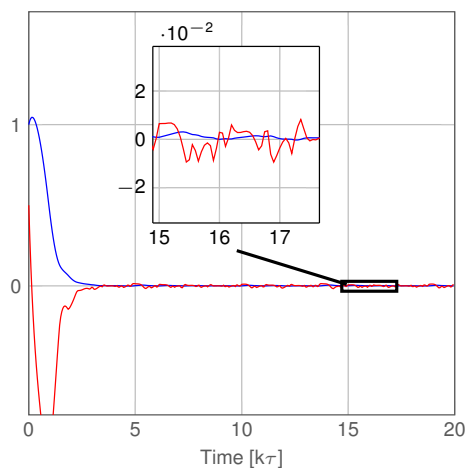


$$\Delta = 0.5 + 0.5 \sin(5k\tau), c = 1, \tau = 0.05$$

# STW vs. FOSM Implicit

$$L = 2.5, \lambda_0 = 1.1, \lambda_1 = 1.5$$

$$\alpha = \lambda_0$$

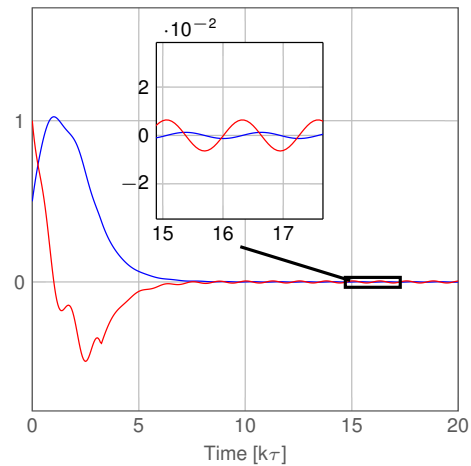
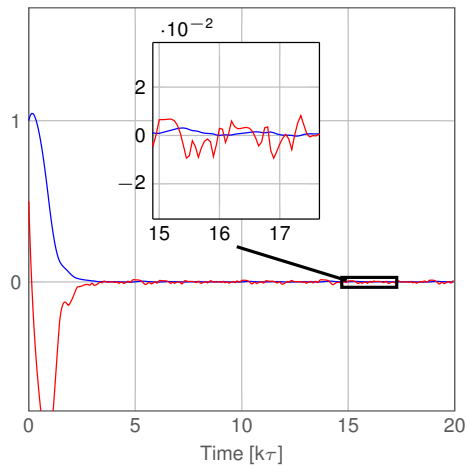


$$\Delta = 0.5 + 0.5 \sin(5k\tau), c = 1, \tau = 0.05$$

# STW vs. FOSM Implicit w. dist. comp.

$$L = 2.5, \lambda_0 = 1.1, \lambda_1 = 1.5$$

$$\alpha = \lambda_0$$



$$\Delta = 0.5 + 0.5 \sin(5k\tau), c = 1, \tau = 0.05$$

## Summary

- Conventional Sliding Mode provides precision  $\mathcal{O}(\tau)$  in the presence of bounded perturbations
- Implicit discretization scheme can remove discretization chattering
  - Additional disturbance compensation can provide for accuracy  $\mathcal{O}(\tau^2)$  in the presence of disturbances having bounded derivatives.
- Super Twisting provides naturally for precision  $\mathcal{O}(\tau^2)$  in the presence of disturbances having bounded derivatives
  - Periodic behavior of switching function is sensitive to initial conditions as well as to the choice of parameters
  - for certain parameters bounds for the switching function have been discussed.

# Outlook

## Conventional Sliding Mode

- Disturbance compensation for nonlinear systems

## Super Twisting

- Basin of attraction and stability properties of periodic orbits
- Best, respectively worst case precision for perturbed and unperturbed STW (relation to periodicity of periodic orbits)
- Implicit Super Twisting?
- Discretization behaviors of next generation Sliding Mode based control algorithms (Continuous Twisting)

# References and Further Reading I

- [1] V. Utkin, *Sliding Modes in Control and Optimization*. Springer-Verlag Berlin Heidelberg, 1992.
- [2] Z. Galias and X. Yu, "Analysis of zero-order holder discretization of two-dimensional sliding-mode control systems," *Circuits and Systems II: Express Briefs, IEEE Transactions on*, vol. 55, pp. 1269–1273, Dec 2008.
- [3] J. Moreno and M. Osorio, "Strict lyapunov functions for the super-twisting algorithm," *Automatic Control, IEEE Transactions on*, vol. 57, pp. 1035–1040, April 2012.
- [4] I. Salgado, I. Chairez, B. Bandyopadhyay, L. Fridman, and O. Camacho, "Discrete-time non-linear state observer based on a super twisting-like algorithm," *Control Theory Applications, IET*, vol. 8, pp. 803–812, July 2014.
- [5] Y. Yan, X. Yu, and C. Sun, "Discretization behaviors of a super-twisting algorithm based sliding mode control system," in *Recent Advances in Sliding Modes (RASIM), 2015 International Workshop on*, pp. 1–5, April 2015.
- [6] B. Bandyopadhyay and S. Janardhanan, *Discrete-time Sliding Mode Control*. Springer-Verlag Berlin Heidelberg, 2006.
- [7] M. Livne and A. Levant, "Accuracy of disturbed homogeneous sliding modes," in *Variable Structure Systems (VSS), 2014 13th International Workshop on*, pp. 1–6, June 2014.
- [8] W.-C. Su, S. Drakunov, and U. Ozguner, "An  $\sigma(t_2)$  boundary layer in sliding mode for sampled-data systems," *Automatic Control, IEEE Transactions on*, vol. 45, pp. 482–485, Mar 2000.

# Discontinuous integral control for mechanical systems

Jaime A. Moreno

Eléctrica y Computación, Instituto de Ingeniería,  
Universidad Nacional Autónoma de México,  
04510 México D.F., Mexico, JMorenoP@ii.unam.mx

## RESUMÉ

We consider a second order system

$$\begin{aligned}\dot{\xi}_1 &= \xi_2 \\ \dot{\xi}_2 &= f(\xi_1, \xi_2, t) + \rho(t) + \tau\end{aligned}\tag{1}$$

where  $\xi_1 \in \mathbb{R}$  and  $\xi_2 \in \mathbb{R}$  are the states,  $\tau \in \mathbb{R}$  is the control variable,  $f(\xi_1, \xi_2, t)$  is some known function, while the term  $\rho(t)$  corresponds to uncertainties and/or perturbations. System 1 can represent a mechanical system, where  $\xi_1$  is the position and  $\xi_2$  is the velocity. An important control task is to track a smooth time varying reference  $r(t)$ , i.e. if one defines the tracking error  $z_1 = \xi_1 - r$  and  $z_2 = \xi_2 - \dot{r}$  the objective is to asymptotically stabilize the origin of system

$$\begin{aligned}\dot{z}_1 &= z_2 \\ \dot{z}_2 &= f(\xi_1, \xi_2, t) + \rho(t) - \ddot{r}(t) + \tau.\end{aligned}\tag{2}$$

With the control  $\tau = u - f(\xi_1, \xi_2, t) + \ddot{r}(t)$  the system becomes

$$\begin{aligned}\dot{x}_1 &= x_2 \\ \dot{x}_2 &= u + \rho(t),\end{aligned}\tag{3}$$

where the perturbation  $\rho(t)$  is a time varying signal, not vanishing at the origin (i.e. when  $x = 0$  the perturbation can still be acting). We notice that it is possible not to feed the second derivative of the reference  $\ddot{r}(t)$  to the control  $\tau$ . In this case it will be considered as part of the perturbation term  $\rho(t)$ .

Under the stated hypothesis it is well known that a continuous, memoryless state feedback  $u = k(x)$  is not able to stabilize  $x = 0$ . This is so, because the controller has to satisfy with the condition  $k(0) = 0$ , since the closed loop has to have an equilibrium at the origin for vanishing perturbation. But if the perturbation does not vanish, then the origin cannot be anymore an equilibrium point. Discontinuous controllers, as the first order Sliding Mode (SM) ones [3], [2] are able to solve the problem for non vanishing (or persistently acting) bounded perturbations. However, they require the design of a sliding surface that is reached in finite time, but the target  $x = 0$  is attained only asymptotically fast, and at the cost of a high frequency switching of the control signal (the so called *chattering*), that has a negative effect in the actuator, and excites unmodelled dynamics of the plant. Higher Order Sliding Modes (HOSM) [4], [7], [6], [5], [9] provide a discontinuous controller for systems of relative degree higher than one to robustly stabilize the origin  $x = 0$  despite of bounded perturbations, but again at the expense of chattering. A natural alternative consists in adding an integrator, i.e. defining a new state  $z = u + \rho(t)$ , with  $\dot{z} = v$  and designing a third order HOSM controller for the new control variable  $v$ . This allows to reach the origin in finite time, and it will be insensitive to Lipschitz perturbations, i.e. with  $\dot{\rho}(t)$  bounded. In this form a continuous control signal  $u$  will be obtained, so that the chattering effect is reduced. However, this requires feedback not only the two states  $x_1$  and  $x_2$  but also the state  $z$ , which is unknown due to the unknown perturbation. Moreover, to implement an output feedback

controller (assuming that only the position  $x_1$  is measured) it is necessary to differentiate two times the position  $x_1$ , with the consequent noise amplification effect.

In the case of (almost) constant perturbations  $\rho(t)$  a classical solution to the robust regulation problem is the use of integral action, as for example in the PID control [1]. The linear solution would consist of a state feedback plus an integral action,  $u = -k_1x_1 - k_2x_2 + z$ ,  $\dot{z} = -k_3x_1$ . This controller requires only to feedback the position and the velocity. For an output feedback it would be only necessary to estimate the velocity (with the D action for example). In contrast to the HOSM controller this PID control is only able to reject constant perturbations, instead of Lipschitz ones, and it will reach the target only exponentially fast, and not in finite time. By the Internal Model Principle it would be possible to reject exactly any kind of time varying perturbations  $\rho(t)$ , for which a dynamical model (an exosystem) is available. However this would increase the complexity (order) of the controller, since this exosystem has to be included in the control law.

Here we provide a solution to the problem, that is somehow an intermediate solution between HOSM and PID control. Similar to the HOSM control our solution uses a discontinuous integral action, it can compensate perturbations with bounded derivative ( $\rho(t)$  is Lipschitz) and the origin is reached in finite time. So it can solve not only regulation problems (where  $\rho$  is constant) but also tracking problems (with  $\rho$  time varying) in finite time and with the same complexity of the controller. Similar to the PID control the proposed controller provides a continuous control signal (avoiding chattering) and it requires only to feedback position and velocity. We also provide for a (non classical) D term, i.e. a finite time converging observer, to estimate the velocity. This basic idea has been already presented in our previous work [10]. In the present one we give a much simpler Lyapunov-based proof, and we also include an observer in the closed loop together with its Lyapunov proof. Our solution can be seen as a generalization of the Super Twisting control for systems of relative degree one [9], [4], [7], [5], [8] to systems with relative degree two. Extensions to arbitrary order is also possible and it will be briefly discussed.

## REFERENCES

- [1] Khalil, H. K. (2002). *Nonlinear Systems*. Prentice Hall
- [2] Utkin, V. (2009). *Sliding Mode Control in Electro-Mechanical Systems*. CRC Press. Second edition. Automatic and Control Engineering.
- [3] Utkin, V. (1992). *Sliding Modes in Control and Optimization*. Springer-Verlag.
- [4] Fridman, L. y A. Levant (2002). *Sliding Mode in Control in Engineering*. Marcel Dekker, Inc. High Order Sliding Modes.
- [5] Levant, A. (2007). Principles of 2-sliding mode design. *Automatica*. **43**, 576–586.
- [6] Levant, A. (2005). Homogeneity approach to higher-order sliding mode design. *Automatica*. **34**, 576–586.
- [7] Levant A. Higher order sliding modes: differentiation and output feedback control. *\emph{Int. J. of Control}*; nov 2003; \textbf{76} (9-10):924–941.
- [8] Moreno, Jaime A.; M. Osorio (2012). Strict Lyapunov functions for the super-twisting algorithm. *IEEE Transactions on Automatic Control*. **54**, 1035–1040.
- [9] Levant, A. (1993). Sliding order and sliding accuracy in sliding mode control. *International Journal of Control*. **6**, 1247–1263.
- [10] Zamora, Cesar; Moreno, J. A.; Kamal, Shyam. Control Integral Discontinuo Para Sistemas Mecánicos. Congreso Nacional de Control Automático 2013. Asociación de México de Control Automático (AMCA). Ensenada, Baja California, 16-18 Octubre 2013. Pp. 11—16. <http://eventos.cicese.mx/amca2013/52.html>

---

# Discontinuous Integral Control for Mechanical Systems

---

Jaime A. Moreno

Universidad Nacional Autónoma de México  
Eléctrica y Computación, Instituto de Ingeniería,  
Universidad Nacional Autónoma de México,  
04510 México D.F., Mexico, JMorenoP@ii.unam.mx



8th. September 2015

19. Steirischen Seminar über Regelungstechnik und  
Prozessautomatisierung, Schloss Retzhof, Austria

◀ ◻ ▶ ◀ ◻ ▶ ◀ ≡ ▶ ◀ ≡ ▶ ≡ ≡ ≡ ≡ ≡ ≡ ≡ ≡ ≡

---

## Overview

---

- ① Introduction
  - Problem
  - Some Previous Solutions
  - Homogeneity
- ② Discontinuous Integral Controller: State Feedback
  - The I-Controller
  - Lyapunov Function
  - Caveat: Lack of Homogeneity
- ③ Discontinuous Integral Controller: Output Feedback
- ④ Conclusions

◀ ◻ ▶ ◀ ◻ ▶ ◀ ≡ ▶ ◀ ≡ ▶ ≡ ≡ ≡ ≡ ≡ ≡ ≡ ≡ ≡



## Overview

### 1 Introduction

- Problem
- Some Previous Solutions
- Homogeneity

### 2 Discontinuous Integral Controller: State Feedback

- The I-Controller
- Lyapunov Function
- Caveat: Lack of Homogeneity

### 3 Discontinuous Integral Controller: Output Feedback

### 4 Conclusions

## Overview

### 1 Introduction

- Problem
- Some Previous Solutions
- Homogeneity

### 2 Discontinuous Integral Controller: State Feedback

- The I-Controller
- Lyapunov Function
- Caveat: Lack of Homogeneity

### 3 Discontinuous Integral Controller: Output Feedback

### 4 Conclusions

## Problem

Second order system of relative degree 2 in normal form (e.g. mechanical system)

$$\begin{aligned}\dot{\xi}_1 &= \xi_2 \\ \dot{\xi}_2 &= f(\xi_1, \xi_2, t) + \tilde{\rho}(t) + \tau\end{aligned}\tag{1}$$

- states  $\xi_1 \in \mathbb{R}$  (position),  $\xi_2 \in \mathbb{R}$  (velocity),
- $\tau \in \mathbb{R}$  control variable,
- $f(\xi_1, \xi_2, t)$  known function,
- $\tilde{\rho}(t)$  uncertainties and/or perturbations.

**Control Task:** Robust tracking of a smooth reference  $r(t)$ .

## Problem reformulation

$$\begin{aligned}\dot{x}_1 &= x_2 \\ \dot{x}_2 &= u + \rho(t),\end{aligned}\tag{2}$$

- $x_1 = \xi_1 - r$ ,  $x_2 = \xi_2 - \dot{r}$  tracking errors,
- $\tau = u - f(\xi_1, \xi_2, t)$ ,  $u$  control variable,
- $\rho(t) = \tilde{\rho}(t) - \ddot{r}(t)$  uncertainties and/or perturbations.

**Control Task:** Robust Asymptotic Stabilization of  $x = 0$ .

## Overview

### 1 Introduction

- Problem
- Some Previous Solutions
- Homogeneity

### 2 Discontinuous Integral Controller: State Feedback

- The I-Controller
- Lyapunov Function
- Caveat: Lack of Homogeneity

### 3 Discontinuous Integral Controller: Output Feedback

### 4 Conclusions

## Some Previous Solutions

- Continuous, memoryless state feedback  $u = k(x)$ .
- Discontinuous, memoryless state feedback:
  - First Order Sliding Mode Controller (FOSM).
  - High Order Sliding Mode Controller (HOSM).
- Extended HOSM Controller.
- Continuous Integral Control (PID).

## Continuous State Feedback

- Continuous, memoryless state feedback  $u = k(x)$ .
  - Not able to robustly stabilize  $x = 0$ .
  - **Because**  $k(0) = 0 \Rightarrow$  Perturbation  $\rho(t)$  vanishing at  $x = 0$ !
  - Asymptotic Convergence with  $\rho(t) = 0$ .
  - Robust, but Sensitive to perturbations: Practical stability.
- Continuous (linear) state feedback controller

$$u = -k_1 x_1 - k_2 x_2$$

- Exponential Convergence with  $\rho(t) = 0$ .
- Continuous Homogeneous state feedback controller

$$u = -k_1 |x_1|^{\frac{1}{3}} - k_2 |x_2|^{\frac{1}{2}}$$

- $|\cdot|^\rho = |\cdot|^\rho \text{sign}(\cdot)$
- Finite Time Convergence with  $\rho(t) = 0$ .

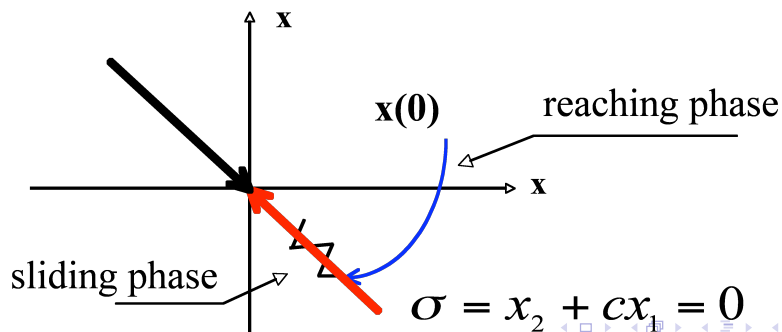
Navigation icons: back, forward, search, etc.

## First Order Sliding Mode Controller

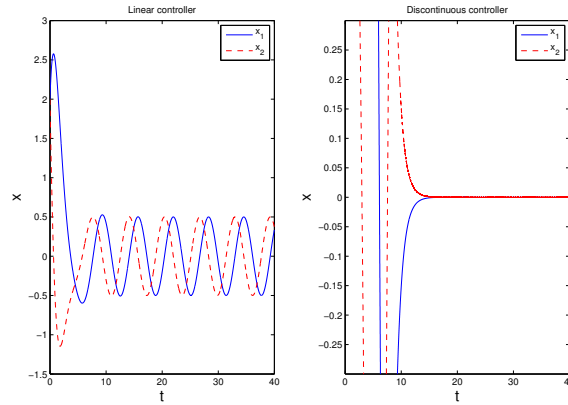
$$\begin{aligned}\dot{x}_1 &= x_2 \\ \dot{x}_2 &= -k_2 \text{sign}(x_2 + k_1 x_1) + \rho(t)\end{aligned}$$

Interpretation as **first order system** with a stable (first order) zero dynamics: with  $\sigma = x_2 + k_1 x_1$  **sliding variable**

$$\begin{aligned}\dot{x}_1 &= -k_1 x_1 + \sigma \\ \dot{\sigma} &= -k_2 \text{sign}(\sigma) + \rho(t)\end{aligned}$$



## Behavior with perturbation



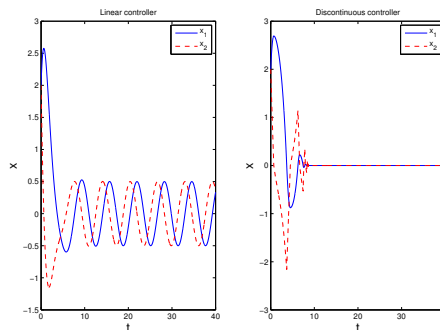
- FOSM control: **exponential** convergence and **insensitive** to perturbation!
- FOSM control **drawback**: Discontinuous control signal  $\Rightarrow$  Chattering

Navigation icons: back, forward, search, etc.

## HOSM: The Twisting Controller

**Finite-time** convergence and **insensitivity** to perturbations:

$$\begin{aligned}\dot{x}_1 &= x_2 \\ \dot{x}_2 &= -k_1 \text{sign}(x_1) - k_2 \text{sign}(x_2) + \rho(t)\end{aligned}$$



**Drawback**: Discontinuous control signal  $\Rightarrow$  Chattering

Navigation icons: back, forward, search, etc.

## Extended HOSM

$$\begin{aligned}\dot{x}_1 &= x_2 \\ \dot{x}_2 &= u + \rho(t) ,\end{aligned}$$

Define:  $x_3 = u + \rho(t)$

$$\begin{aligned}\dot{x}_1 &= x_2 \\ \dot{x}_2 &= x_3 \\ \dot{x}_3 &= v + \dot{\rho}(t),\end{aligned}$$

$v$ : discontinuous Third Order Sliding Mode Controller, e.g.

$$v = -k_3 \text{sign} \left( [\mathbf{x}_3]^{\frac{2}{3}} + k_2 x_2 + k_1 [x_1]^2 \right).$$

- Finite time convergence and **insensitive** to perturbation!
- Continuous control signal  $\Rightarrow$  Chattering reduction.
- **Drawback:** Estimation of the perturbation  $\rho(t)$ !

## Continuous Integral Controller (PID)

- System

$$\begin{aligned}\dot{x}_1 &= x_2 \\ \dot{x}_2 &= u + \rho(t) \, ,\end{aligned}$$

- PID-Controller (e.g. linear)

$$\begin{aligned} u &= -k_1(x_1, x_2) + k_I(x_3) \\ \dot{x}_3 &= -k_2(x_1, x_2), \end{aligned}$$

- $k_{1,2}(x_1, x_2)$  continuous,  $k_I(x_3)$  continuous/discontinuous.
- **Constant** perturbations/references  $\Rightarrow$  Asymptotic convergence and **insensitive** to perturbation!
- Arbitrary perturbations/ref  $\Rightarrow$  Practical convergence.
- Estimation of  $\rho(t)$  is **not** required for implementation.
- More general: Internal Model Principle based controller.

## Proposed Solution

- Combine Integral Action and Discontinuous Control.
- $k_1(x_1, x_2)$  and  $k_I(x_3)$  continuous,  $k_2(x_1, x_2)$  discontinuous.
- **Insensitive** to any Lipschitz perturbation (i.e. with bounded derivative).
- No estimation of the perturbation  $\rho(t)$  required for implementation.
- Continuous control signal  $\Rightarrow$  Chattering reduction.
- For simplicity (!?) we add **Homogeneity**.

## Overview

- 1 Introduction
  - Problem
  - Some Previous Solutions
  - Homogeneity
- 2 Discontinuous Integral Controller: State Feedback
  - The I-Controller
  - Lyapunov Function
  - Caveat: Lack of Homogeneity
- 3 Discontinuous Integral Controller: Output Feedback
- 4 Conclusions

## What is Homogeneity?

- Weighted Homogeneity (Zubov):  $r_i$ : weights,  $\delta$ : degree

$$\Lambda_r = \text{diag}\{\lambda^{r_1}, \dots, \lambda^{r_n}\},$$

$$V(\lambda^{r_1}x_1, \lambda^{r_2}x_2, \dots, \lambda^{r_n}x_n) = V(\Lambda_r x) = \lambda^\delta V(x), \forall \lambda > 0, r_i > 0$$

- Values on the unit sphere define a Homogeneous function.
- A system (vector field or Differential Inclusion) is Homogeneous if  $\dot{x} = f(x)$ , and

$$f(\Lambda_r x) = \lambda^\delta \Lambda_r f(x).$$

- Trajectories:  $\varphi(t, \Lambda_r x_0) = \Lambda_r \varphi(\lambda^\delta t, x_0)$

## Properties of Homogeneous Systems

- Zubov, Hahn, Hermes, Kawski, Rosier, Aeyels, Sepulchre, Grüne, Praly, Efimov, Polyakov,.....
- If  $x = 0$  Locally Attractive (LA)  $\Leftrightarrow$  Globally Asymptotically Stable (GAS)
- If  $x = 0$  GAS and  $\delta < 0 \Leftrightarrow x = 0$  Finite Time Stable
- If  $x = 0$  GAS and  $\delta = 0 \Leftrightarrow x = 0$  Exponentially Stable (e.g. LTI systems)
- If  $x = 0$  GAS and  $\delta > 0 \Leftrightarrow x = 0$  Asymptotically Stable
- If  $x = 0$  GAS  $\Leftrightarrow$  It exists a Homogeneous Lyapunov Function
- Approximation of NL systems: If  $x = 0$  is AS for the Homogeneous approximation  $\Rightarrow x = 0$  is Locally AS for the system.



## Overview

- 1 Introduction
  - Problem
  - Some Previous Solutions
  - Homogeneity
- 2 Discontinuous Integral Controller: State Feedback
  - The I-Controller
  - Lyapunov Function
  - Caveat: Lack of Homogeneity
- 3 Discontinuous Integral Controller: Output Feedback
- 4 Conclusions

## Overview

- 1 Introduction
  - Problem
  - Some Previous Solutions
  - Homogeneity
- 2 Discontinuous Integral Controller: State Feedback
  - The I-Controller
  - Lyapunov Function
  - Caveat: Lack of Homogeneity
- 3 Discontinuous Integral Controller: Output Feedback
- 4 Conclusions

## Continuous and Homogeneous State Feedback Controller

$$u = -k_1 \lceil x_1 \rceil^{\frac{1}{3}} - k_2 \lceil x_2 \rceil^{\frac{1}{2}}$$

Closed Loop System:

$$\begin{aligned}\dot{x}_1 &= x_2 \\ \dot{x}_2 &= -k_1 [x_1]^{\frac{1}{3}} - k_2 [x_2]^{\frac{1}{2}} + \rho(t) ,\end{aligned}$$

Lyapunov Function:

$$V(x_1, x_2, x_3) = \gamma_1 |x_1|^{\frac{5}{3}} + \gamma_{12} x_1 x_2 + |x_2|^{\frac{5}{2}},$$

Sensitive to perturbations.

## Homogeneous Integral + State Feedback Controller

Discontinuous Integral Controller ( $k_1, k_2, k_3 > 0$ ,  $k_4 \in \mathbb{R}$ ,  $L > 0$ )

$$\begin{aligned} u &= -k_1 L^{\frac{2}{3}} [x_1]^{\frac{1}{3}} - k_2 L^{\frac{1}{2}} [x_2]^{\frac{1}{2}} + z \\ \dot{z} &= -k_3 L \left[ x_1 + k_4 L^{-\frac{3}{2}} x_2^{\frac{3}{2}} \right]^0 \end{aligned}$$

Closed Loop System:

$$\begin{aligned}\dot{x}_1 &= x_2 \\ \dot{x}_2 &= -k_1 L^{\frac{2}{3}} [x_1]^{\frac{1}{3}} - k_2 L^{\frac{1}{2}} [x_2]^{\frac{1}{2}} + z + \rho(t) , \\ \dot{z} &= -k_3 L \left[ x_1 + k_4 L^{-\frac{3}{2}} x_2^{\frac{3}{2}} \right]^0\end{aligned}$$

If  $\rho(t) = 0$ : Stability for  $L = 1 \Rightarrow$  Stability for any  $L > 0$ .

## Remarks

- In contrast to the continuous Integral Controller:
  - It tracks exactly, in finite time and robustly
  - arbitrary references with bounded  $\ddot{r}(t)$
  - despite arbitrary (time) Lipschitz perturbations/uncertainties, i.e.  $\|\dot{\rho}(t)\| \leq \Delta$ ,  $\Delta$  constant
  - without an Internal Model.
- For implementation:  $r(t)$  and  $\dot{r}(t)$  are required but not  $\ddot{r}(t)$ .
- Define  $x_3 = z + \rho$ . After convergence  $\Rightarrow x(t) = 0 \Rightarrow z(t) = -\rho(t)$ : Integral action estimates the perturbation!
- Control signal is continuous  $\Rightarrow$  Chattering attenuation.
- Gain selection:
  - Set  $k_1, k_2$  so that state feedback stable and well-behaved without perturbation.
  - Select  $k_4 = 0$ ,  $k_4 > 0$ ,  $k_4 < 0$ .
  - Select  $k_3$  small to assure stability.
  - Select  $L$  sufficiently large to compensate the perturbations/uncertainties.

## Related controllers

- A similar algorithm is the "Continuous Twisting Algorithm". The proof is based on a Generalized Forms technique.

$$\begin{aligned} u &= -k_1 [x_1]^{\frac{1}{3}} - k_2 [x_2]^{\frac{1}{2}} + z \\ \dot{z} &= -k_3 [x_1]^0 - k_4 [x_2]^0 \end{aligned}$$

- The "High-Order Super Twisting"

$$\begin{aligned} u &= -k_1 \left[ x_2 + k_2 \lceil x_1 \rceil^{\frac{2}{3}} \right]^{\frac{1}{2}} + z \\ \dot{z} &= -k_3 \left[ x_2 + k_2 \lceil x_1 \rceil^{\frac{2}{3}} \right]^0 \end{aligned}$$

## Overview

### 1 Introduction

- Problem
- Some Previous Solutions
- Homogeneity

### 2 Discontinuous Integral Controller: State Feedback

- The I-Controller
- Lyapunov Function
- Caveat: Lack of Homogeneity

### 3 Discontinuous Integral Controller: Output Feedback

### 4 Conclusions

## Homogeneous and smooth Lyapunov Function

Homogeneous and smooth Lyapunov Function ( $L = 1$ )

$$V(x_1, x_2, x_3) = \gamma_1 |\xi_1|^{\frac{5}{3}} + \gamma_{12} \xi_1 x_2 + |x_2|^{\frac{5}{2}} + \frac{1}{5} |x_3|^5, \quad \xi_1 = x_1 - \frac{1}{k_1^3} [x_3]^3$$

Derivative  $\dot{V}$  is homogeneous and discontinuous:

$$\dot{V} = W_1(\xi_1, x_2) + W_2(\xi_1, x_2, x_3) + W_3(x, \dot{\rho}),$$

where

$$W_1 = \left( \frac{5}{3} \gamma_1 [\xi_1]^{\frac{2}{3}} + \gamma_{12} x_2 \right) x_2 + \\ - \frac{5}{2} k_2 \left( \frac{2}{5} \gamma_{12} \xi_1 + [x_2]^{\frac{3}{2}} \right) \left( \frac{k_1}{k_2} [\xi_1]^{\frac{1}{3}} + [x_2]^{\frac{1}{2}} \right)$$



## Overview

- 1 Introduction
  - Problem
  - Some Previous Solutions
  - Homogeneity
- 2 Discontinuous Integral Controller: State Feedback
  - The I-Controller
  - Lyapunov Function
  - Caveat: Lack of Homogeneity
- 3 Discontinuous Integral Controller: Output Feedback
- 4 Conclusions

## Caveat

Alternative *Integral + state feedback* controllers:

- Linear Integral + state feedback controller (Homogeneous)

$$\begin{aligned} u &= -k_1 x_1 - k_2 x_2 + x_3 \\ \dot{x}_3 &= -k_3 x_1 \end{aligned}$$

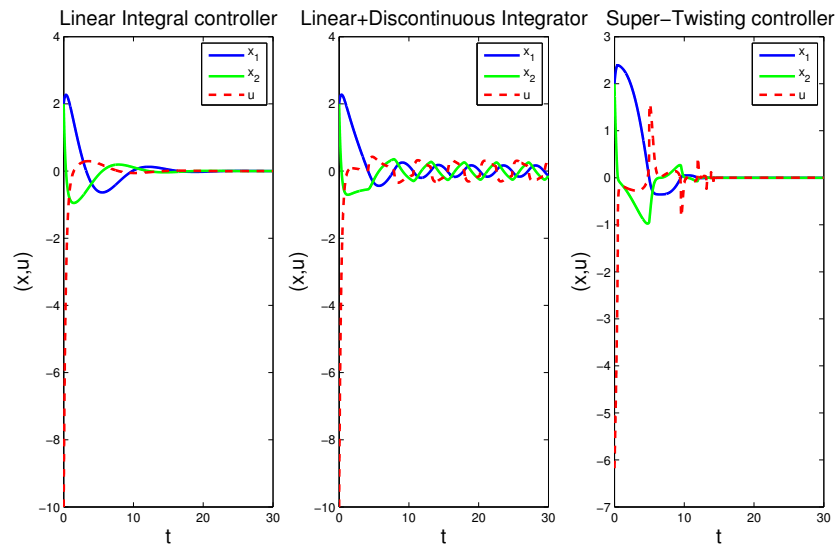
- Linear state feedback + Discontinuous Integral controller (Not Homogeneous)

$$\begin{aligned} u &= -k_1 x_1 - k_2 x_2 + x_3 \\ \dot{x}_3 &= -k_3 \text{sign}(x_1) \end{aligned}$$

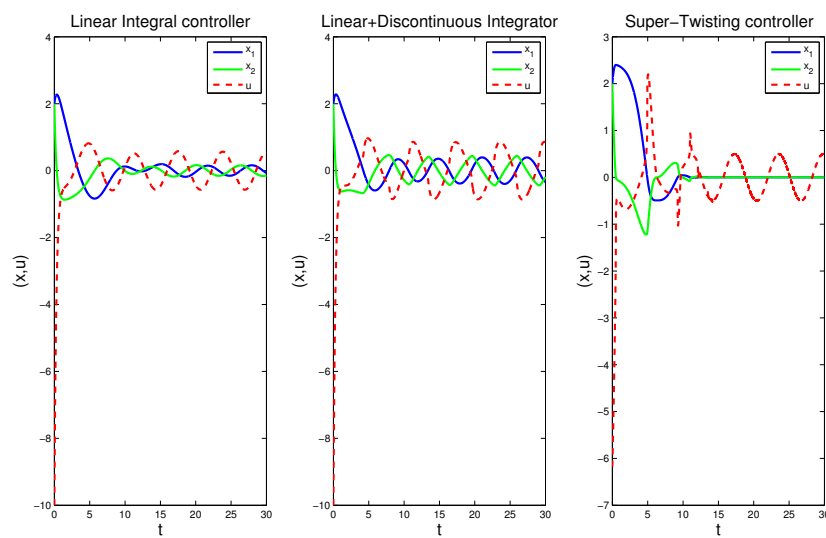
- Discontinuous I-Controller (Extended Super-Twisting) (Homogeneous)

$$\begin{aligned} u &= -k_1 |x_1|^{\frac{1}{3}} \text{sign}(x_1) - k_2 |x_2|^{\frac{1}{2}} \text{sign}(x_2) + x_3 \\ \dot{x}_3 &= -k_3 \text{sign}(x_1) \end{aligned}$$

## Controller without perturbation



## Controller with perturbation I



## Controller with perturbation II

- Linear stabilizes exponentially and is not insensitive to perturbation
- Linear + Discontinuous Integrator causes **oscillations** (Harmonic Balance). This is structural and for any  $n > 2$ . Eliminated by Homogeneity.
- Extended ST: Convergence in finite time and **insensitive to perturbations**.

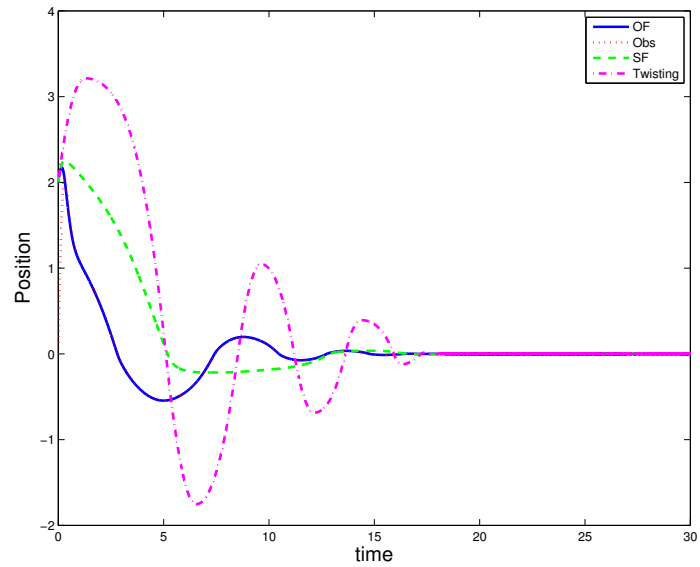
## Overview

- 1 Introduction
  - Problem
  - Some Previous Solutions
  - Homogeneity
- 2 Discontinuous Integral Controller: State Feedback
  - The I-Controller
  - Lyapunov Function
  - Caveat: Lack of Homogeneity
- 3 Discontinuous Integral Controller: Output Feedback
- 4 Conclusions



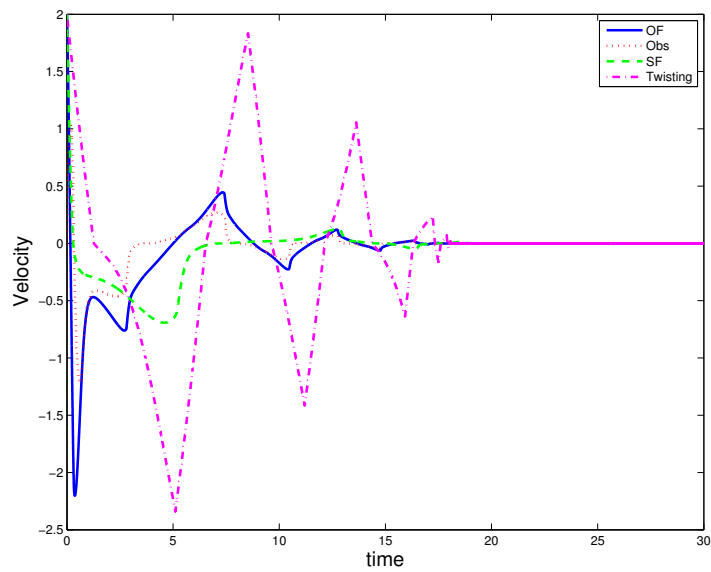


## Simulations



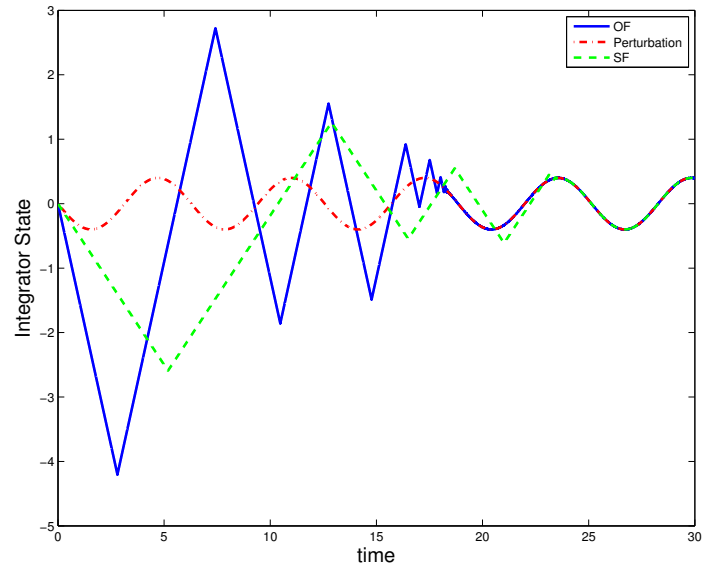
Navigation icons: back, forward, search, etc.

## Simulations



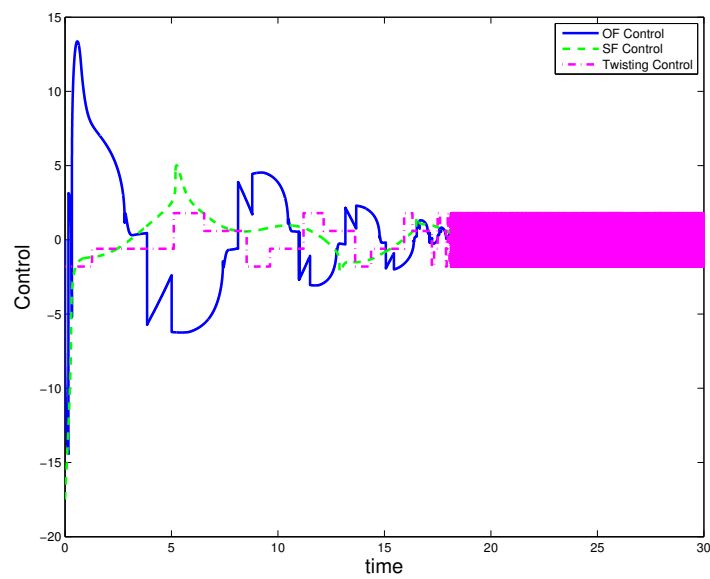
Navigation icons: back, forward, search, etc.

## Simulations



Navigation icons: back, forward, search, etc.

## Simulations



Navigation icons: back, forward, search, etc.

## Overview

- 1 Introduction
  - Problem
  - Some Previous Solutions
  - Homogeneity
- 2 Discontinuous Integral Controller: State Feedback
  - The I-Controller
  - Lyapunov Function
  - Caveat: Lack of Homogeneity
- 3 Discontinuous Integral Controller: Output Feedback
- 4 Conclusions

## Conclusions

- The Discontinuous Integral Controller
  - tracks exactly, in finite time and robustly
  - arbitrary references with bounded  $\ddot{r}(t)$
  - despite arbitrary (time) Lipschitz perturbations/uncertainties, i.e.  $\|\dot{\rho}(t)\| \leq \Delta$ ,  $\Delta$  constant
  - without an Internal Model.
- Separate design of State Feedback and Observer;
- Neither continuous Observer nor continuous State Feedback Controller are **insensitive** to perturbations;
- **Insensitivity** against perturbations is achieved by **discontinuous** Integral Control;
- For implementation:  $r(t)$  is required but not  $\dot{r}(t)$  and  $\ddot{r}(t)$ .
- Design is Lyapunov-Based.
- Generalization to arbitrary order possible.



◀ ◻ ▶ ◀ ◻ ▶ ◀ ≡ ▶ ◀ ≡ ▶ ≡ 🔍 ↺

- A set of navigation icons typically found in Beamer presentations, including symbols for back, forward, search, and other slide controls.

---

## References II





---

-  L. Fridman, Sliding mode enforcement after 1990: main results and some open problems.” Sliding Modes after the First Decade of the 21st Century. Springer Berlin Heidelberg, pp. 3–57, 2011.
-  L. Fridman, J. Moreno, B. Bandyopadhyay, S. Kamal, and A. Chalanga. Continuous Nested Algorithms: The Fifth Generation of Sliding Mode Controllers. In: Recent Advances in Sliding Modes: From control to intelligent mechatronics. Series: Studies in Systems, Decision and Control, vol 24, X. Yu and M. Önder Efe (eds.), Springer International Publisher, Switzerland, pp. 5-35, 2015. DOI: 10.1007/978-3-319-18290-2. eBook ISBN: 978-3-319-18290-2 <http://www.springer.com/gp/book/9783319182896>





---

## References III





---

-  Hardy, G. H., J. E. Littlewood y G. Polya (1951). *Inequalities*. London. Cambridge University Press.
-  Kamal, S.; Chalanga, A; Moreno, J.A; Fridman, L.; Bandyopadhyay, B., ”Higher order super-twisting algorithm,” 13th International Workshop on Variable Structure Systems (VSS), 2014, vol., no., pp.1,5, June 29 2014-July 2 2014. doi: 10.1109/VSS.2014.6881129.
-  Shyam Kamal, Jaime A. Moreno, Asif Chalanga, Bijnan Bandyopadhyay, Leonid M. Fridman. Continuous Terminal Sliding-Mode Controller. Automatica. Submitted 2015.
-  Khalil, H. K. (2002). *Nonlinear Systems*. Prentice Hall

## References IV

-  Levant, A. (1993). Sliding order and sliding accuracy in sliding mode control. *International Journal of Control*. **6**, 1247–1263.
-  A. Levant, Universal single-input-single-output (SISO) sliding-mode controllers with finite-time convergence *IEEE Transactions on Automatic Control*, vol. 6, no. 9, pp. 1447–1451, 2001.
-  Levant A. Higher order sliding modes: differentiation and output feedback control. *Int. J. of Control*; nov 2003; **76** (9-10):924–941.
-  Levant, A. (2005). Homogeneity approach to higher-order sliding mode design. *Automatica*. **34**, 576–586.




## References V

-  Levant, A. (2007). Principles of 2-sliding mode design. *Automatica*. **43**, 576–586.
-  Moreno, Jaime A.; M. Osorio (2012). Strict Lyapunov functions for the super-twisting algorithm. *IEEE Transactions on Automatic Control*. **54**, 1035–1040.
-  Moreno, Jaime A. Osorio, M. (2008). A Lyapunov approach to second-order sliding mode controllers and observers. *Proceedings of the 47th IEEE Conference on Decision and Control*. Cancún, México. Dec. 9–12.
-  Moreno, Jaime A. (2012). Lyapunov function for Levant's second order differentiator, *Proceedings of the 51st IEEE Conference on Decision and Control*. Maui, Hawai, Dec. 10-13, 2012.

---

## References VI


---

-  Torres González, Víctor; Fridman, Leonid M.; Moreno, Jaime A. Continuous Twisting Algorithm. 54th IEEE Conference on Decision and Control (CDC2015). Osaka, Japan. 15-18 December 2015.
-  Utkin, V. (1992). *Sliding Modes in Control and Optimization*. Springer-Verlag.
-  Utkin, V. (2009). *Sliding Mode Control in Electro-Mechanical Systems*. CRC Press. Second edition. Automatic and Control Engineering.

---

## References VII

---

-  Zamora, Cesar; Moreno, J. A.; Kamal, Shyam. Control Integral Discontinuo Para Sistemas Mecánicos. Congreso Nacional de Control Automático 2013. Asociación de México de Control Automático (AMCA). Ensenada, Baja California, 16-18 Octubre 2013. Pp. 11–16.  
<http://eventos.cicese.mx/amca2013/52.html>



# Estimating Parameters and States Using Modulating Functions

Johann Reger<sup>a</sup>

Jerome Jouffroy<sup>b</sup>

Let us first consider SISO-LTI systems of order  $n$ , given in input-output representation

$$y^{(n)} + a_{n-1}y^{(n-1)} + \dots + a_1\dot{y} + a_0y = b_{n-1}u^{(n-1)} + \dots + b_1\dot{u} + b_0u, \quad (1)$$

or as often more compactly written with  $\mathbf{Y} = (-y, -\dot{y}, \dots, -y^{(n-1)}, u, \dot{u}, \dots, u^{(n-1)})^T$  along

$$y^{(n)} = \mathbf{Y}^T \boldsymbol{\theta}. \quad (2)$$

There  $\boldsymbol{\theta} = (a_0, a_1, \dots, a_{n-1}, b_0, b_1, \dots, b_{n-1})^T$  holds unknown system parameters to be identified. For avoiding direct differentiation of probably noisy signals  $y(t)$  we employ the method of modulating functions [10]. We propose to slightly modify the definition given in [5, 6].

Let  $\varphi : \mathbb{R} \times \mathbb{R} \rightarrow \mathbb{R}$  be a sufficiently smooth function and denote  $\varphi^{(i)}(t, t_1) := \frac{\partial^i \varphi}{\partial \tau^i}(\tau, t_1)|_{\tau=t}$ . A function  $\varphi(\cdot, \cdot)$  is called a *modulating function* (of order  $k$ ) if for  $t_0 < t_1$  it satisfies

$$\varphi^{(i)}(t_0, t_1) \cdot \varphi^{(i)}(t_1, t_1) = 0, \quad \forall i \in \{0, 1, \dots, k-1\}. \quad (3)$$

A modulating function for which  $\varphi^{(i)}(t_0, t_1) = 0$  and  $\varphi^{(i)}(t_1, t_1) \neq 0$  is called a *left* modulating function, while a modulating function for which  $\varphi^{(i)}(t_0, t_1) \neq 0$  and  $\varphi^{(i)}(t_1, t_1) = 0$  is called a *right* modulating function. A modulating function whose boundaries verify  $\varphi^{(i)}(t_0, t_1) = \varphi^{(i)}(t_1, t_1) = 0$  is called *total* modulating function.

In view of (3) for total modulating functions we may then enjoy the fundamental property

$$\int_{t_0}^{t_1} \varphi(\tau, t_1) \xi^{(i)}(\tau) d\tau = \int_{t_0}^{t_1} (-1)^i \varphi^{(i)}(\tau, t_1) \xi(\tau) d\tau \quad (4)$$

which allows both to avoid computing signal derivatives of  $\xi$  explicitly and to get rid of its unknown initial and final values [2, 3], in contrast to [9]. This way we may replace (2) with

$$z = \mathbf{w}^T \boldsymbol{\theta} \quad (5)$$

where  $z$  and the vector  $\mathbf{w}$  consists of integrals of the shape in (4). In order to obtain an estimate  $\hat{\boldsymbol{\theta}}$  of  $\boldsymbol{\theta}$ , we may gather a collection of  $m_\phi \geq n$  equations (5), each of them using a different modulating function  $\varphi_k(t)$ . We then get

$$\mathbf{z} = \mathbf{W}^T \boldsymbol{\theta} \quad (6)$$

with  $\mathbf{z} = (z_1, z_2, \dots, z_m)^T$  and regressor  $\mathbf{W} = (\mathbf{w}_1, \mathbf{w}_2, \dots, \mathbf{w}_m)$ . An estimate  $\hat{\boldsymbol{\theta}}^T = (\hat{\mathbf{a}}^T, \hat{\mathbf{b}}^T)$  is finally obtained by simple application of linear least squares, see for example [7, 8, 4]:

$$\hat{\boldsymbol{\theta}} = (\mathbf{W}\mathbf{W}^T)^{-1} \mathbf{W}\mathbf{z}. \quad (7)$$

---

<sup>a</sup>Fachgebiet Regelungstechnik, Technische Universität Ilmenau, Helmholtzplatz 5, D-98693 Ilmenau, E-Mail: johann.reger@tu-ilmenau.de

<sup>b</sup>Mads Clausen Institute, University of Southern Denmark, DK-6400 Alsion 2, E-Mail: jerome@mci.sdu.dk

## Main result

Extending the estimation problem for linear systems, as presented in [1], consider an  $n$ -order single-input system of the form

$$\dot{\mathbf{x}} = \mathbf{A}\mathbf{x} + \mathbf{b}u + \sum_{k=2}^p (\boldsymbol{\alpha}_k x_1^k + \boldsymbol{\beta}_k u^k) + \sum_{k=1}^p \sum_{l=1}^p \boldsymbol{\gamma}_{kl} x_1^k u^l, \quad \mathbf{A} = \left( -\mathbf{a} \left| \begin{array}{c} \mathbf{I}_{n-1} \\ \mathbf{0}_{1 \times (n-1)} \end{array} \right. \right) \quad (8)$$

where the  $n$ -dimensional parameter vectors  $\mathbf{a}$ ,  $\mathbf{b}$ ,  $\boldsymbol{\alpha}_k$ ,  $\boldsymbol{\beta}_k$  and  $\boldsymbol{\gamma}_{kl}$  are all unknown.

Given a set of  $m_\phi \geq np(p+2)$  total modulating functions and  $m_\psi \geq np(p+2)$  left modulating functions, the unknown parameter vectors in (8) and the state  $\mathbf{x}(t_1)$  may be estimated in finite time if some signal dependent matrices  $\mathbf{W}$  and  $\boldsymbol{\Delta}$  both have full rank.

Based on the modulating function method, we derive expressions for such matrices and give estimates for the unknown parameter vectors and the system state that may be obtained in finite time.

- [1] LIU, D.Y., LALEG-KIRATI, T.M., PERRUQUETTI, W. and GIBARU, G.: *Non-asymptotic state estimation for a class of linear time-varying systems with unknown inputs*. IFAC World Congress, Cape Town, South Africa, 2014.
- [2] LOEB, J.M. and CAHEN, G.M.: *More about process identification*. IEEE Transactions on Automatic Control, Vol. 10, No. 3, 359–361, 1965.
- [3] MATHEW, A.V. and FAIRMAN, F.W.: *Identification in the presence of initial conditions*, IEEE Transactions on Automatic Control, Vol. 17, No. 6, 394–396, 1972.
- [4] MEDVEDEV, A. and TOIVONEN, H.T.: *Directional sensitivity of continuous least-squares state estimators*, Systems & Control Letters, Vol. 59, 571–577, 2010.
- [5] PEARSON, A.E. and LEE, F.: *On the identification of polynomial input-output differential systems*, IEEE Transactions on Automatic Control, Vol. 30, No. 8, 778–782, 1985.
- [6] PREISIG, H.A. and RIPPIN, H.W.: *Theory and application of the modulating function method—I. Review and theory of the method and theory of the spline-type modulating functions*, Computers and Chemical Engineering, Vol. 17, No. 1, 1–16, 1993.
- [7] RAO, G.P. and UNBEHAUEN, H.: *Identification of continuous-time systems*, IEE Control Theory and Applications, Vol. 153, no. 2, 185–220, 2006.
- [8] REGER, J. and JOUFFROY, J.: *On algebraic time-derivative estimation and deadbeat state reconstruction*, IEEE Conf. on Decision and Control, Shanghai, 1740–1745, 2009.
- [9] SAHA, D.C. and RAO, G.P.: *A general algorithm for parameter identification in lumped continuous systems—the Poisson Moment Functional approach*, IEEE Transactions on Automatic Control, Vol. 27, No. 1, 223–225, 1982.
- [10] SHINBROT, M.: *On the analysis of linear and nonlinear systems*, Trans. ASME, Vol. 79, No. 3, 547–542, 1957.

# Estimating Parameters and States Using Modulating Functions

Johann Reger<sup>†</sup>, Jerome Jouffroy<sup>‡</sup>

*reger@ieee.org*

<sup>†</sup> Fachgebiet Regelungstechnik, Technische Universität Ilmenau

<sup>‡</sup> Mads Clausen Institute, University of Southern Denmark

September 9, 2015

Retzhof, Steiermark  
Steirisches Seminar über Regelungstechnik und  
Prozessautomatisierung

## Outline

- 1 Modulating functions
- 2 Generalized Modulating Functions
- 3 Main Result
- 4 Simulation
- 5 Conclusions

## Motivation

Identify unknown parameters  $a_i$  and  $b_i$  of an LTI-system

$$y^{(n)} + a_{n-1}y^{(n-1)} + \dots + a_1\dot{y} + a_0y = b_{n-1}u^{(n-1)} + \dots + b_1\dot{u} + b_0u$$

where signals  $u$  and  $y$  are known.

Equivalently, let

$$y^{(n)} = \mathbf{Y}^T \boldsymbol{\theta}$$

and find the constants

$$\boldsymbol{\theta} = (a_0, a_1, \dots, a_{n-1}, b_0, b_1, \dots, b_{n-1})^T$$

when given on some interval of time the signals

$$\mathbf{Y} = (-y, -\dot{y}, \dots, -y^{(n-1)}, u, \dot{u}, \dots, u^{(n-1)})^T.$$

## Definition: Modulating Function

### Challenges

- estimation of time-derivatives
- unknown initial conditions
- attenuation of measurement noise

Circumventing these problems we may use

**Definition (Shinbrot'57, Pearson'85, Preisig'93, Rao'06)**

A function  $\varphi : [0, T] \rightarrow \mathbb{R}$  is called a *modulating function* (of order  $k$ ) if it is sufficiently smooth and if, for some fixed  $T$ , we have

$$\varphi^{(i)}(0) = \varphi^{(i)}(T) = 0$$

for all  $i \in \{0, 1, \dots, k-1\}$ . □

## Definition

For a signal  $\xi$ , conditions  $\varphi^{(i)}(0) = \varphi^{(i)}(T) = 0$  imply

$$\int_0^T \varphi(\tau) \xi^{(i)}(\tau) d\tau = \int_0^T (-1)^i \varphi^{(i)}(\tau) \xi(\tau) d\tau$$

Equivalent to  $y^{(n)} = \mathbf{Y}^T \boldsymbol{\theta}$ , we obtain

$$z = \mathbf{w}^T \boldsymbol{\theta} \quad \text{with} \quad z = \int_0^T (-1)^n \varphi^{(n)}(\tau) y(\tau) d\tau$$

$$w_i = \begin{cases} \int_0^T (-1)^{i-1} \varphi^{(i-1)}(\tau) y(\tau) d\tau, & i = 1, \dots, n \\ \int_0^T (-1)^{i-n-1} \varphi^{(i-n-1)}(\tau) u(\tau) d\tau, & i = n+1, \dots, 2n \end{cases}$$

- No explicit computation of signal derivatives
- No need for knowledge about initial and final conditions

## Least Squares Estimation

For creating  $m \geq 2n$  equations, collect  $m \geq 2n$  different modulating functions  $\varphi_k(t)$  to obtain

$$\mathbf{z} = \mathbf{W}^T \boldsymbol{\theta}$$

with  $\mathbf{z}^T = (z_1, z_2, \dots, z_m)$ ,  $\mathbf{W} = (\mathbf{w}_1, \mathbf{w}_2, \dots, \mathbf{w}_m)$  and  $z_k, \mathbf{w}_k$  as above.

The standard modulating function method then results in the least square estimate

$$\hat{\boldsymbol{\theta}} = (\mathbf{W}\mathbf{W}^T)^{-1} \mathbf{W}\mathbf{z}.$$

Typical modulating functions are for example [Shinbrot'57; Loeb'65]

$$\varphi_k(t) = \left( \sin \frac{k\pi t}{T} \right)^k \quad \text{or} \quad \varphi_k(t) = (T - t)^k t^k$$

## Some related ideas

1) Iterated integration by parts avoiding explicit derivation [**Mathew'72**]:

$$\int_0^t \int_0^{\tau_{k-1}} \dots \int_0^{\tau_1} \xi^{(i)}(\tau_1) d\tau_1 \dots d\tau_{k-1} d\tau_k =$$

$$\int_0^t \int_0^{\tau_{k-i-1}} \dots \int_0^{\tau_1} \xi(\tau_1) d\tau_1 \dots d\tau_{k-i} d\tau_{k-i-1} = \int_0^t \frac{(t-\tau)^{k-i-1}}{(k-i-1)!} \xi(\tau) d\tau$$

2) Poisson Moment Functional method [**Saha'82**]:

$$\int_0^t \frac{(t-\tau)^k}{k!} e^{-\lambda(t-\tau)} \xi^{(i)}(\tau) d\tau = \int_0^t (-1)^i \frac{d^i}{d\tau^i} \left( \frac{(t-\tau)^k}{k!} e^{-\lambda(t-\tau)} \right) \xi(\tau) d\tau$$

Both methods:

- equiv. to modulating function method if  $\xi(0) = \dots = \xi^{(i-1)}(0) = 0$
- admit an expanding or a fixed time horizon

## Definition: (Generalized) Modulating Function

### Definition

Let a function  $\varphi : \mathbb{R} \times \mathbb{R} \rightarrow \mathbb{R}$  be sufficiently differentiable and denote

$$\varphi^{(i)}(t, t_1) := \left. \frac{\partial^i \varphi}{\partial \tau^i}(\tau, t_1) \right|_{\tau=t}.$$

Function  $\varphi$  is called *modulating function* (of order  $k$ ) if for some  $t_0 < t_1$

$$\varphi^{(i)}(t_0, t_1) \varphi^{(i)}(t_1, t_1) = 0 \quad \forall i = 0, 1, \dots, k-1$$

If  $\varphi^{(i)}(t_0, t_1) = 0$  and  $\varphi^{(i)}(t_1, t_1) \neq 0$  then  $\varphi$  is a *left* modulating function.

If  $\varphi^{(i)}(t_0, t_1) \neq 0$  and  $\varphi^{(i)}(t_1, t_1) = 0$  then  $\varphi$  is a *right* modulating function.

If  $\varphi^{(i)}(t_0, t_1) = \varphi^{(i)}(t_1, t_1) = 0$  then  $\varphi$  is called *total* modulating function.

## Definition: Generalized Modulating Function

### Examples

- $(t_1 - t)^k e^{-\lambda(t_1 - t)}$  ... is a right modulating function.
- $(-t)^k$  or  $(\sin k\pi t)^k$  ... are left modulating functions.
- $(t_1 - t)^k t^k$  ... is a total modulating function.

Thus, for a left modulating function  $\varphi_k$  we have

$$\int_{t_0}^{t_1} \varphi_k(\tau) \xi^{(i)}(\tau) d\tau = \int_{t_0}^{t_1} (-1)^i \varphi_k^{(i)}(\tau, t_1) \xi(\tau) d\tau + \boldsymbol{\varphi}_k^T \boldsymbol{\xi}(t_1)$$

with  $\boldsymbol{\xi} = (\xi^{(i-1)}, \xi^{(i-2)}, \dots, \xi^{(0)})^T$  and

$$\boldsymbol{\varphi}_k^T = \left( \varphi_k(t_1, t_1), -\varphi_k^{(1)}(t_1, t_1), \dots, (-1)^{i-1} \varphi_k^{(i-1)}(t_1, t_1) \right)$$

Note that for total modulating functions  $\boldsymbol{\varphi}_k = \mathbf{0}$  (as shown before).

## Problem Statement

Consider an  $n$ -order single-input system of the form

$$\dot{\mathbf{x}} = \mathbf{A}\mathbf{x} + \mathbf{b}u + \sum_{k=2}^p (\boldsymbol{\alpha}_k x_1^k + \boldsymbol{\beta}_k u^k) + \sum_{k=1}^p \sum_{l=1}^p \gamma_{kl} x_1^k u^l$$

with

$$\mathbf{A} = \left( -\mathbf{a} \left| \begin{array}{c} \mathbf{I}_{n-1} \\ \mathbf{0}_{1 \times (n-1)} \end{array} \right. \right)$$

where the  $n$ -dimensional vectors  $\mathbf{a}$ ,  $\mathbf{b}$ ,  $\boldsymbol{\alpha}_k$ ,  $\boldsymbol{\beta}_k$  and  $\gamma_{kl}$  are all unknown.

### Problem

Given  $u(t)$  and measured  $y(t) = x_1(t)$  on  $t \in [t_0, t_1]$ , estimate

- the  $p(p+2)$  parameter vectors  $\mathbf{a}$ ,  $\mathbf{b}$ ,  $\boldsymbol{\alpha}_k$ ,  $\boldsymbol{\beta}_k$  and  $\gamma_{kl}$
- the state vector  $\mathbf{x}(t_1)$

## Main Result: Finite-Time Adaptive Observer

### Theorem

Given  $m_\phi \geq np(p+2)$  total modulating functions and  $m_\varphi \geq np(p+2)$  left modulating functions, the parameter vectors  $\mathbf{a}$ ,  $\mathbf{b}$ ,  $\alpha_k$ ,  $\beta_k$ ,  $\gamma_{kl}$  and the state  $\mathbf{x}(t_1)$  can be estimated in finite-time if  $\mathbf{W}$  and  $\Delta$  have full rank.

In this case, the estimates

$$\hat{\boldsymbol{\theta}}^T = \left( \hat{\mathbf{a}}^T, \hat{\mathbf{b}}^T, \hat{\alpha}_2^T, \dots, \hat{\alpha}_p^T, \hat{\beta}_2^T, \dots, \hat{\beta}_p^T, \hat{\gamma}_{11}^T, \hat{\gamma}_{12}^T, \dots, \hat{\gamma}_{pp}^T \right)^T$$

are given by

$$\hat{\boldsymbol{\theta}} = (\mathbf{W}\mathbf{W}^T)^{-1} \mathbf{W}\mathbf{z}$$

and

$$\hat{\mathbf{x}}(t_1) = \mathbf{P} (\Delta\Delta^T)^{-1} \Delta\mathbf{q}$$

## Sketch of a proof — parameter estimate

Rewrite the state equation in I/O-form

$$\begin{aligned} y^{(n)} = & \sum_{i=1}^n \left( -a(i)y^{(n-i)} + b(i)u^{(n-i)} \right) \\ & + \sum_{k=2}^p \sum_{i=1}^n \left( \alpha_k(i)(y^k)^{(i)} + \beta_k(i)(u^k)^{(n-i)} \right) + \sum_{k,l=1}^p \sum_{i=1}^n \gamma_{kl}(i)(y^k u^l)^{(n-i)} \end{aligned}$$

where  $a(i)$  denotes the  $i$ -th component of vector  $\mathbf{a}$  and so on.

Thus, we obtain  $y^{(n)} = \mathbf{Y}^T \boldsymbol{\theta}$  defining

$$\mathbf{Y}^T = (-\mathbf{y}^T, \mathbf{u}^T, \mathbf{y}^{2T}, \dots, \mathbf{y}^{pT}, \mathbf{u}^{2T}, \dots, \mathbf{u}^{pT}, \mathbf{g}^{11T}, \mathbf{g}^{12T}, \dots, \mathbf{g}^{ppT})^T$$

where  $\mathbf{y}^j := ((y^j)^{(n-1)}, (y^j)^{(n-2)}, \dots, (y^j)^{(0)})^T$  and respectively for  $\mathbf{u}^j$ .

The  $i$ -th component of vector  $\mathbf{g}^{kl}$  is given by  $g^{kl}(i) = (y^k u^l)^{(n-i)}$ .



## Sketch of a proof — parameter estimate

Applying standard modulating function method on the I/O-form

$$z_q = \mathbf{w}_q^T \boldsymbol{\theta} \quad \text{where} \quad z_q = \int_{t_0}^{t_1} (-1)^n \phi_q^{(n)}(\tau, t_1) y(\tau) d\tau$$

with total modulating function  $\phi_q$  and

$$\mathbf{w}_q^T = (-\mathbf{w}_q^{y^T}, \mathbf{w}_q^{u^T}, \mathbf{w}_q^{y^{2^T}}, \dots, \mathbf{w}_q^{y^{p^T}}, \mathbf{w}_q^{u^{2^T}}, \dots, \mathbf{w}_q^{u^{p^T}}, \mathbf{w}_q^{g^{11^T}}, \mathbf{w}_q^{g^{12^T}}, \dots, \mathbf{w}_q^{g^{pp^T}})^T$$

where

$$w_q^{y^j}(i) = \int_{t_0}^{t_1} (-1)^{n-i} \phi_q^{(n-i)}(\tau, t_1) y^j(\tau) d\tau, \quad w_q^{u^j}(i) = \dots$$

Using  $m_\phi$  total modulating functions we get  $\hat{\boldsymbol{\theta}} = (\mathbf{W}\mathbf{W}^T)^{-1} \mathbf{W}\mathbf{z}$  with

$$\mathbf{W} = (\mathbf{w}_1, \mathbf{w}_2, \dots, \mathbf{w}_q, \dots, \mathbf{w}_{m_\phi}).$$

## Sketch of a proof — state estimate

For estimating  $\mathbf{x}(t_1)$ , multiply the I/O-form by a left modulating function  $\varphi_r(\tau, t_1)$  and integrate to get

$$q_r^n + \boldsymbol{\varphi}_r^T \mathbf{y}(t_1) = -\mathbf{a}^T \mathbf{q}_r^y - \mathbf{a}^T \boldsymbol{\Gamma}_r \mathbf{y}(t_1) + \mathbf{b}^T \mathbf{q}_r^u + \mathbf{b}^T \boldsymbol{\Gamma}_r \mathbf{u}(t_1) \\ + \sum_{k=2}^p (\boldsymbol{\alpha}_k^T \mathbf{q}_{r,k}^y + \boldsymbol{\beta}_k^T \mathbf{q}_{r,k}^u + \boldsymbol{\alpha}_k^T \boldsymbol{\Gamma}_r \mathbf{y}^k(t_1) + \boldsymbol{\beta}_k^T \boldsymbol{\Gamma}_r \mathbf{u}^k(t_1)) + \sum_{k,l=1}^p \boldsymbol{\gamma}_{kl}^T (\mathbf{q}_{r,kl}^g + \boldsymbol{\Gamma}_r \mathbf{g}^{kl}(t_1))$$

where

$$q_r^n = \int_{t_0}^{t_1} (-1)^n \varphi_r^{(n)}(\tau, t_1) y(\tau) d\tau$$

$$\boldsymbol{\varphi}_r^T = \left( \varphi_r(t_1, t_1), -\varphi_r^{(1)}(t_1, t_1), \dots, (-1)^{n-1} \varphi_r^{(n-1)}(t_1, t_1) \right)$$

$$\mathbf{q}_r^{y^T} = \int_{t_0}^{t_1} \left( (-1)^{n-1} \varphi_r^{(n-1)}(\tau, t_1), \dots, -\varphi_r^{(1)}(\tau, t_1), \varphi_r(\tau, t_1) \right) y(\tau) d\tau$$

and similarly for  $\mathbf{q}_r^u$ ,  $\mathbf{q}_{r,k}^y$ ,  $\mathbf{q}_{r,k}^u$  and  $\mathbf{q}_{r,kl}^g \dots$

## Sketch of a proof — state estimate

... and matrix  $\Gamma_r$  reads

$$\Gamma_r = \begin{pmatrix} 0 & \varphi_r(t_1, t_1) & \cdots & (-1)^{n-2} \varphi_r^{(n-2)}(t_1, t_1) \\ 0 & 0 & \ddots & \vdots \\ \vdots & \vdots & \ddots & \varphi_r(t_1, t_1) \\ 0 & \dots & \dots & 0 \end{pmatrix}.$$

Solving for the unknowns  $\mathbf{y}(t_1)$ ,  $\mathbf{u}(t_1)$ ,  $\mathbf{y}^k(t_1)$ ,  $\mathbf{u}^k(t_1)$  and  $\mathbf{g}^{kl}(t_1)$  in  $\mathbf{Y}$  and replacing with estimates from  $\hat{\theta}$  yields

$$\begin{aligned} \delta_r^T \mathbf{Y} &= q_r \\ q_r &= -q_r^n - \hat{\mathbf{a}}^T \mathbf{q}_r^y + \hat{\mathbf{b}}^T \mathbf{q}_r^u + \sum_{k=2}^p (\hat{\alpha}_k^T \mathbf{q}_{r,k}^y + \hat{\beta}_k^T \mathbf{q}_{r,k}^u) + \sum_{k,l=1}^p \hat{\gamma}_{kl}^T \mathbf{q}_{r,kl}^g \\ \delta_r^T &= -(\varphi_r^T + \hat{\mathbf{a}}^T \Gamma_r, \hat{\mathbf{b}}^T \Gamma_r, \hat{\alpha}_2^T \Gamma_r, \dots, \hat{\alpha}_p^T \Gamma_r, \hat{\beta}_2^T \Gamma_r, \dots, \hat{\beta}_p^T \Gamma_r, \hat{\gamma}_{11}^T \Gamma_r, \dots, \hat{\gamma}_{pp}^T \Gamma_r)^T \end{aligned}$$

## Sketch of a proof — state estimate

Now using  $m_\varphi$  left modulating functions results in

$$\Delta^T \mathbf{Y} = \mathbf{q}$$

where

$$\Delta = (\delta_1, \delta_2, \dots, \delta_{m_\varphi}) \quad \text{and} \quad \mathbf{q}^T = (q_1, q_2, \dots, q_{m_\varphi})^T.$$

Finally, we obtain

$$\hat{\mathbf{x}}(t_1) = \mathbf{P} (\Delta \Delta^T)^{-1} \Delta \mathbf{q}$$

with  $\mathbf{P}$  by solving the lines of

$$\dot{\mathbf{x}}(t_1) = \mathbf{A} \mathbf{x}(t_1) + \mathbf{b} u(t_1) + \sum_{k=2}^p (\alpha_k (x_1(t_1))^k + \beta_k (u(t_1))^k) + \sum_{k,l=1}^p \gamma_{kl} (x_1(t_1))^k (u(t_1))^l$$

for each state component (linear in  $y$  and  $u$  and its time derivatives).

## Simulation — Van der Pol oscillator

Consider the van der Pol oscillator

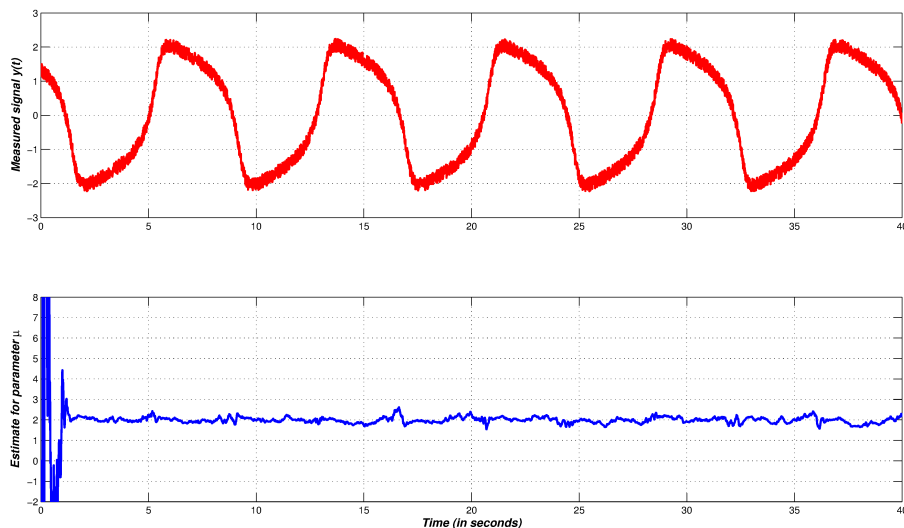
$$\ddot{y} = \mu(1 - y^2)\dot{y} - y \quad \Rightarrow \quad \begin{cases} \dot{x}_1 &= \mu x_1 + x_2 - \frac{\mu}{3} x_1^3 \\ \dot{x}_2 &= -x_1 \\ y &= x_1 \end{cases}$$

Assume that parameter  $\mu$  is unknown.

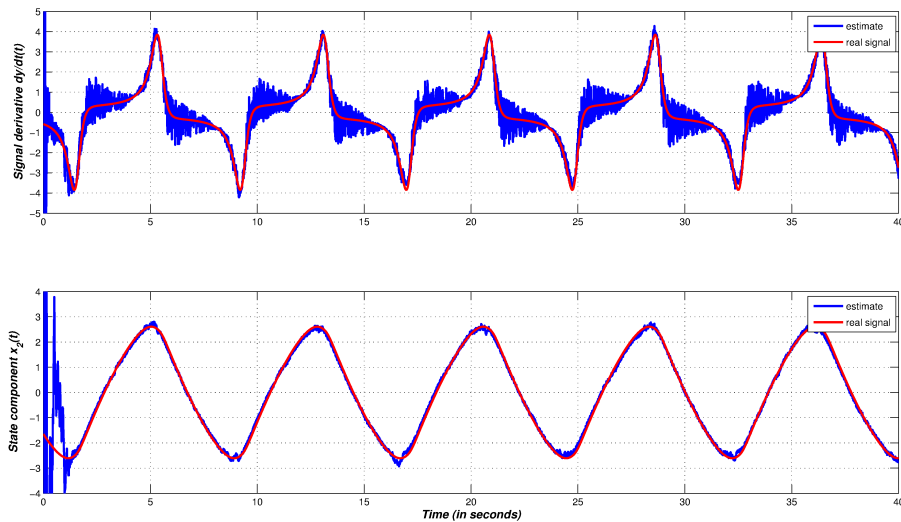
For the simulations:

- $\mu = 2$ , SNR= 22dB wrt. noise, sampling period  $T_s = 0.01$  sec.
- 6 total modulating functions, Loeb and Cahen-like:  $(t_1 - t)^k t^k$
- 2 left modulating functions, Poisson type:  $t^2 e^{-t}$ ,  $t^3 e^{-t}$
- estimation starts with expanding horizon, then switched at  $t = 2$  sec to a receding-horizon of  $T = 2$  sec

## Van der Pol oscillator



## Van der Pol oscillator



## Conclusions

We have presented an approach

- for the modulating function based least squares estimation
- that allows simultaneous estimation of parameters and states
- for observable nonlinear systems SISO-systems
- suitable for expanding and receding horizons

Future work

- specific modulation functions for using FFT and FHT
- extending the system class to convolvable systems
- discretization and recursive issues
- applications, e.g. in underwater navigation

## References

- [1] R. Hermann and A. J. Krener, *Nonlinear controllability and observability*, IEEE TAC, vol. 22, no. 5, pp. 728–740, 1977.
- [2] J. Jouffroy and J. Reger, *An algebraic perspective to singletransponder underwater navigation*, IEEE Int. Conf. on Control Applications, Munich, Germany, 2006.
- [3] T. Kailath, *Linear Systems*, Prentice-Hall, 1980.
- [4] G. Kreisselmeier, *Adaptive observers with exponential rate of convergence*, IEEE TAC, vol. 22, no. 1, pp. 2–8, 1977.
- [5] D.Y. Liu and T.M. Laleg-Kirati and W. Perruquetti and O. Gribu, *Non-asymptotic state estimation for a class of linear time-varying systems with unknown inputs*, IFAC World Congress, Cape Town, South Africa, 2014.
- [6] J. M. Loeb and G. M. Cahen, *More about process identification*, IEEE TAC, vol. 10, no. 3, pp. 359–361, 1965.
- [7] A. V. Mathew and F. W. Fairman, *Identification in the presence of initial conditions*, IEEE TAC, vol. 17, no. 6, pp. 394–396, 1972.
- [8] A. Medvedev, *Continuous least-square observers with applications*, IEEE TAC, vol. 41, no. 10, pp. 1530–1537, 1996.
- [9] A. E. Pearson and F. C. Lee, *On the identification of polynomial input-output differential systems*, IEEE TAC, vol. 30, no. 8, pp. 778–782, 1985.
- [10] H. A. Preisig and H. W. T. Rippin, *Theory and application of the modulating function method—I. Review and theory of the method and theory of the spline-type modulating functions*, Computers and Chemical Engineering, vol. 17, no. 1, pp. 1–16, 1993.
- [11] G. P. Rao and H. Unbehauen, *Identification of continuous-time systems*, IEE Control Theory and Applications, vol. 153, no. 2, pp. 185–220, 2006.
- [12] J. Reger and J. Jouffroy, *On algebraic time-derivative estimation and deadbeat state reconstruction*, IEEE Int. Conf. on Decision and Control, Shanghai, China, 2009.
- [13] D. C. Saha and G. P. Rao, *A general algorithm for parameter identification in lumped continuous systems—the Poisson Moment Functional approach*, IEEE TAC, vol. 27, no. 1, pp. 223–225, 1982.
- [14] M. Shinbrot, *On the analysis of linear and nonlinear systems*, Trans. ASME, vol. 79, no. 3, pp. 547–542, 1957.

# Stability Analysis of interconnected Linear Systems with Coupling Imperfections

Georg Stettinger<sup>a</sup>    Martin Benedikt<sup>a</sup>    Martin Horn<sup>b</sup>    Christian Pötzsche<sup>c</sup>  
Josef Zehetner<sup>d</sup>

This contribution deals with the stability analysis of interconnected systems using a model-based coupling approach to reduce effects of coupling imperfections. Analysis issues are discussed for linear SISO subsystems: first for the time-invariant case, second for the time-invariant in combination with present nonlinearities and third for the time-varying case.

## 1 Introduction

This work deals with the stability analysis of a model-based coupling technique for interconnected linear systems. In general, a model-based coupling approach is introduced to overcome problems arising whenever the interconnections have a non-negligible influence on the overall system behavior. The interaction between two interconnected subsystems via different imperfect communication media is commonly characterized by introduced communication time-delays which degrade the coupling data exchange, see Abb. 1. These time-delays (labeled with  $(t_{s,1}, t_{s,2})$  and  $(t_{r,1}, t_{r,2})$ ) represent dead-times in the closed-loop system and result in so called round-trip-times, which may also be time-variant depending on the communication media utilization. Another important aspect are noisy coupling signals, introduced

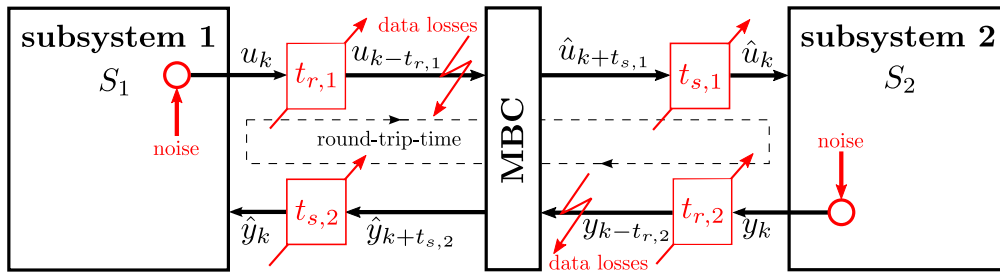


Abbildung 1: Model-based coupling element (MBC) inserted between two coupled subsystems ( $S_1, S_2$ ) to handle non-negligible coupling imperfections [2, 1]

by sensors installed in real-time systems, see Abb. 1. Such noisy measurement signals are

<sup>a</sup>VIRTUAL VEHICLE Research Center, Area E, Inffeldgasse 21a/2, 8010 Graz, E-Mail: georg.stettinger@v2c2.at, martin.benedikt@v2c2.at

<sup>b</sup>Institut für Regelungs- und Automatisierungstechnik, Technische Universität Graz, Kopernikusgasse 24/II, 8010 Graz, E-Mail: martin.horn@tugraz.at

<sup>c</sup>Alpen Adria Universität Klagenfurt, Institute of Mathematics, Universitätsstrasse 65-67, 9020 Klagenfurt, E-Mail: christian.poetzsche@aau.at

<sup>d</sup>AVL List GmbH, Hans-List-Platz 1, 8020 Graz, E-Mail: josef.zehetner@avl.com

problematic especially if signal-based coupling schemes are used. In this case the noise level is typically amplified, which in turn potentially leads to unstable simulations. Coupling data losses (see Abb. 1), caused by disturbances or overload of communication capacity are additional phenomena occurring in coupled systems [2].

## 2 Model-based coupling approach

The model-based coupling scheme in form of a coupling element (labeled with MBC) is inserted between two coupled subsystems, see Abb. 1. To ensure a time-correct coupling the output signal  $u_k$  of subsystem 1 ( $S_1$ ) should arrive at the input of subsystem 2 ( $S_2$ ) without any delay. This is also true for the output  $y_k$  of subsystem 2. However, significant dead-times due to imperfect communication media impose a serious limitation on the control performance of closed-loop systems. To overcome this limitation the proposed model-based coupling algorithm extrapolates the coupling signals  $(u_{k-t_{r,1}}, y_{k-t_{r,2}})$  to  $(\hat{u}_{k+t_{s,1}}, \hat{y}_{k+t_{s,2}})$  based on recursively identified subsystem models. Therefore, at discrete time instant  $k$  the extrapolated values  $\hat{u}_k$  and  $\hat{y}_k$  are already present at the subsystem inputs. This way, the effect of the round-trip-time is compensated. Coupling data losses have a very similar effect as dead-times and can therefore be compensated via additional model-based extrapolations according to the amount of lost data. Furthermore, noise corrupted coupling signals can be considered via adequate parametrizations of the recursive system identification algorithms to perform model-based filtering [1].

## 3 Stability Analysis

Important questions via the use of the model-based coupling approach arise: How do the introduced MBC elements effect the stability of the closed-loop? Can the closed-loop stability properties, without the coupling element, be preserved? In general this stability analysis is a complex task since one has to deal with nonlinear control loops independent of the introduced coupling elements. Therefore, in a first step, the stability analysis is restricted to linear closed-loop dynamics including the proposed coupling elements. The stability analysis is divided into three parts with increasing complexity: first MBC using time-invariant (pre-identified) subsystem models, second the influence of additional nonlinearities at the plant input together with these pre-identified internal models and finally time-varying closed-loop dynamics caused by parameter adaptations of the subsystem models and/or time-varying subsystem dynamics.

- [1] STETTINGER, G., M. HORN, M. BENEDIKT und J. ZEHETNER: *A Model-Based Approach for Prediction-Based Interconnection of Dynamic Systems*. In: *Decision and Control (CDC), 2014 IEEE 53rd Annual Conference on*, Seiten 3286–3291, December 2014.
- [2] STETTINGER, G., M. HORN, M. BENEDIKT und J. ZEHETNER: *Model-based Coupling Approach for non-iterative Real-Time Co-Simulation*. In: *Control Conference (ECC), 2014 European*, Seiten 2084–2089, June 2014.

## Stability Analysis of Interconnected Linear Systems with Coupling Imperfections

Dr. Georg Stettinger, Dr. Martin Benedikt  
VIRTUAL VEHICLE Research Center

Prof. Martin Horn  
Graz University of Technology

Prof. Christian Pöttsche  
Alpen Adria University Klagenfurt

Dr. Josef Zehetner  
AVL List GmbH



COMET K2 Competence Center - Initiated by the Federal Ministry of Transport, Innovation & Technology (BMVIT) and the Federal Ministry of Economics & Labour (BMWFI). Funded by FFG, Land Steiermark and Steirische Wirtschaftsförderung (SFG)

© VIRTUAL VEHICLE

### Agenda

- Introduction
- Model-based Coupling Approach
- Stability Analysis Techniques
- Example: Drivetrain Control-Loop
- Conclusions & Outlook
- Fields of Applications



## Motivation



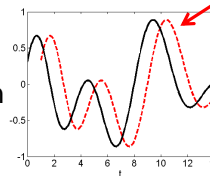
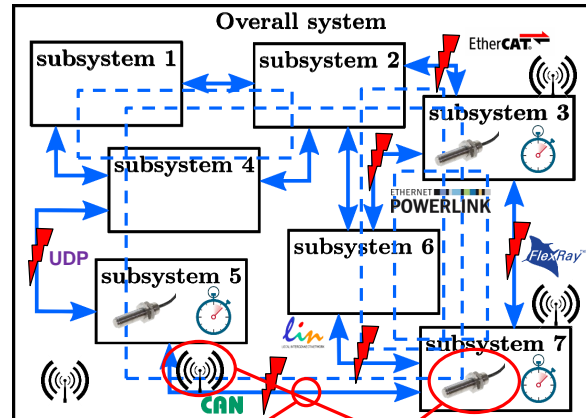
- Entire mechatronic product: “system of systems”, e.g. entire vehicle

### Co-Simulation characteristics:

- Strong interaction
- Bidirectional interdependencies (internal loops)

### Real-time Co-Simulation coupling imperfections:

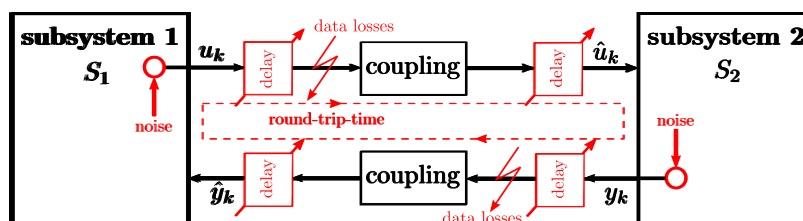
- Time delays**  
(Communication media, A/D resp. D/A converters, sensors/actuators)
- Noise**  
(Sensors)
- Disturbances**  
(data losses due to communication overload)



## Coupling imperfections



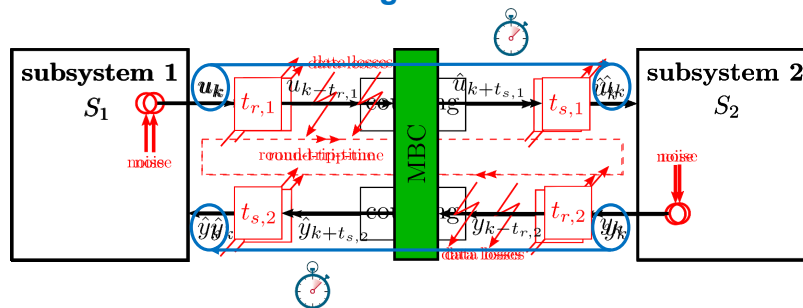
- Caused by incorporation of real-time systems
- Different types:**
  - Communication time-delays** (round-trip-times)
  - Noisy coupling** signals (sensors!)
  - Data-losses** (communication overload, disturbances,...)



## Handling of Coupling imperfections via Model-based Coupling Approach



- **Goal:**  
Compensation of coupling imperfection effects via model-based coupling
- **Coupling element (MBC)** introduction separates round-trip-time into sending ( $t_{s,1}, t_{s,2}$ ) and receiving dead-times ( $t_{r,1}, t_{r,2}$ )
- **Main task:**  
Compensate effects of communication time-delays  
→ “time correct data exchange”



09.09.2015 / Stettinger

Stability Analysis of Interconnected Linear Systems with Coupling Imperfections

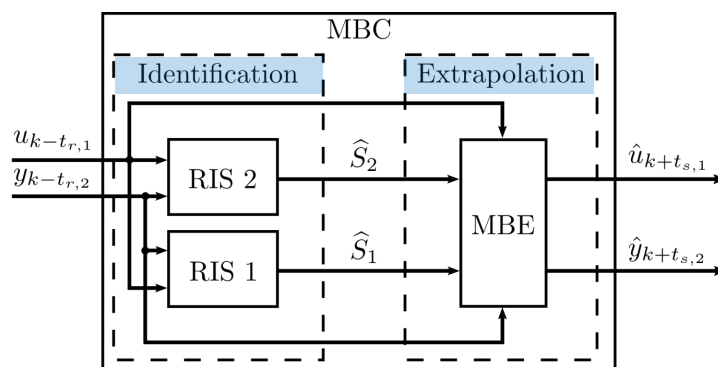
© VIRTUAL VEHICLE

5

## Model-based coupling approach



- **Key functionality:**  
model-based prediction of coupling signals (future estimate)
- **Basis:** subsystem models ( $\hat{S}_1, \hat{S}_2$ )
- **Structure:**
  - Recursive **identification** of subsystem models (RIS2, RIS1)
  - Model-based **extrapolation/prediction** (MBE)



09.09.2015 / Stettinger

Stability Analysis of Interconnected Linear Systems with Coupling Imperfections

© VIRTUAL VEHICLE

6

## Model-based coupling: Identification



- **Subsystem model structure:**  
→ linear time-varying 2<sup>nd</sup> order system

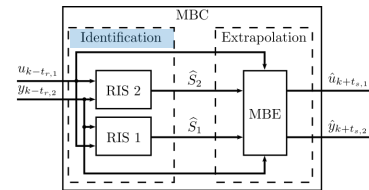
- **Corresponding difference equation:**

$$y_k = -a_{2,k}y_{k-1} - a_{1,k}y_{k-2} + b_{2,k}u_{k-1} + b_{1,k}u_{k-2}$$

- Identification techniques:

- Recursive Least Squares identification
- Kalman Filter based algorithms
- Linear identification problem
- Minimal computational burden
- Prevention of estimator windup via directional tracking algorithms

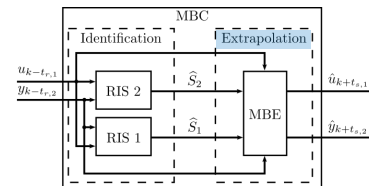
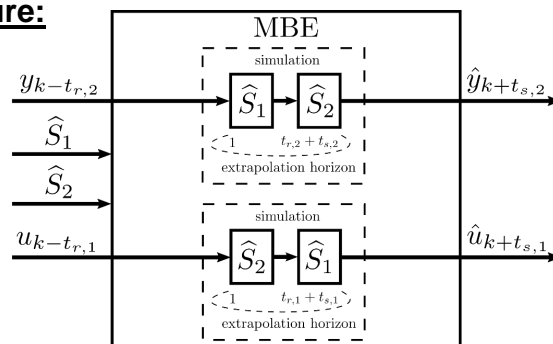
- **Initial identification phase (learning phase) to get subsystem models**( $\hat{S}_1, \hat{S}_2$ )



## Model-based coupling: Extrapolation

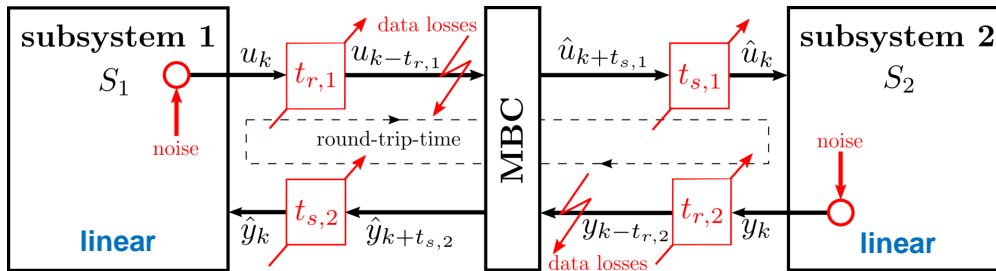


- **Extrapolation via in advance simulation of the estimated closed-loop dynamics**
- Structure:



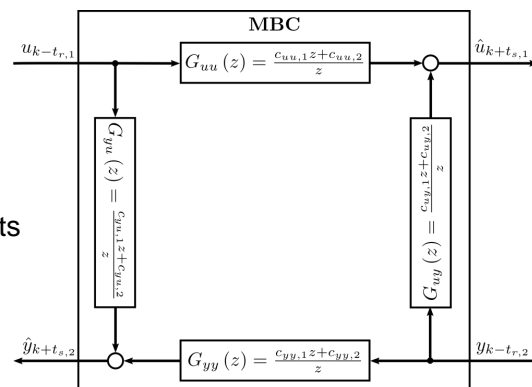
- **Extrapolation horizons given by present sending and receiving dead-times:**
  - y-Extrapolation horizon:  $(t_{r,2} + t_{s,2})$
  - u-Extrapolation horizon:  $(t_{r,1} + t_{s,1})$

- **Goal:**  
Stability properties of closed-loop including the MBC approach
- **Focus:**  
**Linear** subsystems



- **2 different MBC test-cases:**
  - 1) time-invariant subsystem models
  - 2) time-varying subsystem models (parameter adaptation!)

- **whole MBC element (system identification & extrapolation part)**  
can be represented via 4 FIR filters
- **structure independent of the extrapolation horizon and parametrization (only FIR filter coefficients change)**
- **2 different MBC types:**
  - 1) time-invariant subsystem models  
→ constant FIR Filter coefficients
  - 2) time-varying subsystem models (parameter adaptation!)  
→ time-varying FIR Filter coefficients

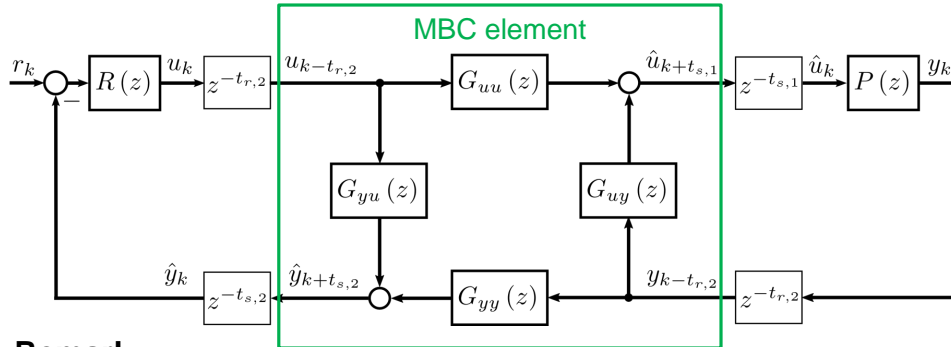


- **Test-case 1 remark:**  
*Time-invariant MBC element is BIBO-stable (assuming finite FIR Filter coefficients)!*

## Stability Analysis Techniques: Time-Invariant Closed-Loop Dynamics



- time-invariant subsystems  $R(z)$ ,  $P(z)$  and MBC element
- preidentified (constant) subsystem models  $\hat{S}_1, \hat{S}_2$   
→ constant FIR Filter coefficients
- MBC element only performs MBEs
- BIBO-stability evaluation based on the overall transfer function  $T(z)$



- **Remark:**  
Additional nonlinearities at the plant input can be considered via absolute stability concepts!

## Stability Analysis Techniques: Time-Variant Closed-Loop Dynamics



- **Sources of time-variations:**
  - time-variant subsystems
  - time-variant MBC element (parameter adaptations!)
  - time-varying delays
  - time-varying extrapolation horizon (time-varying delays resp. data-losses!)

- **Time-variant closed-loop dynamics**

$$\mathbf{x}_{k+1} = \mathbf{A}_k \mathbf{x}_k + \mathbf{B}_k \mathbf{u}_k$$

$$\mathbf{y}_k = \mathbf{C}_k \mathbf{x}_k$$

- **corresponding transition matrix of the free-system**  $\mathbf{x}_{k+1} = \mathbf{A}_k \mathbf{x}_k$

$$\Phi_{k,k_0} = \mathbf{A}_{k-1} \mathbf{A}_{k-2} \dots \mathbf{A}_{k_0} \text{ for all } k > k_0,$$

$$\Phi_{k,k} = \mathbf{I}.$$

## Stability Analysis Techniques: Time-Variant Closed-Loop Dynamics (2)



- **Desirable stability property: UNIFORM EXPONENTIAL STABILITY**  
→ convenient robustness properties

- notion is preserved under small bounded perturbations
- as well as linearly homogeneous perturbations decaying to zero

- **Uniform exponential stability:**

- transition matrix  $\Phi_{k,k_0}$  exponentially decays to zero uniformly

- **Definition:**

A linear free system is called *uniformly exponentially stable* (UES for short), if there exist positive constants  $\alpha \geq 1$  and  $\beta \in [0, 1)$  such that

$$\|\Phi_{k,k_0}\| \leq \alpha \beta^{k-k_0} \quad \text{for all } k_0 \leq k.$$

- **Short-time BIBO property definition:**

A linear system is called *short-time BIBO*, if for specified  $\delta > 0$ ,  $\epsilon > 0$  and  $N > 0$  for  $\mathbf{x}_0 = \mathbf{0}$  and every  $k_0 \in (\kappa, \zeta - N)$ ,  $\|u_k\| < \delta$  implies  $\|y_k\| < \epsilon$  for all  $k \in [k_0, k_0 + N]$ .

( $\kappa$  and  $\zeta$  describe the considered time interval  $K := (\kappa, \zeta)$ ,  $-\infty \leq \kappa < \zeta \leq \infty$ ).

## Stability Analysis Techniques: Time-Variant Closed-Loop Dynamics (3)



- **Short-time BIBO property characterization:**

- **Impulse response matrix:**

$$\mathbf{G}_{k,i} = \mathbf{C}_k \Phi_{k,i+1} \mathbf{B}_i$$

- **Theorem:**

A linear system is short time BIBO for specified  $\delta, \epsilon > 0$  and integers  $N > 0$ , if and only if for all  $k_0 \in (\kappa, \zeta - N)$  and  $k \in [k_0, k_0 + N]$  one has

$$\sum_{i=k_0}^{k-1} \|\mathbf{G}_{k,i}\| < \frac{\epsilon}{\delta}.$$

- **Different techniques to obtain UES:**

- Stability of asymptotically time-invariant systems
- Stability based on the Bohl exponent
- (Stability according to Lyapunov-Perron-Malkin)

## Stability of asymptotically time-invariant systems



- **Goal:**  
UES verification
- **Special case:**  
subsystem model parameters converge to constant values
- **Theorem:**  
If a linear free system fulfills

$$\mathbf{A}_k \rightarrow \mathbf{A} \text{ as } k \rightarrow \infty$$

with a Schur matrix  $\mathbf{A}$ , then the linear system is UES.

## Stability based on the Bohl exponent



- **Goal:**  
UES verification
- **General case:**  
no assumptions about the parameter adaptations (no convergence required!)
- **Eigenvalues (resp. Schur matrix) are of no use**
- **Two counterparts to eigenvalue moduli for time-varying systems**
  - Lyapunov exponent indicates asymptotic stability
  - Bohl exponent indicates UES (robustness properties!)

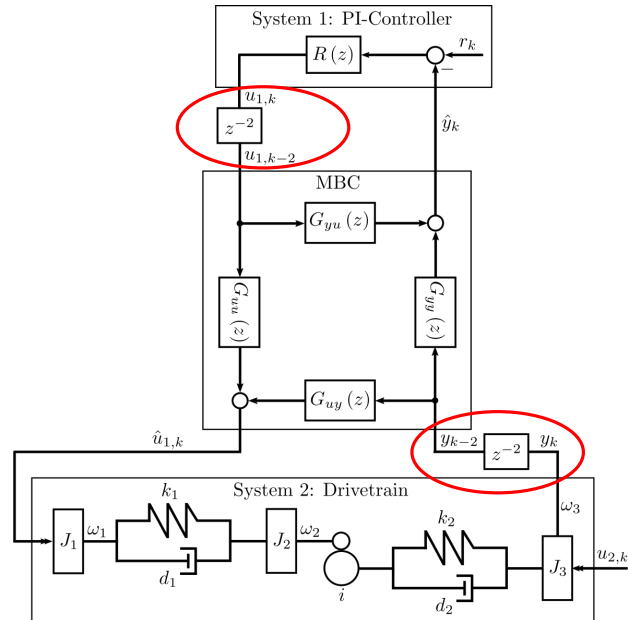
$$\bar{\beta}(\mathbf{A}) = \limsup_{i \rightarrow \infty} \sup_{k \geq 0} \|\Phi_{k+i,k}\|^{\frac{1}{i}} = \inf_{i > 0} \sup_{k \geq 0} \|\Phi_{k+i,k}\|^{\frac{1}{i}}$$

- **Necessary and sufficient condition for UES**  
 $\bar{\beta}(\mathbf{A}) < 1$

## Example: Drivetrain Control-Loop



- **Goal:**  
Reference speed tracking
- **Sample-time:**  
 $\Delta T = 10\text{ms}$
- **2 receiving time-delays:**  
 $t_{r,1} = t_{r,2} = 2 \times \Delta T$



09.09.2015 / Stettinger

Stability Analysis of Interconnected Linear Systems with Coupling Imperfections

© VIRTUAL VEHICLE

17

## Example: Drivetrain Control-Loop



### System 1: PI-Controller:

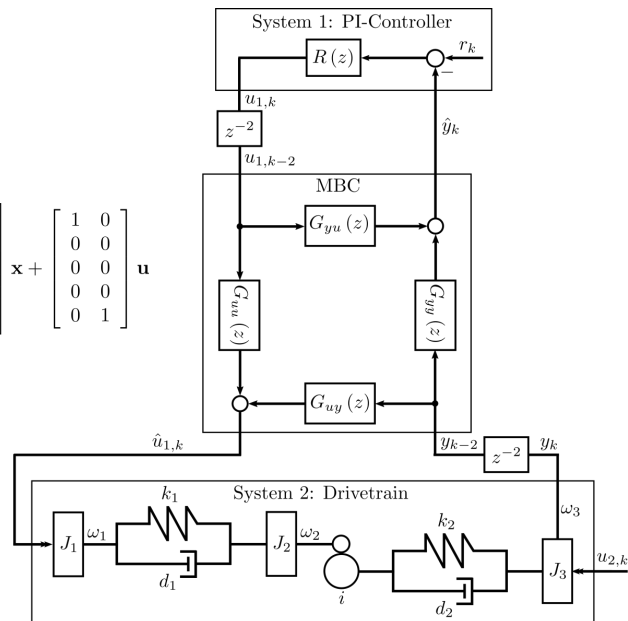
$$R(z) = \frac{10000(z - 0.975)}{z - 1}$$

### System 2: Drivetrain:

$$\dot{\mathbf{x}} = \begin{bmatrix} -\frac{d_1}{J_1} & -\frac{k_1}{J_1} & -\frac{d_1}{J_1} & 0 & 0 \\ 1 & 0 & -1 & 0 & 0 \\ \frac{d_1}{J_2} & \frac{k_1}{J_2} & -\frac{d_1}{J_2} & -\frac{k_2}{J_2} & \frac{d_2}{J_2} \\ 0 & 0 & \frac{1}{J_2} & 0 & -1 \\ 0 & 0 & \frac{d_2}{J_3} & \frac{k_2}{J_3} & -\frac{d_2+d_0}{J_3} \end{bmatrix} \mathbf{x} + \begin{bmatrix} 1 & 0 \\ 0 & 0 \\ 0 & 0 \\ 0 & 0 \\ 0 & 1 \end{bmatrix} \mathbf{u}$$

$$y = [0 \ 0 \ 0 \ 0 \ 1]^T \mathbf{x}$$

$$\mathbf{x} = \begin{bmatrix} x_1 \\ x_2 \\ x_3 \\ x_4 \\ x_5 \end{bmatrix} = \begin{bmatrix} \omega_1 \\ \varphi_1 - \varphi_2 \\ \omega_2 \\ \frac{1}{i}\varphi_2 - \varphi_3 \\ \omega_3 \end{bmatrix} \text{ and } \mathbf{u} = \begin{bmatrix} u_1 \\ u_2 \end{bmatrix}$$



09.09.2015 / Stettinger

Stability Analysis of Interconnected Linear Systems with Coupling Imperfections

© VIRTUAL VEHICLE

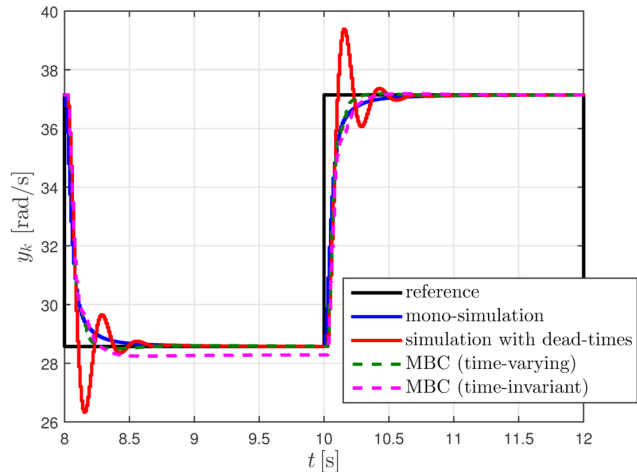
18



## Results: Drivetrain Control-Loop



- **Mono-simulation:**  
Reference solution without communication time-delays
- Distinct overshoots due to introduced dead-times
- Compensation of time-delay effects via MBC
  - time-varying MBC  
→ most accurate results!
  - time-invariant MBC  
→ offset!



09.09.2015 / Stettinger

Stability Analysis of Interconnected Linear Systems with Coupling Imperfections

© VIRTUAL VEHICLE

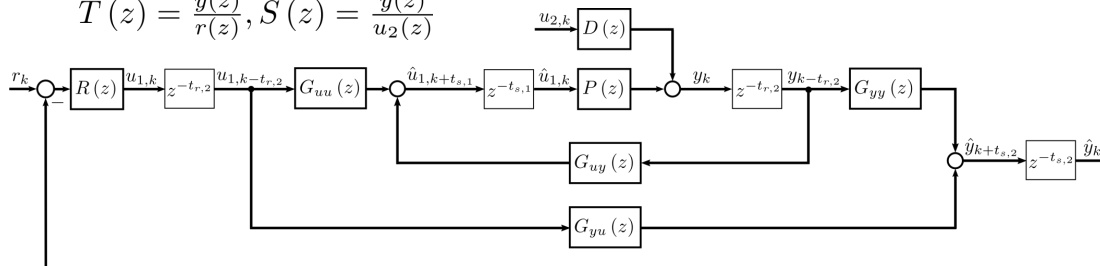
19

## Stability Analysis: Time-Invariant Closed-Loop Dynamics



- Time-invariant MBC (constant subsystem model-parameters)
- **Goal:**  
state BIBO stability
- BIBO-stability verification via two overall transfer functions

$$T(z) = \frac{\hat{y}(z)}{r(z)}, S(z) = \frac{\hat{y}(z)}{u_2(z)}$$



- **Result:**  
 $|\text{poles}(T(z))| < 1, |\text{poles}(S(z))| < 1$



BIBO stable Time-Invariant Closed-Loop Dynamics

09.09.2015 / Stettinger

Stability Analysis of Interconnected Linear Systems with Coupling Imperfections

© VIRTUAL VEHICLE

20

## Stability Analysis:

### Time-Variant Closed-Loop Dynamics



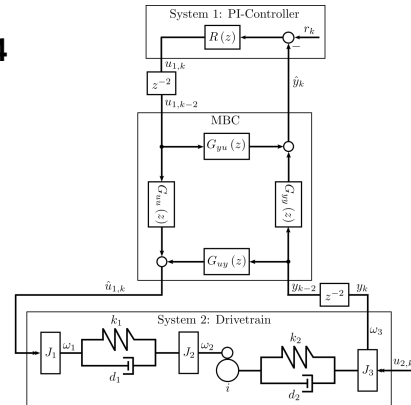
- Resulting time-variant system of order 14

$$\mathbf{x}_{k+1} = \mathbf{A}_k \mathbf{x}_k + \mathbf{B}_k \mathbf{u}_k, \quad \mathbf{u}_k = \begin{bmatrix} r_k \\ u_{2,k} \end{bmatrix}$$

$$y_k = \mathbf{C}_k \mathbf{x}_k$$

- Analysis via perturbed linear system

$$\mathbf{A}_k = \underbrace{\mathbf{A}}_{\text{constant}} + \underbrace{\mathbf{D}_k}_{\text{time-varying}}$$



- spectral radius  $\rho(\mathbf{A}) \approx 0.9744 < 1 \rightarrow$  Schur matrix
- furthermore  $\lim_{k \rightarrow \infty} \mathbf{D}_k = \mathbf{0}$



UES Time-Variant Closed-Loop Dynamics

## Stability Analysis:

### Time-Variant Closed-Loop Dynamics (2)



- Short-time BIBO stability evaluation

- simulation time

$$T_{sim} = n_{sim} \Delta T$$

- numerical calculation of the Bohl exponent

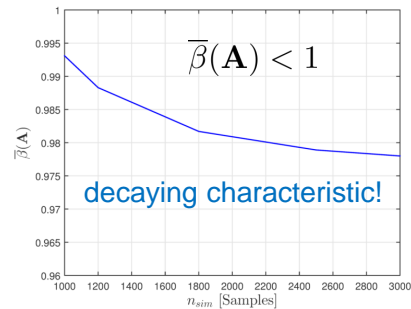
$$\bar{\beta}(\mathbf{A}) = \lim_{i \rightarrow \infty} \sup_{k \geq 0} \left\| \Phi_{k+i,k} \right\|^{\frac{1}{i}} = \inf_{i > 0} \sup_{k \geq 0} \left\| \Phi_{k+i,k} \right\|^{\frac{1}{i}}$$

- evaluation via minimum of the individual row-maxima of  $\mathbf{M}$ :

$$\mathbf{M} = \begin{matrix} & k=0 & \dots & k=\frac{n_{sim}}{2} \\ \begin{matrix} i=1 \\ \vdots \\ i=\frac{n_{sim}}{2} \end{matrix} & \begin{bmatrix} \left\| \Phi_{1,0} \right\|^{\frac{1}{1}} & \dots & \left\| \Phi_{\frac{n_{sim}}{2}+1, \frac{n_{sim}}{2}} \right\|^{\frac{1}{1}} \\ \vdots & \ddots & \vdots \\ \left\| \Phi_{\frac{n_{sim}}{2}, 0} \right\|^{\frac{1}{\frac{n_{sim}}{2}}} & \dots & \left\| \Phi_{n_{sim}, \frac{n_{sim}}{2}} \right\|^{\frac{1}{\frac{n_{sim}}{2}}} \end{bmatrix} \end{matrix}$$

## Stability Analysis: Time-Variant Closed-Loop Dynamics (2)

- Results of the numerical approximation:



### UES Time-Variant Closed-Loop Dynamics

- UES:**  $\|\Phi_{k,k_0}\| \leq \alpha \beta^{k-k_0}$  for all  $k_0 \leq k$  and  $\beta \in (\bar{\beta}(\mathbf{A}), 1)$ ,  $\alpha \geq 1$

- Short-time BIBO stability:**

$$\sum_{i=k_0}^{k-1} \|\mathbf{G}_{k,i}\| \leq \sum_{i=k_0}^{k-1} \underbrace{\|\mathbf{C}_k\|}_{K_C} \underbrace{\|\Phi_{k,i}\|}_{\beta} \underbrace{\|\mathbf{B}_i\|}_{K_B}$$

$$\leq K_C K_B \alpha \frac{\beta}{1-\beta} = c < \frac{\epsilon}{\delta}.$$



### Short-Time BIBO Stable Time-Variant Closed-Loop Dynamics

## Conclusions & Outlook

- MBC is suitable to compensate coupling imperfection effects**
- MBC is the key to solve Real-Time Co-Simulation problems**
- Successful Closed-Loop Stability Analysis for linear Subsystems**



- Open tasks:**

- Closed-Loop Stability Analysis for nonlinear Subsystems
- Usability improvement (Parametrization and Integration)



- Real-Time Co-Simulation
- Networked Control Systems (NCS)
- Consensus Control of Multi-Agent Systems
- Time-Delay Systems
- Systems of Systems Engineering (SoSE)
- Decentralized Control
- Smart Grid Applications
- Signal Conditioning



Dr. Georg Stettinger, Dr. Martin Benedikt  
VIRTUAL VEHICLE Research Center, Graz, Austria  
[georg.stettinger@v2c2.at](mailto:georg.stettinger@v2c2.at), [martin.benedikt@v2c2.at](mailto:martin.benedikt@v2c2.at)

# Model based control of a biomass fired steam boiler

Christopher Zemann<sup>a,b</sup>

Viktor Unterberger<sup>a,b</sup>

Markus Gölles<sup>a</sup>

## Introduction

In terms of system theory, a biomass furnace with steam boiler is a non-linear, coupled multivariable system with several inputs and outputs. Conventional control strategies currently applied to these plants usually consist of decoupled linear sub-controllers, just partially or even not at all considering the coupled and non-linear behaviour of furnace and boiler. The goal of this work was to develop a new control strategy that utilizes a mathematical model of the process to improve the plant's operating behaviour and apply this control to an industrial plant for the production of process steam.

## Plant description

The industrial plant, illustrated in Figure 1, has a nominal capacity of 6 MW and is designed for the combustion of wood chips. The fuel is fed onto a declining reciprocating grate by a hydraulic stoker. There it is heated up due to the high temperatures in the furnace. As a result, the water that is bound in the fuel is evaporated and the fuel's volatile components are released to the gas phase (devolatilization). The remaining charcoal is burned with primary air supplied beneath the grate, providing the heat necessary for the evaporation and devolatilization. The resulting flue gas moves from the primary combustion chamber to the secondary combustion chamber where additional air (secondary air) is added, ensuring a complete burnout of the fuel. Both the primary and the secondary combustion chambers are surrounded by refractory lining which physically resembles a heat storage continuously exchanging heat with the flue gas passing through the combustion chamber. Finally, the flue gas enters the steam boiler where most of the heat released by the combustion is transferred to water, leading to its evaporation. A part of the flue gas is recirculated into the primary combustion chamber, thus enabling the control of the temperature in the combustion chamber.

## Modelling and control

The modelling of biomass furnace and steam boiler investigated has been performed separately for all relevant parts, namely the fuel bed, the gas phase combustion, the heat storage effect of the refractory lining and the evaporation of the water in the boiler. The mathematical model for the fuel bed consists of two first-order ordinary differential equations representing mass balances for the mass of water and dry fuel on the grate. They describe the correlation between the supplied primary air and fuel mass flows as well as the fuel composition and the mass flows of evaporated water and thermally decomposed dry fuel. The static model for the gas phase combustion equals a standard combustion calculation. It considers the water and fuel released from the fuel bed, the supplied air and the recirculated

---

<sup>a</sup>Bioenergy 2020+ GmbH, Inffeldgasse 21b, A-8010 Graz, E-Mail: christopher.zemann@bioenergy2020.eu

<sup>b</sup>Institut für Regelungs- und Automatisierungstechnik, Technische Universität Graz, Kopernikusgasse 24/II, 8010 Graz

flue gas and provides the adiabatic combustion temperature as well as the mass flow and the chemical composition of the resulting flue gas. The heat storage effect of the refractory lining is modeled by one linear first order ordinary differential equation describing the correlation of the adiabatic combustion temperature and the temperature of the flue gas at the end of the secondary combustion chamber. The evaporation of water in the steam boiler as well as the heat transfer from the flue gas to the water is described by two first order non-linear ordinary differential equations.

Similar to conventional control strategies, the variables controlled by the developed strategy are the steam pressure, the water level in the boiler, the temperature of the flue gas at the end of the secondary combustion zone and the oxygen content of the flue gas at boiler outlet. The developed control is based on the method of Exact Input-Output Linearization in combination with an Extended Kalman Filter.

### Results of the implementation at an industrial plant

The control strategy developed has been implemented and validated at the industrial biomass plant described previously where it led to significant improvements of the plant's operating behaviour, with all controlled variables being kept closer to the desired values. In particular, a better control of the oxygen content in the flue gas has been achieved, indicating a more regular and complete burnout of the fuel. Furthermore, the new control reacts more quickly to the rapid changes of the heat demand occurring in this plant, providing an overall more stable plant behaviour and consequently a more stable steam pressure as illustrated in Figure 2.

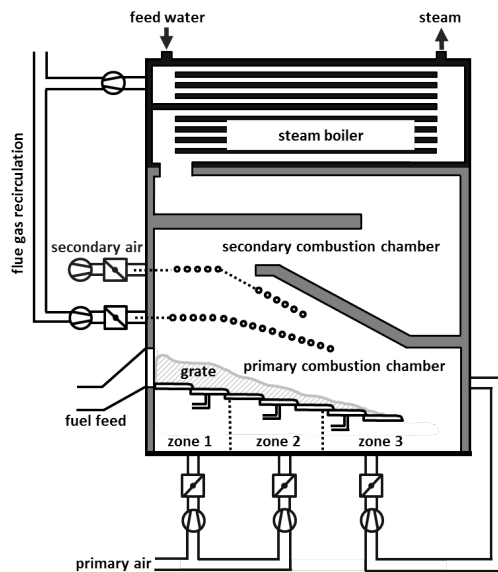


Figure 1: Biomass fired steam boiler

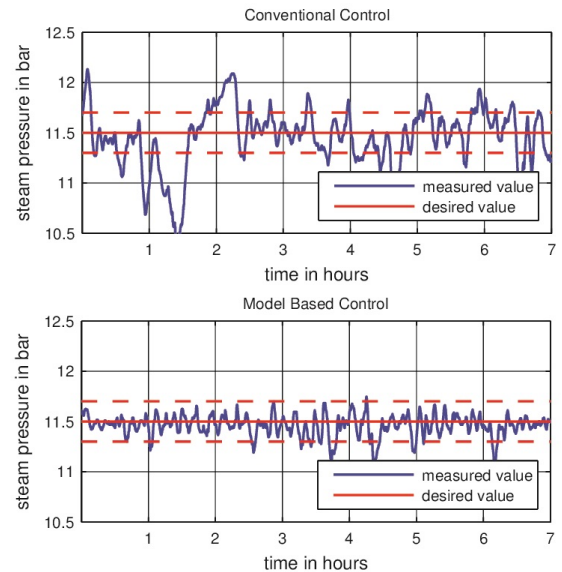


Figure 2: Stabilization of steam pressure



bioenergy2020+



## Model based control of a biomass fired steam boiler

Christopher Zemann<sup>a,b</sup>, Viktor Unterberger<sup>a,b</sup>, Markus Gölls<sup>a</sup>

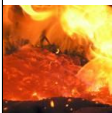
Schloss Retzhof, 09.09.2015

<sup>a</sup> Bioenergy 2020+ GmbH, Inffeldgasse 21b, A-8010 Graz, E-Mail: [christopher.zemann@bioenergy2020.eu](mailto:christopher.zemann@bioenergy2020.eu)

<sup>b</sup> Institute of Automation and Control, Graz University of Technology, Kopernikusgasse 24/II, 8010 Graz



bioenergy2020+



## Model based control of biomass furnaces

- In terms of system theory, a biomass furnace with steam boiler is a
    - non-linear
    - coupled multivariable system
    - with several inputs and outputs
  - Currently applied control strategies are based on decoupled PI-controllers ignoring the couplings and non-linear behaviour.
- **Development and application of a model based control strategy to improve the operating behavior.**



## Content of the presentation

- Description of the biomass fired steam boiler
- Modelling of the biomass furnace
- Modelling of the steam boiler
- Model based control of the biomass fired steam boiler
- Results and summary

Slide 3



## Description of the biomass fired steam boiler

Slide 4





## Fuel: wood chips

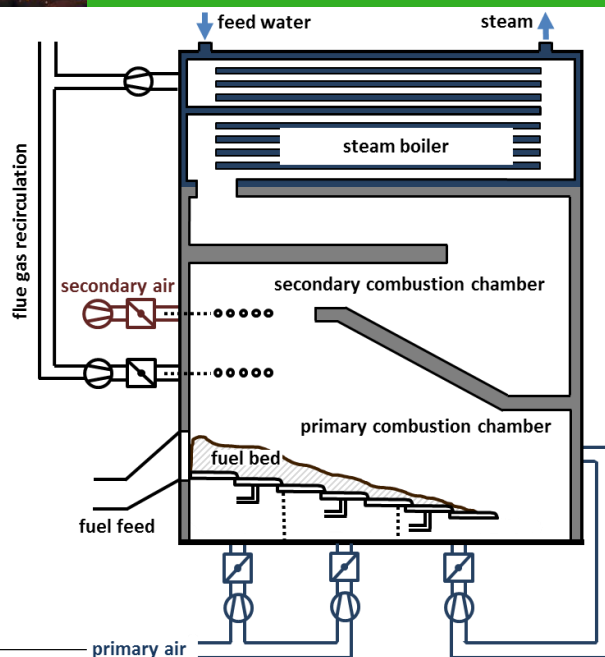


- wood chips
- water content
  - typically 30% - 60% of the overall weight
- calorific value
  - typically ~4,3 kWh / kg
  - for comparison:
    - hard coal: 7 – 8 kWh / kg

Slide 5



## Description of the biomass fired steam boiler



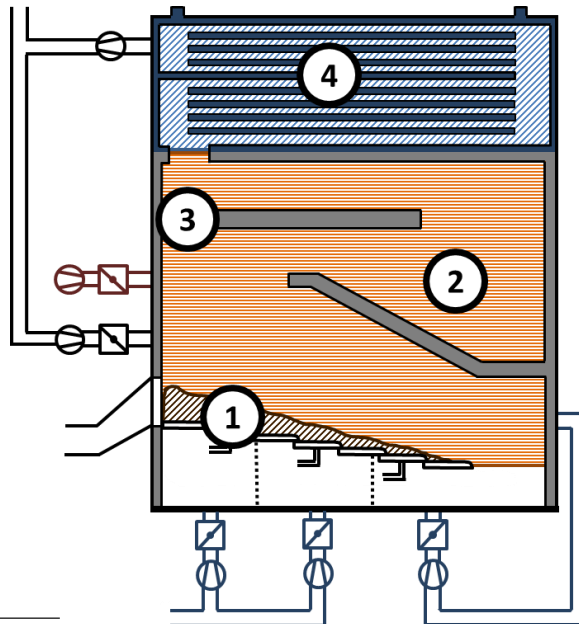
- industrial steam boiler
- production of process steam (dairy industry)
- nominal capacity: **6 MW<sub>th</sub>**
- saturated steam produced at nominal load: **9.2 t/h**

Slide 6



## Modelling of the plant

### Separate modeling of the relevant parts



- **(1) fuel bed:**  
evaporation of the water and thermal decomposition of the dry fuel
- **(2) gasphase combustion:**  
combustion of the decomposed dry fuel
- **(3) thermal storage in the refractory lining:**  
heat stored in the refractory lining
- **(4) steam boiler:**  
transfer of the heat released by the combustion to the water and evaporation of the water

Slide 7



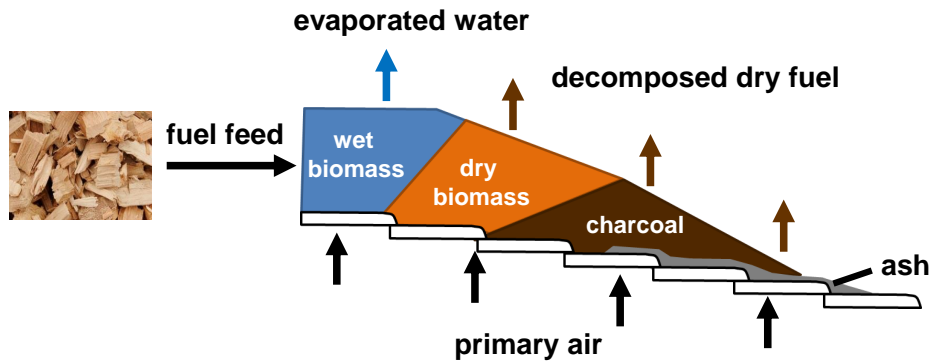
## Modelling of the biomass furnace

- (1) fuel bed
- (2) gasphase combustion
- (3) thermal storage in the refractory lining

Slide 8



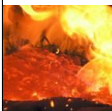
## Modelling of the biomass furnace (1) fuel bed



Utilization of an existing mathematical model based on a mass balance

$$\frac{d}{dt}(\text{mass of fuel in the fuel bed}) = \text{entering mass flow} - \text{released mass flow}$$

Slide 9



## Modelling of the biomass furnace (1) fuel bed

- differential equation for the water in the evaporation zone  $m_w$

$$\frac{dm_w(t)}{dt} = \underbrace{-c_{wev} m_w(t)}_{\text{evaporated water}} + \underbrace{\frac{dm_{w,inlet}(t - T_d(t))}{dt}}_{\text{entering water}}$$

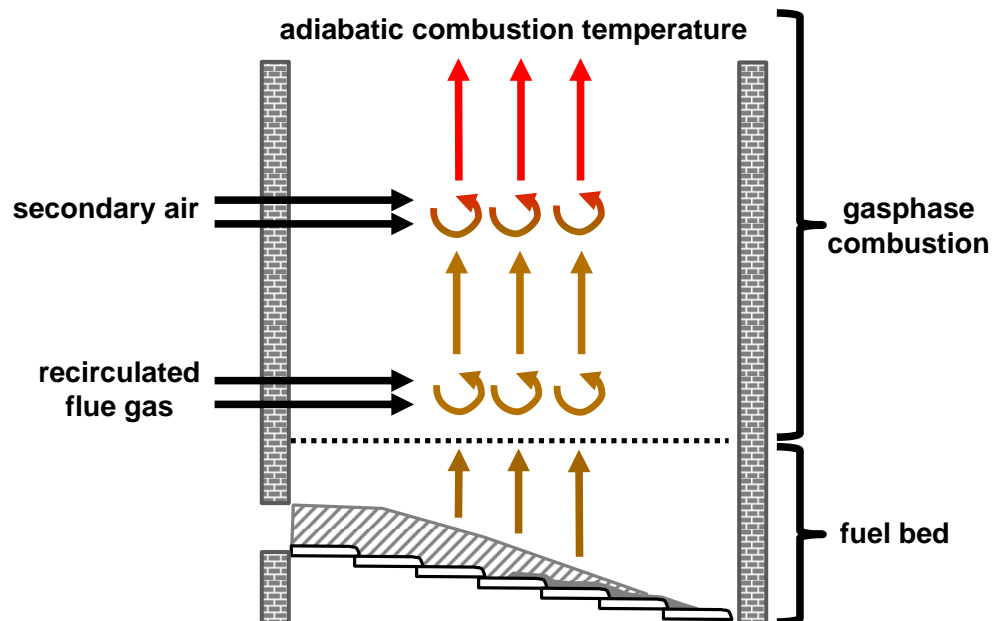
- differential equation for the dry fuel in the thermal decomposition zone  $m_{ds}$

$$\frac{dm_{ds}(t)}{dt} = \underbrace{-c_{thd} [\dot{m}_{pa}(t) + c_{pa,0}] m_{ds}(t)}_{\text{decomposed dry fuel}} + \underbrace{\frac{dm_{ds,inlet}(t - T_d(t))}{dt}}_{\text{entering dry fuel}}$$

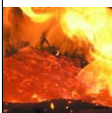
Slide 10



## Modelling of the biomass furnace (2) gasphase combustion



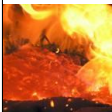
Slide 11



## Modelling of the biomass furnace (2) gasphase combustion

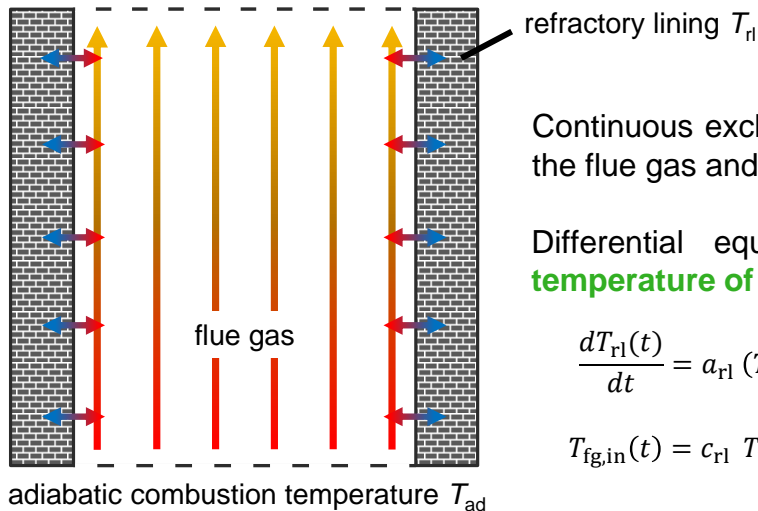
- **combustion of volatiles and char**
  - ordinary mass and energy balance (combustion calculation)
  - **nonlinear algebraic equations**
- **outputs**
  - adiabatic combustion temperature
  - mass flow of the flue gas

Slide 12



## Modelling of the biomass furnace (3) thermal storage in the refractory lining

resulting temperature of the flue gas  $T_{fg,in}$



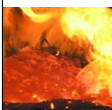
Continuous exchange of heat between the flue gas and the refractory lining.

Differential equation for the **mean temperature of the refractory lining**:

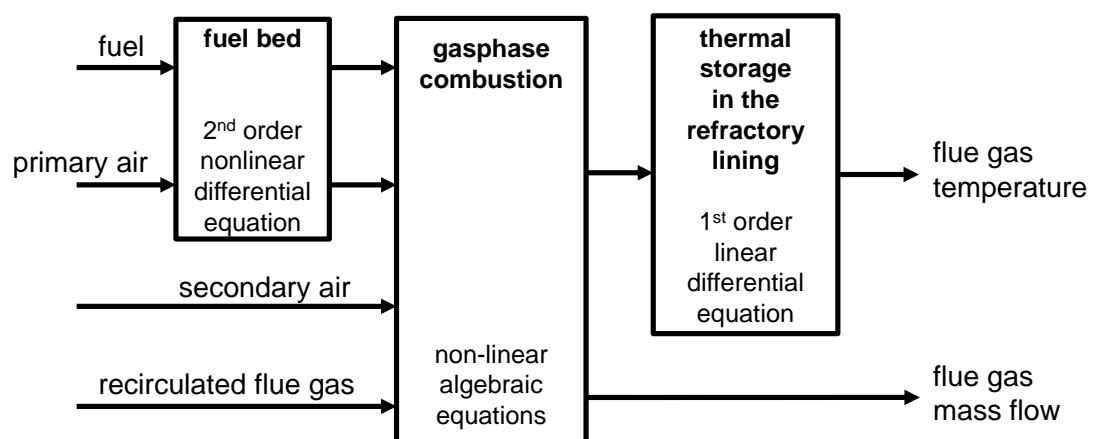
$$\frac{dT_{rl}(t)}{dt} = a_{rl} (T_{ad}(t) - T_{rl}(t))$$

$$T_{fg,in}(t) = c_{rl} T_{rl}(t) + (1 - c_{rl}) T_{ad}(t)$$

Slide 13



## Structure of the overall model of the biomass furnace



Slide 14



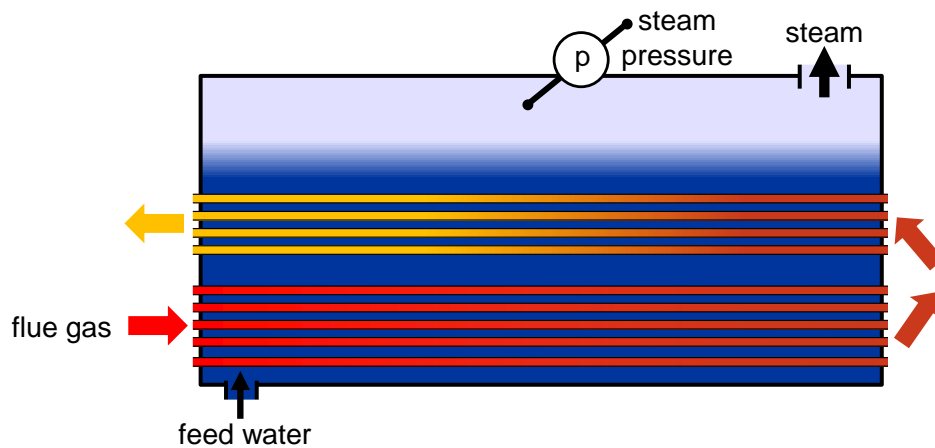
## Modelling of the steam boiler

Slide 15



## Modelling of the steam boiler

### Description of the steam boiler



Application of mass and energy balance equations  
for modelling the steam boiler.

Slide 16



## Modelling of the steam boiler

### Mass balance equation

- conservation of mass in the steam boiler

$$\frac{d}{dt} \underbrace{(m_{\text{water}} + m_{\text{steam}})}_{\text{mass of water and steam in the boiler}} = \underbrace{\dot{m}_{\text{feed}} - \dot{m}_{\text{steam}}}_{\text{mass flows of entering feed water and emanating steam}}$$

- $m = \rho V$

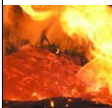
$$\frac{d}{dt} (\rho_{\text{water}} V_{\text{water}} + \rho_{\text{steam}} V_{\text{steam}}) = \dot{m}_{\text{feed}} - \dot{m}_{\text{steam}}$$

with

$$\rho_{\text{water}} = \rho_{\text{water}}(\text{pressure, temperature}) \quad \dots \text{density of water}$$

$$\rho_{\text{steam}} = \rho_{\text{steam}}(\text{pressure, temperature}) \quad \dots \text{density of steam}$$

Slide 17



## Modelling of the steam boiler

### Energy balance equation

- conservation of energy in the steam boiler

$$\underbrace{\frac{dU}{dt}}_{\text{stored energy}} = \underbrace{\sum \dot{H}_{\text{in}} - \sum \dot{H}_{\text{out}}}_{\text{energy flux across the system boundaries}}$$

$$\frac{d}{dt} (U_{\text{water}} + U_{\text{steam}} + U_{\text{metal}}) = \dot{H}_{\text{feed}} - \dot{H}_{\text{steam}} + \Delta \dot{H}_{\text{fg}}$$

with

$$U_x \sim \rho_x \cdot V_x \cdot h_x \quad \dots \text{internal energy}$$

$$\dot{H}_x = \dot{m}_x \cdot h_x \quad \dots \text{energy flux}$$

$$h_x = h_x(\text{pressure, temperature}) \quad \dots \text{specific enthalpy}$$

Slide 18



## Modelling of the steam boiler

### Saturated steam

- The properties of water and steam (density and specific enthalpy) are **nonlinear functions of the temperature and the pressure**.

→ Assumption: **saturated steam**

$$\rho_x = \rho_x(\text{pressure})$$

$$h_x = h_x(\text{pressure})$$

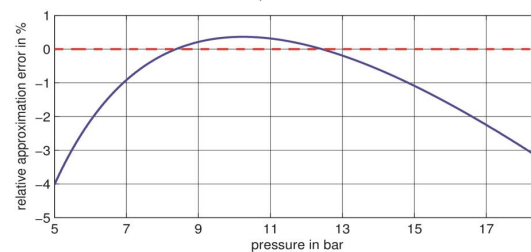
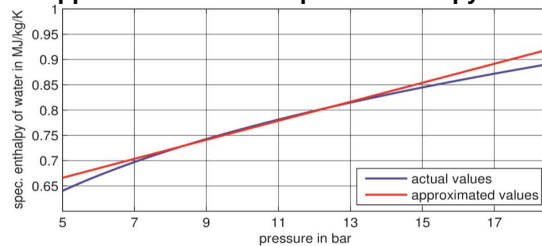
$$\rho_{\text{water}} = a_{w,1} p + a_{w,0}$$

$$\rho_{\text{steam}} = a_{s,1} p + a_{s,0}$$

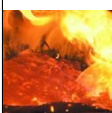
$$h_{\text{water}} = b_{w,1} p + b_{w,0}$$

$$h_{\text{steam}} = b_{s,1} p + b_{s,0}$$

approximation of the specific enthalpy of water



Slide 19



## Modelling of the steam boiler

### Resulting overall model

The resulting mathematical model of the steam boiler is a system of two coupled, non-linear ordinary differential equations:

$$\begin{bmatrix} \frac{dV_{\text{water}}}{dt} \\ \frac{dp}{dt} \end{bmatrix} = \begin{bmatrix} \alpha_1 \cdot p + \alpha_0 & \beta_1 \cdot V_{\text{water}} + \beta_0 \\ \gamma_1 \cdot p^2 + \gamma_1 \cdot p + \gamma_0 & \Delta_3 \cdot V_{\text{water}} \cdot p + \Delta_2 \cdot V_{\text{water}} + \Delta_1 \cdot p + \Delta_0 \end{bmatrix}^{-1} \cdot \left( - \begin{bmatrix} 1 \\ \varepsilon_1 \cdot p + \varepsilon_0 \end{bmatrix} \dot{m}_{\text{steam}} + \begin{bmatrix} 1 & 0 \\ h_{\text{feed}} & 1 \end{bmatrix} \cdot \begin{bmatrix} \dot{m}_{\text{feed}} \\ \Delta \dot{H}_{\text{fg}} \end{bmatrix} \right)$$

- state variables**

→  $p$  ... steam pressure

→  $V_{\text{water}}$  ... volume of water in the boiler

- input variables**

→  $\dot{m}_{\text{feed}}$  ... feed water mass flow

→  $\Delta \dot{H}_{\text{fg}}$  ... heat flux transferred from flue gas to the steam boiler

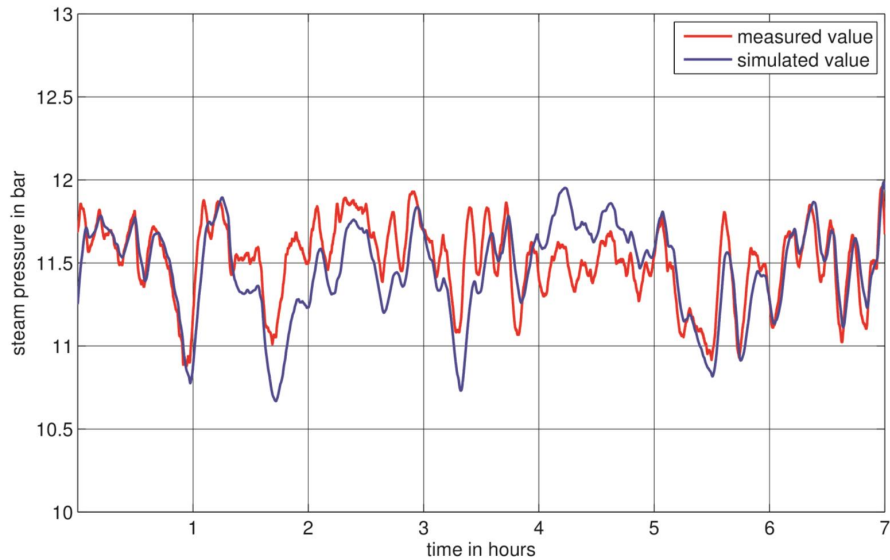
Slide 20





## Modelling of the steam boiler

### Verification of the mathematical model of the steam boiler



**The mathematical model of the steam boiler matches the measured data sufficiently well.**

Slide 21

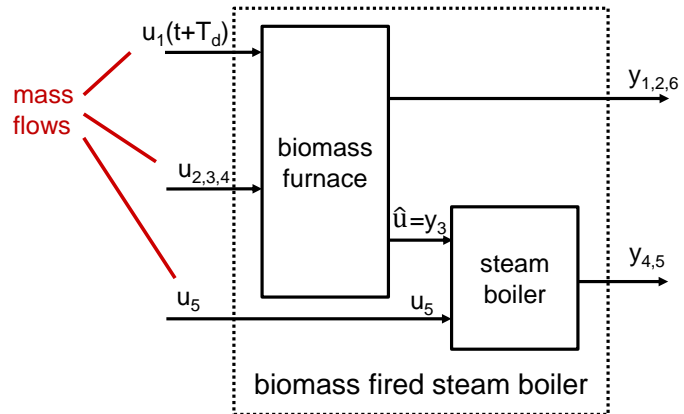


## Model based control of the biomass fired steam boiler

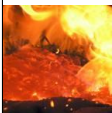
Slide 22



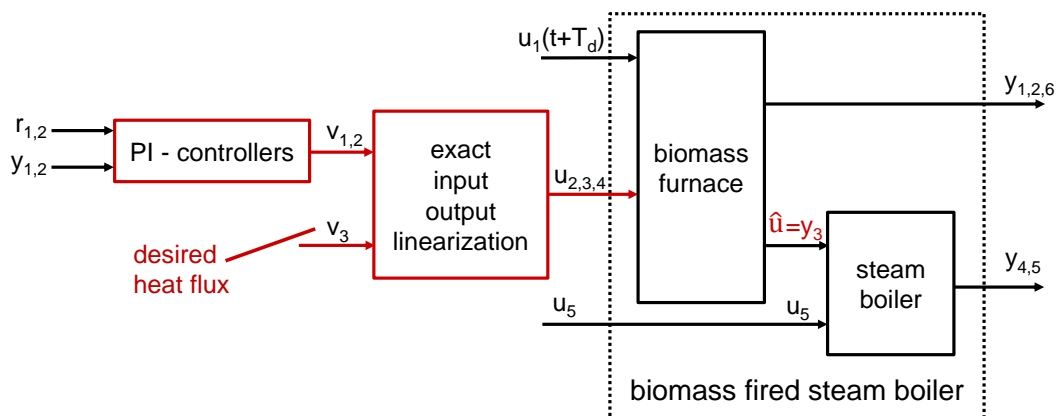
## Control of the biomass fired steam boiler



Slide 23



## Control of the biomass fired steam boiler



Slide 24



## Control of the biomass fired steam boiler

### Mathematical model of the biomass furnace

$$\begin{aligned}\frac{dx_1}{dt} &= -\frac{c_{11}}{1 + c_{12}d_1}x_1 + \frac{d_1}{1 + c_{12}d_1}u_1 \\ \frac{dx_2}{dt} &= \frac{c_{21}}{1 + c_{12}d_1}x_1 - c_{22}x_2u_2 + \frac{1}{1 + c_{12}d_1}u_1 \\ \frac{dx_3}{dt} &= \frac{-c_{31}x_1 + c_{32}x_2u_2 + c_{33}u_3 + c_{34}u_4}{c_{11}x_1 + c_{12}x_2u_2 + u_3 + u_4}\end{aligned}$$

#### ■ state variables

- $x_1 = m_w$  ... mass of water in the evaporation zone
- $x_2 = m_{ds}$  ... mass of dry fuel in the thermal decomposition zone
- $x_3 = T_{rl}$  ... mean temperature of the refractory lining

Slide 25



## Control of the biomass fired steam boiler

### Exact input-output linearization of the biomass furnace

#### ■ output variables

- $y_1$  ... residual oxygen content of the flue gas
- $y_2$  ... temperature of the flue gas
- $y_3$  ... heat flux transferred from flue gas to the steam boiler

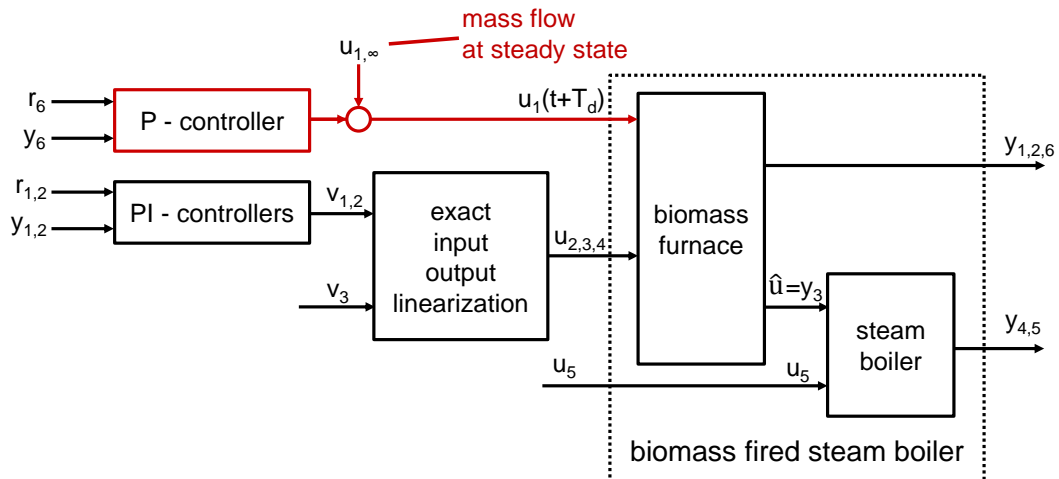
#### ■ exact input – output linearization with desired transfer functions

$$\left. \begin{aligned}y_1 &= v_1 \\ y_2 &= v_2 \\ y_3 &= v_3\end{aligned} \right\} \xrightarrow{\text{exact linearization}} \left. \begin{aligned}u_2 \\ u_3 \\ u_4\end{aligned} \right\}$$

Slide 26



## Control of the biomass fired steam boiler



Slide 27



## Control of the biomass fired steam boiler Fuel mass flow

$$u_1 = \dot{m}_{ds,inlet}(t - T_d(t)) \quad \dots \text{mass flow of dry fuel}$$

→ the method of exact input – output linearization is not applicable

- separate control for the fuel bed

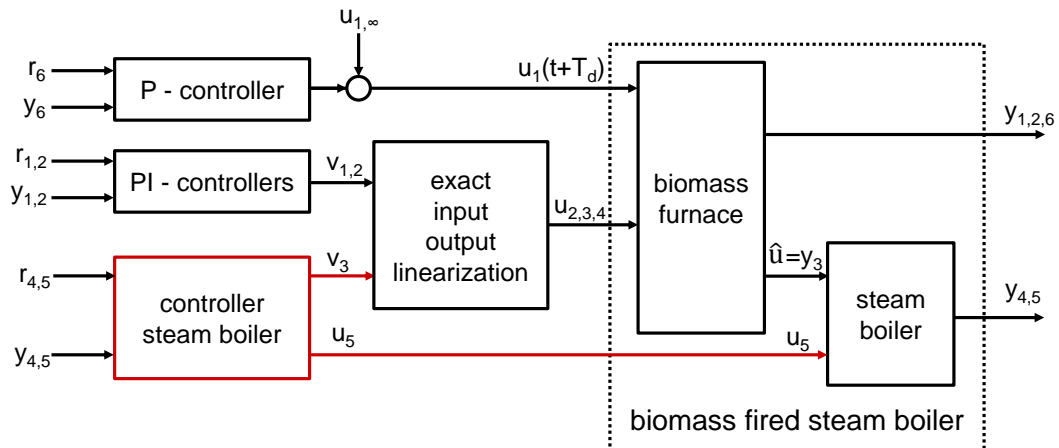
$$u_1 = u_{1,\infty} + \underbrace{k_p (r_6 - y_6)}_{\text{proportional controller}}$$

- $y_6$  ... mass of dry fuel in the thermal decomposition zone
- $u_{1,\infty}$  ... mass flow of dry fuel at steady state conditions

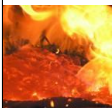
Slide 28



## Control of the biomass fired steam boiler



Slide 29



## Control of the biomass fired steam boiler

### Mathematical model of the steam boiler

$$\begin{aligned} \frac{dx_4}{dt} &= \frac{(-c_{f,7} x_4 x_5 - c_{f,5} x_4 - c_{f,8} x_5 - c_{f,9} + c_{f,1} x_4 d_5 + c_{f,3} d_5) u_5}{F(x_4, x_5)} \\ &\quad + \frac{(c_{f,1} x_4 + c_{f,3}) \hat{u}}{F(x_4, x_5)} + \frac{(c_{K,7} x_4 x_5 + c_{K,8} x_4 + c_{K,9} x_5 + c_{K,10}) d_4}{F(x_4, x_5)} \\ \frac{dx_5}{dt} &= \frac{(-c_{f,4} x_5^2 - c_{f,5} x_5 - c_{f,6} + c_{f,1} x_5 d_5 + c_{f,2} d_5) u_5}{-F(x_4, x_5)} \\ &\quad + \frac{(c_{f,1} x_5 + c_{f,2}) \hat{u}}{-F(x_4, x_5)} + \frac{(c_{K,11} x_5^2 + c_{K,12} x_5 + c_{K,13}) d_4}{-F(x_4, x_5)} \end{aligned}$$

- state variables and output variables
  - $x_4 = y_4 = V_{\text{water}}$  ... volume of water in the boiler
  - $x_5 = y_5 = p$  ... steam pressure
- input variables
  - $u_5$  ... mass flow of feed water
  - $\hat{u} (= y_3)$  ... heat flux transferred from flue gas to the steam boiler

Slide 30



## Control of the biomass fired steam boiler

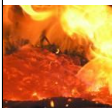
### Exact input-output linearization of the steam boiler

- exact input – output linearization with desired transfer functions

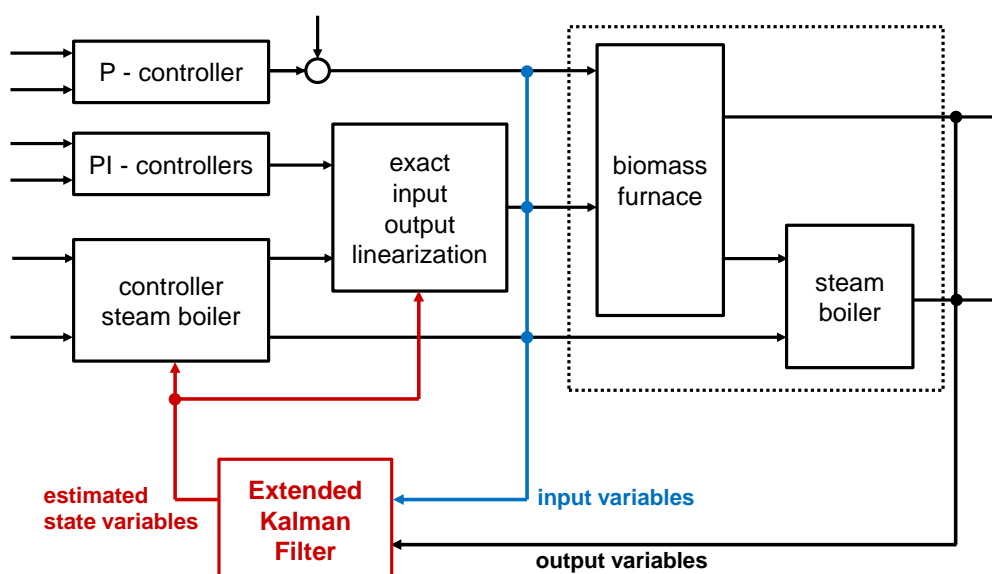
$$\left. \begin{aligned} w_{4,1} y_4 + \frac{dy_4}{dt} &= w_{4,0} v_4 \\ w_{5,1} y_5 + \frac{dy_5}{dt} &= w_{5,0} v_5 \end{aligned} \right\} \xrightarrow{\text{exact linearization}} \begin{cases} u_5 \\ \hat{u} \end{cases}$$

- control of steam pressure and volume of water
  - PI - controllers

Slide 31



## Control of the biomass fired steam boiler



Slide 32



## Results and summary

Slide 33



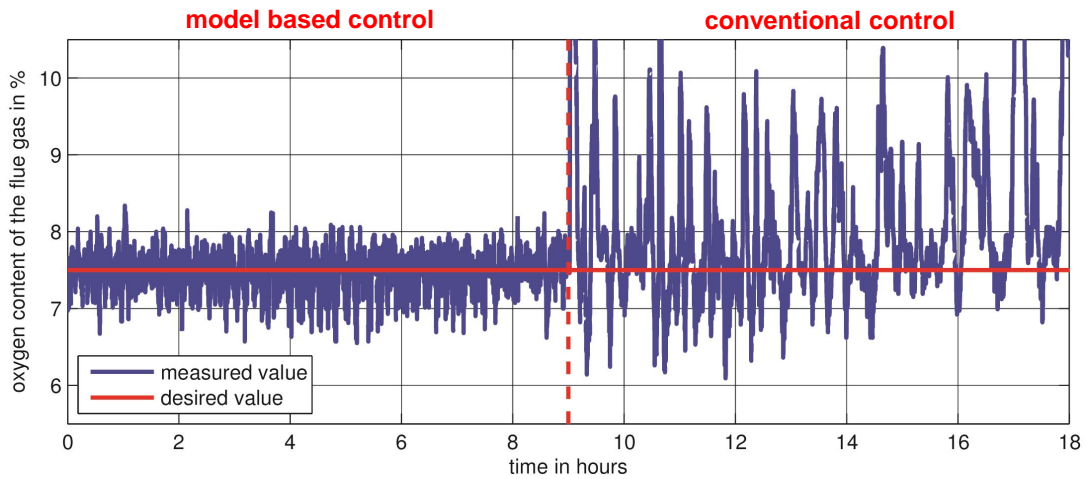
## Results

- Comparison of the biomass plant's operating behaviour controlled by
  - the newly developed model based control strategy
  - the conventional control strategy (PI-controllers) originally applied
- Switching between both controls
  - initialization of the integral controller to enable a smooth transition
- Comparing:
  - $y_1$  ... residual oxygen content of the flue gas
  - $y_2$  ... flue gas temperature in the secondary combustion chamber
  - $y_3$  ... steam pressure

Slide 34

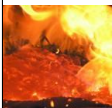


## Results oxygen content of the flue gas

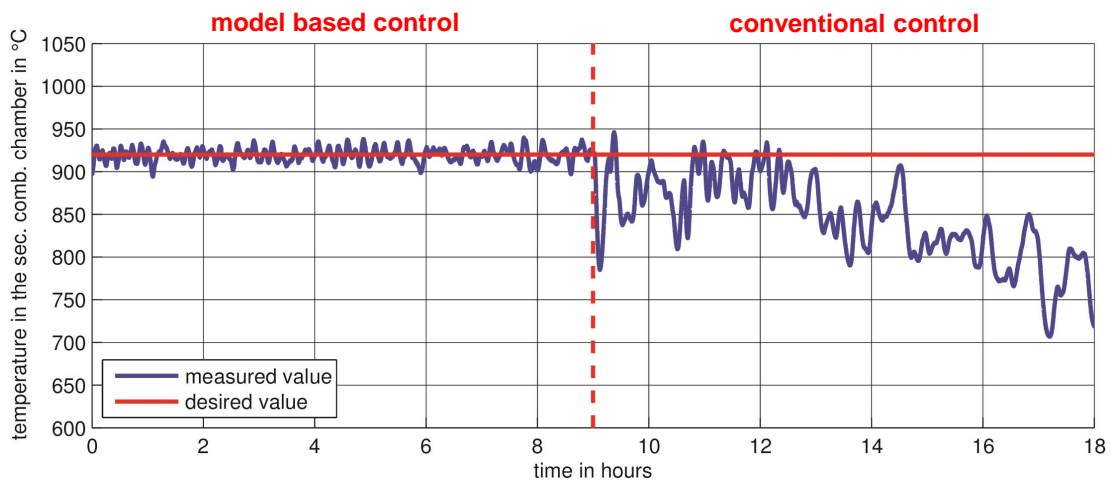


→ model based control keeps the oxygen content closer to the desired value  
(reduction of standard deviation: 1.15 → 0.25 vol.% w.b.)

Slide 35



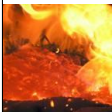
## Results temperature of the flue gas



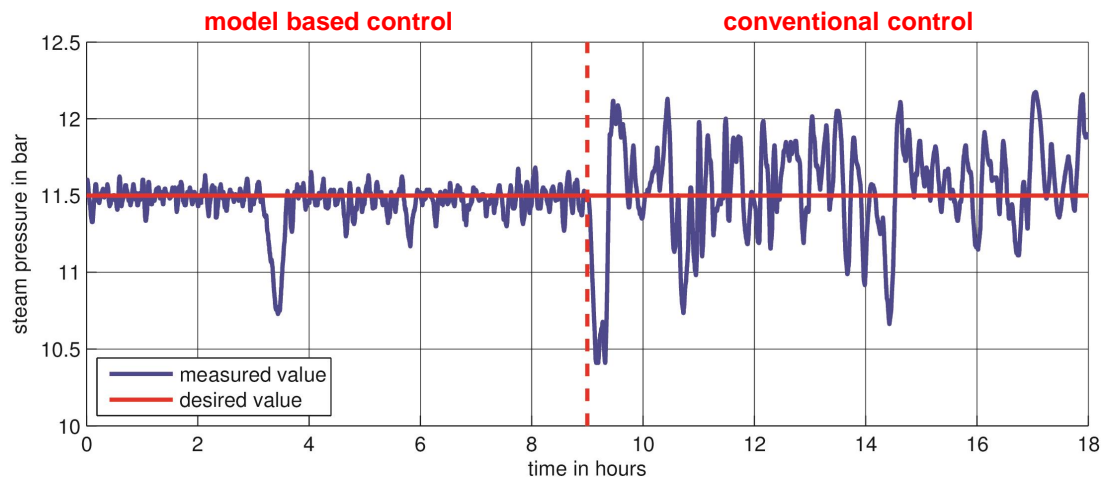
→ model based control keeps temperature in the secondary combustion chamber closer to the desired value

Slide 36



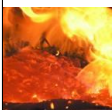


## Results steam pressure



→ model based control keeps the steam pressure closer to the desired value  
(reduction of standard deviation: 0.33 → 0.12 bar)

Slide 37



## Summary

- Development of a mathematical model for biomass fired steam boilers.
  - **biomass furnace:** 3<sup>rd</sup> order non-linear differential equation
  - **steam boiler:** 2<sup>nd</sup> order non-linear differential equation
- Application of a model based control strategy.
  - exact input-output linearization of the biomass furnace
  - superimposed controller for the steam boiler (exact put-output linearization)

**The application of the control at an industrial plant led to a significant improvement of the plant's operating behavior.**

Slide 38



## Model based control of a biomass fired steam boiler

Christopher Zemmann<sup>a,b</sup>, Viktor Unterberger<sup>a,b</sup>, Markus Göllers<sup>a</sup>

Schloss Retzhof, 09.09.2015

<sup>a</sup> Bioenergy 2020+ GmbH, Inffeldgasse 21b, A-8010 Graz, E-Mail: [christopher.zemann@bioenergy2020.eu](mailto:christopher.zemann@bioenergy2020.eu)

<sup>b</sup> Institute of Automation and Control, Graz University of Technology, Kopernikusgasse 24/II, 8010 Graz